University of Southampton

Faculty of Engineering and Physical Sciences

School of Chemistry

Developing New Metal-Based Complexes for ^{18}F-based Positron Emission Tomography (PET) Applications

by

Madeleine Serena Woodward

Thesis for the degree of Doctor of Philosophy

May 2023

University of Southampton

Abstract

Faculty of Engineering and Physical Sciences
Chemistry
Doctor of Philosophy

By Madeleine Serena Woodward

Developing New Metal-Based Complexes for ^{18}F-based Positron Emission Tomography (PET) Applications

The coordination chemistry of Group 14 fluoride complexes towards hard N– and O-donor ligands was developed. The pseudo-octahedral complexes $[SnF_4(L)_2]$ have been prepared and further characterisation detail has been acquired than present in the literature. The reactions of $[SnF_4(L)_2]$ with trimethylsilyl trifluoromethanesulfonate (TMSOTf) and one equivalent of appropriate ligand gave the novel, octahedral cationic complexes $[SnF_3(L)_3][OTf]$ (L = dmf, dmso, pyridine N-oxide (pyNO), pyridine (py) and $OPPh_3$). Further tests on removing fluoride in the presences of $OPPh_3$ showed that it was possible to prepare and characterise the first reported example of a phosphine oxide dicationic tin(IV) fluoride phosphine oxide complex, $[SnF_2(OPPh_3)_4][OTf]_2$.

Similarly, the novel complexes $[GeF_4(L)_2]$ (L = dmso, dmf and pyNO) and known complexes $[GeF_4(L')_2]$ (L' = py, $OPPh_3$, $OPMe_3$ and $OAsPh_3$) were prepared from reactions of $[GeF_4(MeCN)_2]$ with the appropriate ligand. The reactions of $[GeF_4(L)_2]$ with TMSOTf and one equivalent of appropriate ligand gave the novel, octahedral cationic complexes $[GeF_3(L)_3][OTf]$ (L = dmso, dmf, pyNO, py, $OPPh_3$, $OPMe_3$ and $OAsPh_3$). All of the complexes have been characterised by microanalysis, IR, ^{1}H, ^{31}P{^{1}H}, ^{19}F{^{1}H} and spectroscopy, where appropriate.

Reactions of $[MF_4(MeCN)_2]$ (M = Sn, Ge) with tetradentate macrocyclic ligands, 1,4,8,11-tetramethyltetraazacyclotetradecane (Me_4-cyclam) and 1,4,7,10-tetramethyltetraazacyclododecane (Me_4-cyclen), yields the rare Group 14 difluoride dicationic complexes, *cis*-$[MF_2(Me_4$- cyclam)$][OTf]_2$ and $[MF_2(Me_4$-cyclen$)][OTf]_2$, the former a mixture of *cis* and *trans* isomers. Similar attempts using SiX_4 (X = Cl or I) did not produced the dicationic complexes.

A new hydrothermal synthesis route to $[GaF_3(pyNO)(H_2O)_2]$ was developed and the complex was tested to determine whether it could be used as a synthon to access a new route to $[GaF_3(BnMe_2tacn)]$ in the absence of a highly coordinating solvent or competing anions. An attempt at a [^{18}F]fluoride radiolabelling experiment demonstrated that this route did produce a more radio-stable formulation of $[Ga^{18}F^{19}F_2(BnMe_2tacn)]$, showing a radiochemical purity (RCP) of >99% after three hours, however repeat experiments were unable to replicate these results.

The automation of the synthesis of $[Fe^{18}F^{19}F_2(BnMe_2tacn)]$ has been developed and optimised using the GE HealthCare's FASTlab, a commercially available synthesis module. Variation of parameters including pH, eluent concentration, temperature and organic:aqueous solvent ratio were undertaken. The RCP of the finalised reaction at a precursor concentration of 2.68 μM was >99% at t=0. High activity work (up to 30 GBq) was undertaken at Addenbrooke's Hospital subsequently and several radiostabilisers were tested for their suitability; a reaction starting at 26.1 GBq, the RCP of $[Fe^{18}F^{19}F_2(BnMe_2tacn)]$ was shown to have a radio-stability of 86% at t = 3 h in the presence of nicotinamide (5 mg/mL). This work showed that it is feasible to transfer these systems over to automation, as a proof of concept, and will allow more work on similar Fe(III) systems with bioconjugates by starting with this developed protocol.

Table of Contents

Table of Tables

Table of Tables

Table of Figures

Table of Figures

Table of Figures

Table of Figures

Table of Figures

List of Accompanying Materials

Appendix 1: General experimental details

Appendix 2: Crystallographic information files

Research Thesis: Declaration of Authorship

Madeleine Woodward

Developing New Metal-Based Complexes for ^{18}F-based Positron Emission Tomography (PET) Applications

I, Madeleine S. Woodward, declare that this thesis and the work presented in it are my own and has been generated by me as the result of my own original research.

I confirm that:

1. This work was done wholly or mainly while in candidature for a research degree at this University;
2. Where any part of this thesis has previously been submitted for a degree or any other qualification at this University or any other institution, this has been clearly stated;
3. Where I have consulted the published work of others, this is always clearly attributed;
4. Where I have quoted from the work of others, the source is always given. With the exception of such quotations, this thesis is entirely my own work;
5. I have acknowledged all main sources of help;
6. Where the thesis is based on work done by myself jointly with others, I have made clear exactly what was done by others and what I have contributed myself;
7. Parts of this work have been published as:

Fluoro-Germanium (IV) Cations with Neutral Co-Ligands—Synthesis, Properties and Comparison with Neutral GeF_4 Adducts. Madeleine S. Woodward; Rhys P. King; Robert D. Bannister; Julian Grigg; Graeme McRobbie; William Levason; Gillian Reid. *Inorganics* **2022**, *10*, 107.

Tin(IV) fluoride complexes with neutral phosphine coordination and comparisons with hard N- and O-donor ligands. Rhys P. King; Madeleine S. Woodward; Julian Grigg; Graeme McRobbie; William Levason; Gillian Reid. *Dalton Transactions* **2021** 50, 14400-14410.

Signature: ..... Date: .....

Acknowledgements

The work in this thesis is the product of three and a half years of work that I could not have done without the support of my supervisors Professor Gill Reid and Professor Bill Levason. Gill, your support, encouragement and kindness has been so significant in helping me reach the end of this PhD.

A big thank you to Vicki, Daniie, Kelsey, Rhys, and Charley for being there in the lab. Thanks to all the NCS staff, especially Dr Rob Bannister for the help in solving difficult X-ray crystal structures. Thanks to Dr Julie Herniman and the whole MS team for running my direct injection MS samples.

A big thanks to the GE team, to Dr Graeme McRobbie for your fantastic supervision during the radiochemistry experiments, your knowledge and patience has been invaluable and I have really appreciated all the time we've spent at KCL and Addenbrookes, and to Dr Julian Grigg for your insight during our catch-up meetings.

Thanks to EPSRC and GE HealthCare for funding and to the University of Southampton for providing excellent X-ray crystallography, NMR and MS facilities.

Big shout out to Molly for the countless coffees, bottles of wine and good food, your company and support has been something I will treasure forever. Thank you to Emily, my long suffering friend, for being there since the very beginning and always bringing me back down to earth, you never fail to make me cry from laughing so hard. Thank you to Angus who put up with me throughout our undergraduate degrees, hopefully there's plenty more pálinka and Diana Ross to come.

It has been quite the journey and I could not have done this without the support of my family. The biggest thank you of all goes to my Mum, Dad, and Al for your continuous love and encouragement, and to my Grandparents for being my biggest cheerleaders. It means more than you'll ever know.

Finally, to Fred, thank you for being there, words cannot express my gratitude for your support and love. I could not have got through this without you.

Definitions and Abbreviations

{^{1}H}..... Proton decoupled

^{18}F..... Fluorine-18

Bar^{F} ..... Tetrakis(3,5-bis(trifluoromethyl)phenyl)borate

BIMEt ..... Tris(1-ethyl-benzoimidazol-2-ylmethyl)amine)

Bipy ..... 2, 2'-Bipyridine

Bn..... Benzyl

br..... Broad

CT ..... Computed tomography

Cyclam 1,4,8,11-tetraazacyclotetradecane

Cyclen 1,4,7,10-tetraazacyclododecane

DMF ..... Dimethylformamide

DMSO..... Dimethyl sulfoxide

EA..... Elemental analysis

efg ..... Electric field gradient

Fac..... Facial

GBq ..... Giga-Becquerel

GC ..... Gas chromatography

GMP ..... Good manufacturing practice

HER3 ..... Human epidermal growth factor receptor 3

HLB..... Hydrophilic-lipophilic balanced

HSA ..... Human serum albumin

Hz ..... Hertz

IR ..... Infrared

J ..... Coupling constant

Kryptofix 2.2.2 ..... 4,7,13,16,21,24-Hexaoxa-1,10-diazabicyclo[8.8.8]hexacosane

m ..... Multiplet

m/z ..... Mass to charge ratio

MBq ..... Mega-Becquerel

Me ..... Methyl

MeCN ..... Acetonitrile

Mer ..... Meridional

Mes ..... Mesityl

MRI ..... magnetic resonance imagine

ng ..... Nanogram

NMR ..... Nuclear Magnetic Resonance

NODA 1,4,7-triazacyclononane-1,4-diacetate

NOE ..... Nuclear Overhauser effect

NOTA ..... 1,4,7-triazacyclononane-1,4,7-triacetic acid

$OAsPh_3$ ..... Triphenyl arsine oxide

$OPMe_3$ ..... Trimethyl phosphine oxide

$OPPh_3$ ..... Triphenyl phosphine oxide

OTf ..... Triflate

PBS ..... Phosphate-buffered saline

PET ..... Positron Emission Tomography

ppm ..... Parts per million

Py ..... Pyridine

PyNO ..... Pyridine N-Oxide

QMA ..... Quaternary methyl ammonium

RAC ..... Radioactivity concentration

RCP ..... Radiochemical purity

RCY ..... Radiochemical yield

s ..... Sharp

s ..... Singlet

SPE ..... Solid-phase extraction

tach ..... Triaza-cyclohexane

Tacn 1, 4, 7-Triazacyclononane

TBA..... Tetrabutylammonium

Terpy..... 2, 2', 6', 2''-Terpyridine

TMA ..... Tetramethylammonium

TMHD..... Tris(2,2,6,6-tetramethyl-3,5-heptanedionato)chromium(III)

TMS..... Tetramethylsilane

δ ..... Chemical shift

1 Introduction

1.1 Positron Emission Tomography

1.1.1 The History of PET

Positron emission tomography (PET) as a medical imaging technique was invented in the 1950s by Wrenn and co-workers for the localisation and detection of brain tumours, where it was first described as a promising technique for imaging within neurosurgery.[1] However, it wasn't until the late 1990s that it became a major diagnostic tool across the clinic. The technique suffers from relatively low resolution (typically 4-10 mm), in contrast to its high sensitivity, and therefore attempts were made to combine PET with another diagnostic technique such as computed tomography (CT) or magnetic resonance imaging (MRI) and fuse the anatomical images together. In the late 1980s, this was achieved for the detection of cancer in the head and neck, and this works well for rigid organs such as the brain.[2, 3]

1.1.2 Overview of PET

PET is a nuclear imaging technique used widely within oncology, cardiology, and neurology for diagnostics. A radiotracer is injected into the patient, the radioactive isotope then decays in the body through positron emission.[4] The emitted positrons (β^+) collide with electrons in close proximity in the surrounding tissues, this results in an annihilation event, which produces two gamma rays that are emitted in opposite directions, in a coincidence line almost 180 ° to each other. These β^+ emitters can be detected by a PET camera and a 3D image is reconstructed, Figure 1.1 shows the annihilation event and the process to develop a PET image.[5] A positron-emitting radionuclide can also be conjugated to a biomolecule, this can then accumulate in an area of interest, such as cells that metabolise glucose rapidly, this is the case for the most commonly used PET radiotracer in the clinic today, [^{18}F]fluorodeoxyglucose (FDG).[6]

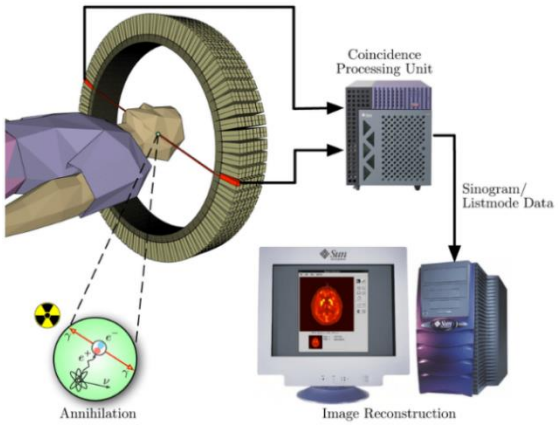

Figure 1.1: PET scan process and annihilation event.[7]

Important features of fluorine-18 are its positron-emitting capability, its short, but manageable half-life of approximately 110 minutes, the ability to form the radioisotope in an onsite cyclotron and the lack of any toxic products from the decay process (non-toxic ^{18}O is formed,

Scheme 1). The most common method for the production of [^{18}F] is *via* the irradiation of ^{18}O (the $^{18}O(p,n)^{18}F$ reaction), this results in [^{18}F]F^- in water, which can give radioactive levels greater than 100 GBq, this can be achieved after only one hour of bombardment.[8]

$$^{18}F \longrightarrow {}^{18}O + \beta^+ + \nu$$

Scheme 1: Decay of an ^{18}F isotope by positron emission, resulting in the formation of non-toxic ^{18}O, a positron (β^+) and a neutrino (ν).[9]

The diagnostic technique, PET, has a high sensitivity and a so very small amount of radiotracer can be used and subsequently detected. It can also have high resolution, but this can depend on the type of energy that is emitted. The greater the energy of the positron, the longer distance it can travel before an annihilation event occurs and thus the lower the resolution. Table 1 shows selected properties of certain commonly used positron-emitting radioisotopes.

Table 1: Selected physical properties of select positron-emitting radioisotopes. Edited from Reference.[8]

Radioisotope	Half-life (min)	Positron decay (%)	Max. energy (MeV)
^{18}F	110.0	97	0.64
^{11}C	20.3	99	0.97
^{13}N	10.0	100	1.20
^{15}O	2.0	100	1.74
^{68}Ga	68.1	89	1.90

The most widely used PET radiotracers are organofluorine molecules, where ^{18}F-radiolabelling of small molecules is achieved by the formation of a covalent bond between [^{18}F]fluoride and a carbon atom. The organofluorine tracer synthesis can often require many steps and time-consuming purification post-radiolabelling and is often achieved under conditions too harsh for a biomolecule. To form C-^{18}F bonds, nucleophilic substitution involving $^{18}F[F]^-$ is often undertaken and there is a limit on the organic chemistry possible for a ^{18}F-radiotracer production.[10]

1.1.3 [^{18}F]FDG

The most widely used PET radiotracer is [^{18}F]FDG, the structure of which is shown in Figure 1.2.[8, 11] [^{18}F]FDG is synthesised *via* a nucleophilic substitution mechanism (Scheme 2).

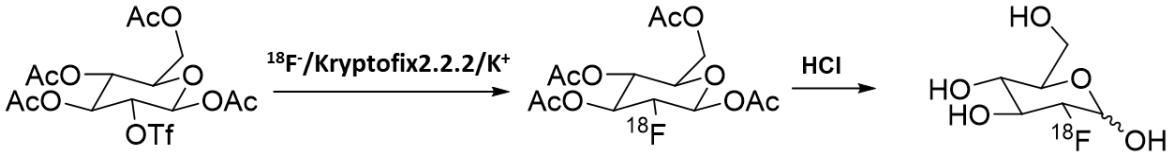

Scheme 2: Synthesis of ^{18}F[FDG].

[^{18}F]FDG is used to study the metabolism of glucose, and for example can be used in patients with altered cerebral metabolism, which can be indicative of certain cerebrovascular diseases, or for characterisation of tumours in secondary breast cancer patients.[12, 13] However its low specificity has been shown to be a problem, requiring higher than ideal concentrations, increasing the chance of false negatives and preventing early diagnoses.[14] Limitations also exist with tumours that do not get tagged effectively by [^{18}F]FDG, for example in prostate cancer, and in non-cancerous tissues that have a high uptake of [^{18}F]FDG and lead to false positives.[10, 15-17] Early diagnosis is vital to identify disease manifestations and treat individuals, maximising quality of life and increasing the chances of successful treatment.[6]

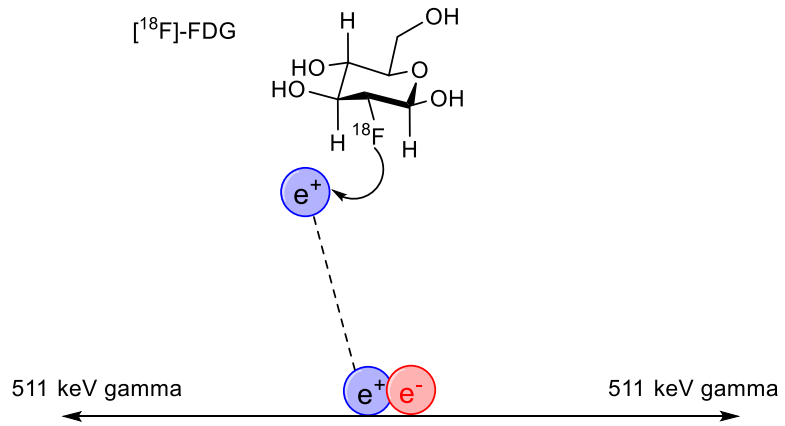

Figure 1.2: [^{18}F]FDG emitting a positron, a positively charged electron, colliding with an electron, and causing an annihilation event.

[^{18}F]fluoride is a poor nucleophile in water and is therefore often unable to undergo nucleophilic substitution with organic species within aqueous media. Hence these reactions require the rigorous exclusion of water. This is a significant challenge in production of organofluorine radiotracers.[18] A drying step is incorporated into the synthesis and the radioactive species is transferred in an aprotic solvent. A phase transfer catalyst, Kryptofix 2.2.2, is used to elute the radioactive fluoride anions, as illustrated in Scheme 3. These additional steps are time-consuming and undesirable given the short half-life of [^{18}F]fluoride. The encapsulation of the potassium ion leads to the formation of the K^+ salt, which in turn prevents the formation of unreactive ^{18}F[KF], which is insoluble in non-polar media, and the potassium acts as a counterion. This increases the solubility and reactivity of the fluoride source in non-aqueous media.

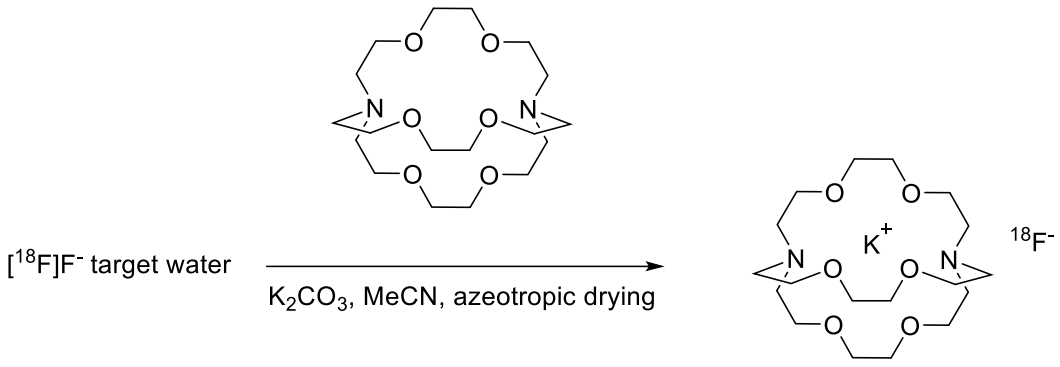

Scheme 3: Kryptofix on [^{18}F]fluoride target water.

The synthesis of [^{18}F]FDG often uses triflate, a good leaving group, but other leaving groups have been used previously, such as sulfonate ($R–SO_2O^-$) or tosylate ($CH_3C_6H_4SO_2O^-$)[19] The existence of other functional groups can add further complication to the system. To circumvent the issues that arise from the synthesis of organofluorine PET radiotracers, there has been a surge in research

into the development of new methods of late stage radiofluorination of inorganic compounds, an approach which exploits the strong bond between the fluoride and the inorganic acceptor.

1.1.4 [^{18}F]FDOPA

[^{18}F]FDOPA is an amino acid based radiotracer and is frequently used in diagnoses in neuro-oncology and Parkinsonian syndromes.[20, 21] It is synthesised *v*ia an electrophilic radiofluorination mechanism using [^{18}F]F_2, this can be produced by the ^{18}O(p,n)^{18}F nuclear reaction, using $^{18}O_2$ as the target.[22] The maximum radiochemical yield that can be achieved using this method is 50%, since only one fluorine atom in [^{18}F]F_2 is radioactive. Due to the highly reactive nature and low selectivity, it can lead to several by-products. Despite this, [^{18}F]FDOPA can be produced *vi*a regioselective demetallation on aryltrimethyltin, with a radiochemical yield of 25%, its synthesis route is shown in Scheme 4.[23]

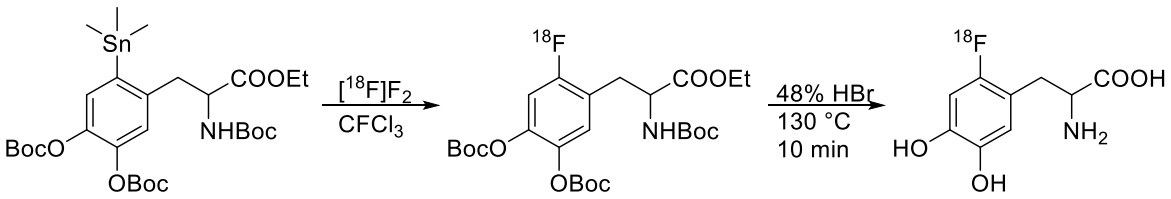

Scheme 4: Radiochemical synthesis of [^{18}F]FDOPA using electrophilic [^{18}F]F_2.[24]

The gaseous [^{18}F]F_2 also presents issues in handling and has resulted in new methods of accessing electrophilic $^{18}F^-$.[21, 23]

1.1.5 Cassette-based radiochemistry

A convenient, reliable, and easy to use method for the delivery of a radiolabelled PET tracer is desirable. Ideally, this would be through a fully automated process that is good manufacturing practice (GMP) compliant. However, adaptation to full optimisation can prove challenging for many tracer syntheses.[25, 26] Details of automation and clinically used synthesis platforms are discussed in Chapter 6.

1.2 Overview of Group 13 and Group 14 M-F coordination chemistry

1.2.1 Group 13

The coordination chemistry of Group 13 halides has been extensively explored with neutral ligands, where the +3 oxidation state dominates, due to the elements having an electronic ground state of $ns^2 3p^1$, however Ga(I) and Al(I) can be accessed under certain conditions.[27, 28]

The small Al(III) centre favours a tetrahedral or octahedral geometry upon coordination, however as you descend the Group 13 elements, the larger Ga(III) and In(III) can form complexes with four to eight ligands.[29, 30]

The literature is dominated by the trivalent halides, the Lewis acidity of which generally falls from the trifluorides being the most Lewis acidic to the triiodides being the least. The anhydrous trifluoride complexes are inert and polymeric (fluoride-bridged) , however their hydrates, $MF_3.3H_2O$ are more reactive, but have poor solubility in commonly used solvents.

1.2.2 Group 14

The Group 14 elements have a ground state electronic configuration of ns^2np^2 and are most commonly found in the +2 or +4 oxidation states, the geometry and coordination chemistry of Group 14 complexes are governed by their oxidation state and the coordination number.[31] Some of the physical properties of these Group 14 elements are shown in Table 2.

Table 2: Select properties of Group 14 elements.[32, 33]

Property	C	Si	Ge	Sn	Pb
Atomic number	6	14	32	50	82
Electronic configuration	$[He]2s^22p^2$	$[Ne]3s^23p^2$	$[Ar]3d^{10}4s^24p^2$	$[Kr]4d^{10}5s^25p^2$	$[Xe]4f^{14}5d^{10}6s^26p^2$
Number of naturally occurring isotopes	2	3	5	10	4
Atomic weight	12.01	28.09	72.61	118.71	207.21
Electronegativity	2.5	1.8	1.8	1.8	1.9

The Group 14 elements are diverse in their classifications and properties; carbon is classed as a non-metal, whilst germanium and silicon are semi-metals and tin and lead are metals. The metals are less electropositive than the s-block metals and are more likely to form covalent bonds.[31] The *s-p* separation increases as the elements in the group get larger and there is a trend towards greater stability in the +2 oxidation state, rather than the +4 state. This is demonstrated by PbF_4 being a highly reactive fluorinating agent, whereas $SnCl_2$ is a widely used reducing agent in acidic

solutions.[34, 35] However, as discussed later on in Chapters 2, 3 and 4, Sn and Ge complexes exist for both oxidation states, with the novel work in this thesis focused on the +4 oxidation state.[32, 36]

The Si-F bond is the strongest amongst the Group 14 halide bonds and generally bond dissociation energies decrease as the group is descended. There is an increase in covalent and van der Waals (vDW) radii of each element as you descend Group 14, except for a small dip for Sn-Pb for the vdW radii.[36]

The reactions of neutral Group 14 tetrahalides with monodentate ligands can typically result in the formation of complexes of the type $[MX_4(L)_2]$, or $[MX_4(L\text{-}L)]$ with bidentate ligands, with the latter only able to form the *cis*-geometry and the former forming both *cis* and *trans* isomers. Examples of these can be seen in Chapter 2 and 3, for both Sn(IV) and Ge(IV) tetrafluoride systems, the majority of which contain both *cis* and *trans* isomers in solution. The displacement or abstraction of one halide, either from the addition of a desirable ligand or *via* the addition of a halide abstractor, can lead to the formation of trihalide complexes with three neutral donor ligands, often forming cationic complexes. These can form two different isomers: *fac* and/or *mer*, many of which are presented in this thesis. Literature examples prior to the work described in this thesis using halide abstractors are discussed further in Chapter 2 and 3.[37]

The first Group 14 cation was reported in 1887, the trityl cation, $[Ph_3C]^+$.[38-40]Analogous cations exist with silicon, silylium cations being widely explored due to their high electrophilicity and strong Lewis acidity, which are used extensively across organic catalytic transformations.[41] However, unlike the carbenium ions, silylium cations are significantly more difficult to stabilise and sterically bulky anions are required in order to truly isolate them, $[Mes_3Si][HCB_{11}Me_5Br_6]$ was the first silylium cation to be isolated in 2002 (Figure 1.3).[42] Analogues for both tin and germanium have also been reported.[43-45]

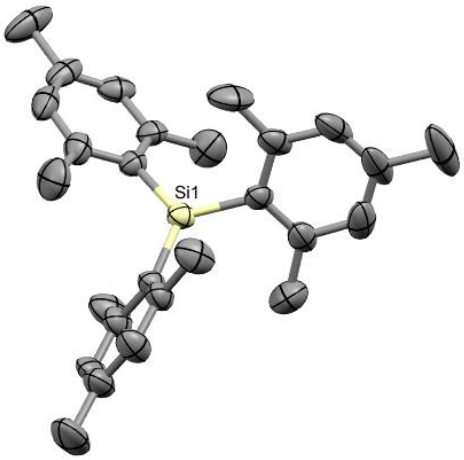

Figure 1.3: Crystal structure of the cation, $[Mes_3Si]$, in the complex $[Mes_3Si][HCB_{11}Me_5Br_6]$. Hydrogen atoms and anion are omitted for clarity.[42]

In the +2 oxidation state, Sn and Ge cations have extensive literature; there are many examples of complexes with N- and O-donor ligands. For example, the reaction of $SnCl_2$ with half an equivalent of the 15-crown-5 ether, forming $[Sn(15\text{-crown-}5)_2][SnCl_3]_2$.[46] Similar complexes also exist for Ge(II) and Pb(II) with crown ether ligands, with the geometry dependent on the ring-size of the crown ether and on which metal it is coordinated to.[47]

1.3 Inorganic-based approaches to radiopharmaceuticals

Nearly all elements can form fluorides, with many also forming oxo-fluorides. The Lewis acidity of the metal fluorides is shown best by their formation of fluoro-anions.[48] When these are not formed, it is often due to the formation of "coordinatively saturated" fluorides, like SF_6. For metal complexes with neutral ligands, such as 1,4,7-triazacyclononane (tacn) derivatives, other influences need to be considered.[48] An important aspect of metal fluoride complexes is the ability of a fluoride to form very strong bridges between metal centres and so there is competition between the coordination of the M-F fragment to a ligand *versus* polymerisation of the binary fluoride.[49] This contrasts with heavier halides, which generally form weaker bridges, and where this competition does not come into play.[48, 50] Some classes of metal fluorides that are of interest are shown below:

- An example of a strongly polymerised metal fluoride that can be converted into a useful molecular synthon is SnF_2 to $[SnF_4(MeCN)_2]$, whereby the acetonitrile ligands are readily substituted and the Sn(IV) centre is easily accessed.[51]

- A metal trifluoride hydrate that can react to form useful coordination complexes. For example, anhydrous GaF_3, which is an inert polymeric solid *versus* $GaF_3.3H_2O$, which is mononuclear and more reactive and therefore opens ups the Ga-F chemistry possibilities towards PET radiotracers.[52]
- Organo-main group species such as [^{18}F]Me_3SiF, which was made in 1985, then opened up Si-F chemistry and the development of silicon based [^{18}F]fluoride complexing agents that have been shown to attach to some biomolecules.[53-56]
- Boron containing fluoride complexes, for example zwitterionic alkylammonium trifluoroborates species have been shown to have high stability both *in vitro* and *in vivo* and can be successfully radiolabelled with [^{18}F]fluoride.[57]
- The formation of transition metal complexes *fac*-[FeF_3(Me_3tacn)] and *fac*-[FeF_3($BnMe_2$tacn)], which has been shown to be ^{18}F-radiolabelled successfully.[50, 58]

Inorganic systems are of interest due to their high bond dissociation energies with fluorine and their ability to be radiolabelled under mild conditions, e.g., aqueous solution, low temperatures and close to physiological pH. These mild conditions also allow for ^{18}F-radiolabelling to occur after bioconjugation, instead of attaching the [^{18}F]fluoride to the organic molecule first before conjugation, this increases efficiency and decreases the number of steps required for the reaction.[50] Potential inorganic [^{18}F]fluoride radiotracers have been investigated, including systems based on Si-F and B-F, and also coordination complexes based around Sb-F, P-F, Ga-F and Al-F systems.[56, 59-61]

The desired properties of a chosen metal chelate complex include:

- Formation of a strong M-F bond
- Stable in water, highly resistant to hydrolysis
- Stable to common ions such as hydroxide, chloride, acetate, carbonate, and phosphate under physiological conditions
- Fast ^{18}F incorporation, preferable from [^{18}F]fluoride in water
- Fixed coordination number and limited redox capability

Developing these inorganic fluoride complexes could allow for ^{18}F radiolabelling under milder conditions, this not only simplifies the clinical synthesis but improves the compatibility with a more diverse range of biomolecules and therefore has a greater effect on the specificity and diagnostic capability of a PET radiotracer.

Table 3 outlines a select number of M-F bond dissociation energies.

Table 3: M-F bond dissociation energies of metal fluorides covered in this work.[62]

Bond	Bond dissociation enthalpy, 298 K, $kJmol^{-1}$
Al-F	664
Ga-F	577
In-F	506
Si-F	540
Ge-F	485
Sn-F	467

Isotopic exchange reactions in ^{18}F PET radiotracers offers an advantageous pathway over alternative methods, due to limiting the potential for by-product formation with minimal crude products present post radiolabelling; the precursor, the radiolabelled product and unreacted [^{18}F]fluoride. The precursor and the radio-product are chemically identical and so the purification steps are simpler than those reactions that have several other by-products that need to be removed (these often require time consuming preparative HPLC procedures). The reaction can often also be performed in one step, in a short amount of time, even as little as 10 minutes.[52, 63]

The co-ligands also play an important role in these properties. The co-ligand must be strongly bound to the metal centre and be retained within the coordination sphere, so that the M-^{18}F fragment remains bound in the body. The ligand must remain bound in variable conditions, not only during radiolabelling, but also over different pH variations and in the presence of common, competitive ions.

Cationic complexes *versus* their neutral counterparts could play a different role in transport, absorption, and release in the body. Their counterions must be tailored so not to interact with the body in a harmful way. For example, for cationic Sn systems, the anion could be $[SnF_6]^{2-}$ which would likely cause the complex to be more insoluble due to the higher charge and could also interfere during ^{18}F radiolabelling. Triflate (OTf^{--}, $CF_3SO_3^-$) offers enhanced solubility, it is only weakly coordinating and is already an anion to some cationic drugs on the market.[64]

1.3.1 Boron

Organotrifluoroborate systems have been studied extensively within Suzuki-Miyaura cross-coupling reactions, due to their stability and resistance against oxidation, forming the highly thermodynamically stable bond B-F (~ 730 kJ mol^{-1}).[62, 65-68] Organotrifluoroborate systems, $[^{18}F]RBF_3^-$, can be synthesised by converting a boronic ester to the trifluoroborate equivalent, or by utilising an isotopic exchange reaction, these often require the use of a Lewis acid promoter, like $SnCl_4$. [53, 69-71] The RBF_3^- anions can hydrolyse and so an aryl group (Figure 1.4) can be utilised to provide structural stability. A zwitterion was also synthesised to test the stability of the trifluoroborate moiety. These systems have been conjugated to biomolecules such as biotin and avidin.[61, 72, 73]

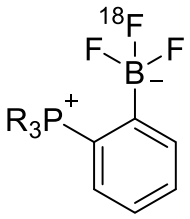

Figure 1.4: Zwitterionic boron compounds tested for radiofluorination and *in vivo* stability by Gabbaï and co-workers. Where R = Ph_2Me, iPr_2Me or $(HO_2C(CH_2)_2)Ph_2$.[61]

Perrin and co-workers developed a radiofluorination protocol for the ^{18}F radiolabelling of an aryltrifluoroborate conjugate, using the fluoride source $[^{18}F]KHF_3$, this is a nucleophilic ^{18}F carrier (Scheme 5).[72] This is a single step route and therefore advantageous when translating such a synthesis to the clinic, it avoids the need for time consuming and complex purification techniques.

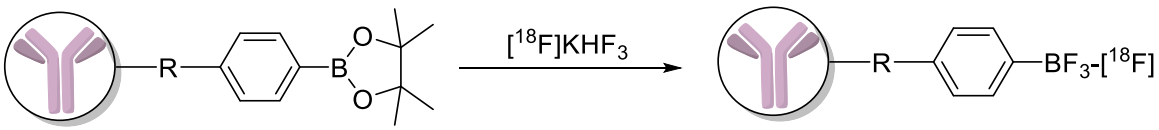

Scheme 5: Perrin and co-workers arylfluoroborate conjugate radiolabelling experiment.[72]

Perrin and co-workers synthesised several phenyl boronic esters to show that they can be used as prosthetic groups for PET imaging.[69, 74, 75] A kit-based method, developed on microgram production level quantities, has also been demonstrated using $[^{18}F]ArBF_3^-$, providing further evidence that B-^{18}F pharmaceuticals could have applications within the clinic and regular PET imaging.[71] However this approach does require purification by HPLC and carbon filtering which is less than ideal when considering its use in the clinic.

The radiofluorination of N-heterocyclic carbene (NHC) boron trifluoride adducts can be conducted by $^{18}F/^{19}F$ isotopic exchange reactions using the Lewis acid promoter $SnCl_4$, the backbone of the NHC can be functionalised with a bioconjugate. Gabbaï and co-workers demonstrated this by the addition of a maleimide functionality, which enables conjugation. They presented an *in vivo* model with the peptide H-Cys-Phe-OH. The reaction for its synthesis is shown in Scheme 6.

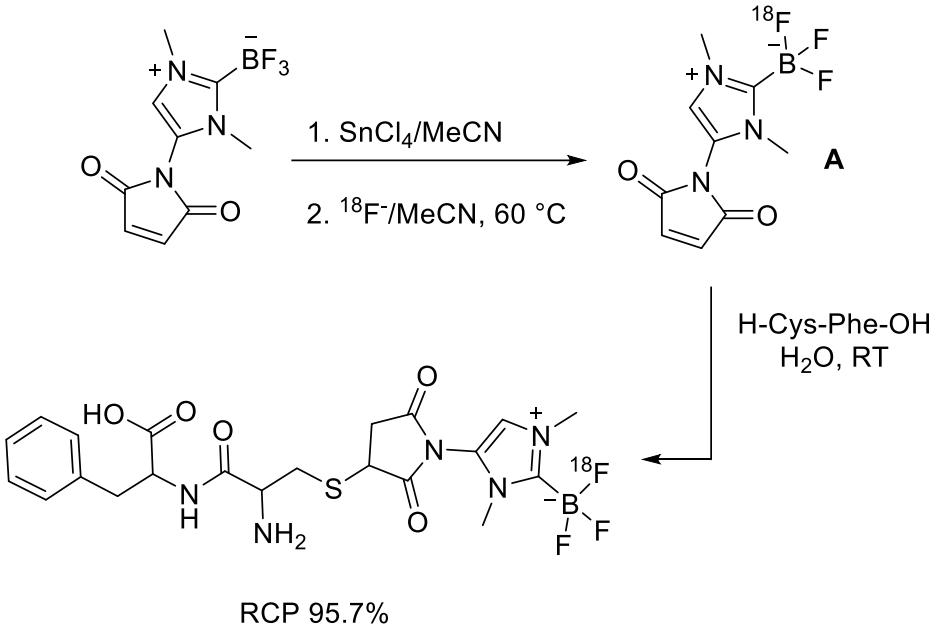

Scheme 6: The synthesis of [^{18}F]**A**-H-Cys-Phe-OH.[76]

[^{18}F]**A**-H-Cys-Phe-OH was shown to have substantial stability in phosphate-buffered saline (PBS), with the RCP remaining greater than 90% after two hours. *In vivo* PET/CT imaging showed important results, with urinary and liver clearance of the tracer after several hours and negligible uptake of [^{18}F]fluoride by the bone after four hours, showing that there is no release of the radiofluorinated carbene.[76]

Gabbaï and co-workers also successfully developed a ^{18}F radiolabelling protocol on an NHC-PF_5 system, an analogue to the NHC-BF_3 chemistry. An imidazolylidene derivative underwent $^{18}F/^{19}F$ isotopic exchange under Lewis acid promotion using $SnCl_4$ with [^{18}F]TBAF in MeCN, giving a RCY of up to 6% (Scheme 7).[77]

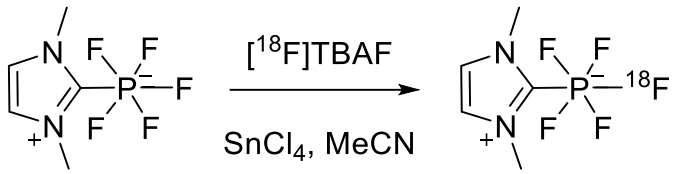

Scheme 7: ^{18}F radiolabelling of NHC-PF_5.[77]

This system was evaluated in female nude mice and using microPET, scans were obtained after three hours post-infection. No bone-uptake was seen, therefore showing that negligible amounts of [^{18}F]fluoride was released over this time period.

1.3.2 Silicon

The Si-F bond is of interest within radiochemistry using ^{18}F due to its high bond dissociation energy of approximately 570 kJ mol^{-1}, *versus* 318 kJ mol^{-1} for C-F.[62] Additionally, silicon has a greater covalent radius when compared to carbon and this provides a greater driving force for nucleophilic substitution at the silicon centre, compared to its carbon analogues. Tetravalent silicon will also react readily with Lewis bases due to its vacant low energy d-orbitals. These all play a part in why [^{18}F]organofluorosilanes are a good choice for the development of PET radiotracers.[78]

The complex [^{18}F]SiF_4 was first identified in 1958, with isotopic exchange reactions producing [^{18}F]Me_3SiF not long after, with the latter being reported as a hypothetical intermediate in the reaction of hexamethylsiloxane with [^{18}F]HF.[79-82] However, it wasn't until the mid-2000s that these systems were shown to have potential applications as PET radiotracers. The SiFA complex shown in Figure 1.5 was successfully radiolabelled under mild conditions at room temperature with ^{18}F/Kryptofix2.2.2./K^+complex in MeCN, with a RCY as high as 97% recorded.

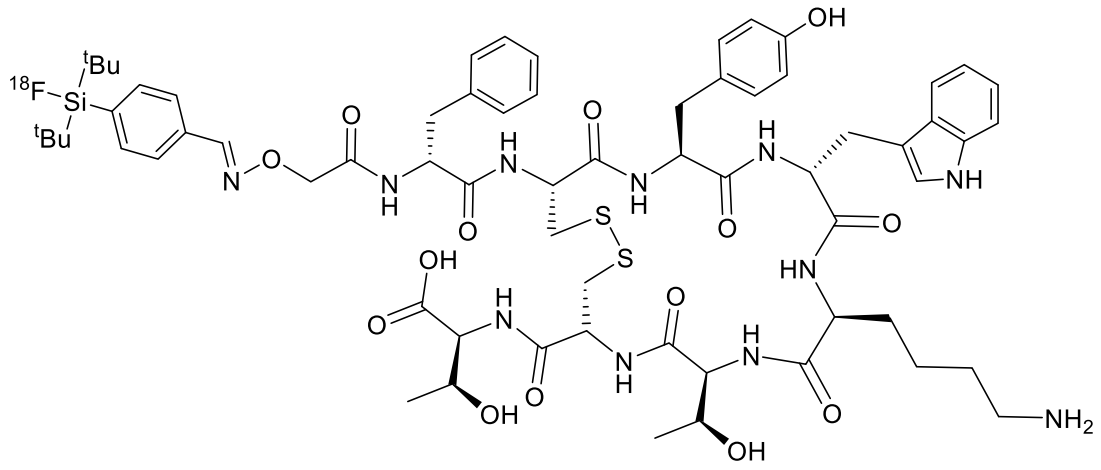

Figure 1.5: SiFA Tyr^3-octreotate system developed by Schirrmacher and co-workers.[56]

Niedermoser and co-workers demonstrated that [^{18}F]SiFA-somatostatin analogues can be radiolabelled in one step, with high RCYs and an RCP of greater than 99% in plasma after two hours. *In vivo* studies were also undertaken using AR42J-bearing nude mice (a pancreatic cancer cell-line), which showed high IC_{50} values and tumour uptake greater than 15%.[83] This overcame the issues that were faced with first-generation SiFA systems, whereby their high lipophilicity

hampered any *in vivo* studies due to almost exclusive hepatobiliary metabolism and near zero target tissue uptake.

A kit formulation on a SiFA system was developed by Wessmann and co-workers in 2012, this reduced the amount of time that would classically be required for the drying step (such as azeotropic drying), therefore providing a better route to ease of automation and production of these ^{18}F-radiopharmaceuticals for clinical use.[84] The technique developed consisted of the elution of dry [^{18}F]fluoride from an anion exchange cartridge, with Kryptofix 2.2.2./K^+ in anhydrous MeCN, which can be performed in 3-5 minutes at room temperature (Scheme 8).

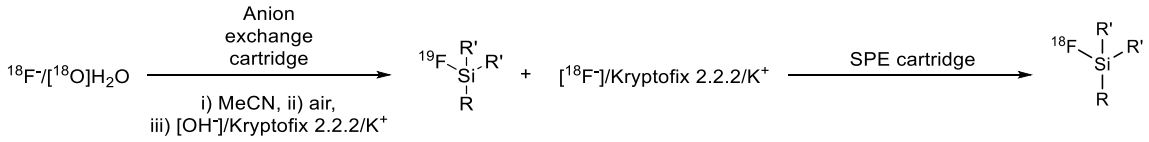

Scheme 8: Scheme for the general method of the kit production procedure developed by Wessmann and co-workers.[84]

Clinical studies in patients with prostate cancer provided promising results for the SiFA candidate, [^{18}F]rhPSMA-7, showing comparable imaging to that of the clinically-utilised [^{68}Ga]Ga-PSMA-11, especially so in patients with low amounts of prostate-specific antigen, therefore providing a greater chance of detecting the cancer at an earlier stage and improving the prognosis for the patient (Figure 1.6).[85, 86]

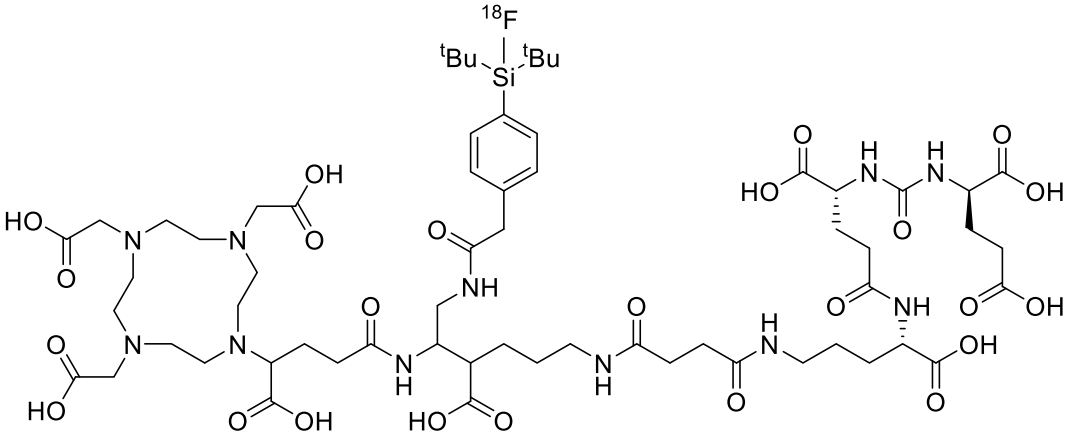

Figure 1.6: The general structure of [^{18}F]rhPSMA-7, synthesised by Wester and co-workers.[86]

However, radiolabelling methods in aqueous conditions have been investigated and hydrolysis of the Si-F bond has proved to be a problem and has presented a challenge to a more widespread use of these systems as potential PET radiotracers.[87]

1.3.3 Aluminium

Aluminium has a high affinity towards fluorine, aluminium trifluoride trihydrate exists in two forms; as a discrete molecule, $[AlF_3(OH_2)_3]$, or in the polymeric β-form, $[\{AlF_2(OH_2)_2(\mu\text{-}F)\}n].nH_2O$.[88] Little of the chemistry of the Group 13 trifluorides had been explored until recently. This may be due to the low reactivity and highly polymerised trifluorides, and poor solubility of the metal fluoride hydrates.[28, 48]

Hydrothermal conditions have been exploited previously to overcome the lack of solubility of $AlF_3.3H_2O$ to prepare complexes with neutral nitrogen donor ligands, such as Me_3tacn, $BnMe_2$tacn, terpy, phen and bipy, the crystal structure of the latter of which is shown in Figure 1.7.

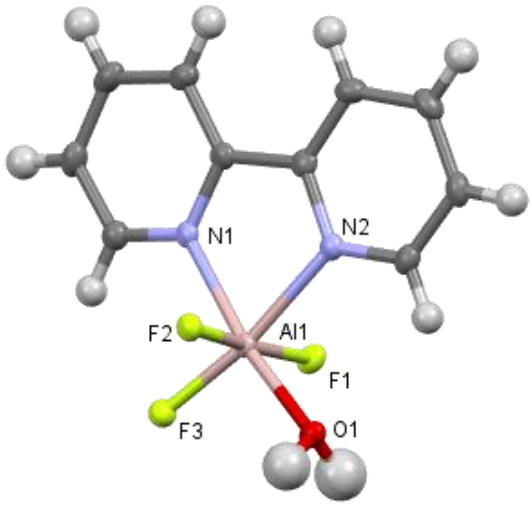

Figure 1.7: Crystal structure of $[AlF_3(OH_2)(bipy)]$. No ellipsoid data available. Two lattice water molecules omitted for clarity. Image redrawn from Reference.[89]

McBride and co-workers have demonstrated that the choice of ligand type enables easier access to ^{18}F compounds based on Al-tacn-derived macrocyclic complexes, an example of which is shown in Figure 1.8.[90] The use of the modified dianionic NOTA derivative was investigated with aluminium trifluoride, which is a strong Lewis acid with limited redox chemistry. The macrocycle binds to 5 of the 6 available coordination sites on the metal.[91] An example of the peptide attached is octreotide, a somatostatin analogue used for targeting prostate cancer.[92]

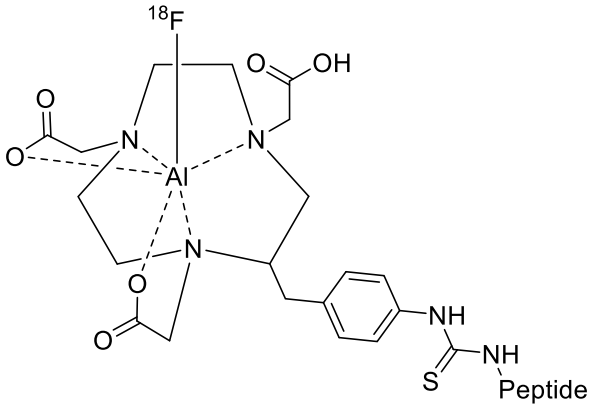

Figure 1.8: Promising AlF-NOTA system demonstrated by McBride and co-workers.[90]

This work exploits the high bond dissociation energy between Al-F and the stability provided by the NOTA macrocycle scaffold. Halide exchange reactions were first used to produce $[^{18}F]AlF^{2+}$, which was then reacted with the NOTA macrocycle in water in a CH_3COONa buffer at ~ pH 4, at a temperature greater than 100 ˚C, *via* a two-step one-pot reaction.[93, 94] This high temperature is a shortcoming, as many biomolecules are sensitive to heat and therefore work on these metal-tacn complexes needs to be focused on near to room temperature reactions in aqueous media. The use of neutral tacn ligands with Group 13 metals (Ga, Al) were further investigated and $[MCl_3(BnMe_2tacn)$ (M = Ga, Al) and $[GaF_3(BnMe_2$-tacn)] were successfully ^{18}F-radiolabelled through Cl/F halide exchange and $^{19}F/^{18}F$ isotopic exchange, respectively.[50, 59]

Research into AlF chemistry has been developing rapidly in recent years and Al-NOTA complexes have been conjugated to several other biomolecules. These include: HER3, a human epidermal growth factor linked to breast, cervical, ovary, lung, head, and neck cancers when overexpressed and serum albumin, a plasma protein that is highly abundant in the blood and can be used to study the movement of radioactivity in the blood (for example to look at cardiac function).[95, 96] The reactions to form both of these conjugated AlF chelate complexes were performed at 100 °C and at pH 4.

Cleeren and co-workers demonstrated two encouraging acyclic chelators conjugated to a urea-based inhibitor of the PSMA antigen for $[^{18}F]AlF$ complexation at a significantly milder temperature of 40 °C, with a good RCY (>90%).[97] The acyclic chelators conjugated to Al-^{18}F are shown in Figure 1.9 as H_1L3 and H_3L3. However, these systems were shown to be poorly stable *in vitro* and they were improved by utilising a cyclohexyl moiety which imparted structural rigidity and stability onto the molecule, (±)-H_3RESCA, this was radiolabelled at room temperature and was shown to be stable in rat plasma after four hours.[98]

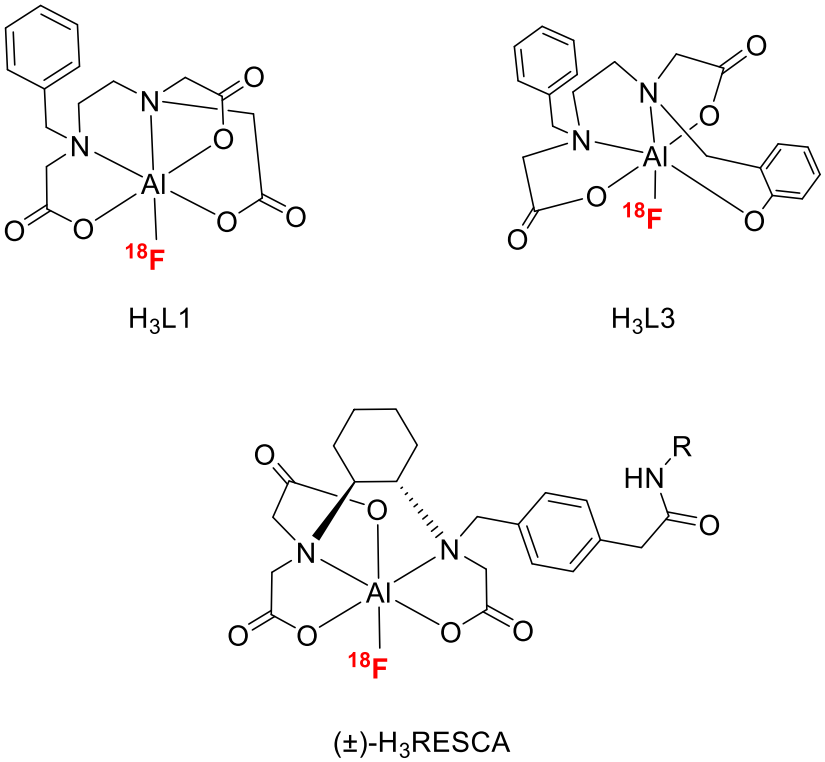

Figure 1.9: The structures of the acycic AlF chelators developed by Cleeran and co-workers.[99]

AlF-(±)-H_3RESCA was conjugated to serum albumin (RCY 52-63%) and an affibody molecule that targets HER2 receptors (RCY 20±7%), demonstrating the utility of this chelator complex.[98]

1.3.4 Gallium

Gallium has radionuclides of significant importance within nuclear medicine. ^{67}Ga, a gamma–emitter with a half-life of 3.26 days, has long been used in nuclear medicine as a therapeutic imaging agent for lymphoma and infections.[100-102] ^{68}Ga, a positron-emitter, has been used extensively within PET imaging, it has a half-life of 68 minutes, which is long enough for quick radiochemistry and for distribution of most small molecules and biomolecules, but short enough to keep the radioactive dose relatively low. It is delivered as $^{68}Ga(NO_3)_3$ in an aqueous solution, and is frequently bound to an aza-macrocyclic ligand, such as DOTA derivatives with peptide conjugates, for example, DOTATATE and DOTATOC, these target somatostatin receptors (Figure 1.10).[103-105]

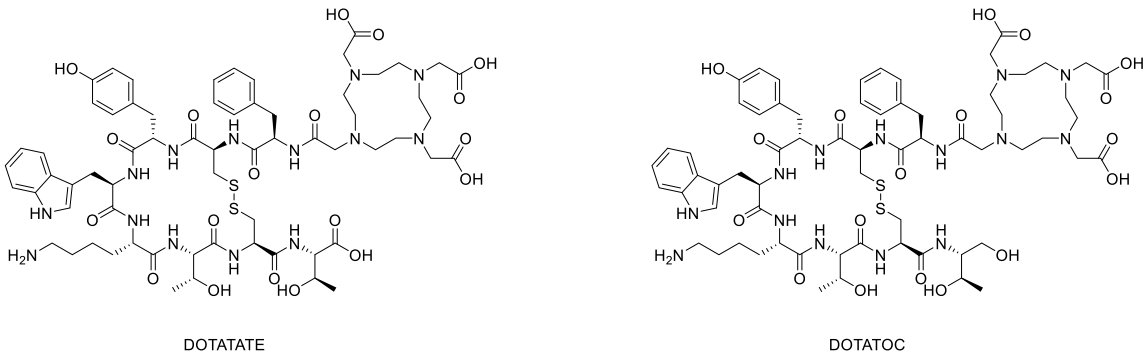

Figure 1.10: The chemical structures of the DOTATATE and DOTATOC macrocyclic ligands used in ^{68}Ga imaging applications.

However, the labelling conditions required for chelation of DOTA derivatives to ^{68}Ga(III) require relatively harsh conditions (30 minutes, 90 °C, low pH) and these conditions will not always be compatible with a biomolecule. Other ligands, such as the TRAP derivatives (Figure 1.11), have been utilised and shown to significantly improve the conditions required for chelation, therefore opening up the scope for this radiochemistry.[106, 107]

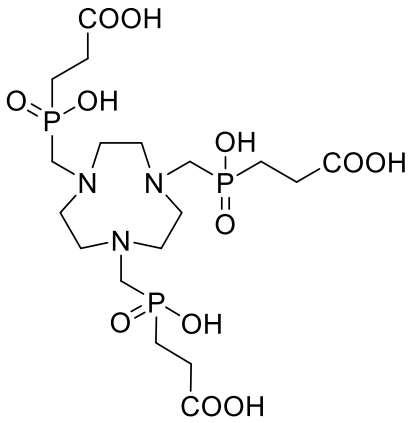

Figure 1.11: Tri-valent TRAP ligand using as chelator towards radioactive ^{68}Ga(III) ions for applications within PET imaging.

These developments also opened up the potential for Ga(III) macrocyclic complexes to be inorganic binding sites for the radionuclide ^{18}F, a contrast to the most common bond in ^{18}F PET imaging, C-^{18}F.

Ga-^{18}F systems reported by the Reid group include the ^{18}F radiolabelling halide exchange reactions on [$GaCl_3$($BnMe_2$tacn)] and [GaCl(Bn($CH_2COO)_2$-tacn)], and also the isotopic exchange reactions on "cold" [GaF_3($BnMe_2$tacn)], as shown in Scheme 9.

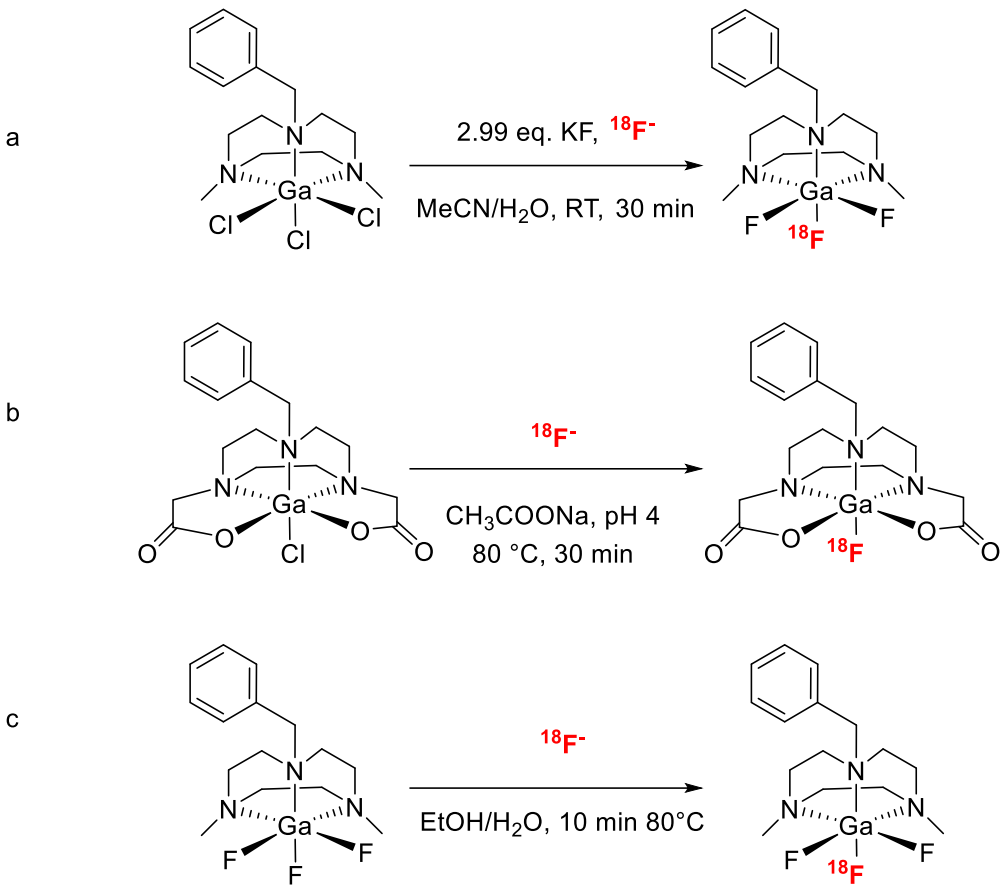

Scheme 9: Schematics for the ^{18}F radiolabelling conditions for a) [$GaCl_3$($BnMe_2$tacn)], b) [GaCl(Bn($CH_2COO)_2$-tacn)] and c) [GaF_3($BnMe_2$tacn)] developed previously by the Reid group.[59, 63, 108]

Successful radiofluorination of the preformed chloride complex, [$GaCl_3$($BnMe_2$tacn)] (a) at a 1 mg (2.36 μM) concentration, was achieved under relatively mild conditions (aqueous MeCN, room temperature, 30 min). The crude RCY was 30%, the radio-product was purified and formulated in a 10% EtOH/PBS (pH = 7.2) solution, the RCP remained greater than 98% over two hours. However, attempts to radiolabel the precursor at lower concentrations (nmol) were unsuccessful, nano-molar scale or less is the required concentration for PET radiotracers of this type in clinical applications.[109]

[GaCl(Bn($CH_2COO)_2$-tacn)] (b) was radiolabelled at a 0.1 mg (268 nM) concentration in the presence of a sodium acetate buffer at pH 4 at 80 °C, for 30 min, the crude RCY was 70%, and the RCP remained >95% at three hours. However, when formulated in a 10% EtOH/PBS (pH = 7.5) solution, the product was highly unstable, with an initial RCP post-purification of 98%, this decreased dramatically to 2% after 90 minutes. Showing that the stability of complex b is highly pH dependant.[108]

Lastly, [GaF_3($BnMe_2$tacn)] (c) was radiolabelled at concentrations as low as 0.01 mg (27 nM), the crude RCY was 37%, the purified radio-product was formulated in a 20% EtOH/PBS solution and the RCP dropped from 99% at t = 0 to 77% at 2 h. Further details on this work is explored in Chapter 5.[63]

1.4 Macrocycles

1.4.1 Trimethyltriazacyclononane: synthesis and coordination chemistry

Me_3tacn was successfully synthesised using a multi-step route and is shown in Figure 1.12. A comprehensive review set out by Chaudhuri and Wieghardt demonstrates the synthesis and methodologies of triazacyclononane derivatives.[110, 111]

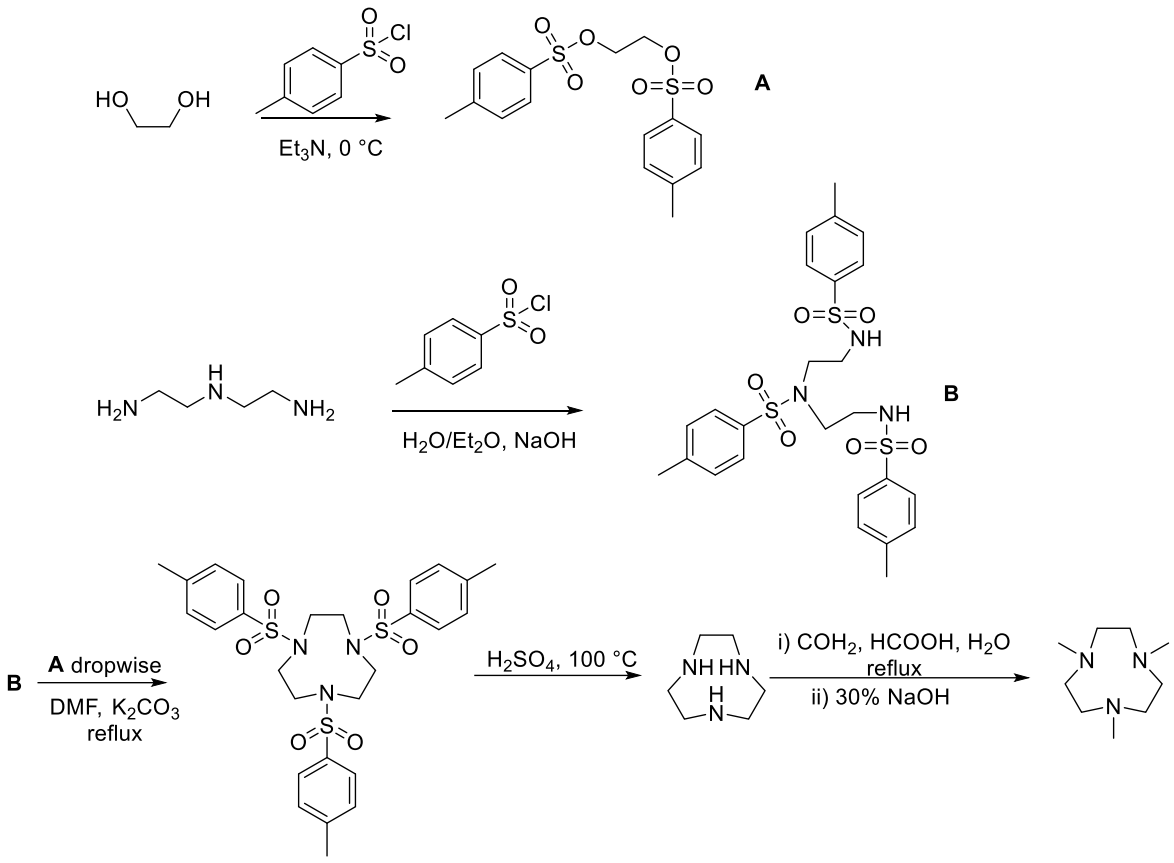

Figure 1.12: Synthesis of Me_3tacn.[112]

The initial reactions involve producing the precursors – a tosyl protected triamine and a tosyl diol. The cyclisation step, addition of **A** to **B**, forms the protected tacn product and can be seen in Figure 1.12, this involves equimolar amounts of the two starting materials. The 48-hour reaction in the presence of K_2CO_3 in DMF, led to the desired cyclic tritosylate product as a white powder.

This was confirmed using NMR spectroscopy and comparison with the literature; ^{1}H NMR ($CDCl_3$, 298 K): δ ppm = 7.20-7.75 (dd, [12H], ArH), 3.35 (s, [12H], tacn-CH_2), 2.40 (s, [9H], Ar-CH_3).[6] The following stages consist of the deprotection of Ts_3-tacn using 97% sulfuric acid and then the *in situ* methylation of the neutralised deprotection mixture with formic acid and formaldehyde, after which the pH is adjusted to 14.[113]

The $BnMe_2$tacn ligand used in radiolabelling experiments is synthesised *via* a different route, and it is outlined in Figure 1.13.

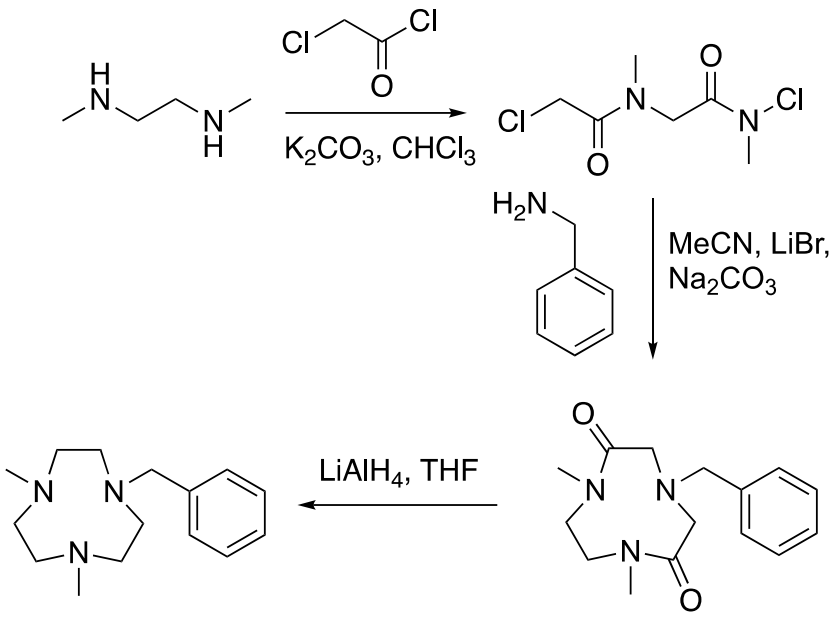

Figure 1.13: Synthesis of $BnMe_2$tacn.[111]

Tacn is a small triaza ring, it stabilises a complex through the macrocyclic effect and blocks one side of the face to substitution, thus allowing the other face to undergo further chemistry. The three nitrogens can be functionalised to provide a range of derivatives which may be tuned for a certain application or property. The strong preference for Me_3tacn in tridentate coordination has been demonstrated previously, including cleavage of a strong Si-F bond from the SiF_4 fragment as shown in the work by Levason and co-workers in the formation of $[SiF_3(Me_3tacn)]^+$ from SiF_4 without the need for a halide abstractor.[114] The complex cation was found to be resistant to hydrolysis in water and unaffected by MeCN, a potential donor solvent; this suggests that this and similar complexes may prove to be promising candidates as PET tracers, as they may stand up to physiological conditions and competitive media.[114]

1.4.2 Macrocyclic effect

Macrocycles are cyclic hydrocarbons, typically with ring sizes of 9 or more and containing donor atoms such as O, N, or S capable of binding to metal ion guests. The cyclic structures are more

restricted and have less rotational and conformational degrees of freedom than their linear analogues, for a macrocycle, which is itself relatively rigid, coordination only leads to a small reduction in its conformational flexibility. For example, the work undertaken by Busch and co-workers on the synthesis of Cu(II) cyclam complexes, which was studied against its acyclic counterpart, N,N'-di(2-aminoethyl)- propylenediamine (ligands shown in Figure 1.14). The macrocyclic complex was shown to be 10,000 times more stable than the non-cyclic complex; this was measured by assessing the stability of the complexes in the presence of acid at variable temperatures. A stability constant measures the of strength the interaction between reagents and the driving force for a complex to form.

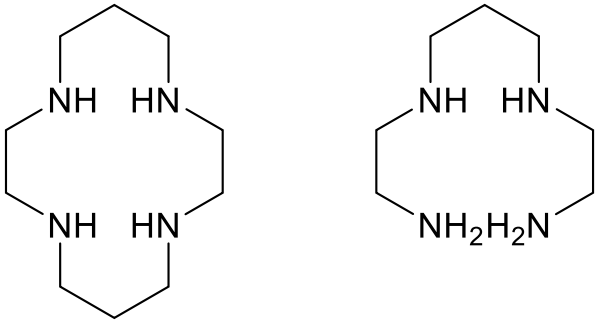

Figure 1.14: Cyclam (left) and acyclic 1, 4, 8, 11-tetraazaundecane[115, 116]

1.5 Radiolabelling and characterisation

Radiochemistry studies the chemistry behind radioactive compounds. The radiolabelling experiments carried out in this work were conducted in St Thomas' Hospital in London in King's College London research laboratories and also at Addenbrooke's Hospital in Cambridge. The hospitals have an on-site cyclotron for the production of target water, [^{18}F]fluoride, this is produced *via* ^{18}O(p, n)^{18}F. Target water is used in a clinical setting for the production of [^{18}F]FDG and for research purposes.

Handling radiation requires strict containment and protection methods. Everyone handling radioactivity must undergo training and wear body and finger dosimeters, these are replaced every other month and record the amount of radioactivity a person has been exposed to. When performing radiolabelling experiments the handling of reagents is carried out in a lead-shielded workstation, and the containers holding the radioactive solutions are further shielded in lead pots.

The amount of radiation that a person is exposed to should be limited as much as possible, with manipulation time kept to a minimum and the distance from the radioactive source being maximised by using tongs.

1.5.1 A typical radiolabelling experiment

In a typical radiolabelling experiment, the precursor is dissolved in a suitable solvent, such as MeCN, EtOH, or buffer solution (sodium acetate at pH 4) and a solution of the target water is added. The radioactivity is measured (MBq) and the reaction mixture is allowed to stir at a suitable temperature, typically 80 °C for the work reported here, for 10 minutes. Once completed, an aliquot of the reaction mixture is diluted with water and injected onto an analytical HPLC system, which is used to analyse the crude product.[52] The HPLC has a UV-Vis and radioactivity detector, this enables the detection of non-radioactive material that contain a chromophore and radioactive species. In the chromatogram there is nearly always a large peak between 2 and 3 minutes that corresponds to unreacted [^{18}F]fluoride and the product peak usually has a longer retention time (Rt), coming between 6-7 minutes. The integration of these two peaks gives the RCY.

If the desired product has been observed in the radio-HPLC, then a purification step is undertaken through solid-phase extraction (SPE). The steps for this are as follows:

1. A solution of the crude product is passed through the cartridge, where it is trapped.
2. The product is washed by passing water through the cartridge to remove any unreacted [^{18}F]fluoride.
3. The product is eluted by passing an organic solvent, typically EtOH, through the cartridge.

Typically, the organic solution was formulated in water or pH 7.4 phosphate-buffered saline (PBS). The purified product was then injected back into the HPLC system to check the RCP of the sample, this is often conducted after different time intervals (t = 0, t = 2-4 h) to gauge the radiostability of the complex over time.

If a product is unstable, several factors could be at play, with it being commonly attributed to radiolysis. Radiolysis is defined as the degradation process of a radiolabelled compound due to free radicals. A radiostabiliser, such sodium ascorbate, can be used to limit radiolysis. It does this by scavenging free radicals and should not interfere with the radiolabelled complex nor be toxic to the body.[117]

It is likely that $^{19}F/^{18}F$ isotopic exchange on the Ga(III) fluoride complex occurs *via* a dissociative mechanism, whereby a five-coordinate intermediate is formed and so it is expected that only one ^{19}F atom will undergo the exchange (Scheme 10).

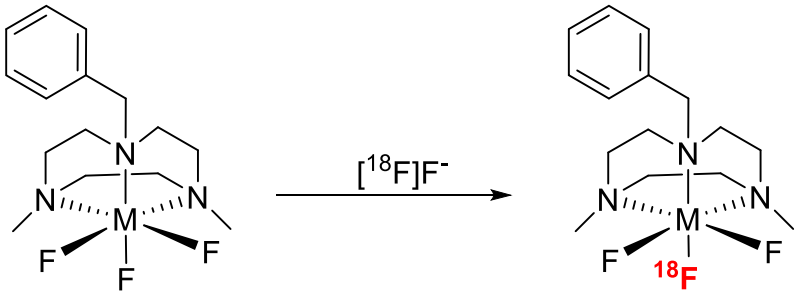

Scheme 10: Generic schematic for the formation of radiolabelled octahedral metal fluoride complex, M= Ga(III), Fe(III) etc

Previous work was done to test the dissociative mechanism hypothesis on $[GaF_3(BnMe_2tacn)]$, whereby a $^{18}F/^{19}F$ isotopic exchange reaction was performed in the presence of dmso. Dmso is highly coordinating and it was thought that it would quench the five-coordinate intermediate species and reduce the expected RCY of the radio-product. The reaction was performed at 80 °C for 10 min and the RCY was 14%, this provided supporting evidence to the dissociative mechanism.

Being able to radiolabel a pre-formed metal chelate complex in the final step of the synthesis, limits the amount of ^{18}F decay and so a smaller amount would be required to undertake the radiolabelling experiment. This offers advantages over McBride and co-workers' system, whereby their Al-^{18}F moiety is formed prior to chelation.[90, 118]

1.5.2 High-performance liquid chromatography (HPLC)

HPLC allows for the identification and purification of compounds from a reaction mixture and is very useful when only small amounts of sample are available; it is widely used in radiochemistry. During this work, analytical HPLC was employed. An experiment involves dissolving a sample in an appropriate solvent, a mobile phase that contains a mixture of solvents and a stationary phase (the column). A pump pushes the sample onto the column, along with the mobile phase and the sample is separated according to the nature of the species within it. The separated fractions are eluted off at different retention times and detected.

A reverse phase HPLC was used, this contained a polar mobile phase and a silica column, whereby hydrophilic species are eluted off the column at a shorter Rt in comparison to compounds that

contain organic moieties, which will elute at longer Rt. Unreacted $[^{18}F]F^-$ will elute much earlier than our desired radiolabelled complexes. A UV-Vis detector adjoined with a radiodetector allows for the identification based on the Rt and quantification of the species based on the integration of the area under the curve.

1.6 Characterisation and Analytical Techniques

Several techniques have been used to characterise and analyse the compounds synthesised in the work presented in this thesis.

1.6.1 Infrared Spectroscopy (IR)

IR spectra were obtained as Nujol mulls between CsI plates It can show whether water is present in a sample and if solvents or other ligands are present. In addition to the fingerprint bands associated with organics and ligands, in the present study IR spectroscopy was used to determine the presence of M-X stretching vibrations and hence to probe the molecular symmetry and halide type present. When a sample is irradiated with a certain energy that corresponds to vibrational transitions within the molecule, the radiation is absorbed. The subsequent subtraction of these absorbed energies from a pre-recorded background gives a spectrum.

For certain species, Group Theory can be used to determine the number of vibrational bands present in a molecule and its molecular symmetry. For example, the number of M-F stretching frequencies present in an IR spectrum for an octahedral complex of the type $[MX_3(L)_3]$ can help determine if the complex is the *meridional* or *facial* isomer, or for those of the type $[MX_4(L)_2]$, where the number of M-F stretches can be used to determine if the complex is the *cis* or *trans* isomer. However, it does not consider intermolecular interactions which can cause broadening of peaks and may mask some of the M-X peaks resulting in fewer peaks being observed than expected.

Table 4: M-X stretching modes for $[MX_3(L)_3]$ and $[MX_4(L)_2]$ complexes relevant to the present study.

	Symmetry point group	ν(M-X)*
fac-$[MX_3(L)_3]$	C_{3v}	$A_1 + E$
mer-$[MX_3(L)_3]$	C_{2v}	$2A_1 + B_1$
cis-$[MX_4(L)_2]$	C_{2v}	$2A_1 + B_1 + B_2$
trans-$[MX_4(L)_2]$	D_{4h}	E_u

Table 4 shows that for octahedral complexes of the type *fac*-$[MX_3(L)_3]$ and *mer*-$[MX_3(L)_3]$, with C_{3v} and C_{2v} symmetry, there should be two and three ν(M-X) IR active bands, respectively. However, for *cis*-$[MX_4(L)_2]$ with C_{2v} symmetry, there should be four ν(M-X) IR active bands and for *trans*-$[MX_4(L)_2]$, with D_{4h} symmetry, there should be only one band.

1.6.2 NMR Spectroscopy

The main technique for analysis of solution state behaviour of the complexes synthesised and demonstrated in this thesis is NMR spectroscopy. NMR is a method that exploits the magnetic properties of atomic nuclei. The nuclear spins of each element resonate at distinctive frequencies and detailed information such as chemical environment and structure of the molecules that contain the NMR active nuclei can be determined from a spectrum.[119] The ligand present, coordination number, oxidation state, geometry and NMR solvent all have significant effects on the chemical shifts and gives information on the coordination environment around a metal centre.

Table 5: Selected properties of NMR active isotopes relevant to the present study.[119]

Isotope	Spin	Natural Abundance (%)	Resonance Frequency (MHz)	Quadrupole Moment (10^{-28} m^2.A)
^{27}Al	5/2	100	52.1418	0.15
^{19}F	1/2	100	188.2543	0
^{69}Ga	3/2	60.4	48.034	0.19
^{71}Ga	3/2	39.6	61.0248	0.12
^{1}H	1/2	100	200.10673	0
^{117}Sn	1/2	7.6	71.2896	0
^{119}Sn	1/2	8.6	74.58430	0

Nuclei have nuclear angular momentum; this has an associated magnetic field which is comparable to the generated magnetic field. The nuclear spin tries to align with the applied magnetic field. An electric field gradient (efg) at the nucleus is present in a molecule due to the asymmetry of local charge distribution caused by electrons and other nuclei close by and a compound must be diamagnetic for conventional NMR spectroscopy. Those nuclei with I = ½ have long lifetimes and so relaxation is slow and NMR peaks are sharp and there are only small amounts of Heisenberg broadening. However, for quadrupolar nuclei with spin > ½, such as ^{69}Ga and ^{27}Al, the nuclei are constantly trying to orientate to the lowest possible energy level. In other than highly symmetrical geometries (O_h, T_d, *etc*), this considerably shortens the lifetime of the excited state and results in broader lines in an NMR spectrum, or complete loss of the signal. However, when nuclei are in a relatively highly symmetrical environment, such as in C_{3v} symmetry, where the electric field gradient may be very close to zero, only slight broadening may be observed and it may be possible to observe the couplings.[52] In contrast, if an environment is highly unsymmetrical then a spectrum may not be observed at all.

1.6.2.1 Fluorine NMR spectroscopy

^{19}F NMR spectroscopy has been used extensively in these studies, ^{19}F (I = ½, 100% abundance) is a sensitive technique with a wide chemical shift range and can provide useful information on diamagnetic complexes. The other halogens only have quadrupolar nuclei which are not observable in low symmetry environments of complexes containing halide ligands. The technique often has to be performed at low temperature due to dynamic processes, e.g., labile co-ligands

that undergo reversible dissociation at room temperature. ^{19}F NMR spectroscopy is also useful in detecting impurities formed in fluorination reactions or decomposition products formed during stability studies with competitive ions.

1.6.2.2 Tin NMR spectroscopy

There are three NMR active isotopes of tin: ^{115}Sn, ^{117}Sn and ^{119}Sn. The ^{119}Sn isotope has the greatest abundance and receptivity and is therefore the isotope of choice in NMR studies. It has a large negative gyromagnetic ratio and therefore the NMR resonances from proton decoupled spectra are greatly affected by a reduction in signal intensity due to the nuclear Overhauser effect (NOE).[120] The addition of an inert (unreactive) relaxation agent, such as $[Cr(acac)_3]$, helps to supress the NOE by introduction of another relaxation mechanism which helps in reducing the overall relaxation times and enhances the signal intensities.

^{119}Sn NMR chemical shifts are affected by:

- Electronegativity
- Ligand donor type
- Oxidation state
- Geometry
- Coordination number

The chemical shift range, relative to tetramethyltin (δ = 0 ppm), is usually between 700 and -1900 ppm. In NMR spectra of nuclei bound directly to tin, and often present in $^{19}F\{^1H\}$ NMR spectra in this work, tin satellite couplings can be observed to both ^{119}Sn and ^{117}Sn, resulting in low intensity doublets symmetrically disposed around the main ^{19}F resonance when the satellites are fully resolved.

1.6.3 Elemental Analysis

Elemental analysis is used to determine the quantity of a certain element present in a bulk compound. In this report, C, H, and N analysis have been performed offsite at MEDAC Ltd or the Elemental Analysis Service at London Metropolitan University, through combustion analysis. The sample is burned completely in an oxygen-rich atmosphere and the CO_2, H_2O and N_2 produced are measured by GC and used to calculate the percentages of C, H and N present, with accuracy within +/- 0.4%. It is used to confirm the purity of the bulk sample and whether the sample is free of solvents or to what degree of lattice solvation is present (in tandem with NMR data).

1.6.4 Electrospray ionisation mass spectrometry

Mass spectrometry (MS) can provide both quantitative and qualitative information. The sample is first introduced to an ionisation source in the mass spectrometer, where molecules are converted to ions, which could be positively or negatively charged. The ions will then move through a path, the mass analyser, and arrive at different sections depending on its mass-to-charge (*m/z*) ratio. Once the ions reach the detector, signals are recorded and displayed as a mass spectrum, showing their relative abundancies, isotope pattern and *m/z* ratios.

Electrospray ionisation (ESI) is used in the analysis of large molecules, inorganic complexes, salts, and peptides, as well as for a range of other compounds where volatility is low. The compound is dissolved fully in an appropriate solvent, which carries the low volatile compounds into the vapour as an aerosol. It uses electrical energy to transfer ions from solution into the gaseous phase and ionic species can therefore be analysed by ESI-MS. ESI-MS often allows the whole molecular ion to be observed due to only small amount of fragmentation and can be used to detect both cations and anions.

The metals used in this work and their natural abundances give characteristic distribution of peaks in the mass spectrum, with relative intensities and therefore can be easily identified and isotope patterns are readily simulated for comparison.

1.6.5 Single crystal X-ray diffraction

Single crystal X-ray diffraction allows for the clear determination of the structure of a compound that is formed as a single crystal. This powerful technique depends on the ability to grow suitable single crystals; these can be attained *via* different methods, such as vapour diffusion of different solvents, solvent evaporation, or slow cooling. With conditions such as temperature and pressure being altered depending on requirement. A crystal can be regarded as repeating units of the same structure, this structure can be for atoms, ions, or molecules. The crystal system can be classified depending on the geometry of its unit cell.[121] The unit cell is an imaginary parallelopiped and is made up of parameters in three dimensions; three sides (*a, b, c*) and three angles (α, β, γ).

Table 6: Crystal systems.[122]

System	Unit cell parameters
Triclinic	$a \neq b \neq c$, $\alpha \neq \beta \neq \gamma \neq 90$ °
Monoclinic	$a \neq b \neq c$, $\alpha = \gamma = 90$ °, $B \neq 90$ °

Orthorhombic	a ≠ b ≠c, $\alpha = \beta = \gamma = 90$ °
Rhombohedral	a = b = c, $\alpha = \beta = \gamma \neq 90$ °
Tetragonal	a = b ≠ c, $\alpha = \beta = \gamma = 90$ °
Hexagonal	a = b ≠ c, $\alpha = \beta = 90$ °C, $\gamma \neq 120$ °
Cubic	a = b = c, $\alpha = \beta = \gamma = 90$ °

In a single crystal X-ray experiment, images are produced in each position in which the X-rays hit the crystal and the beam is diffracted by electrons associated with the different atoms. Each image shows spots of different intensities and these represent a set of parallel planes in the crystal. When Bragg's law is satisfied, a spot is observed by the detector (Equation 1).

The asymmetric unit of a crystal contains the structural and symmetry information of the unit cell and can consist of a whole or part of a molecule. The unit cell can be determined by applying symmetry operations onto the asymmetric unit and the space group can be discovered.

Equation 1: Bragg equation.

$$\lambda = 2d_{hkl}sin\theta$$

Where λ = wavelength of X-ray beam; d= distance between planes, *hkl* = integers which define the orientation within the unit cell and θ = angle between the plane and incoming/outgoing beam. The conditions to satisfy Bragg's law can only be satisfied by a few reflections in a randomly orientated crystal, this is why rotations of a single crystal is required to obtain all reflections that appear as a spot on the detector.

Crystals are mounted onto a support and the information is acquired at 100 K, to decrease the thermal motion of atoms in the crystal.

This technique is highly valuable due to the depth of information it can provide such as the positions and types of atoms, bond lengths, bond angles and the intra- and inter-molecular bonding interactions.

1.7 Project Aims

The overarching aim of this project was to develop new inorganic-fluoride complexes with macrocyclic co-ligands as potential carriers for ^{18}F towards the development of new PET imaging agents.

The objectives of this thesis can be described by the following:

- To develop a series of Group 14 metal fluoride coordination complexes with neutral O- and N-donor ligands and explore the use of TMSOTf as a halide abstractor. The work here is to broaden knowledge of the preparations and properties of new Group 14 fluoride complexes, in particular comparing neutral *versus* cationic complexes.
- To advance the research and develop the coordination chemistry of cationic Group 14 metal fluorides with aza-macrocyclic ligands and establish whether these systems are promising for potential applications in PET imaging.
- To further investigate the radiochemistry of the Group 13 metal fluoride complex, $[GaF_3(BnMe_2tacn)]$, and develop new methods for its synthesis, avoiding strongly coordinating solvents, especially dmso, and other anions which could interfere with radiolabelling experiments. Previous work has shown that $[GaCl_3(BnMe_2tacn)]$ can be successfully radiofluorinated at μM concentrations via Cl/F exchange affording excellent radiochemical stability, however the stability of the same $[Ga^{18}F^{19}F_2(BnMe_2tacn)]$ complex produced from the trifluoride *via* $^{19}F/^{18}F$ isotopic exchange was rather lower (88-77% after 2 h when formulated in EtOH). This was unexpected and there is a need to better understand the factors that affect the ^{18}F radiolabelling experiments and the radiochemical stability of these systems. The synthesis and subsequent $^{19}F/^{18}F$ radiolabelling experiments (Chapter 5) will provide insights into these queries.[63]
- To develop and optimise a protocol for radiolabelling $[FeF_3(BnMe_2tacn)]$ using GE HealthCare's FASTlab synthesis module and assessment of whether this complex can be successfully radiolabelled using high activity (approx. 30 GBq) and the identification of suitable radiostabilisers, where applicable.

1.8 References

1. Wrenn, F. R.; Good, M. L.; Handler, P., *Science* **1951,** *113*, 525-527.

2. Pelizzari, C. A.; Chen, G. T. Y.; Spelbring, D. R.; Weichselbaum, R. R.; Chen, C.-T., *Journal of Computer Assisted Tomography* **1989,** *13*.

3. Woods, R. P.; Mazziotta, J. C.; Cherry, R.; Simon, *Journal of Computer Assisted Tomography* **1993,** *17*.

4. Cole, E. L.; Stewart, M. N.; Littich, R.; Hoareau, R.; Scott, P. J. H., *Current topics in medicinal chemistry* **2014,** *14*, 875-900.

5. Cherry, S. R.; Dahlbom, M., Cherry, S. R.; Dahlbom, M.; Phelps, M. E., PET: Physics, Instrumentation, and Scanners. In *PET: Physics, Instrumentation, and Scanners*, Eds. Springer New York: New York, NY, 2006; pp 1-117.

6. Yu, S., *Biomedical Imaging and Intervention Journal* **2006,** *2*, e57.

7. Benning, M.; Kosters, T.; Wubbeling, F.; Schafers, K.; Burger, M. 2008 IEEE Nuclear Science Symposium Conference Record, 19-25 Oct. 2008; 2008; pp 4472-4477.

8. Ametamey, S. M.; Honer, M.; Schubiger, P. A., *Chemical Reviews* **2008,** *108*, 1501-1516.

9. Miller, P. W.; Long, N. J.; Vilar, R.; Gee, A. D., *Angewandte Chemie International Edition* **2008,** *47*, 8998-9033.

10. Pery, C.; Meurette, G.; Ansquer, C.; Frampas, E.; Regenet, N., *Gastroenterology in Clinical Biology* **2010,** *34*, 465-74.

11. Zhan, C.-G.; Dixon, D. A., *The Journal of Physical Chemistry A* **2004,** *108*, 2020-2029.

12. Dundar, A.; Bold, M. S.; Agac, B.; Kendi, A. T.; Friedman, S. N., *Radiology Case Reports* **2019,** *14*, 1447-1451.

13. Reivich, M.; Kuhl, D.; Wolf, A.; Greenberg, J.; Phelps, M.; Ido, T.; Casella, V.; Fowler, J.; Hoffman, E.; Alavi, A.; Som, P.; Sokoloff, L., *Circulation Research* **1979,** *44*, 127-37.

14. Lind, P.; Igerc, I.; Beyer, T.; Reinprecht, P.; Hausegger, K., *European Journal of Nuclear Medicine and Molecular Imaging* **2004,** *31*, S125-S134.

15. Lubezky, N.; Metser, U.; Geva, R.; Nakache, R.; Shmueli, E.; Klausner, J. M.; Even-Sapir, E.; Figer, A.; Ben-Haim, M., *Journal of Gastrointestinal Surgery* **2007,** *11*, 472-478.

16. Liu, S.; Chang, J.; Ng, S.; Chan, S.; Yen, T., *The British Journal of Radiology* **2004,** *77*, 257-260.

17. Tu, Z.; Xu, J.; Jones, L. A.; Li, S.; Dumstorff, C.; Vangveravong, S.; Chen, D. L.; Wheeler, K. T.; Welch, M. J.; Mach, R. H., *Journal of Medicinal Chemistry* **2007,** *50*, 3194-3204.

18. Smith, G. E.; Sladen, H. L.; Biagini, S. C. G.; Blower, P. J., *Dalton Transactions* **2011,** *40*, 6196.

19. Brown, L. J.; Ma, N.; Bouvet, D. R.; Champion, S.; Gibson, A. M.; Hu, Y.; Jackson, A.; Khan, I.; Millot, N.; Topley, A. C.; Wadsworth, H.; Wynn, D.; Brown, R. C. D., *Organic & Biomolecular Chemistry* **2009,** *7*, 564-575.

20. Darcourt, J.; Schiazza, A.; Sapin, N.; Dufour, M.; Ouvrier, M. J.; Benisvy, D.; Fontana, X.; Koulibaly, P. M., *The Quarterly Journal of Nuclear Medicine and Molecular Imaging* **2014,** *58*, 355-65.

21. Chen, W.; Silverman, D. H.; Delaloye, S.; Czernin, J.; Kamdar, N.; Pope, W.; Satyamurthy, N.; Schiepers, C.; Cloughesy, T., *Journal of Nuclear Medicine* **2006,** *47*, 904-11.

22. Bishop, A.; Satyamurthy, N.; Bida, G.; Hendry, G.; Phelps, M.; Barrio, J. R., *Nuclear Medicine in Biology* **1996,** *23*, 189-99.

23. Namavari, M.; Bishop, A.; Satyamurthy, N.; Bida, G.; Barrio, J. R., *International Journal of Radiation Applications and Instrumentation* **1992,** *43*, 989-96.

24. Oldendorf, W., *American Journal of Physiology-Legacy Content* **1973,** *224*, 967-969.

25. Mach, R. H.; Schwarz, S. W., *PET Clinics* **2010,** *5*, 131-153.

26. Li, S.; Schmitz, A.; Lee, H.; Mach, R. H., *EJNMMI Radiopharmacy and Chemistry* **2016,** *1*, 15.

27. McCleverty, J. A.; Meyer, T. J., *Comprehensive Coordination Chemistry II*, 2004; p 1-7861.

28. Downs, A. J., *Chemistry of aluminium, gallium, indium, and thallium*, New York, 1993.

29. Hsieh, W.-Y.; Liu, S., *Inorganic Chemistry* **2004,** *43*, 6006-6014.

30. Shannon, R. D., *Acta Crystallographica Section A* **1976,** *32*, 751-767.

31. Fulton, J. R., Constable, E. C.; Parkin, G.; Que Jr, L., 3.10 - Germanium, Tin and Lead. In *Comprehensive Coordination Chemistry III*, Eds. Elsevier: Oxford, 2021; pp 281-320.

32. Mantina, M.; Chamberlin, A. C.; Valero, R.; Cramer, C. J.; Truhlar, D. G., *The Journal of Physical Chemistry A* **2009,** *113*, 5806-5812.

33. Greenwood, N. N.; Earnshaw, A., *Chemistry of the Elements*, 2nd Edition, Eds. Butterworth-Heinemann: Oxford, 1997; pp 367-405.

34. Bissell, E. R.; Fields, D. B., *The Journal of Organic Chemistry* **1964,** *29*, 1591-1593.

35. Teruaki, M.; Koji, T.; Takeshi, O., *Chemistry Letters* **1985,** *14*, 1359-1362.

36. Cordero, B.; Gómez, V.; Platero-Prats, A. E.; Revés, M.; Echeverría, J.; Cremades, E.; Barragán, F.; Alvarez, S., *Dalton Transactions* **2008**, 2832-2838.

37. Woodward, M. S.; King, R. P.; Bannister, R. D.; Grigg, J.; McRobbie, G.; Levason, W.; Reid, G., *Inorganics* **2022,** *10*, 107.

38. Baeyer, A.; Villiger, V., *Berichte der deutschen chemischen Gesellschaft* **1902,** *35*, 1189-1201.

39. Henderson, G. G., *Journal of the Chemical Society, Transactions* **1887,** *51*, 224-228.

40. Gomes de Mesquita, A. H.; MacGillavry, C. H.; Eriks, K., *Acta Crystallographica* **1965,** *18*, 437-443.

41. Lee, V. Y.; Sekiguchi, A., Lee, V. Y., Chapter 5 - Silicon-Centered Cations. In *Organosilicon Compounds,* Ed. Academic Press: 2017; pp 197-230.

42. Kim, K. C.; Reed, C. A.; Elliott, D. W.; Mueller, L. J.; Tham, F.; Lin, L.; Lambert, J. B., *Science* **2002,** *297*, 825-7.

43. Lambert, J. B.; Lin, L.; Keinan, S.; Müller, T., *Journal of the American Chemical Society* **2003,** *125*, 6022-6023.

44. Zharov, I.; Weng, T.-C.; Orendt, A. M.; Barich, D. H.; Penner-Hahn, J.; Grant, D. M.; Havlas, Z.; Michl, J., *Journal of the American Chemical Society* **2004,** *126*, 12033-12046.

45. Sekiguchi, A.; Fukawa, T.; Lee, V. Y.; Nakamoto, M., *Journal of the American Chemical Society* **2003,** *125*, 9250-9251.

46. Hough, E.; Nicholson, D. G.; Vasudevan, A. K., *Dalton Transactions* **1989**, 2155-2159.

47. Swidan, A. a.; Macdonald, C. L. B., *Chemical Society Reviews* **2016,** *45*, 3883-3915.

48. Benjamin, S. L.; Levason, W.; Reid, G., *Chemical Society Reviews* **2013,** *42*, 1460-1499.

49. Leblanc, M.; Maisonneuve, V.; Tressaud, A., *Chemical Reviews* **2015,** *115*, 1191-1254.

50. Levason, W.; Monzittu, F. M.; Reid, G., *Coordination Chemistry Reviews* **2019,** *391*, 90-130.

51. D. Tudela, F. P., Wiley, *Inorganic Syntheses*, 1997; Vol. 31.

52. Monzittu, F.Main group and transiton metal-based chelates for PET applications. PhD Thesis. University of Southampton, Southampton, 2018.

53. Chansaenpak, K.; Vabre, B.; Gabbaï, F. P., *Chemical Society Reviews* **2016,** *45*, 954-971.

54. Liang, Q.; Satyamurthy, N.; Barrio, J. R.; Toyokuni, T.; Phelps, M. P.; Gambhir, S. S.; Herschman, H. R., *Gene Therapy* **2001,** *8*, 1490-8.

55. Gambhir, S. S.; Barrio, J. R.; Herschman, H. R.; Phelps, M. E., *Nuclear Medicine and Biology* **1999,** *26*, 481-490.

56. Schirrmacher, R.; Bradtmöller, G.; Schirrmacher, E.; Thews, O.; Tillmanns, J.; Siessmeier, T.; Buchholz, H. G.; Bartenstein, P.; Wängler, B.; Niemeyer, C. M.; Jurkschat, K., *Angewandte Chemie International Edition* **2006,** *45*, 6047-6050.

57. Liu, Z.; Pourghiasian, M.; Radtke, M. A.; Lau, J.; Pan, J.; Dias, G. M.; Yapp, D.; Lin, K. S.; Bénard, F.; Perrin, D. M., *Angew Chem Int Ed Engl* **2014,** *53*, 11876-80.

58. Blower, P. J.; Levason, W.; Luthra, S. K.; McRobbie, G.; Monzittu, F. M.; Mules, T. O.; Reid, G.; Subhan, M. N., *Dalton Transactions* **2019,** *48*, 6767-6776.

59. Bhalla, R.; Darby, C.; Levason, W.; Luthra, S. K.; McRobbie, G.; Reid, G.; Sanderson, G.; Zhang, W., *Chemical Science* **2014,** *5*, 381-391.

60. Ting, R.; Aguilera, T. A.; Crisp, J. L.; Hall, D. J.; Eckelman, W. C.; Vera, D. R.; Tsien, R. Y., *Bioconjugate Chemistry* **2010,** *21*, 1811-1819.

61. Li, Z.; Chansaenpak, K.; Liu, S.; Wade, C. R.; Conti, P. S.; Gabbaï, F. P., *Medicinal Chemistry Communications* **2012,** *3*, 1305-1308.

62. Dean, J. A., *Lange's Handbook Of Chemistry*, Eleventh Edition ed.; McGraw Hill, New York, 1973; Vol. 13, p 12A-12A.

63. Monzittu, F. M.; Khan, I.; Levason, W.; Luthra, S. K.; McRobbie, G.; Reid, G., *Angewandte Chemie International Edition* **2018,** *57*, 6658-6661.

64. Reiß, M.; Brietzke, A.; Eickner, T.; Stein, F.; Villinger, A.; Vogel, C.; Kragl, U.; Jopp, S., *RSC Advances* **2020,** *10*, 14299-14304.

65. Molander, G. A.; Ellis, N., *Accounts of Chemical Research* **2007,** *40*, 275-286.

66. Quach, T. D.; Batey, R. A., *Organic Letters* **2003,** *5*, 4397-4400.

67. Vedejs, E.; Chapman, R. W.; Fields, S. C.; Lin, S.; Schrimpf, M. R., *The Journal of Organic Chemistry* **1995,** *60*, 3020-3027.

68. Molander, G. A.; Bernardi, C. R., *The Journal of Organic Chemistry* **2002,** *67*, 8424-8429.

69. Ting, R.; Harwig, C.; auf dem Keller, U.; McCormick, S.; Austin, P.; Overall, C. M.; Adam, M. J.; Ruth, T. J.; Perrin, D. M., *Journal of the American Chemical Society* **2008,** *130*, 12045-12055.

70. Liu, Z.; Li, Y.; Lozada, J.; Schaffer, P.; Adam, M. J.; Ruth, T. J.; Perrin, D. M., *Angewandte Chemie International Edition* **2013,** *52*, 2303-2307.

71. Liu, Z.; Li, Y.; Lozada, J.; Wong, M. Q.; Greene, J.; Lin, K.-S.; Yapp, D.; Perrin, D. M., *Nuclear Medicine and Biology* **2013,** *40*, 841-849.

72. Ting, R.; Adam, M. J.; Ruth, T. J.; Perrin, D. M., *Journal of the American Chemical Society* **2005,** *127*, 13094-13095.

73. auf dem Keller, U.; Bellac, C. L.; Li, Y.; Lou, Y.; Lange, P. F.; Ting, R.; Harwig, C.; Kappelhoff, R.; Dedhar, S.; Adam, M. J.; Ruth, T. J.; Bénard, F.; Perrin, D. M.; Overall, C. M., *Cancer Research* **2010,** *70*, 7562-9.

74. Harwig, C. W.; Ting, R.; Adam, M. J.; Ruth, T. J.; Perrin, D. M., *Tetrahedron Letters* **2008,** *49*, 3152-3156.

75. Ting, R.; Lo, J.; Adam, M. J.; Ruth, T. J.; Perrin, D. M., *Journal of Fluorine Chemistry* **2008,** *129*, 349-358.

76. Chansaenpak, K.; Wang, M.; Wu, Z.; Zaman, R.; Li, Z.; Gabbaï, F. P., *Chemical Communications* **2015,** *51*, 12439-12442.

77. Vabre, B.; Chansaenpak, K.; Wang, M.; Wang, H.; Li, Z.; Gabbaï, F. P., *Chemical Communications* **2017,** *53*, 8657-8659.

78. Bernard-Gauthier, V.; Wängler, C.; Schirrmacher, E.; Kostikov, A.; Jurkschat, K.; Wängler, B.; Schirrmacher, R., *BioMed research international* **2014,** *2014*, 454503-454503.

79. Fry, B. W.; Whitford, G. M.; Pashley, D. H., *International Journal of Applied Radiation and Isotopes* **1978,** *29*, 123-125.

80. Poole, R. T.; Winfield, J. M., *Dalton Transactions* **1976**, 1557-1560.

81. Gens, T. A.; Wethongton, J. A.; Brosi, A., *The Journal of Physical Chemistry* **1958,** *62*, 1593-1593.

82. Winfield, J. M., *Journal of Fluorine Chemistry* **1980,** *16*, 1-17.

83. Niedermoser, S.; Wängler, C.; Chin, J.; Kostikov, A.; Bartenstein, P.; Jugold, M.; Schirrmacher, E.; Schirrmacher, R.; Wängler, B., *Journal of Nuclear Medicine* **2013,** *54*, 60-60.

84. Wessmann, S.; Henriksen, G.; Wester, H.-J., *Nuklearmedizin-NuclearMedicine* **2012,** *51*, 1-8.

85. Gower-Fry, L.; Kronemann, T.; Dorian, A.; Pu, Y.; Jaworski, C.; Wängler, C.; Bartenstein, P.; Beyer, L.; Lindner, S.; Jurkschat, K.; Wängler, B.; Bailey, J. J.; Schirrmacher, R., *Pharmaceuticals (Basel, Switzerland)* **2021,** *14*, 701.

86. Wester, H. J.; Schottelius, M., *Seminars in Nuclear Medicine* **2019,** *49*, 302-312.

87. Schirrmacher, E.; Wängler, B.; Cypryk, M.; Bradtmöller, G.; Schäfer, M.; Eisenhut, M.; Jurkschat, K.; Schirrmacher, R., *Bioconjugate Chemistry* **2007,** *18*, 2085-2089.

88. Kemnitz, E.; Groß, U.; Rüdiger, S.; Scholz, G.; Heidemann, D.; Troyanov, S. I.; Morosov, I. V.; Lemée-Cailleau, M. H., *Solid State Sciences* **2006,** *8*, 1443-1452.

89. Bhalla, R.; Levason, W.; Luthra, S. K.; McRobbie, G.; Monzittu, F. M.; Palmer, J.; Reid, G.; Sanderson, G.; Zhang, W., *Dalton Transactions* **2015,** *44*, 9569-9580.

90. McBride, W. J.; Sharkey, R. M.; Karacay, H.; D'Souza, C. A.; Rossi, E. A.; Laverman, P.; Chang, C. H.; Boerman, O. C.; Goldenberg, D. M., *Journal of Nuclear Medicine* **2009,** *50*, 991-8.

91. Schmitt, S.; Moreau, E., *Coordination Chemistry Reviews* **2023,** *480*, 215028.

92. Tshibangu, T.; Cawthorne, C.; Serdons, K.; Pauwels, E.; Gsell, W.; Bormans, G.; Deroose, C. M.; Cleeren, F., *EJNMMI Radiopharmacy and Chemistry* **2020,** *5*, 4.

93. McBride, W. J.; D'Souza, C. A.; Sharkey, R. M.; Karacay, H.; Rossi, E. A.; Chang, C.-H.; Goldenberg, D. M., *Bioconjugate Chemistry* **2010,** *21*, 1331-1340.

94. Dijkgraaf, I.; Franssen, G. M.; McBride, W. J.; D'Souza, C. A.; Laverman, P.; Smith, C. J.; Goldenberg, D. M.; Oyen, W. J. G.; Boerman, O. C., *Journal of Nuclear Medicine* **2012,** *53*, 947-952.

95. Niu, G.; Lang, L.; Kiesewetter, D. O.; Ma, Y.; Sun, Z.; Guo, N.; Guo, J.; Wu, C.; Chen, X., *Journal of Nuclear Medicine* **2014,** *55*, 1150-6.

96. Da Pieve, C.; Allott, L.; Martins, C. D.; Vardon, A.; Ciobota, D. M.; Kramer-Marek, G.; Smith, G., *Bioconjugate Chemistry* **2016,** *27*, 1839-1849.

97. Cleeren, F.; Lecina, J.; Billaud, E. M. F.; Ahamed, M.; Verbruggen, A.; Bormans, G. M., *Bioconjugate Chemistry* **2016,** *27*, 790-798.

98. Cleeren, F.; Lecina, J.; Ahamed, M.; Raes, G.; Devoogdt, N.; Caveliers, V.; McQuade, P.; Rubins, D. J.; Li, W.; Verbruggen, A.; Xavier, C.; Bormans, G., *Theranostics* **2017,** *7*, 2924-2939.

99. Archibald, S. J.; Allott, L., *EJNMMI Radiopharmacy and Chemistry* **2021,** *6*, 30.

100. Even-Sapir, E.; Israel, O., *European Journal of Nuclear Medicine and Molecular Imaging* **2003,** *30 Suppl 1*, S65-81.

101. Goldsmith, S. J.; Vallabhajosula, S., *Seminars in Nuclear Medicine* **2009,** *39*, 2-10.

102. Draisma, A.; Maffioli, L.; Gasparini, M.; Savelli, G.; Pauwels, E.; Bombardieri, E., *Tumori Journal* **1998,** *84*, 434-441.

103. Banerjee, S. R.; Pomper, M. G., *Applied Radiation and Isotopes* **2013,** *76*, 2-13.

104. Velikyan, I., *Theranostics* **2014,** *4*, 47-80.

105. Blower, P. J., *Dalton Transactions* **2015,** *44*, 4819-4844.

106. Price, E. W.; Orvig, C., *Chemical Society Reviews* **2014,** *43*, 260-290.

107. Burke, B. P.; Clemente, G. S.; Archibald, S. J., *Journal of Labelled Compounds and Radiopharmaceuticals* **2014,** *57*, 239-243.

108. Bhalla, R.; Levason, W.; Luthra, S. K.; McRobbie, G.; Sanderson, G.; Reid, G., *Chemistry – A European Journal* **2015,** *21*, 4688-4694.

109. Bhalla, R.; Levason, W.; Luthra, S. K.; McRobbie, G.; Reid, G.; Sanderson, G.; Zhang, W., *Chemical Communications* **2014,** *50*, 12673-12675.

110. Joshi, T.; Kubeil, M.; Nsubuga, A.; Singh, G.; Gasser, G.; Stephan, H., *ChemPlusChem* **2018,** *83*, 554-564.

111. Chaudhuri, P.; Wieghardt, K., *The Chemistry of 1,4,7-Triazacyclononane and Related Tridentate Macrocyclic Compounds.* In Progress in Inorganic Chemistry,35 ed.; 1987; Vol. 70, p 329.

112. Wieghardt, K.; Chaudhuri, P.; Nuber, B.; Weiss, J., *Inorganic Chemistry* **1982,** *21*, 3086-3090.

113. Batal, D. J.; Madison, S. A. *Improved synthesis of 1,4,7-triazacyclononane*, 1992.

114. Cheng, F.; Hector, A. L.; Levason, W.; Reid, G.; Webster, M.; Zhang, W., *Chemical Communications* **2009**, 1334-1336.

115. Cabbiness, D. K.; Margerum, D. W., *Journal of the American Chemical Society* **1969,** *91*, 6540-6541.

116. J. Hubin, T.; M. McCormick, J.; R. Collinson, S.; H. Busch, D.; W. Alcock, N., *Chemical Communications* **1998**, 1675-1676.

117. Liu, S.; Ellars, C. E.; Edwards, D. S., *Bioconjugate Chemistry* **2003,** *14*, 1052-1056.

118. McBride, W. J.; Goldenberg, D. M.; Sharkey, R. M., *Journal of Nuclear Medicine* **2014,** *55*, 1043.

119. Iggo, J. D., Linda, *Journal of Chemical Education* **2001,** *78*, 1469.

120. Grindley, T. B., *Advanced Carbohydrate Chemistry and Biochemistry* **1998,** *53*, 17-142.

121. Giacovazzo, C.; Monaco, H. L.; Artioli, G.; Viterbo, D.; Milanesio, M.; Gilli, G.; Gilli, P.; Zanotti, G.; Ferraris, G.; Catti, M., *Fundamentals of Crystallography,* 3 ed.; Oxford University Press: Oxford, 2011; p 864.

122. Bennett, D. W., *Wiley-VCH*: Weinheim, 2010.

2 Synthesis of neutral and cationic tin(IV) fluoride complexes with neutral hard N- and O-donor ligands

2.1 Introduction

The Sn(IV) halides, SnX_4 (where X = Cl, Br, or I) are tetrahedral monomers that can be used as Lewis acids and as synthons towards Sn(IV) complexes. They are soluble in common, weak, or non-coordinating solvents and their coordination chemistry has been explored extensively. Sn(IV) chloride and bromide are strong Lewis acids and form a wide range of adducts with neutral ligands, contrasting to Sn(IV) iodide which is a very weak Lewis acid and forms unstable complexes with neutral ligands that are often heavily dissociated in solution.[1-3] A wide range of six-coordinate $SnCl_4$ adducts with neutral ligands are known, of the type $[SnCl_4(L)_2]$. The majority of the ligands in the literature are with hard N- and O-type donors, however there are examples with softer ligands, for example, PR_3, AsR_3, SR_2, SeR_2 or TeR_2.[4] Complexes such as *trans*-$[SnCl_4(PEt_3)_2]$ and $[SnCl_4\{Et_2P(CH_2)_2PEt_2\}]$ have been synthesised from $SnCl_4$ (Figure 2.1 shows the crystal structure of the former).[5, 6]

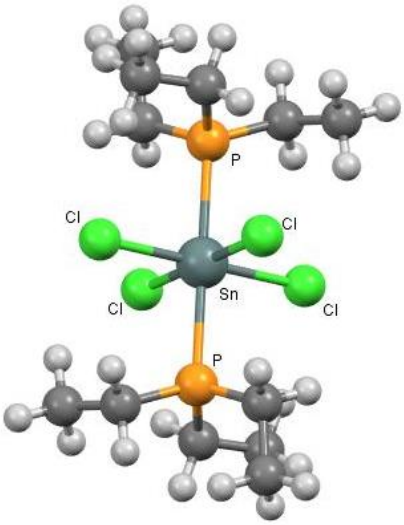

Figure 2.1: Crystal structure of [*trans*-$[SnCl_4(PEt_3)_2]$. Redrawn from Reference[6]. No ellipsoid data available.

The Reid group have previously reported SnX_4 systems with soft donor ligands including di-thioethers, di-selenoethers, di-phosphines and thia-macrocycles.[7-10] However, less work has been

undertaken on the lighter analogue, GeX_4. Ge(IV) halides exhibit less Lewis acidity than their Sn(IV) analogues, but have higher bond dissociation energies associated with the smaller Ge centre and work on Ge(IV) chemistry has been described in Chapter 3.[3, 7, 11-14]

On very few occasions it has been shown that neutral ligands displace a coordinated halide from a Sn(IV) centre, in the formation of "self-ionisation" cationic complexes; this has been demonstrated with the macrocycles 1,4,7-trimethyl-1,4,7-triazacyclononane, 1,3,5-trimethyl-1,3,5-triazacyclohexane and 1,4,7-trithiacyclonane (Figure 2.2), whereby they generate complexes of the type $[SnX_3(L_3)]_2[SnX_6]$, where X = Cl or Br.[15, 16] The formation of these Sn(IV) halide cationic complexes when X = Cl or Br can be achieved by using halide abstractors, these include; $AlCl_3$, TMSOTf or $Na[Bar^F]$.[11, 16, 17]

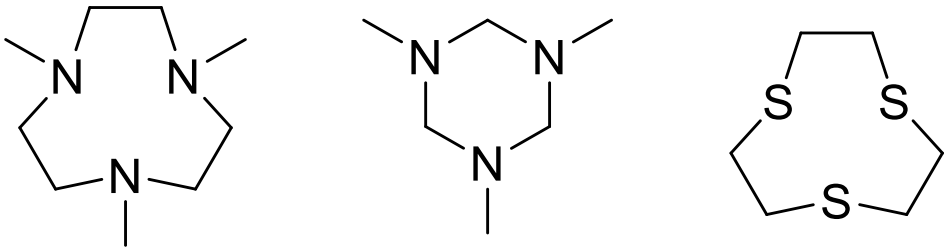

Figure 2.2: Structures of Me_3tacn, Me_3tach, $[9]aneS_3$.

2.1.1 Complexes of Sn(IV) fluoride with neutral ligands

Compared to the heavier halides, there are fewer reported Sn(IV) fluoride complexes with neutral ligands and where there is data, most of the early work focused on Mössbauer, IR or elemental analysis studies for characterisation.[18] However, as the area has advanced, multinuclear NMR spectroscopy and X-ray crystallography have become the most common analytical tools for understanding these complexes.

In contrast to the heavier halide analogues, SnF_4 is an ionic solid and it contains a six-coordinated Sn(IV) in vertex sharing octahedra with a polymeric sheet structure. As a result, it is highly unreactive towards neutral ligands and poorly soluble and therefore is an inconvenient entry point into Sn(IV) fluoride coordination chemistry.[19, 20] A key development in this chemistry was first demonstrated by Tudela and co-workers in 1989, which showed a much more convenient route to Sn-F complexes *via* the molecular synthon $[SnF_4(MeCN)_2]$.[18, 21] It is a soluble monomer with labile MeCN ligands that can be substituted readily by neutral Lewis base ligands. As a key precursor for the work in this project, it was made by refluxing SnF_2 in excess MeCN and I_2, the

SnI_4 by-product does not form a stable adduct with MeCN and is readily removed by washing in CS_2 (

Scheme 11).

$$2\ SnF_2 + 2I_2 \xrightarrow[90\ ^\circ C,\ 2\ h]{MeCN} [SnF_4(MeCN)_2] + SnI_4$$

Scheme 11: Reaction scheme for $[SnF_4(MeCN)_2]$.[18]

The displacement of MeCN ligands in $[SnF_4(MeCN)_2]$ has helped in the development of SnF_4 chemistries with a number of ligands. This method has been used to synthesise a variety of neutral tin tetrafluoride complexes, including, $[SnF_4(thf)_2]$, $[SnF_4(OPPh_3)_2]$, $[SnF_4(py)_2]$ and $[SnF_4(2, 2'\text{-bipy})]$, the latter being the first reported structure of an SnF_4 complex and this has the expected *cis*-octahedral configuration (Figure 2.3).[22, 23] The complexes containing the nitrogen donor ligands are unaffected upon exposure to air and not readily decomposed, despite being slightly moisture sensitive in solution. This is a promising attribute for these systems for potential PET applications, as ease of handling and stability is a must when it comes to developing a new radiotracer.

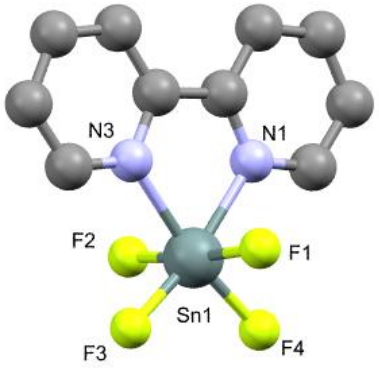

Figure 2.3: The structure of $[SnF_4(2,2'\text{-bipy})]$ showing the octahedral geometry. Redrawn from Ref.[23] No ellipsoid data available. Hydrogen atoms and solvent CH_3NO_2 molecule omitted for clarity.

For hard oxygen donor ligands, a range of Sn(IV) complexes have been isolated successfully, including the thf adduct, $[SnF_4(thf)_2]$, was isolated as the *trans* isomer in the solid state and identified by IR and Mössbauer spectroscopy by Tudela and co-workers. Only the chloride and bromide analogues were elucidated by X-ray crystallography.[18] Also, *cis*-$[SnF_4\{MeO(CH_2)_2OMe\}]$ was synthesised by the direct reaction of the ligand with $[SnF_4(MeCN)_2]$ and crystals were grown by layering a CH_2Cl_2 solution with *n*-hexane.[5, 24] The structure of *cis*-$[SnF_4\{MeO(CH_2)_2OMe\}]$ showed Sn–O bond lengths of 2.156(2) and 2.144(2) Å, which are significantly shorter than the Sn-O bond lengths seen for $[SnCl_4(thf)_2]$, both complexes undergo extensive ligand exchange in

solution at room temperature.[5] Reactions of two equivalents of ligand (L = $OPMe_3$, $OAsMe_3$ and $OPPh_3$) with $[SnF_4(MeCN)_2]$ forms complexes of the type $[SnF_4(L)_2]$.[22] The solution NMR data show that these complexes are dynamic in solution, with both *cis* and *trans* isomers present; single X-ray crystal data showed that $[SnF_4(OPMe_3)_2]$ adopts a *trans* geometry in the solid state (Figure 2.4). However, these complexes rapidly hydrolyse in air and persistently retain lattice solvent molecules, which is evident in the ^1H NMR spectra. For bidentate phosphine oxide ligands, only the expected *cis*-octahedral geometry was present in solution and solid states.[22]

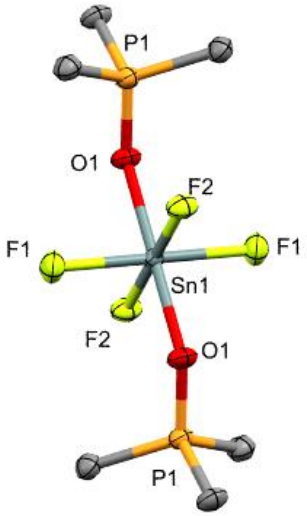

Figure 2.4: Crystal structure of $[SnF_4(OPMe_3)_2]$. Redrawn from Reference.[22]

Previous work in the Reid group has also demonstrated the ability to synthesise SnF_4 complexes with soft dithioether ligands in a CH_2Cl_2 solution, including $[SnF_4\{RS(CH_2)_2SR\}]$ (where R = Me, Et or ^{i}Pr).[25] The studies showed that these complexes dissociate extensively in solution at room temperature and the ^1H NMR spectrum of $[SnF_4\{^iPrS(CH_2)_2S^iPr\}]$ in CD_2Cl_2 at 298 K showed single resonances for the three different proton environments, with only a minor shift to higher frequency from "free" ligand, indicative of lability and fast reversible ligand exchange in solution. However, upon cooling to 223 K, the resonances associated with the coordinated dithioether were present. Further confirmation of these complexes was shown from X-ray crystal structural determination, as show in Figure 2.5.

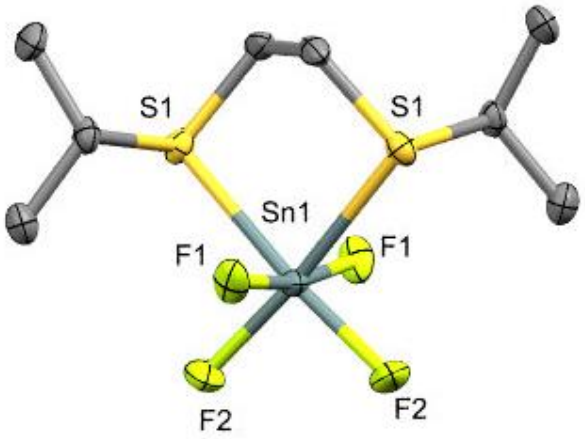

Figure 2.5: Crystal structure of *cis*-[SnF_4{$^{i}PrS(CH_2)_2S^{i}Pr$}]. Redrawn from Reference.[25]

2.1.2 Cationic Sn(IV) fluoride complexes synthesised using halide abstractors

There are few examples of cationic tin(IV) fluoride complexes, with focus on organotin cationic complexes with applications in catalysis.[26] In terms of other cationic tin fluoride complexes, previous work in the Reid group has shown the successful formation of cationic Sn(II) fluoride complexes, for example [Sn(18-crown-6)F][PF_6] (Figure 2.6), this was formed by the reaction of $Sn(PF_6)_2$, 18-crown-6 and KF in MeCN and water.[27]

Figure 2.6: Structure of the cation, $[Sn(18\text{-crown-6})F]^+$, in the complex [Sn(18-crown-6)F][PF_6]. $[PF_6]^-$ anion omitted for clarity. Redrawn from Reference.[27]

The fluoride is in an unusual axial position and this originates from the degradation of the $[PF_6]^-$ counterion, this is further confirmed by a $^{19}F\{^1H\}$ NMR spectroscopy, with a resonance at -96.5 ppm, this is in addition to the $[PF_6]^-$ anion.

Since cationic complexes of Sn(IV) fluoride do not readily form with most neutral ligands through self-ionisation, halide abstractors can be utilised. Burford and co-workers presented an

alternative route to cationic Sn(IV) fluoride complexes; $SnF_4(MeCN)_2$ was reacted with $BIMEt_3$ ($BIMEt_3$ = tris((1-ethyl-benzoimidazol-2-yl)methyl)amine, chemical structure shown in Figure 2.7) and TMSOTf in a 1:1:1 ratio in MeCN, to form $[SnF_3(BIMEt_3)][OTf]$,this was confirmed by the presence of a quartet in the ^{119}Sn NMR spectrum due to the three equivalent fluorides. They also demonstrated the sequential fluoride abstraction to form the dication and trication complexes, this is shown in Scheme 12.[28]

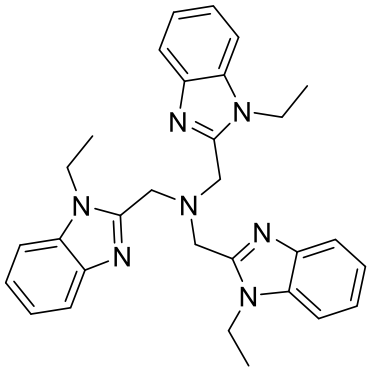

Figure 2.7: The $BIMEt_3$ ligand.

$$BIMEt_3 + SnF_4 \xrightarrow[TMSOTf]{MeCN} [(BIMEt_3)SnF_3][OTf] \xrightarrow[TMSOTf]{CH_2Cl_2} [(BIMEt_3)SnF_{4-x}][OTf]_x$$

Scheme 12: Reaction of SnF_4 with TMSOTf and $BIMEt_3$ and sequential fluoride abstractions. Redrawn from Reference.[28]

The reaction of $[Sn(BIMEt_3)][OTf]_2$ with the fluoride source XeF_2 results in the aggressive evolution of xenon gas, consistent with a redox process, and numerous fluorine containing compounds were observed in the $^{19}F\{^1H\}$ NMR spectrum.[28] However, for the equivalent germanium reaction, a pure sample of the Ge(IV) complex, $[GeF_2(BIMEt_3)][OTf]_2$ was isolated, with crystal data showing a distorted octahedral geometry for the dicationic complex, with the fluorides in the *cis*-configuration (Scheme 13).[29] This is similar to other germanium halide complexes with phosphine oxide ligands, of the type $[GeX_2(OPMe_3)_4][X]_2$ (X= Cl or Br).[19] Treatment of $[GeF_2(BIMEt_3)][OTf]_2$ with TMSOTf generates $[GeF(BIMEt_3)OTf][OTf]_2$, whereby a triflate coordinates to the Ge(IV) centre to complete the six-coordinate complex.

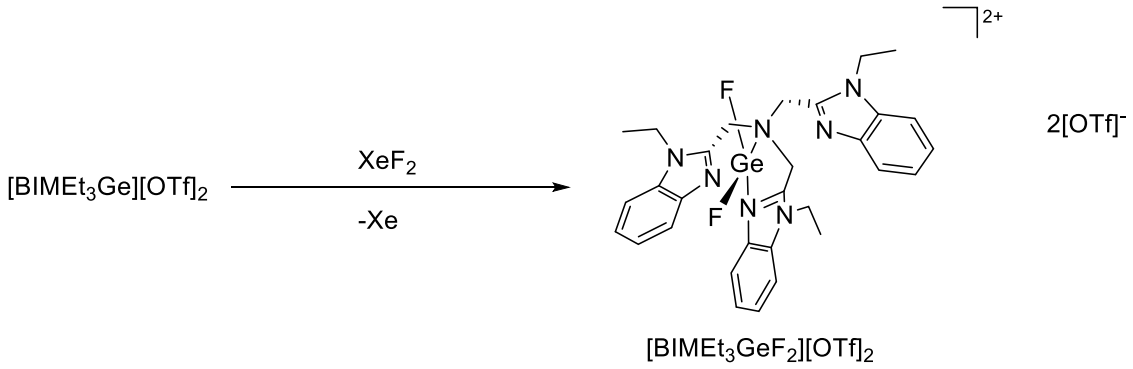

Scheme 13: Schematic for the synthesis of $[GeF_2(BIMEt_3)][OTf]_2$, from Reference.[29]

Cationic complexes of the type $[Sn(L)R_3][ClO_4]$ where R = Ph or ^nBu and L = 2 py, 2 γ-picoline, 2,2'-bipy or 1,10-phen can be synthesised from the reaction of R_3SnCl with $AgClO_4(L)$ or directly from SnR_3ClO_4 and (L).[30, 31]

This approach is exemplified by the use of $AlCl_3$ as a halide abstractor to remove a chloride (forming $AlCl_4^-$) from various Sn(IV) chloride phosphine complexes, forming cationic complexes such as $[SnCl_3(PR_3)_2][AlCl_4]$, $[SnCl_2(PR_3)_2][AlCl_4]_2$ (R = Me, Et), and $[SnCl_2\{o\text{-}C_6H_4(PMe_2)_2\}][AlCl_4]_2$.[11, 17] Using $Na[BAr^F]$ ($BAr^F = [B\{3,5\text{-}CF_3(C_6H_3)_4\}]^-$) with the corresponding neutral tin tetrachloride complex has been shown to produce $[SnCl_3(PEt_3)_2][BAr^F]$ and $[SnCl_3(AsEt_3)_2][BAr^F]$ salts.[11] Similarly, $SiCl_4$ complexes containing the smaller Group 14 centre, Si(IV), have also been shown to react successfully with $Na[BAr^F]$. For example, the reaction of $SiCl_4$ and $Na[BAr^F]$ in toluene with the triamine, N,N,N',N'',N''-pentamethyldiethylenetriamine (pmdta), leads to the formation of the complex $[SiCl_3(pmdta)][BAr^F]$, the crystal structure of which shows a *mer* geometry. The reaction of $SiCl_4$ with the tridentate macrocycle Me_3tacn leads to the spontaneous displacement of a chloride ligand, forming the salt $[SiCl_3(Me_3tacn)]Cl$ with a *fac*-octahedral geometry.[32] The crystal structures for both are shown in Figure 2.8, outlining their different geometries.

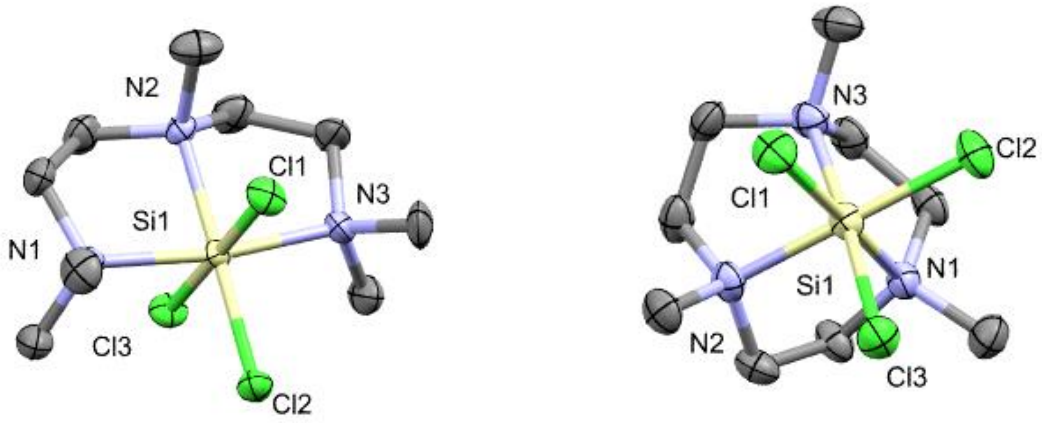

Figure 2.8: Crystal structures of cations $[SiCl_3(pmdta)]^+$ in $[SiCl_3(pmdta)][BAr^F]$ complex and $[SiCl_3(Me_3tacn)]^+$in $[SiCl_3(Me_3tacn)]Cl$ complex. Anions are omitted for clarity. Redrawn from Reference.[32]

Since soft phosphine ligands cannot displace fluoride directly from a Sn(IV) centre to generate Sn(IV) fluoride cationic complexes, the Reid group researched whether the use of a halide abstractor would work to develop this chemistry. $Na[BAr^F]$ was chosen first to explore this chemistry, its structure is shown in Figure 2.9. It is bulkier than many other weakly coordinating anions, such as OTf^- and its diffuse charge makes it less likely to coordinate, however there had been no reported work with Group 14 fluoride complexes at the time this work was undertaken. Work in the Reid group by Dr. Rhys King demonstrated the use of $Na[BAr^F]$ to form cationic five-coordinate Sn(IV) complexes of the type $[SnCl_3(L)_2][BAr^F]$, where L is the soft donor ligand, PEt_3, PMe_3, o-$C_6H_4(PMe_2)_2$ and $AsEt_3$. In the case of the latter complex, $[SnCl_3(AsEt_3)_2][BAr^F]$, its synthesis was clean and a pure sample was isolated, in contrast to attempts using the two other halide abstractors, $AlCl_3$ and TMSOTf.[11] NMR data for a select number of complexes are presented in Table 7. It was shown that $Na[BAr^F]$ can successfully remove one chloride from many neutral complexes to generate a monocationic complex, however upon addition of more $Na[BAr^F]$, no further chlorides could be abstracted.

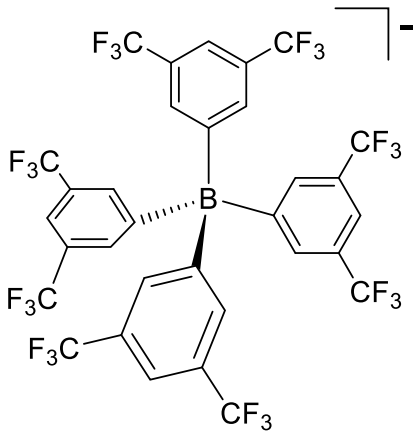

Figure 2.9: The $[BAr^F]^-$ anion: four fluorinated aryl groups coordinated tetrahedrally around a central boron atom.

Table 7: Selected NMR data for Sn(IV) pnictine complexes with [OTf] and $[BAr^F]$ in CD_2Cl_2 at 298 K (unless stated otherwise), edited from Reference.[11]

Complex	$\delta(^{31}P\{^1H\})$ / ppm	$\delta(^{119}Sn)$ / ppm	$^1J_{^{119}Sn\text{-}^{31}P}$ / Hz
$[SnCl_3(PMe_3)_2(OTf)]$	+8.7	–516	2963
$[SnCl_3(PEt_3)_2(OTf)]$	+33.4[a]	–535[a]	2737[a]
$[SnCl_3(PEt_3)_2][BAr^F]$	+37.1	–379	2311
$[SnCl_3(AsEt_3)_2(OTf)]$	N/A	–620	N/A
$[SnCl_3(AsEt_3)_2][BAr^F]$	N/A	–388[a]	N/A

[a] recorded at 183 K

In equivalent Sn(IV) fluoride systems, AlF_3 is an inert polymer and therefore cannot behave as a fluoride abstractor and $Na[BAr^F]$ often leads to incomplete reactions, hence TMSOTf is being explored.[33, 34] TMSOTf has been shown to be an efficient halide abstractor for both tin fluoride and chloride phosphine complexes, as well as germanium fluoride phosphine complexes, however, many of these reactions resulted in neutral complexes with a coordinated triflate rather than forming a cationic species.[11, 34, 35] Examples of this include $[SnF_{4\text{-}n}(PMe_3)_2(OTf)_n]$ and $[GeF_{4-n}\{o\text{-}C_6H_4(PMe_2)_2\}(OTf)_n]$ (n= 1- 3) (Figure 2.10 shows the crystal structures of both complexes when n = 1).

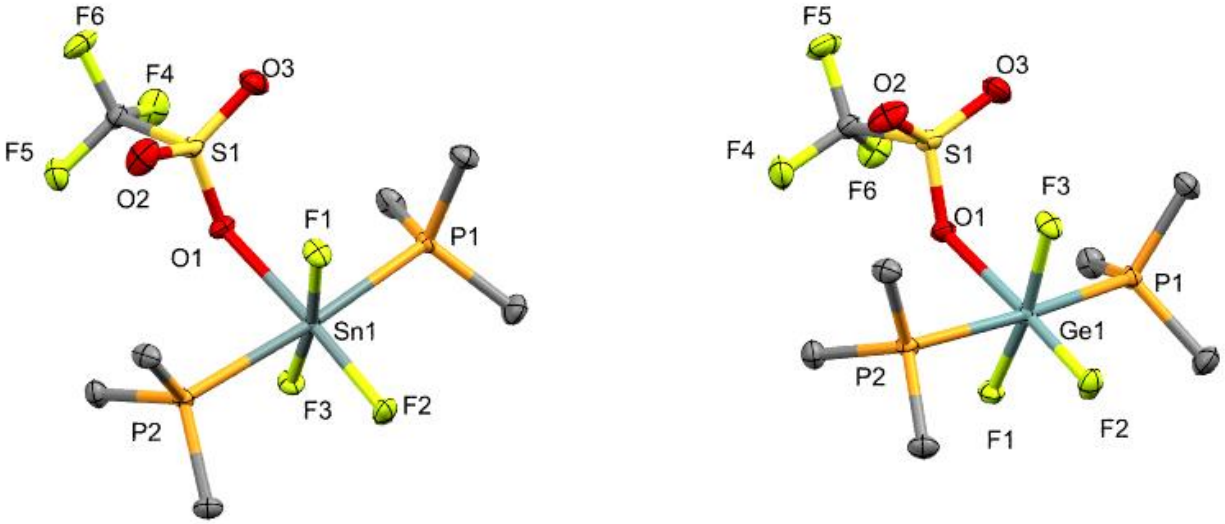

Figure 2.10: Crystal structures of $[SnF_3(PMe_3)_2(OTf)]$ and $[GeF_3(PMe_3)_2(OTf)]$. Redrawn from References.[34, 35]

Very recent work by Kuziola and co-workers demonstrated the successful synthesis of a series of cationic fluorotriarylbismuthonium salts, use $Na[BAr^F]$ as a fluoride abstractor to form a unique mononuclear fluorotrimesitylbismuthonium cation, as shown in Scheme 14. This is the first known example of $Na[BAr^F]$ being used effectively in the removal of a fluoride ligand from Bi(V).[36]

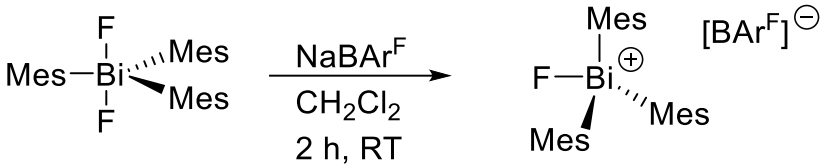

Scheme 14: Synthesis of cationic fluorotrimesitylbismuthonium. Redrawn from Reference.[36]

2.1.3 Aims

The aims of the work in this chapter were:

i) to develop the underlying coordination chemistry of tin(IV) fluoride to develop a systematic series of SnF_4 complexes of the type $[SnF_4(L)_2]$ with neutral nitrogen and oxygen donor ligands;

ii) to test the sequential removal of fluoride from these complexes to form cationic species using a halide abstractor and to investigate how the choice of neutral ligand affects the reaction outcome;

iii) to use the results to allow comparisons to be drawn with the work in the following Chapters, 3 and 4.

Complexes have predominantly been characterised by IR spectroscopy and elemental analysis in the solid state, multinuclear NMR spectroscopy in solution, and by X-ray crystallography in some cases.

2.2 Results and Discussion

2.2.1 Reactions of $SnF_4(MeCN)_2$ with neutral N- and O-donor monodentate ligands

In this study, several neutral tin complexes of the type $[SnF_4(L)_2]$ (L = dmso, pyNO, dmf, $OPPh_3$ or py) were synthesised, these complexes have been reported previously but mostly the published data was limited to IR spectroscopy and microanalysis and the first three complexes were synthesised under a modified procedure (Scheme 15).[5, 22, 37, 38] $[SnF_4(MeCN)_2]$ was suspended in an excess of the appropriate ligand, when the ligand is the solvent, or reacted with 2 equivalents of the ligand in CH_2Cl_2 and stirred for 2 h, resulting in the precipitation of the desired complexes in good yield.

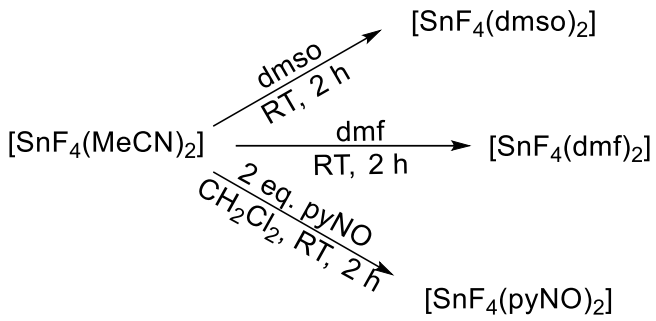

Scheme 15: Schematic showing the synthesis of $[SnF_4(L)_2]$ (L = dmso, pyNO, dmf).

The colourless solids were filtered and washed in anhydrous hexane to remove excess unreacted ligand. These complexes were moderately air sensitive, hence they were stored in a dry, N_2 filled glovebox. They are poorly soluble in common NMR solvents, such as $CDCl_3$ or CD_2Cl_2. NMR studies of these complexes were performed in CD_3NO_2 as this provided sufficient solubility for the complexes and because it is a weakly coordinating solvent and so there is little risk of ligand exchange in solution, which could occur in other solvents such as MeCN, thf or dmso.

The crystal structures of *trans*-$[SnF_4(OPR_3)_2]$ (R= Me or Ph) have been determined previously, however the structures of *trans*-$[SnF_4(pyNO)_2]$ and *trans*-$[SnF_4(py)_2]$ were determined in this work and are shown in Figure 2.11; colourless crystals were isolated by slow evaporation from a CH_3NO_2 solution.[22]

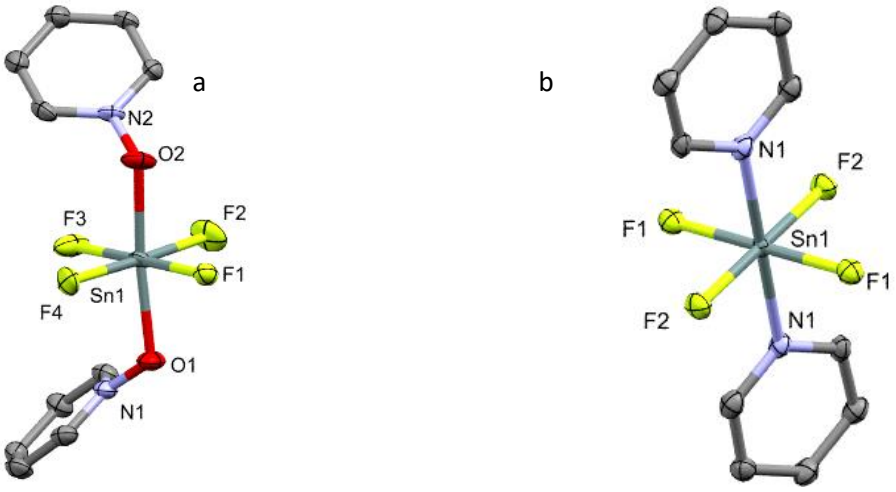

Figure 2.11: Crystal structures of $[SnF_4(pyNO)_2]\cdot CH_2Cl_2$ (a) and the centrosymmetric $[SnF_4(py)_2]$ (b) showing the atom labelling schemes. The ellipsoids are drawn at the 50% probability level and H atoms and lattice CH_2Cl_2 are omitted for clarity. There are two crystallographically independent $[SnF_4(pyNO)_2]\cdot CH_2Cl_2$ moieties in asymmetric unit and only one is shown. Selected bond lengths (Å) and angles (°) are: (a) Sn1–F1 = 1.945(3), Sn1–F2 = 1.945(4), Sn1–F3 = 1.943(4), Sn1–F4 = 1.953(3), Sn1– O1 = 2.081(3), Sn1–O2 = 2.081(3), N1–O1 = 1.364(5), N1–O2 = 1.359(5), O1–Sn1–O2 = 172.29(15), F1–Sn1–F3 = 177.59(16), F2–Sn1–F4 = 177.20 (16); (b) Sn1–F1 = 1.954(7), Sn1–F2 = 1.956(7), Sn1–N1 = 2.175(10), F1– Sn1–F2 = 90.1(3), F1–Sn1–N1 = 90.0(3), F2–Sn1–N1 = 90.0(3).

The $^{19}F\{^1H\}$ NMR spectra for most of the $[SnF_4(L)_2]$ complexes show both *cis* and *trans* isomers in solution, with varying amounts of each (Figure 2.12). The ^1H NMR spectra for the neutral complexes reported in this section showed the expected shifts of the ligand resonances to a higher frequency upon coordination to the Sn(IV) centre.

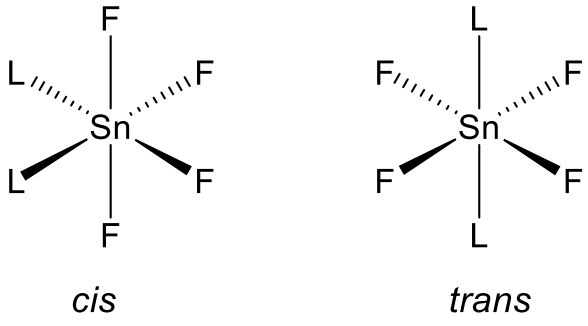

Figure 2.12: Structures of *cis*- and *trans*- isomers of the type $[SnF_4(L)_2]$.

Table 8 outlines the key NMR spectroscopic data for this set of neutral Sn(IV) fluoride complexes.

Table 8: Selected NMR spectroscopic data[b] for $[SnF_4(L)_2]$ complexes.

Compound	Isomer	δ $^{19}F\{^1H\}$ / ppm (multiplicity)	δ $^{31}P\{^1H\}$ / ppm (multiplicity)	$\delta(^{119}Sn)$ / ppm (multiplicity)	$^1J(^{19}F-^{119}Sn)$ / Hz	$^1J(^{19}F-^{117}Sn)$ / Hz	$^2J(^{19}F-^{19}F)$ / Hz
$[SnF_4(dmso)_2]$	*trans*	-149.0 (s)	N/A	-778.4 (quin)	1850	1767	-
	cis	-149.3 (t)		n.o.	1952	1661	52
		-161.6 (t)			2030	1737	52
$[SnF_4(dmf)_2]$	*trans*	-161.8 (s)	N/A	n.o.	a	a	-
	cis	-161.9 (t)		n.o.	1907	a	50
		-169.5 (t)			2015	a	50
$[SnF_4(pyNO)_2]$	*trans*	-164.2 (s)	N/A	-779-1 (quin)	1951	1864	-
	cis	-166.5 (t)	-	n.o.	2081	1729	51
		-168.7 (t)	-		2030	1891	51
$[SnF_4(py)_2]$[c]	*trans*	-163.8 (s)	N/A	-670.8 (quin)	1983	a	-
$[SnF_4(OPPh_3)_2]$	*cis*	-159.8 (t), -146.2 (t)	42.3	-775.1 (ttt)			
	trans	-149.8 (s)	42.5	-770.0 (quin)			

[a] Unable to determine $^1J(^{19}F-^{119/117}Sn)$ due to satellite overlap, [b] In CD_3NO_2 [c] data from reference[18]

The isomers present in solution are readily identified from the $^{19}F\{^1H\}$ NMR spectra, with the *trans* isomer showing a sharp singlet resonance and the *cis* isomer showing two triplets, with accompanying $^{117/119}Sn$ satellites. The isomer ratio is likely solvent dependant. The $\delta(^{19}F)$ ranges between -146 and -170 ppm and with $^1J(^{19}F-^{119/117}Sn)$ between 1660-2030 Hz. These are similar to values in substituted fluorostannates(IV).[39] The magnitudes of the coupling constants are consistent with the expectation based on $\gamma^{119}Sn/\gamma^{117}Sn$ (1.046), where γ is the gyromagnetic ratio for each isotope.[4] A typical example is shown in Figure 2.13 for the complex $[SnF_4(dmso)_2]$.[34]

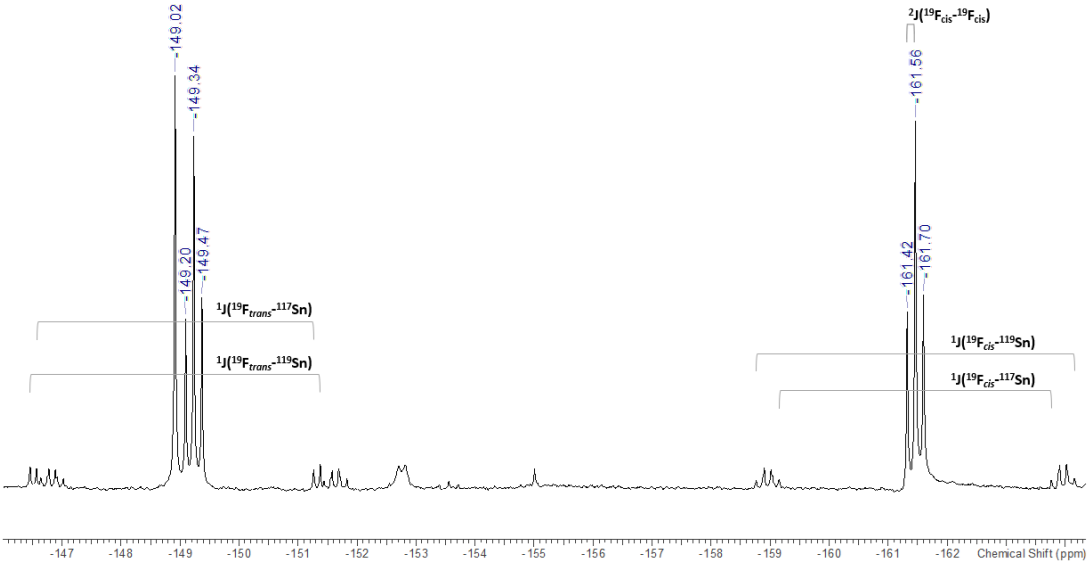

Figure 2.13: $^{19}F\{^{1}H\}$ NMR spectrum of $[SnF_4(dmso)_2]$ showing the resonance of the *cis* and *trans* isomers with the $^{117/119}Sn$ satellites (298 K, CD_3NO_2).

Acquiring ^{119}Sn NMR spectra proved more challenging due to a combination of aspects, this includes the presence of two isomers that can lead to complex multiplet patterns overlapping. Typically, the central lines were identified and allowed for the identification of $\delta(^{119}Sn)$. $[SnF_4(dmf)_2]$ failed to exhibit a ^{119}Sn resonance in CH_3NO_2 at 253 K, likely due to reversible neutral ligand dissociation. The ^{119}Sn NMR spectrum of $[SnF_4(pyNO)_2]$ (253 K, CD_3NO_2) is shown in Figure 2.14, it is likely that the two outer lines for the expected quintet are hidden in the noise.

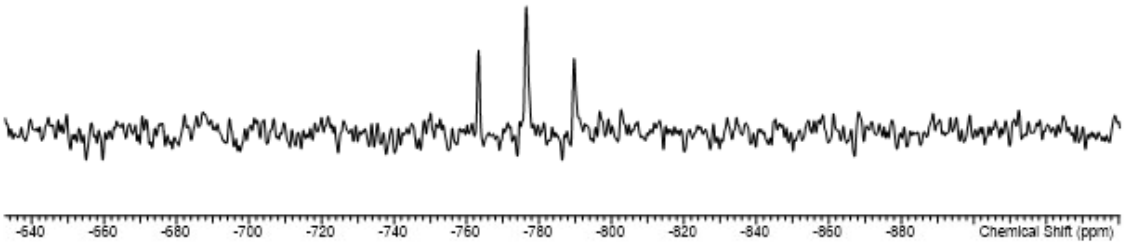

Figure 2.14: ^{119}Sn NMR spectrum of $[SnF_4(pyNO)_2]$ (253 K, CD_3NO_2).

The IR spectra of $[SnF_4(L)_2]$ complexes typically show four ν/(Sn-F) bands between 588 and 522 cm^{-1}, indicating a mixture of *cis* and *trans* isomers and in the case of $[SnF_4(dmso)_2]$ also two sharp ν/(S=O) bands at 936 and 908 cm^{-1}, relating to the two coordinated dmso environments. Despite the theory that there should be five different Sn-F bands, this is a common feature in IR spectroscopy where some expected bands can be lost in the noise or amongst stronger IR peaks. The elemental analyses confirmed the desired complexes had been isolated in a pure state in each case.

2.2.2 Reactions of $[SnF_4(L)_2]$ and TMSOTf with N- and O-donor monodentate ligands

Having demonstrated the ability to synthesise neutral complexes of the type $[SnF_4(L)_2]$, it was postulated whether the corresponding $[SnF_3(L)_3][OTf]$ (L = dmso, py, pyNO, DMF or $OPPh_3$) salts could be accessed *via* the addition of one equivalent of the halide abstractor, TMSOTf, to remove another fluoride (as TMSF), followed by the addition of one molar equivalent of the appropriate ligand, L, in anhydrous CH_2Cl_2. Triflate can act as a counter anion and/or coordinate to the metal centre, depending on the driving force and stoichiometries used.[11, 34]

The approach to use TMSOTf has been exemplified due to previous explorations of other halide abstraction reagents, for example $AlCl_3$ can be used to remove chlorides from various Sn(IV) complexes with soft phosphine ligands, forming cationic complexes of the type $[SnCl_3(PR_3)_2][AlCl_4]$, $[SnCl_2(PR_3)_2][AlCl_4]_2$ (R = Me, Et), $[SnCl_3\{o\text{-}C_6H_4(PMe_2)_2\}][AlCl_4]$ and $[SnCl_2\{o\text{-}C_6H_4(PMe_2)_2\}][AlCl_4]_2$, as mentioned in Section 2.1[11, 17] Similar reactions with another halide abstractor, $Na[BAr^F]$, has also been shown to successfully remove a chloride from a neutral tetrachloride tin complex and form the 5-coordinate complex $[SnCl_3(PEt_3)_2][BAr^F]$.[11] However, in corresponding tin fluoride systems both AlF_3 and $Na[BAr^F]$ are not sufficient; AlF_3 is an inert polymer and therefore does not act as a fluoride abstractor, while reactions with $Na[BAr^F]$ did not go to completion.[33, 34]

Formation of cationic complexes would be expected to increase the Lewis acidity of the Group 14 metal centre, of which there are very few in the literature.[11] These experiments were conducted to test the method for the formation of cationic complexes containing the SnF_3^+ fragment and later, whether they could act as synthons to macrocyclic systems (see Chapter 4).

The reaction of $[SnF_4(L)_2]$ with TMSOTf and the corresponding ligand in a 1:1:1 ratio in CH_2Cl_2 leads to the formation of complexes of the type $[SnF_3(L)_3][OTf]$ (Scheme 16).

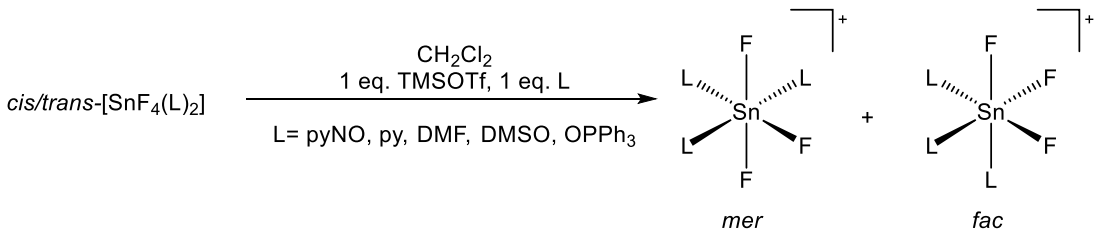

Scheme 16: Reaction of $[SnF_4(L)_2]$ with 1 eq. of TMSOTf and 1 eq. of ligand.

The $^{19}F\{^{1}H\}$ NMR spectra show that both the *fac* and *mer* isomers are present in solution, in varying amounts depending on the ligand and NMR solvent. The *fac* isomer shows a sharp singlet and the *mer* isomer gives rise to a doublet and a triplet resonance, attributed to $^{2}J_{FF}$, all with accompanying $^{117/119}Sn$ satellites. A typical example for the cation in $[SnF_3(dmso)_3][OTf]$ is shown in Figure 2.15. The triflate resonance has been omitted from the spectrum for clarity, however it is present at -79 ppm, which is indicative of anionic triflate. By comparing the NMR data for the monocationic complexes to the related neutral complexes, it can be noted that δ $^{19}F\{^{1}H\}$ generally shifts to a lower frequency (more negative). Also, the $^{2}J_{FF}$ coupling constants are consistently larger for the cationic complexes, therefore providing evidence that there are stronger interactions with the more Lewis acidic cation.

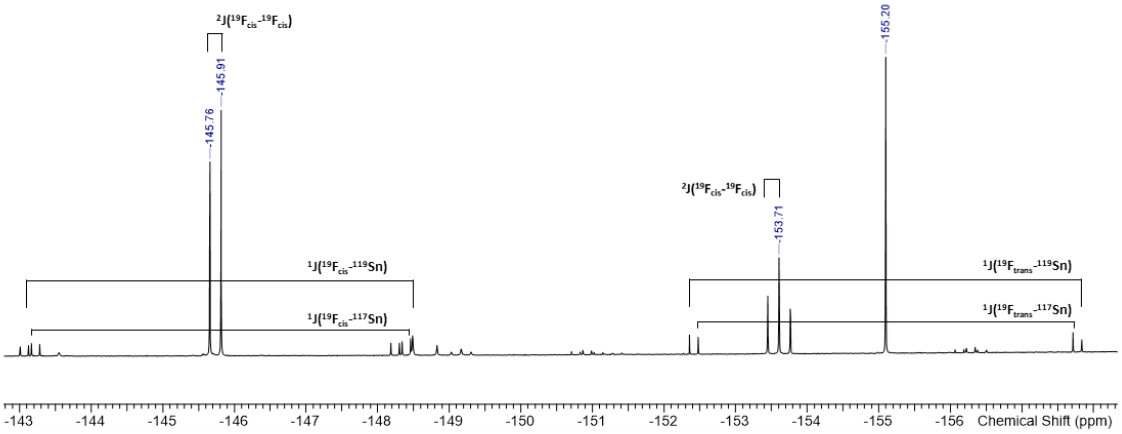

Figure 2.15: $^{19}F\{^{1}H\}$ NMR spectrum $[SnF_3(dmso)_3][OTf]$ (CD_3NO_2 298 K). Triflate resonance omitted for clarity.

Select NMR data for these complexes are shown in Table 9.

Table 9: Selected multinuclear NMR data[a, b]

Compound		δ ^{19}F{H}[c] / ppm (multiplicity)	$^{1}J(^{19}F-^{119}Sn)$ / Hz	δ ^{119}Sn / ppm (multiplicity)	$^{2}J(^{19}F-^{19}F)$ / Hz
$[SnF_3(dmso)_3][OTf]$	*fac*	-155.2 (s)	2063	-735 (q)	-
	mer	-145.8 (t) -153.7 (d)	2063, 2181	-744 (m)	59 59
$[SnF_3(dmf)_3][OTf]$	*fac*	-168.8 (s)	2150	n.o.	-
	mer	-169.2 (t) -164.0 (d)	2143, 1985	n.o.	55 55
$[SnF_3(pyNO)_3][OTf]$[a]	*fac*	-172.36 (s)	2159	~ -770	-
	mer	-171.6 (t) -169.9 (d)	2268, 2244	~ -770	57 57
$[SnF_3(py)_3][OTf]$[a]	*fac*	-157.2 (s)	1588	-763 (q)	-
	mer	-165.8 (t) -158.8 (d)	1717 1737	-771 (m)	40 40
$[SnF_3(OPPh_3)_3][OTf]$	*fac*	-142.1 (s)	1878	n.o.	-
	mer	-141.2 (t) -134.5 (d)	1811 2000	n.o.	61 61
$[SnF_2(OPPh_3)_4][OTf]_2$	*trans*	-123.1 (s)	1812	n.o.	-
	cis	-122.4 (s)	2069	n.o.	-

[a] NMR data from CH_3NO_2 solution at 298 K. [b] Full data found in Experimental section. [c] Non-triflate resonances. n.o. = not observed

The IR spectrum of $[SnF_3(dmso)_3][OTf]$ showed two broad Sn-F stretches, while Group theory predicts two bands for the *facially* coordinated complex, with C_{3v} symmetry (A_1 and E), and three bands for the *mer* isomer, which has C_{2v} symmetry ($2A_1$ and B_1). It is likely that these bands are partially overlapping in the Sn-F region and this explains why the expected five bands are not all observed.

Gaining good quality ^{119}Sn NMR spectra has proved difficult, this is due to a number of factors:

- Modest receptivity of ^{119}Sn – the receptivity relative to ^{1}H natural abundance is 4.53 x10^{-3}.[9]
- Poor solubility of the complexes in common NMR solvents.
- Melting point of nitromethane is a limiting factor for acquiring data at sufficiently low temperatures to reach the low temperature limiting spectrum.
- Presence of different isomers complicating the spectrum.

Typically, central lines of the multiplets were observed, but often the weaker outer lines of the expected multiplets were not easily distinguished from the baseline and were difficult to assign. The complexes $[SnF_3(dmf)_3][OTf]$, $[SnF_3(OPPh_3)_3][OTf]$ and $[SnF_2(OPPh_3)_4][OTf]_2$, failed to exhibit a ^{119}Sn resonance (in CH_3NO_2 at 253 K), this is likely due to the lability of the complex and ligand dissociation in solution on the ^{119}Sn NMR timescale.[40]

The $[SnF_3(L)_3][OTf]$ complexes are less stable in solution than the neutral $[SnF_4(L)_2]$ and resonances that correspond to decomposition or disproportionation products can also be observed in some cases. This is especially so for the systems containing dmf and $OPPh_3$. It is noteworthy that the crystal used to determine the structure of $[SnF_4(py)_2]$ (shown in Figure 2.11) was grown from the sample of $[SnF_3(py)_3][OTf]$, therefore suggesting that some ligand re-distribution also occurs in solution in these systems.

It should also be noted that at no point did we see evidence for the coordination of a triflate to the metal centre, in contrast to related complexes with soft donor phosphine ligands, where a triflate binds to the metal centre rather than an extra phosphine ligand to form a neutral complex, $[SnF_3(PR_3)_2(OTf)]$. This is likely due to all the ligands used in this study being harder Lewis bases and more strongly coordinating than triflate.[34]

Work was undertaken to assess the possibility of abstracting further fluorides from the $[SnF_3(L)_3][OTf]$ complexes in this study to form dications and trications. Attempts to isolate pure samples of difluoro tin(IV) dications of type, $[SnF_2(L)_4][OTf]_2$, from $[SnF_4(L)_2]$ with two equivalents of TMSOTf and excess ligand proved challenging (Scheme 17 shows the synthesis of $[SnF_2(OPPh_3)_4][OTf]_2$). The target complexes were identified in the $^{19}F\{^{1}H\}$ NMR spectra, however often they were present as mixtures with the trifluoro species. The difficulty in isolating pure samples of the dications further adds to the suggestion that some ligand distribution does occur in solution. Nevertheless, it was possible to isolate a rare example of a Sn(IV) dication, the analytically pure sample of $[SnF_2(OPPh_3)_4][OTf]_2$ (NMR data can be seen in the last row of Table 9).

$$[SnF_4(OPPh_3)_2] + 2\ TMSOTf + 2\ OPPh_3 \xrightarrow[4\ h]{CH_2Cl_2,\ RT} [SnF_2(OPPh_3)_4][OTf]_2 + 2TMSF$$

Scheme 17: Schematic for the synthesis of $[SnF_2(OPPh_3)_4][OTf]_2$.

The ^{1}H NMR spectrum of the difluoride complex, $[SnF_2(OPPh_3)_4][OTf]_2$, contained the expected broad multiplet for the phenyl protons from 7.3-7.9 ppm. The resonances in the $^{19}F\{^{1}H\}$ and $^{31}P\{^{1}H\}$ NMR spectra correspond to both the *cis* and *trans* isomers, with the *cis* isomer predominant in the CD_3NO_2 solution. There was no ^{119}Sn NMR resonance observed at 253 K, which is the lower limit of the CD_3NO_2 solvent. However, colourless crystals suitable for single crystal X-ray analysis were obtained by slow evaporation from a CH_3NO_2 solution and the structure clearly showed the 1:4 Sn to $OPPh_3$ ratio, with the fluorides *trans* to each other (Figure 2.16). The elemental analysis further confirmed the formation of a pure bulk sample of $[SnF_2(OPPh_3)_4][OTf]_2$.

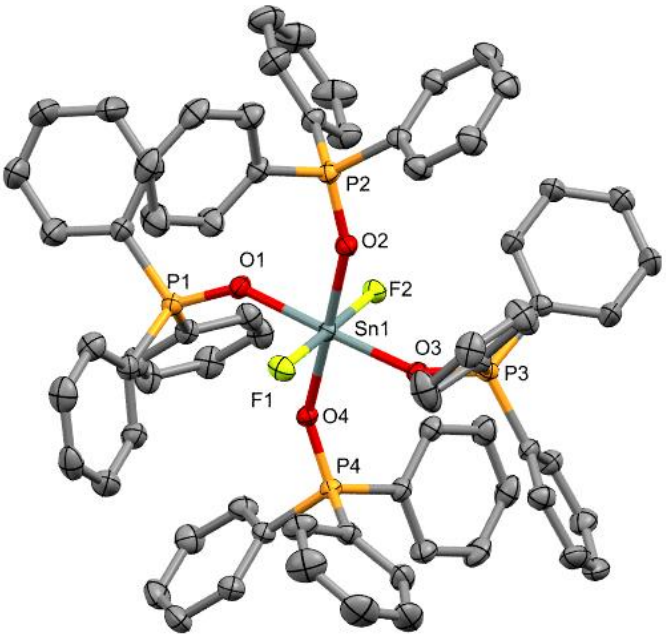

Figure 2.16: Structure of the dication in $[SnF_2(OPPh_3)_4][OTf]_2$ showing the atom labelling scheme. The ellipsoids are drawn at the 50% probability level and H atoms and OTf anions are omitted for clarity. Selected bond lengths (Å) and angles (°) are: Sn1–F2 = 1.9314(16), Sn1–F1 = 1.9164(17), Sn1–O3 = 2.040(2), Sn1–O4 = 2.0447(19), Sn1–O2 = 2.040(2), Sn1–O1 = 2.057(2), F1–Sn1–F2 = 178.78(7), O3–Sn1–O1 = 176.24(8), O–2Sn1– O4 = 178.85(8).

The tin environment is close to that of a regular octahedron and the d(Sn-F) are markedly shorter than in the neutral $[SnF_4(L)_2]$ (L= pyNO, py) complexes above, although the d(Sn-O) are not significantly different to its corresponding neutral complex *trans*-$[SnF_4(OPPh_3)_2]$.[22]

Table 10: Selected bond lengths and angle for $[SnF_4(OPPh_3)_2]$ and $[SnF_2(OPPh_3)_4][OTf]_2$.

Bond length (Å) or bond angle (°)	$[SnF_4(OPPh_3)_2]$	$[SnF_2(OPPh_3)_4][OTf]_2$
Sn1-F1	1.928(3)	1.916(1)
Sn1-F2	1.934(3)	1.931(1)
Sn1-O($-_{trans}$O)	2.050(3)	2.057(2)
F_{trans}-Sn1-F_{trans}	90.56(12)	178.78(7)

2.3 Conclusions

A range of distorted octahedral Sn(IV) fluoride complexes with hard N- and O-donor ligands, of the type $[SnF_4(L)_2]$, $[SnF_3(L)_3][OTf]$ and $[SnF_2(L)_4][OTf]_2$ have been successfully synthesised. The products have been analysed by infrared spectroscopy, ^1H, $^{19}F\{^1H\}$ and $^{31}P\{^1H\}$ NMR spectroscopy (where applicable). ^{119}Sn NMR spectra and elemental analysis were obtained when possible. It has been demonstrated that in the presence of a further equivalent of a neutral ligand, L, TMSOTf can be used to abstract one fluoride reliably from the neutral *cis*/*trans*-$[SnF_4(L)_2]$ complexes to form novel monocations as their OTf^- salts, *fac*/*mer*-$[SnF_3(L)_3][OTf]$, this is contrast to similar Sn(IV) fluoride complexes with soft phosphine donor ligands ,that give complexes with coordinated triflate ligand(s), instead of allowing incorporation of further phosphine or arsine ligand. In some cases, it was possible to abstract a further fluoride to form $[SnF_2(L)_4]^{2+}$, identified by solution NMR spectroscopy, however, despite repeated attempts with longer reaction times, excess of the neutral ligand or elevated temperature, most reactions did not go to completion to form pure samples of Sn(IV) dications. It did prove possible to isolate an analytically pure sample of $[SnF_2(OPPh_3)_4][OTf]_2$, the first of its kind, which was confirmed as the *trans* isomer in the solid state by single crystal X-ray analysis.

This work with monodentate ligands provided a solid grounding in the formation of cationic Sn(IV) fluoride complexes and helped in identifying a method for the formation of systems containing the SnF_3^+ (and SnF_2^{2+}) fragment, which paves the way to the work on macrocyclic systems containing these described in Chapter 4.

2.4 Experimental

$[SnF_4(MeCN)_2]$, $[SnF_4(py)_2]$, $[SnF_4(OPPh_3)_2]$, $[SnF_4(OAsPh_3)_2]$, $[SnF_4(OPMe_3)_2]$ were synthesised following literature methods, $[SnF_4(dmso)_2]$ was prepared by a modified procedure.[18, 22]

2.4.1 $[SnF_4(dmso)_2]$

$[SnF_4(MeCN)_2]$ (0.20 g, 0.72 mmol) was suspended in excess dmso and stirred for 5 min. The white powder was filtered and dried *in vacuo*. Yield 0.120 g, 47%. Required for $C_4H_{12}F_4O_2S_2Sn$ (351.0): C, 13.7; H, 3.5. Found: C, 13.1; H, 3.5%. IR (Nujol/cm^{-1}): ν = 936s, 908sh (SO), 573vs, 552sh, 522m (SnF). ^1H NMR (CD_3NO_2, 298 K): δ = 3.1 (s), 3.0 (s). $^{19}F\{^1H\}$ NMR (CD_3NO_2, 298 K): δ = -161.6 (t, $^1J_{119SnF}$ = 2030, $^2J_{FF}$ = 52 Hz), -149.3 (t, $^1J_{119SnF}$ = 2020, $^2J_{FF}$ = 52 Hz), -149.0 (s, $^1J_{119SnF}$ = 2466 Hz). ^{119}Sn NMR (CD_3NO_2, 253 K): δ = -778.4.

2.4.2 $[SnF_4(pyNO)_2]$

$[SnF_4(MeCN)_2]$ (0.15 g, 0.54 mmol) was dissolved in CH_2Cl_2 and pyNO (0.10 g, 1.08 mmol) was added. The solution was stirred for 2 h. The white powder was filtered, washed in hexane (3 x 5 mL) and dried *in vacuo.* Yield 0.125 g, 60%. Required for $C_{10}H_{10}F_4N_2O_2Sn$ (384.9): C, 31.2; H, 2.6; N, 7.3. Found: C, 31.4; H, 2.6; N, 7.1%. IR (Nujol/cm^{-1}): ν = 1202m (NO), 573br (Sn-F). ^1H NMR (CD_3NO_2, 298 K): δ = 8.7 (m, [2H]), 8.2 (m, [1H]), 7.9 (m, [2H]). $^{19}F\{^1H\}$ NMR (CD_3NO_2, 298 K): δ = -168.7 (t, $^1J_{119SnF}$ = 2030, $^2J_{FF}$ =51 Hz), -166.5 (t, $^1J_{119SnF}$ = 2081, $^2J_{FF}$ = 51 Hz), -164.2 (s, $^1J_{119SnF}$ = 1951). ^{119}Sn NMR (CD_3NO_2, 253 K): δ = -778.5.

2.4.3 $[SnF_4(dmf)_2]$

$[SnF_4(MeCN)_2]$ (0.20 g, 0.72 mmol) was added to an excess of dmf (5 mL) in CH_2Cl_2 (10 mL). The suspension was stirred for 2 h. The white precipitate was filtered, washed in hexane (3 x 3 mL) and dried *in vacuo.* Yield 0.195 g, 80%. Required for $SnF_4C_6H_{14}N_2O_2.CH_2Cl_2$ (425.8): C, 19.74; H, 3.79; N, 6.58. Found C, 19.54; H, 3.81; N, 7.42%. IR (Nujol/cm^{-1}): ν = 1669 (CO), 585s (Sn-F). ^1H NMR (CD_3NO_2, 298 K): δ = 8.2 (s), 7.9 (s) (H), 3.3 (s), 3.3 (s), 3.1 (s), 3.1 (s). $^{19}F\{^1H\}$ NMR (CD_3NO_2, 298 K): δ = -169.5 (t, $^1J_{119SnF}$ = 2015 Hz, $^2J_{FF}$ = 50 Hz), -161.9 (t, $^1J_{119SnF}$ = 1907 Hz, $^2J_{FF}$ = 50 Hz), -161.8 (s). ^{119}Sn NMR (CH_3NO_2, 253 K): n.o.

2.4.4 $[SnF_3(dmso)_3][OTf]$

$[SnF_4(dmso)_2]$ (0.15 g, 0.43 mmol) was suspended in CH_2Cl_2 (10 mL). To this TMSOTf (0.035 g, 0.43 mmol) in CH_2Cl_2 (5 mL) was added and the solution stirred for 2 h. Dmso (0.04 g, 0.43 mmol) in

MeCN (5 mL) was then added and the solution was again stirred for 2 h. The solvent and volatiles were removed and dried *in vacuo,* which yielded a colourless, gel-like solid which was recrystalised from MeCN/Et_2O to a colourless powder. Yield 0.11 g, 46%. Required for $C_7H_{18}F_6O_6S_4Sn$ (559.2): C, 15.0; H, 3.2. Found C, 14.9; H, 3.2%. IR (Nujol/cm^{-1}): ν = 912 vbr (SO), 574br, 519br (SnF). ^1H NMR (CD_3NO_2, 298 K): δ = 3.1 (s), 3.1 (s), 3.1 (s). $^{19}F\{^1H\}$ NMR (CD_3NO_2, 298 K): δ = -155.2 (s, $^1J_{119SnF}$ = 2063 Hz), -153.7 (t, $^1J_{117SnF}$ = 1852, $^1J_{119SnF}$ = 2181 Hz), -145.8 (d, $^1J_{117SnF}$ = 1847, $^1J_{119SnF}$ = 2063 Hz, $^2J_{FF}$ = 59 Hz), -79.5 (s, OTf). ^{119}Sn NMR (CD_3NO_2, 253 K): δ = -744, -735.

2.4.5 $[SnF_3(pyNO)_3][OTf]$

$[SnF_4(pyNO)_2]$ (0.30 g, 0.78 mmol) was suspended in CH_2Cl_2. To this TMSOTf (0.17 g, 0.78 mmol) was added in MeCN (5 mL). The solution was stirred for 2 h. PyNO (0.074 g, 0.78 mmol) was added and the solution was stirred for a further 2 h. The solvent was then removed *in vacuo* which yielded a colourless, gel-like solid which was recrystallised from MeCN/Et_2O to give a white powder. Yield: 0.22 g, 46%. Required for $C_{16}H_{15}F_6N_3O_6Sn.1/2CH_2Cl_2$ (652.54): C, 30.4; H, 2.5; N, 6.4. Found: C, 30.3; H, 2.9; N, 6.6%. IR (Nujol/cm^{-1}): ν = 1225m (NO), 574br,s, 517m (Sn-F). ^1H NMR (CD_3CN, 298 K): δ = 8.8 (m, [2H]), 8.2 (m, [1H]), 7.9 (m, [2H]). $^{19}F\{^1H\}$ NMR (CD_3CN, 298 K): δ = -172.4 (s, $^1J_{119SnF}$ =2159 Hz), -171.6 (t, $^1J_{119SnF}$ = 2268 Hz, $^2J_{FF}$ = 59 Hz), -169.9 (d, $^1J_{119SnF}$ = 2244 Hz, $^2J_{FF}$ = 59 Hz), -78.7 (s, OTf). ^{119}Sn NMR (CD_3NO_2, 253 K): δ ~ -770 (multiplets for the two isomers are almost coincident).

2.4.6 $[SnF_3(dmf)_3][OTf]$

$[SnF_4(dmf)_2]$ (0.31 g, 0.91 mmol) was suspended in CH_2Cl_2. To this TMSOTf (0.20 g, 0.91 mmol) was added in CH_2Cl_2. The solution was stirred for 2 h. DMF (0.067 g, 0.91 mmol) in MeCN was then added and the solution was stirred for 2 h. Addition of n-hexane formed a viscous oil from which the solvent was decanted, and the residue was washed with further hexane and dried in vacuo, leaving a colourless glassy solid. Yield 0.085 g, 17%. . Although we were unable to obtain satisfactory microanalytical data for this complex, likely due to the glassy nature of the product, the spectroscopic data are in accordance with the formulation above. IR (Nujol/cm^{-1}): ν = 1666 (C=O), 582s (Sn-F), 518s (Sn-F). ^1H NMR (CD_3NO_2, 298 K): δ = 8.3 (br s), 8.2 (s), 3.3 (m), 3.2 (m). $^{19}F\{^1H\}$ NMR (CD_3NO_2, 298 K): δ = -169.2 (t, $^1J_{119SnF}$ = 2143 Hz, $^2J_{FF}$ = 55 Hz), -168.8 (s, $^1J_{119SnF}$ = 2150 Hz), -164.0 (d, $^1J_{119SnF}$ = 1985 Hz, $^2J_{FF}$ = 55 Hz). ^{119}Sn NMR (CH_3NO_2, 253 K): n.o.

2.4.7 $[SnF_3(py)_3)][OTf]$

$[SnF_4(py)_2]$ (0.104 g, 0.28 mmol) was suspended in CH_2Cl_2 (10 mL). To this TMSOTf (0.063 g, 0.28 mmol) was added in CH_2Cl_2 (5 mL). The solution was stirred for 2 h. Pyridine (0.022 g, 0.28 mmol) was added, and the solution was stirred for a further 2 h. The solvent was then removed *in vacuo* which yielded a colourless, gel-like solid which was recrystallised from MeCN/Et_2O to a white powder. Although we were unable to obtain satisfactory microanalytical data for this complex, likely due to the glassy nature of the product, the spectroscopic data are in accordance with the formulation above. IR (Nujol/cm^{-1}): ν = 568br,s (Sn-F). ^{1}H NMR (CD_3NO_2, 298 K): δ = 8.9 (m), 8.8 (m), 8.4 (m), 8.3 (m), 7.9 (m), 7.8 (m). $^{19}F\{^1H\}$ NMR (CD_3NO_2, 298 K): δ = -165.8 (m, $^1J_{117SnF}$ = 1637 Hz, $^1J_{119SnF}$ = 1717 Hz, $^2J_{FF}$ = 40 Hz), -158.8 (d, $^1J_{117SnF}$ = 1658 Hz, $^1J_{119SnF}$ = 1737 Hz, $^2J_{FF}$ = 40 Hz), -157.2 (s), $^1J_{117SnF}$ = 1515 Hz, $^1J_{119SnF}$ = 1588 Hz), -79.9 (s, OTf). ^{119}Sn NMR (CH_3NO_2, 253 K): n.o.

2.4.8 $[SnF_3(OPPh_3)_3][OTf]$

$[SnF_4(OPPh_3)_2]$ (0.073 g, 0.097 mmol) was dissolved in CH_2Cl_2 (10 mL). To this TMSOTf (0.20 g, 0.91 mmol) was added in CH_2Cl_2 (5 mL). The solution was stirred for 2 h. To this $OPPh_3$ (0.027 g, 0.097 mmol) then added and the solution was stirred for 2 h. The solution was concentrated *in vacuo* and excess hexane was added, the solvent was removed, and the resulting white powder was dried *in vacuo*. Yield 0.070 g, 63%. Required for $C_{55}H_{45}F_6O_6P_3SSn{\cdot}2.5CH_2Cl_2$ (1372.0): C, 50.34; H, 3.67. Found: C, 50.00; H, 3.50%. IR (Nujol/cm^{-1}): ν = 1145sh, 1059 P=O), 554m, 537m (Sn-F). ^{1}H NMR (CD_2Cl_2, 298 K): δ = 7.9-7.3(m). $^{19}F\{^1H\}$ NMR (CD_2Cl_2, 298 K): δ = -142.1 (s), -141.2 (t, $^2J_{FF}$ = 61 Hz), -134.5(d, $^2J_{FF}$ = 61 Hz), -79.1 (s, OTf). $^{31}P\{^1H\}$ NMR (CD_2Cl_2, 298 K): δ = 46.0 (s), 43.9 (s), 41.7 (s). ^{119}Sn NMR (CH_3NO_2, 253 K): n.o.

2.4.9 $[SnF_2(OPPh_3)_4][OTf]_2$

$[SnF_4(OPPh_3)_2]$ (0.085 g, 0.11 mmol) was dissolved in CH_2Cl_2 (5 mL). To this TMSOTf (0.050 g, 0.23 mmol) was added in CH_2Cl_2 (5 mL). The suspension was stirred for 2 h and then $OPPh_3$ (0.063 g, 0.23 mmol) was added, and the solution was stirred for a further 2 h. The solution was concentrated *in vacuo* and excess hexane was added, the solvent was decanted, and the resulting white powder was dried *in vacuo*. Yield 0.08 g, 47%. Required for $C_{74}H_{60}F_8O_{10}P_4S_2Sn{\cdot}CH_2Cl_2$ (1652.9): C, 54.5; H, 3.8. Found: C, 54.6; H, 3.8%. IR (Nujol/cm^{-1}): ν = 1150s, 1060 (P=O), 550s, 537s, 517m (Sn-F). ^{1}H NMR (CD_3NO_2, 298K): δ = 7.3-7.9 (m). $^{19}F\{^1H\}$ NMR (CD_3NO_2, 298 K): δ = -123.1 (s, $^1J_{117SnF}$= 1730, $^1J_{119SnF}$= 1812 Hz), -122.4 (s, $^1J_{117SnF}$= 1977, $^1J_{119SnF}$= 2069 Hz), -79.8 (s, OTf). $^{31}P\{^1H\}$ NMR (CD_3NO_2, 298 K): δ = 50.5 (s, $^2J_{SnP}$= 78 Hz), 48.4 (s, $^2J_{SnP}$= 78 Hz), 47.1 (s, $^1J_{SnP}$= 96 Hz) average ^{117}Sn/^{119}Sn; separate couplings were not resolved. ^{119}Sn NMR (CH_3NO_2, 253 K): n.o.

2.5 X-ray crystallographic data

Table 11: Table of X-ray crystallographic data[a] for the crystal structures described in 2.

Compound	$[SnF_4(pyNO)_2]\cdot CH_2Cl_2$	$[SnF_4(py)_2]$	$[SnF_2(OPPh_3)_4][OTf]_2$
Formula	$C_{22}H_{24}Cl_4F_8N_4O_4Sn_2$	$C_{10}H_{10}F_4N_2Sn$	$C_{74}H_{60}F_8O_{10}P_4S_2Sn$
M	469.82	342.81	1567.91
Crystal system	Triclinic	Triclinic	Triclinic
Space group (no.)	P-1 (2)	P-1 (2)	P-1 (2)
a /Å	9.4615(3)	6.3696(4)	13.7031(3)
b /Å	11.2482(3)	7.2222(4)	15.6126(4)
c /Å	15.4968(5)	7.2263(3)	18.1412(4)
α /°	90.899(3)	117.933(5)	69.740(2)
β /°	103.213(3)	91.612(4)	70.468(2
γ /°	101.930(3)	109.045(5)	76.875(2)
U /Å^3	1567.47(9)	271.02(3)	3404.20(15)
Z	4	1	2
μ(Mo-K_α) /mm^{-1}	2.019	2.387	0.613
F(000)	911.269	160	1596
Total number reflns	20963	6755	80126
R_{int}	0.077	0.043	0.050
Unique reflns	7617	1396	17545
No. of params, restraints	397, 0	79, 0	892, 0
GOF	1.0361	1.182	1.020
R_1, wR_2 [I > 2σ(I)][b]	0.055, 0.156	0.067, 0.211	0.047, 0.116
R_1, wR_2 (all data)	0.068, 0.164	0.067, 0.211	0.066, 0.130

[a]Common items: T = 293 K; wavelength (Mo-K_α) = 0.71073 Å; θ(max) = 27.5°; [b] $R_1 = \Sigma||Fo|-|Fc||/\Sigma|Fo|$; $wR_2=[\Sigma w(Fo^2-Fc^2)^2/\Sigma wFo^4]^{1/2}$

2.6 References

1. Harrison, P. G., Blackie, *Chemistry of tin*; Chapman and Hall: Glasgow; New York, 1989.

2. Ruzicka, S. J.; Merbach, A. E., *Inorganica Chimica Acta* **1976,** *20*, 221-229.

3. Ruzicka, S. J.; Merbach, A. E., *Inorganica Chimica Acta* **1977,** *22*, 191-200.

4. Davis, M.The Synthesis and Characterisation of Complexes of Tin and Germanium Fluorides with Soft Donor Ligands. PhD Thesis, University of Southampton, 2008.

5. Davis, M. F.; Clarke, M.; Levason, W.; Reid, G.; Webster, M., *European Journal of Inorganic Chemistry* **2006,** *2006*, 2773-2782.

6. Mather, G. G.; McLaughlin, G. M.; Pidcock, A., *Journal of the Chemical Society, Dalton Transactions* **1973**, 1823-1827.

7. Levason, W.; Matthews, M. L.; Patel, R.; Reid, G.; Webster, M., *New Journal of Chemistry* **2003,** *27*, 1784-1788.

8. E. Dann, S.; R. J. Genge, A.; Levason, W.; Reid, G., *Journal of the Chemical Society, Dalton Transactions* **1997**, 2207-2214.

9. Dann, S. E.; Genge, A. R. J.; Levason, W.; Reid, G., *Journal of the Chemical Society, Dalton Transactions* **1996**, 4471-4478.

10. Genge, A. R. J.; Levason, W.; Reid, G., *Inorganica Chimica Acta* **1999,** *288*, 142-149.

11. Greenacre, V. K.; King, R. P.; Levason, W.; Reid, G., *Dalton Transactions* **2019,** *48*, 17097-17105.

12. Harrison, P.; Lane, B.; Zuckerman, J., *Inorganic Chemistry* **1972,** *11*, 1537-1543.

13. Abel, E. W.; Bhargava, S. K.; Orrell, K. G.; Sik, V., *Inorganica Chimica Acta* **1981,** *49*, 25-30.

14. Burt, J.; Levason, W.; Reid, G., *Coordination Chemistry Reviews* **2014,** *260*, 65-115.

15. R. Willey, G.; J. Woodman, T.; Somasundaram, U.; R. Aris, D.; Errington, W., *Dalton Transactions* **1998**, 2573-2576.

16. Willey, G. R.; Jarvis, A.; Palin, J.; Errington, W., *Dalton Transactions* **1994**, 255-258.

17. MacDonald, E.; Doyle, L.; Chitnis, S. S.; Werner-Zwanziger, U.; Burford, N.; Decken, A., *Chemical Communications* **2012,** *48*, 7922-7924.

18. Tudela, D.; Rey, F., *Zeitschrift für anorganische und allgemeine Chemie* **1989,** *575*, 202-208.

19. Cheng, F.; Davis, M. F.; Hector, A. L.; Levason, W.; Reid, G.; Webster, M.; Zhang, W., *European Journal of Inorganic Chemistry* **2007,** *2007*, 2488-2495.

20. Bork, M.; Hoppe, R., *Zeitschrift für anorganische und allgemeine Chemie* **1996,** *622*, 1557-1563.

21. D. Tudela, F. P., Wiley, *Inorganic Syntheses*: 1997; Vol. 31.

22. Davis, M. F.; Levason, W.; Reid, G.; Webster, M., *Polyhedron* **2006,** *25*, 930-936.

23. Adley, A. D.; Bird, P. H.; Fraser, A. R.; Onyszchuk, M., *Inorganic Chemistry* **1972,** *11*, 1402-1409.

24. Gerald R. Willey; Timothy J. Woodman; Robert J. Deeth; William Errington, *Main Group Metal Chemistry* **1998,** *21*, 583-592.

25. Davis, M. F.; Levason, W.; Reid, G.; Webster, M.; Zhang, W., *Dalton Transactions* **2008**, 533-538.

26. Chandrasekhar, V.; Singh, P., *Dalton Transactions* **2011,** *40*, 114-123.

27. Beattie, C.; Farina, P.; Levason, W.; Reid, G., *Dalton Transactions* **2013,** *42*, 15183-15190.

28. Suter, R.; Swidan, A. a.; Zijlstra, H. S.; Macdonald, C. L. B.; McIndoe, J. S.; Burford, N., *Dalton Transactions* **2018,** *47*, 16729-16736.

29. Suter, R.; Swidan, A. a.; Macdonald, C. L. B.; Burford, N., *Chemical Communications* **2018,** *54*, 4140-4143.

30. Basu Baul, T.; Basaiawmoit, *J. Indian Chemistry Society.* **1993,** *70*, 151-152.

31. Baul, T. S. B.; Dey, D.; Mishra, D. D.; Basaiawmoit, W. L.; Rivarola, E., *Journal of Organometallic Chemistry* **1993,** *447*, 9-13.

32. Everett, M.; Jolleys, A.; Levason, W.; Light, M. E.; Pugh, D.; Reid, G., *Dalton Transactions* **2015,** *44*, 20898-20905.

33. Benjamin, S. L.; Levason, W.; Reid, G., *Chemical Society Reviews* **2013,** *42*, 1460-1499.

34. King, R. P.; Woodward, M. S.; Grigg, J.; McRobbie, G.; Levason, W.; Reid, G., *Dalton Transactions* **2021,** *50*, 14400-14410.

35. King, R. P.; Levason, W.; Reid, G., *Dalton Transactions* **2021,** *50*, 17751-17765.

36. Kuziola, J.; Magre, M.; Nöthling, N.; Cornella, J., *Organometallics* **2022**.

37. Michelson, C. E.; Dyer, D. S.; Ragsdale, R. O., *Journal of Inorganic and Nuclear Chemistry* **1970,** *32*, 833-838.

38. Wilkins, C. J.; Haendler, H. M., *Journal of the Chemical Society (Resumed)* **1965**, 3174-3179.

39. Dean, P. A. W.; Evans, D. F., *Journal of the Chemical Society A: Inorganic, Physical, Theoretical* **1968**, 1154-1166.

40. Clark, H.; Kwon, J.; Reeves, L.; Wells, E., *Canadian Journal of Chemistry* **1963,** *41*, 3005-3012.

3 Synthesis of neutral and cationic germanium(IV) fluoride complexes with hard N- and O-donor ligands

Previous work on hard O- and N-donor ligands, such as phosphine oxide and amine ligands, has demonstrated that GeF_4 has a much greater affinity for these ligands than the analogous heavier halides, GeX_4, where X = Cl, Br or I.[1-3] As an extension of this work, the reactions of GeF_4 with a wider range of hard donor ligands has been explored, similar to those studied with SnF_4 in Chapter 2, allowing for the key spectroscopic data for $[GeF_4(L)_2]$ and $[GeF_3(L)_3]^+$ to be directly compared to the Sn(IV) analogues. The knowledge of $^{19}F\{^1H\}$ NMR chemical shifts for analogous tin complexes, in particular, provides a useful guide for the germanium systems. DFT calculations have been used to explore the changes in electronic structure and bonding as fluoride ligands are sequentially removed from the Ge(IV) centre.

3.1 Introduction

Germanium is in Group 14 of the periodic table and has a smaller covalent radius than tin, 1.22 Å compared to 1.41 Å, respectively.[4] Germanium has one NMR active nucleus, ^{73}Ge, with a nuclear spin of 9/2, a natural abundance of 7.76% and a very low receptivity of 0.617.[5] It has a large quadrupole moment and therefore, other than in highly symmetrical environments, typically gives NMR spectroscopic signals that are very broad or unobtainable and so there are very few ^{73}Ge NMR resonances reported in the literature, and given the low symmetry of the complexes, no ^{73}Ge NMR studies were undertaken in this work.

3.1.1 Neutral complexes of Ge(IV) fluoride

As with the SnF_4 chemistry described in Chapter 2, a more convenient pathway into GeF_4 chemistry is through the molecular synthon $[GeF_4(MeCN)_2]$, whereby the weakly bound MeCN ligands can be readily displaced by other ligands. GeF_4 is a gas at atmospheric pressure, with a boiling point of -36.5 °C, and it is not convenient to handle. The acetonitrile adduct is a colourless solid and is easier to handle and therefore, easier to control its stoichiometry in a reaction. The $[GeF_4(MeCN)_2]$ was synthesised according to the literature method by bubbling GeF_4 gas through an anhydrous acetonitrile solution (Scheme 18), whereby the complex immediately precipitates out of solution as a colourless solid, which can be stored for months under anhydrous conditions.[6] The IR spectrum for this complex contains broad ν/(Ge-F) bands at 688, 657, 639 cm^{1}.

$$GeF_4 \xrightarrow{MeCN} [GeF_4(MeCN)_2]$$

Scheme 18: Schematic for the synthesis of $[GeF_4(MeCN)_2]$.[7]

The reaction of $[GeF_4(MeCN)_2]$ with the bidentate N-donor ligands; 2,2'-bipy, 1,10-phen and $Me_2N(CH_2)_2NMe_2$ (L-L) in a 1:1 molar ratio in anhydrous MeCN forms isolatable solids of the form $[GeF_4(L\text{-}L)]$, which are air and moisture stable.[2] The $^{19}F\{^1H\}$ NMR spectra for these complexes show two triplets of equal intensity, consistent with the presence of the *cis* isomer only, the expected result due to the ligand "locking" the geometry of the complex. The crystal structure of $[GeF_4(1,10\text{-phen})]$ is shown in Figure 3.1.[2]

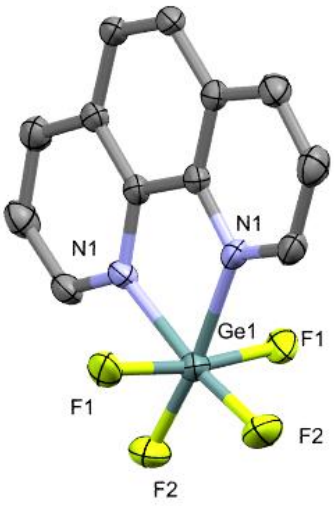

Figure 3.1: Structure of $[GeF_4(1,10\text{-phen})]$. Redrawn from Reference.[2]

Stable complexes have also been isolated from the reaction of $GeCl_4$ and KSCN with both 2,2'-bipy and 1,10-phen.[8] The direct reaction of Me_4cyclam and $[GeF_4(MeCN)_2]$ leads to the formation of $[GeF_4(\kappa^2\text{-}Me_4cyclam)]$, with two coordinated nitrogens in a *meso* configuration and the other two nitrogen atoms bent away and not interacting with the metal centre (Figure 3.2), with the four fluorides retained. It was rationalised that they did not form *endocyclic* dications due to the displacement of two fluorides being energetically unfavourable.[2]

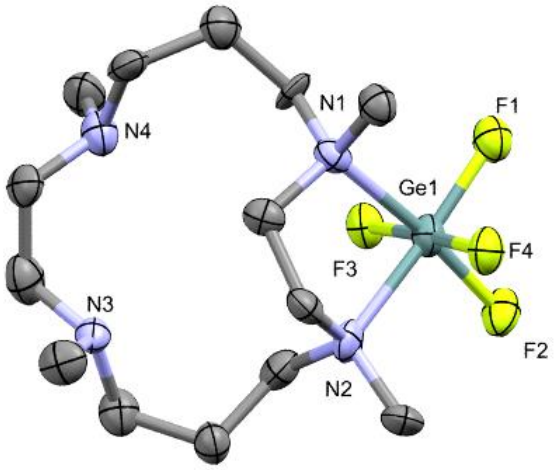

Figure 3.2: Structure of [$GeF_4(\kappa^2$-Me_4cyclam)]. Redrawn from Reference.[2]

Germanium(IV) fluoride can also form stable complexes with hard O-donor ligands, with early examples of [$GeF_4(L)_2$] adducts, where L = H_2O, CH_3OH and $(CH_3)_2CO$, being characterised by vibrational spectroscopy.[9, 10] The reactions of [$GeF_4(MeCN)_2$] with R_3PO (R = Me, Et or Ph) in a 1:2 molar ratio yielded colourless powders in the form [$GeF_4(R_3PO)_2$]. Both *cis* and *trans* isomers are present in the $^{19}F\{^1H\}$ NMR spectra, but only the *trans* isomers are identified in the solid state using X-ray crystallography.[1] Crystals of both *trans*-[$GeF_4(Me_3PO)_2$] and *trans*-[$GeF_4(Et_3PO)_2$] were grown from the evaporation of a MeCN solution, whereas *trans*-[$GeF_4(Ph_3PO)_2$] crystals were unexpectedly grown from the reaction of [$GeF_4(MeCN)_2$] and Ph_3P in CH_2Cl_2, due to oxidation by adventitious air (oxygen).[11]

Reactions of [$GeF_4(MeCN)_2$] with soft thioether donor ligands, $RS(CH_2)_2SR$ (R = Me or Et), to form [$GeF_4\{RS(CH_2)_2SR\}$], are the only known examples of complexes of this type and they are highly moisture sensitive (the crystal structure of [$GeF_4\{MeS(CH_2)_2SMe\}$] is shown in Figure 3.3). They have a distorted octahedral geometry and contain weakly coordinating, chelating thioethers.[12] These complexes are very labile and are extensively dissociated in solution at ambient temperature and ^1H and $^{19}F\{^1H\}$ NMR spectroscopy experiments in CH_2Cl_2 at -90 °C show that the low temperature limiting spectra were not reached, it was thought that this was most likely due to fast pyramidal inversion still occurring.

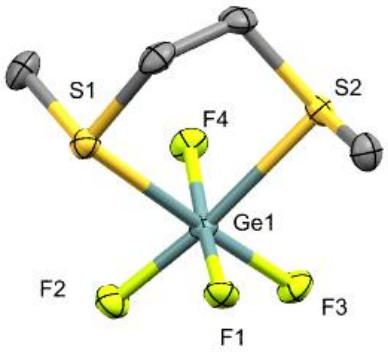

Figure 3.3: Crystal structure of $[GeF_4\{MeS(CH_2)_2SMe\}]$, redrawn from Reference.[13]

Soft donor ligand complexes of GeF_4 with tertiary phosphine ligands also exist. These include *trans*-$[GeF_4(PR_3)_2]$ (R = Me, Ph, ^{i}Pr), *cis*-$[GeF_4\{R_2P(CH_2)_2PR_2\}]$ (R = Me, Et, Ph, Cy), and *cis*-$[GeF_4\{o\text{-}C_6H_4(PR_2)_2\}]$ (R = Me, Ph), all of which have been characterised systematically, with crystal structures of $[GeF_4\{Ph_2P(CH_2)2PPh_2\}]$ and $[GeF_4\{o\text{-}C_6H_4(PMe_2)_2\}]$ being identified. These phosphine complexes slowly convert to the corresponding phosphine oxide complexes, however, the corresponding reactions with arsine ligands formed complexes that were significantly less stable and none have been isolated or characterised in the literature. Contrastingly, moving to the heavier halides, reactions of $GeCl_4$ with arsine ligands have demonstrated the formation of stable $[GeCl_4(AsR_3)_2]$ (R = Me or Et) complexes, however the reaction of $GeCl_4$ with PMe_3 produces $[PMe_3Cl][GeCl_3]$, *via* a redox reaction.[13]

3.1.2 Cationic Ge(IV) complexes

There are relatively few reports of cationic germanium(IV) fluoride complexes in the literature, the cation $[GeF_3(Me_3tacn)]^+$ being one that was successfully synthesised in 2007.[2] The corresponding reaction of $[GeF_4(MeCN)_2]$ with the triaza-macrocycle, Me_3tacn, forms an isolatable solid of $[GeF_3(Me_3tacn)]_2[GeF_6]$, which was found to be insoluble in all common NMR solvents. A crystal structure of $[GeF_3(Me_3tacn)]Cl$ was however isolated (as shown in Figure 3.4), with the chloride anion thought to be derived from the reaction solvent, CH_2Cl_2. The structure confirms the presence of a *fac* GeF_3N_3 unit in the cation.[2]

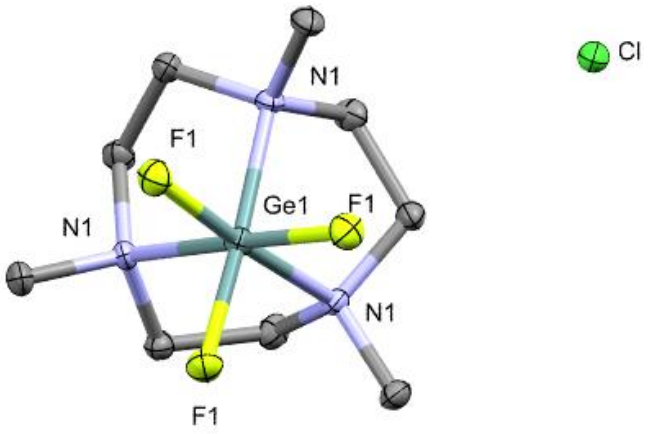

Figure 3.4: Structure of $[GeF_3(Me_3tacn)]Cl$. Redrawn from Reference.[2]

The soft donor analogue $[9]aneS_3$ was shown to not be a strong enough donor to displace fluoride from $[GeF_4(MeCN)_2]$; however the $^{19}F\{^1H\}$ NMR spectrum at 243 K shows a mixture of $[GeF_4(MeCN)_2]$ and $[9]aneS_3$, as well as two triplets of equal intensity, which were attributed to the formation of *cis*-$[GeF_4(\kappa^2\text{-}[9]aneS_3)]$.[13]

Dicationic germanium(IV) complexes can also be synthesised *via* oxidation of Ge(II) complexes using a fluoride source. For example, the reaction of $[Ge(BIMEt_3)][OTf]_2$ with the oxidising agent XeF_2 yields pure $[GeF_2(BIMEt_3)][OTf]_2$ as mentioned in Section 2.1.2.[14] The X-ray crystal structure of this complex reveals a distorted octahedron with *cis* fluorines. The treatment of $[GeF_2(BIMEt_3)][OTf]_2$ with the halide abstractor TMSOTf yields the Ge(IV) monofluoride complex, $[GeF(BIMEt_3)OTf][OTf]_2$, with one triflate coordinating to the germanium centre and completing the distorted octahedron, the crystal structures of both Ge(IV) fluoride complexes can be seen in Figure 3.5.

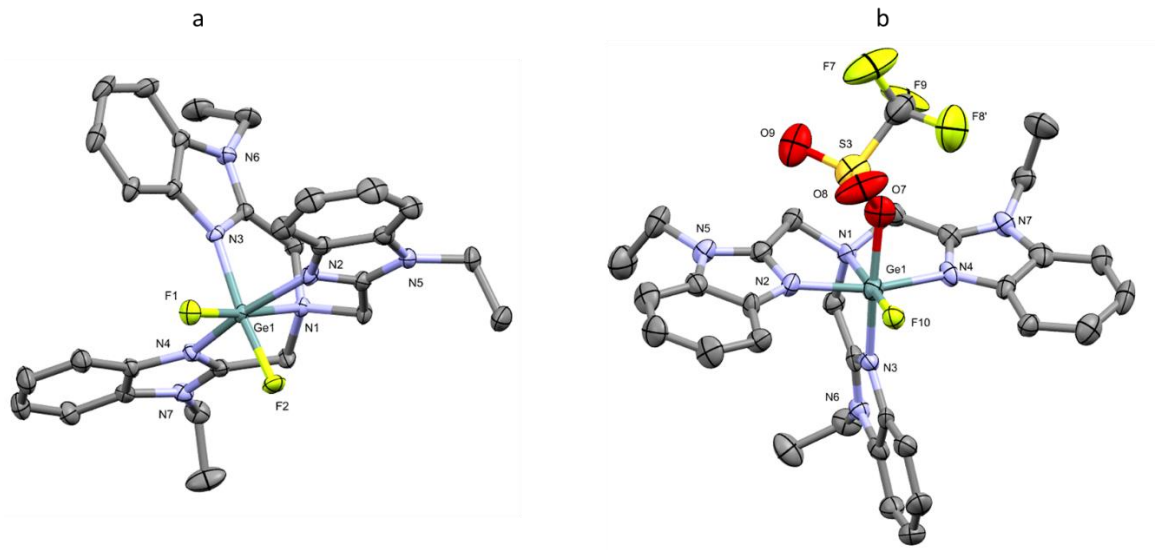

Figure 3.5: X-Ray crystal structures of cationic Ge(IV) complexes $[GeF_2(BIMEt_3)]^{2+}$ (a) and $[GeF(BIMEt_3)(OTf)]^{2+}$ (b).[14]

The reactions of the phosphine complex, $[GeF_4(PMe_3)_2]$, with one molar equivalent of TMSOTf has been investigated, leading to the formation of $[GeF_3(PMe_3)_2(OTf)]$ (Figure 3.6). It can be noted that the triflate binds directly to the Ge(IV) centre, instead of forming a cationic complex with a discrete triflate anion, as demonstrated in the Sn(IV) fluoride chemistry in Chapter 2 and the Ge(IV) fluoride chemistry below. The analogous tin tetrachloride reaction results in the formation of the cationic complex, $[SnCl_3(PMe_3)_2]^+$.[15]

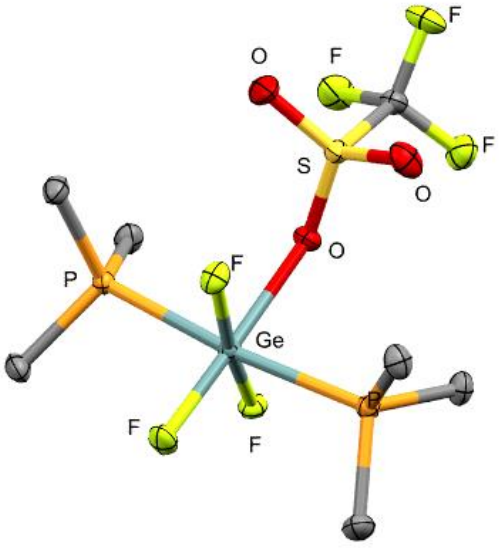

Figure 3.6: The crystal structure of $[GeF_3(PMe_3)_2(OTf)]$ with *mer* fluorines and *trans* phosphines.[16]

Other examples include $[GeF_{4-n}(PMe_3)_2(OTf)_n]$ (n = 1- 3), and $[GeF_{4-n}\{o\text{-}C_6H_4(PMe_2)_2\}(OTf)_n]$ (n = 1-3). However, with the bulkier ligand, ^{i}Pr, $[GeF_3(^{i}Pr_3P)_2][OTf]$ was believed to be formed, containing the $[GeF_3(^{i}Pr_3P)_2]^+$ cation. The tri-isopropyl phosphine ligand has a much greater Tolman cone angle than PMe_3 and therefore there is a greater steric crowding at the Ge(IV) centre, hindering coordination of the triflate.[16]

3.1.3 Aims

The aim of this Chapter was to develop the underlying coordination chemistry of Ge(IV) fluoride:

i. to develop a systematic series of GeF_4 complexes with neutral ligands, with the emphasis on hard nitrogen and oxygen donor ligands;
ii. to test the sequential removal of a fluoride using TMSOTf to form cationic complexes and to draw comparisons with the tin(IV) fluoride chemistry discussed in Chapter 2.

This work will also help us to understand whether a similar approach can be used to form triaza and tetra-aza macrocyclic complexes and whether they could be suitable candidates to assess as potential ^{18}F carriers for PET imaging.

Complexes have predominantly been characterised by ^{1}H, $^{19}F\{^{1}H\}$ and $^{31}P\{^{1}H\}$ NMR and IR spectroscopy, along with microanalyses, with the structures of two novel complexes elucidated using X-ray crystallography.

3.2 Results and Discussion

3.2.1 Reactions of GeF_4 with neutral, monodentate N- and O-donor ligands

$[GeF_4(L)_2]$ complexes were prepared by the reaction of $[GeF_4(MeCN)_2]$ with the appropriate ligand (L = dmso, dmf, pyNO, py, $OPPh_3$, $OPMe_3$, $OAsPh_3$). Whilst the dmso complex, $[GeF_4(dmso)_2]$, was synthesised successfully from the acetonitrile adduct, residual dmso proved difficult to remove completely from the isolated complex and therefore an alternative route was found. This involved directly reacting GeF_4 gas in hexane, containing dmso (0.5 mL). The corresponding complexes with py, $OPPh_3$, $OPMe_3$, and $OAsPh_3$ ligands have been described in previous work, with crystal structures of the latter three being reported.[1, 2] The three novel complexes and their reactions that were developed in this work are shown in Scheme 19.

$$[GeF_4(MeCN)_2] \xrightarrow[CH_2Cl_2,\ 2\ h,\ 50\ °C]{\text{excess dmf}} [GeF_4(dmf)_2]$$

$$[GeF_4(MeCN)_2] \xrightarrow[CH_2Cl_2,\ 2\ h,\ RT]{\text{excess pyNO}} [GeF_4(pyNO)_2]$$

$$GeF_4 \xrightarrow[hexane,\ 1\ h,\ RT]{\text{dmso}} [GeF_4(dmso)_2]$$

Scheme 19: Schematics for the synthesis of $[GeF_4(dmf)_2]$, $[GeF_4(pyNO)_2]$ and $[GeF_4(dmso)_2]$, developed in this work.

In solution, generally at low temperatures, the $^{19}F\{^1H\}$ NMR spectroscopic data typically show two 1:2:1 triplets with equal integrations for the *cis* isomer, with $^2J_{FF}$ between 55 and 64 Hz, as well as a singlet, representing the *trans* isomer. However, at ambient temperatures, some of the NMR spectroscopic data for $[GeF_4(L)_2]$ (L= dmso, dmf, py, pyNO, $OPPh_3$, $OPMe_3$, $OAsPh_3$) show that the complexes are exchanging and that the ratio of each isomer in solution differs depending on complex and solvent conditions, see Table 12 for details.

Typical examples of the $^{19}F\{^1H\}$ NMR spectra obtained for these complexes are shown in Figure 3.7 for $[GeF_4(dmf)_2]$ in CD_3NO_2. The spectrum at 298 K shows one sharp singlet (due to the *trans* isomer) and two very broad resonances. However, upon cooling to 253 K the broad lines resolve into two sharp triplets, as expected for the *cis* isomer. This observation is indicative of dissociation of the neutral ligand in solution, suggesting that exchange of the ligand is easier for the *cis* isomer than the *trans* isomer, and that the *trans* isomer is not involved in this process.

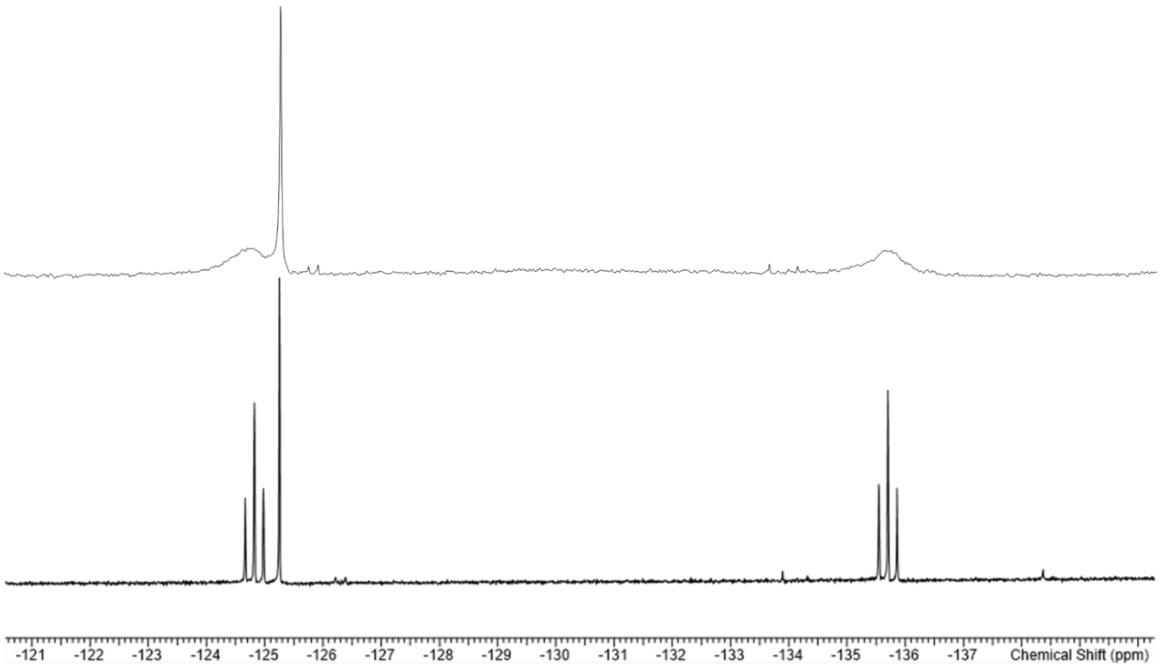

Figure 3.7: $^{19}F\{^{1}H\}$ NMR spectra of the *cis/trans* isomer mixture from $[GeF_4(dmf)_2]$ at 298 K (top spectrum) and at 253 K (bottom spectrum) (CD_3NO_2).

Table 12: Selected NMR spectroscopic data of $[GeF_4(L)_2]$ (L= dmso, dmf, py, pyNO, $OPPh_3$, $OPMe_3$, $OAsPh_3$ and MeCN).[17]

	Solvent Temperature	$^{19}F\{^{1}H\}$ NMR / ppm[a]	$^{2}J_{FF}$ /Hz	$^{31}P\{^{1}H\}$ NMR / ppm	
$[GeF_4(dmso)_2]$ *cis* *trans*	CD_3NO_2 253K	-115.3 (t), -129.8 (t) -115.4 (s)	61		This work
$[GeF_4(dmf)_2]$ *cis* *trans*	CD_3NO_2 253K	-125.4 (t), -135.8 (t) -125.4 (s)	59		This work
$[GeF_4(py)_2]$ *trans*	$CDCl_3$ 253K	-125.7(s)			Reference[18]

$[GeF_4(pyNO)_2]$ *trans*	CD_3NO_2 298K	-142.8(br s)			This work
$[GeF_4(OPPh_3)_2]$ *cis* *trans*	$CDCl_3$ 253K	-100.9(t), -120.6(t) -105.3(s)	64	40.8(s) 40.2(s)	Reference[1]
$[GeF_4(OPMe_3)_2]$ *cis* *trans*	CD_2Cl_2 298K	-107.6(t), -121.6(t) -109.9(s)	58	65.1(s) 65.8(s)	Reference[1]
$[GeF_4(OAsPh_3)_2]$ *cis* *trans*	CD_2Cl_2 298K	-94.4(t), -112.9(t) -98.2(s)	60		Reference[1]
$[GeF_4(MeCN)_2]$ *cis* *trans*	CD_2Cl_2 180K	-101.2(t), -134.2 (t) -108.2(s)	55		Reference[7]

3.2.2 Reactions of $[GeF_4(MeCN)_2]$ and TMSOTf with N- and O-donor monodentate ligands

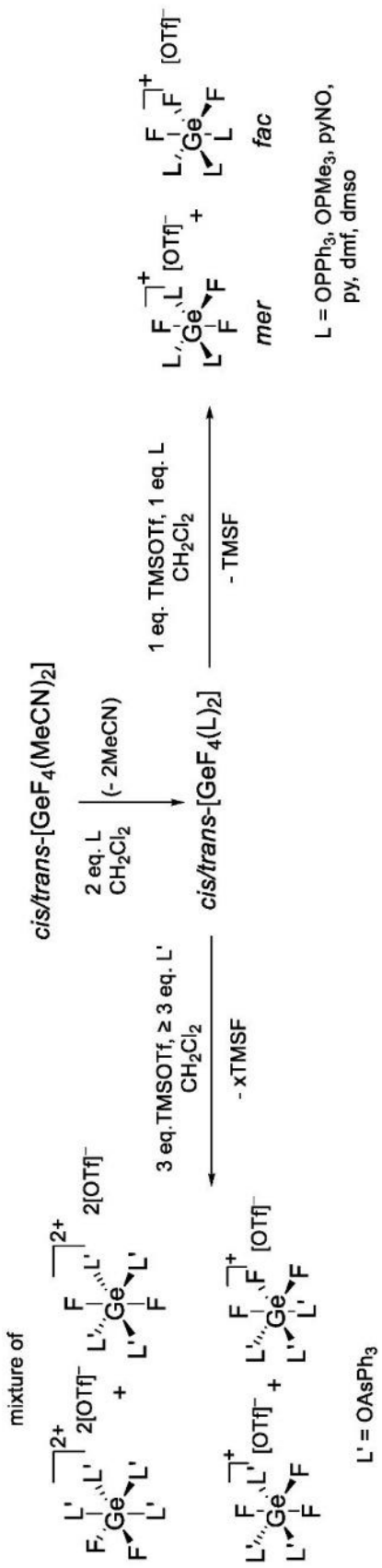

Scheme 20: The generic schematic for the synthesis of Ge(IV) cationic complexes, where L = $OPPh_3$, $OAsPh_3$, $OPMe_3$, pyNO, py, DMF, DMSO and L' = $OAsPh_3$.

The synthesis of the Ge(IV) fluoride cationic complexes required significantly longer reaction times than the Sn(IV) analogues and it proved more difficult to drive the reactions to completion; this can be rationalised by the higher bond dissociation energies associated with the smaller Ge centre, i.e., stronger Ge-F bonds, when comparing it to the Sn-F bond, hence abstraction is more difficult and this therefore affects the energy barrier for the substitution mechanism. The Lewis acidity may also have a small influence, with the lower acceptor power of Ge(IV) in comparison to Sn(IV). Similarly to the work in Chapter 2, the general approach to the synthesis of these $[GeF_3(L)_3]^+$ cations was the reaction of $[GeF_4(L)_2]$ with one equivalent of TMSOTf in anhydrous CH_2Cl_2, followed by addition of one equivalent of L, where L = dmso, dmf, py, pyNO, $OPPh_3$, $OPMe_3$ or $OAsPh_3$. An attempt to react $[GeF_4(MeCN)_2]$ with TMSOTf and further MeCN ligand was unsuccessful, causing decomposition.[17]

The reaction to form $[GeF_3(dmso)_3][OTf]$ (Scheme 21) took 72 hours to reach completion. Its $^{19}F\{^1H\}$ NMR spectrum is similar to that of the tin analogue which only required four hours, as seen in Chapter 2.2.2.

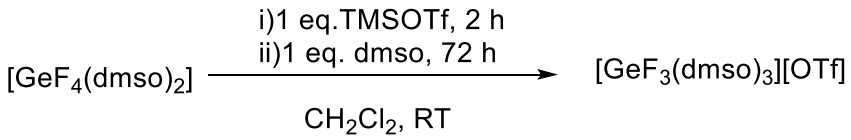

Scheme 21: Schematic for the synthesis of $[GeF_3(dmso)_3][OTf]$.

The $^{19}F\{H\}$ NMR spectrum for $[GeF_3(dmso)_3][OTf]$ in Figure 3.8 shows a singlet at -122.2 ppm and a triplet and doublet at -121.7 and -109.8 ppm ($^2J_{FF}$ = 71 Hz), corresponding to the *fac* and *mer* complexes, respectively. An unknown, minor impurity peak, which does not correspond to the starting materials is also present at -116.9 ppm. It is hypothesised that this could be the *trans* difluoride species, possibly resulting from the difficulties in measuring the very small volumes of TMSOTf required to achieve the intended 1:3 Ge to ligand stoichiometry.

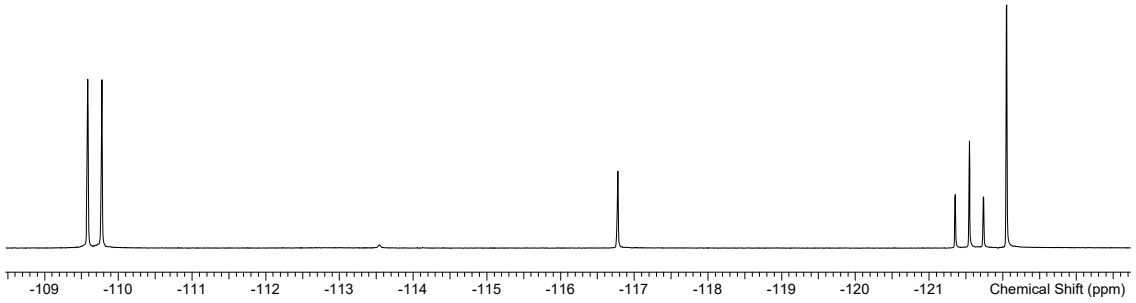

Figure 3.8: $^{19}F\{^1H\}$ NMR spectrum of $[GeF_3(dmso)_3][OTf]$ (CD_3NO_2, 298 K). Triflate resonance at -79 ppm omitted for clarity.

The expected spectroscopic results were also obtained for $[GeF_3(dmf)_3][OTf]$, with a sharp singlet at -134.7 ppm for the *fac* isomer and a sharp triplet and doublet at -135.2 and -126.5 ppm, respectively, with a $^2J_{FF}$ coupling constant of 66 Hz in the $^{19}F\{^1H\}$ NMR spectrum.

Attempts to isolate a pure sample of $[GeF_3(pyNO)_3][OTf]$ were unsuccessful. The products that were obtained were difficult to isolate due to their viscous nature and NMR spectroscopic studies consistently showed a mixture of both $[GeF_4(pyNO)_2]$ and $[GeF_3(pyNO)_3][OTf]$ species, despite particular care given to achieve the target reagent stoichiometries. The $^{19}F\{^1H\}$ NMR spectrum of the mixture is shown in Figure 3.9. However, the desired cationic product does form, but is somewhat unstable in CD_3NO_2 solution and degrades over time. The elemental analysis shows close to the expected CHN composition for the desired cationic complex, with one CH_2Cl_2 solvent molecule i.e., $C_{16}H_{15}F_6GeN_3O_6S{\cdot}CH_2Cl_2$ (648.9): calcd. C, 31.46, H 2.64, N 6.48; found C 31.62, H, 2.94, N, 7.18%. This further adds to the likelihood that it is unstable in solution, but not in the solid phase.

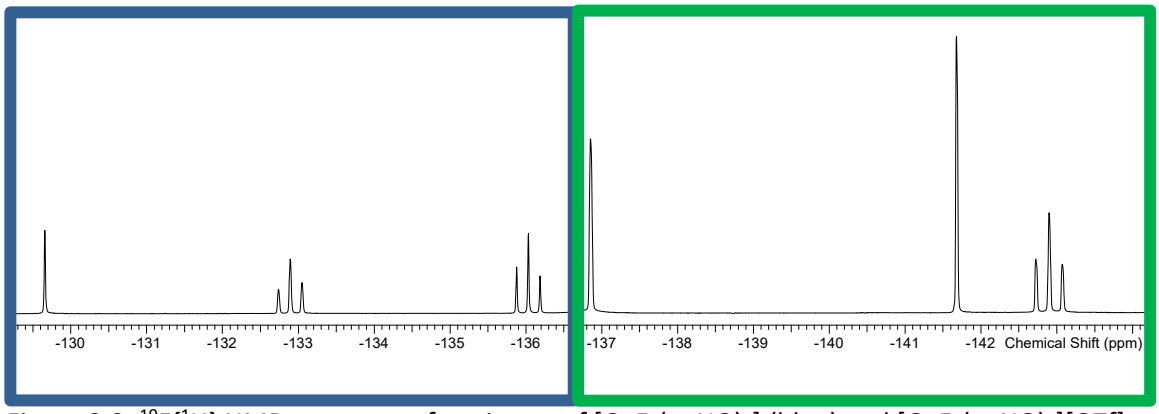

Figure 3.9: $^{19}F\{^1H\}$ NMR spectrum of a mixture of $[GeF_4(pyNO)_2]$ (blue) and $[GeF_3(pyNO)_3][OTf]$ (green) (CD_3NO_2, 298 K). Triflate resonance at -79 ppm omitted for clarity.

Obtaining crystals for the series of $[GeF_3(L)_3]^+$ type cations proved challenging, presumably due to reversible ligand exchange in solution. However, crystals of $[GeF_3(OPPh_3)_3][OTf]$ were obtained from a CH_2Cl_2 solution by slow evaporation and the X-ray structure solution revealed them to be of the *mer* isomer, as shown in Figure 3.10.

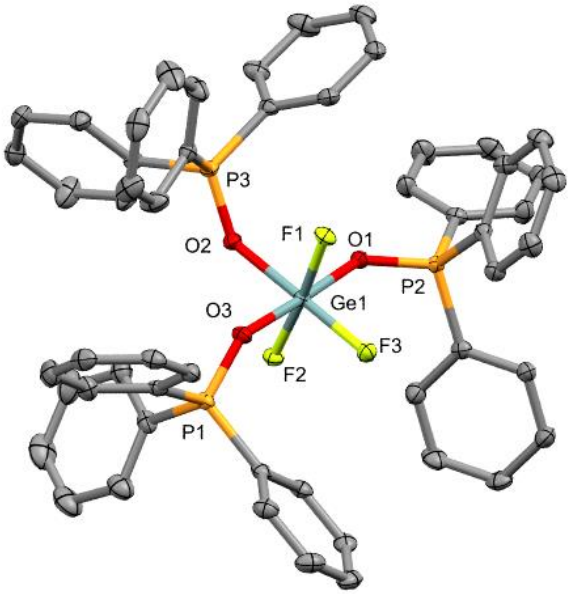

Figure 3.10: Crystal structure of *mer*-$[GeF_3(OPPh_3)_3]^+$ showing the atom labelling scheme. There are two crystallographically independent molecules in the asymmetric unit, only one of which is shown, the second is very similar. The ellipsoids are drawn at the 50% probability level and H atoms and OTf anions are omitted for clarity. Selected bond lengths (Å) and angles (°) are: Ge1-F3 = 1.7598(11), Ge1-F1 = 1.7679(11), Ge1-F2 = 1.7628(11), Ge1-O2 = 1.8950(13), Ge1-O3 = 1.9076(13), Ge1-O1 = 1.8990(13), P3-O3 = 1.5287(14), P2-O2 = 1.5298(13), P1-O1 = 1.5232(13), F3-Ge1-F2 = 91.99(5), F2-Ge1-F1 92.69(5), O2-Ge1-O3 = 88.38(6), O2-Ge1-O1 = 89.30(6).

The structure of $[GeF_3(OPPh_3)_3][OTf]$ reveals a close to regular octahedron with the *cis* F-Ge-F angles somewhat greater than 90 ° and *cis* O-Ge-O angles somewhat smaller than 90 °. The d(Ge-F) and d(Ge-O) showing no significant effect on the *trans* ligands. Comparing this to the neutral structure of *trans*-$[GeF_4(OPPh_3)_2]$, the d(Ge-F) are identical, but the d(Ge-O) are slightly longer for the latter, consistent with the weaker Lewis acidity of the neutral GeF_4 unit. The $^{19}F\{^1H\}$ NMR spectrum of this complex is shown in Figure 3.11 and it can be clearly seen that both the *fac* and *mer* isomers are present in the solution state.

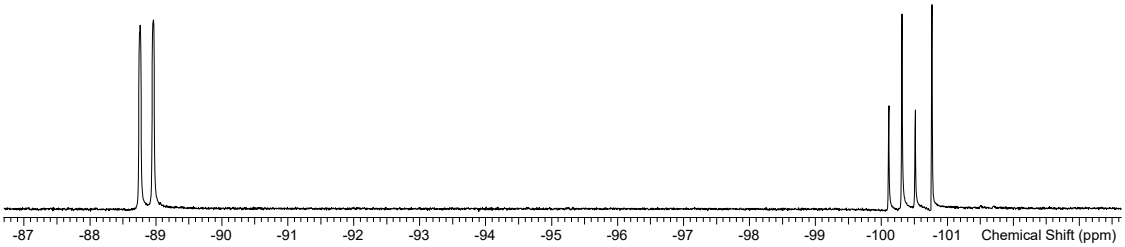

Figure 3.11: $^{19}F\{^1H\}$ NMR spectrum of the *mer/fac* isomer mixture in $[GeF_3(OPPh_3)_3][OTf]$ (CD_2Cl_2, 298 K). Triflate resonance omitted for clarity.

The complex $[GeF_3(OPMe_3)_3][OTf]$ was obtained in good yield, with the *mer* isomer the major form in a CD_3NO_2 solution. In the $^{19}F\{^1H\}$ and $^{31}P\{^1H\}$ NMR spectra, additional small couplings of ~ 7 Hz were seen and tentatively assigned as $^3J_{FP}$, Figure 3.12 shows the $^{19}F\{^1H\}$ NMR spectra for this complex with an expanded image of the triplet, showing the further splitting. These were also seen in the spectra for $[GeF_3(OPPh_3)_3][OTf]$ but were less well resolved.

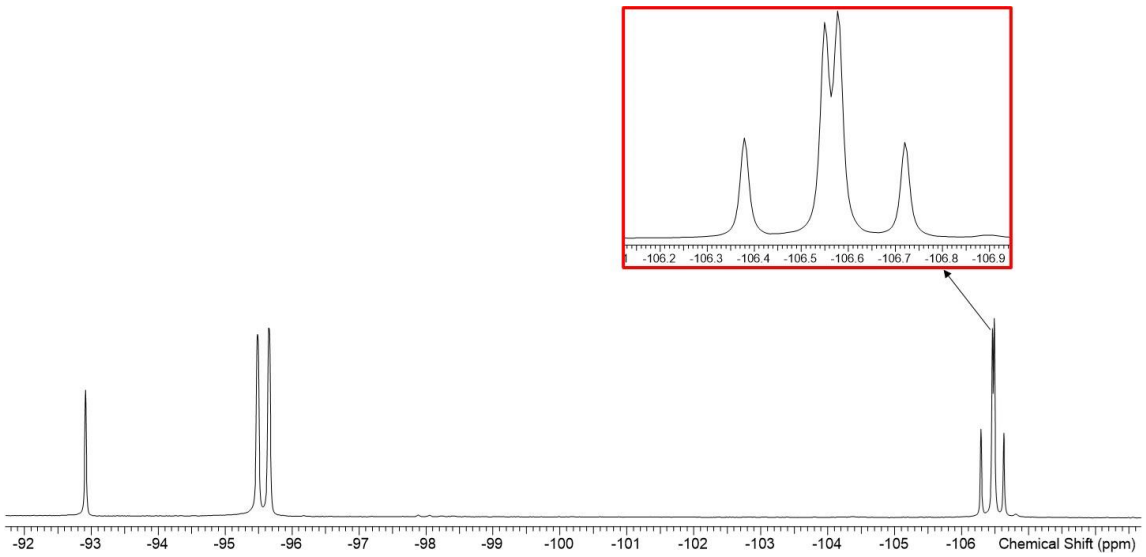

Figure 3.12: $^{19}F\{^1H\}$ NMR spectrum of $[GeF_3(OPMe_3)_3][OTf]$ demonstrating further splitting assigned as $^3J_{FP}$. Triflate resonance omitted for clarity.

The addition of one equivalent of TMSOTf and terpyridine to $[GeF_4(MeCN)_2]$ lead to the abstraction of a fluoride and the formation of *mer*-$[GeF_3(terpy)][OTf]$ as a colourless solid in good yield. The IR spectrum showed strong, broad features for ν(Ge-F), with a broad band at 637 cm^{-1} and a sharp band at 573 cm^{-1}, three stretches are expected for the *mer*-trifluoride ($2A_1 + B_1$). The ^1H NMR spectrum in CD_2Cl_2 shows multiplet resonances for the terpy protons at a higher chemical shift to free ligand, whilst the $^{19}F\{^1H\}$ NMR spectrum (Figure 3.13) is weak due to the poor solubility of the complex, but its identity is not in doubt. Two resonances are present in a 2:1 ratio due to F_{transF} and F_{transN}, respectively. The $^{19}F\{^1H\}$ NMR resonances for $[GeF_3(terpy)][OTf]$ show a doublet at -115.9 and a triplet at -153.0 ppm, (plus a OTf resonance at -79.0 ppm), with $^2J_{FF}$

couplings of 68 Hz.[19] It is notable that these $^{19}F\{^{1}H\}$ NMR resonances are significantly more negative than any of the other germanium cations discussed above.

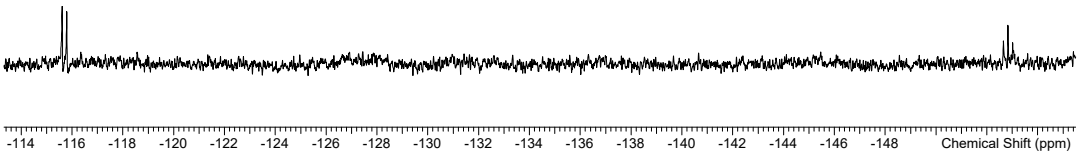

Figure 3.13: $^{19}F\{^{1}H\}$ NMR spectrum of $[GeF_3(terpy)][OTf]$ (CD_2Cl_2, 298 K). Triflate resonance omitted for clarity.

In an earlier study the direct reaction of GeF_4 with terpy in CH_2Cl_2 gave an insoluble product, which had the formula $[(GeF_4)_3(terpy)_2]$ *via* elemental analysis. The IR spectrum of this complex showed no signs of $[GeF_6]^{2-}$ and therefore it was suggested that it was oligomeric with bridging and chelating terpyridine and did not form the cation with tridentate terpy directly.[2, 20]

It is notable that the $^{19}F\{^{1}H\}$ NMR chemical shift values are also significantly less negative than the neutral Group 13 analogue, *mer*-$[GaF_3(terpy)].3H_2O$, the Ga(III) complex has resonances at -154.5 and -188.9 ppm. This complex also proved to be significantly more stable to hydrolysis than $[GeF_3(terpy)][OTf]$. When the Group 14 complex is added to a D_2O solution the resonances for the complex are lost and additional resonances for F^- and HF_2^- and other unidentified species are present (most likely organofluorine species). As a result of the instability of this complex in the presence of water, it was concluded that it would not be a potential candidate for radiofluorination due to its inherent instability in aqueous media.

The $^{19}F\{^{1}H\}$ NMR resonances for all the synthesised $[GeF_3(L)_3]^+$ monocations occur in the range δ = -80 to -155 ppm, depending upon the isomer and the neutral ligand present and overlap with those of the $[GeF_4(L)_2]$ complexes, although δ(F) *trans* F are always of a higher frequency than δ(F) *trans* N/O for a particular complex. The cations were generally poorly soluble in chlorocarbons and spectra were mostly obtained from CH_3NO_2/CD_3NO_2 solutions, due to the weakly coordinating and solubilising nature of nitromethane. The details of which, along with coupling constants and $^{31}P\{^{1}H\}$ NMR chemical shifts (where applicable), are shown in Table 13.

Table 13: Selected NMR spectroscopic data of $[GeF_3(L)_3][OTf]$ (L= dmso, dmf, py, pyNO, $OPPh_3$, $OPMe_3$, $OAsPh_3$ and L_3= terpy) complexes.

Complex	**Solvent** **Temp.**	**$^{19}F\{^{1}H\}$ NMR/ ppm[a]**	**$^{2}J_{FF}$ /Hz**	**$^{31}P\{^{1}H\}$ NMR/ ppm**	

$[GeF_3(dmso)_3][OTf]$ *mer* *fac*	CD_3NO_2 253K	–109.8(d), –121.7(t) -122.2 (s)	71	N/A	This work
$[GeF_3(dmf)_3][OTf]$ *mer* *fac*	CD_3NO_2 253K	-126.1 (d) -135.0 (t) -134.5 (s)	64	N/A	This work
$[GeF_3(pyridine)_3][OTf]$ *mer* *fac*	CD_2Cl_2 298K	-122.0 (t), -137.3 (t) -149.2 (s)	55	N/A	This work
$[GeF_3(pyNO)_3][OTf]$* *mer* *fac*	CD_3NO_2 253 K	-136.8 (d), -143.0 (t) -129.8 (s)	65	N/A	This work
$[GeF_3(OPPh_3)_3][OTf]$ *mer* *fac*	CD_2Cl_2 298 K	-89.0 (d), -100.4 (t), -100.9(s)	76	44.1(s), 41.7(s) 43.7 (s)	This work
$[GeF_3(OPMe_3)_3][OTf]$ *mer* *fac*	CD_3NO_2 298 K	-95.6 (d), -106.6 (t) -93.01(s)	64	67.4 (m), 66.9 (m) 70.4 (s)	This work
$[GeF_3(OAsPh_3)_3][OTf]$*[b] *mer* *fac*	CD_3NO_2 298 K	-79.3 (d), -89.5 (t) -89.9 (s)	68	N/A	This work

$[GeF_2(OAsPh_3)_4][OTf]_2$*[b] *cis* *trans*	CD_3NO_2 298 K	 -65.1 (s) -59.1 (s)	 N/A	 N/A	This work
$[GeF_3(terpy)][OTf]$ *mer*	CD_2Cl_2 298 K	 -115.9 (d), -153.0 (t)	 68	 N/A	This work

[a]. triflate resonances omitted. * Resonances picked out from mixtures in NMR data. [b] not isolated in the pure state, data is from a mixture with $[GeF_2(OAsPh_3)_4][OTf]_2$ and $[GeF_3(OAsPh_3)_3][OTf]$.

3.2.3 Attempts to remove further fluoride ligands

Attempts to remove a second fluoride using a second equivalent of TMSOTf with the addition of a further equivalent of the neutral ligand, L, were mostly unsuccessful. Predominantly $[GeF_3(L)_3][OTf]$ and degradation products formed for the reactions when L = dmf, $OPMe_3$ and $OPPh_3$. However, the reaction of $[GeF_4(MeCN)_2]$, TMSOTf and $OAsPh_3$ in a 1:1:3 molar ratio in CH_2Cl_2 precipitated a colourless solid. The $^{19}F\{^1H\}$ NMR spectrum in CD_3NO_2 showed the expected resonances for the monocation $[GeF_3(OAsPh_3)_3][OTf]$, $\delta = -89.9$ ppm (s) for the *fac* isomer and -89.5 (t, $^2J_{FF} = 66$ Hz), -79.3 ppm($^2J_{FF} = 67$ Hz) for the *mer* isomer, and -79.9 ppm (s, OTf), along with two strong singlets at $\delta = -65.1$ and -59.1 ppm (Figure 3.14). With the latter two singlets assigned as *cis* and *trans* $[GeF_2(OAsPh_3)_4][OTf]_2$, integration of the mixture in the spectrum suggested the ratio of the complexes was $[GeF_3(OAsPh_3)_3][OTf]$:$[GeF_2(OAsPh_3)_4][OTf]_2$ ~ 3: 1 and attempts to obtain a pure sample of either by increasing the temperature and time of the reactions were unsuccessful, although their identities are not in serious doubt.

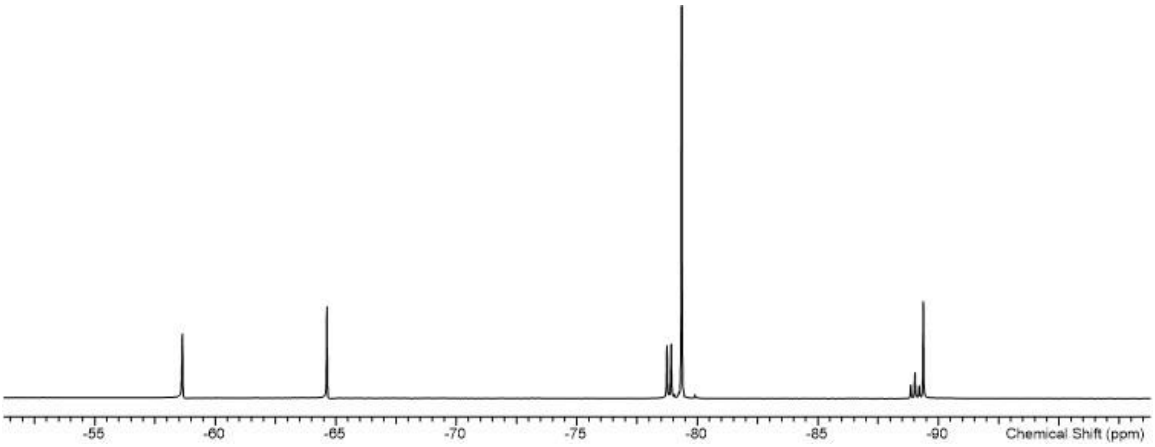

Figure 3.14: $^{19}F\{^{1}H\}$ NMR spectrum (CD_3NO_2, 298 K) mixture of $[GeF_3(OAsPh_3)_3][OTf]$ and $[GeF_2(OAsPh_3)_4][OTf]_2$.

The capability for the $[GeF_2(OAsPh_3)_4][OTf]_2$.complex to form directly contrasts with all the other ligands used in this work, including the analogous phosphine oxide ligands. This indicates that the arsine oxide ligand is a stronger donor towards the Ge(IV) centre. Comparison of other X-ray crystallographic data on several isostructural phosphine oxide complexes show that the M-OAs bond distance was shorter than the M-OP bond distance, providing supporting evidence for stronger bonding of $OAsPh_3$ to hard acceptors such as Ge(IV).[21-23]

Attempts were also made to synthesise Ge(IV) cationic complexes bearing the soft thioether macrocycles, [9]aneS_3, [12]aneS_4 and [14]aneS_4 (Figure 3.15), however no evidence for complexation was observed, despite several attempts in different solvents (CH_3NO_2, CH_2Cl_2 and hexane). Therefore, this work was not pursued. Attempts were then made to synthesise $[GeF_3([9]aneS_3)][OTf]$ from the preformed $[GeF_3(dmf)_3][OTf]$, however this also proved unsuccessful.

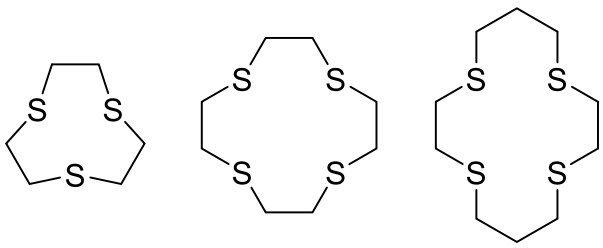

Figure 3.15: Structures of the ligands [9]aneS_3, [12]ane$S_4$and [14]aneS_4, respectively.

3.2.4 DFT calculations

DFT calculations were performed on the neutral *cis*/*trans*-$[GeF_4(OPMe_3)_2]$, the monocationic, *mer*/*fac*-$[GeF_3(OPMe_3)_3]^+$, and the dicationic *cis*/*trans*-$[GeF_2(OPMe_3)_4]^{2+}$ complexes by Dr. Rhys

King using the B3LYP-D3 functional and 6-311G(d) basis set. The initial geometry of *trans*-[$GeF_4(OPMe_3)_2$] was taken from the published crystal structure, whilst the *cis* isomer was constructed starting from the *trans* geometry.[1] Both structures were optimised and the calculations converged with no imaginary frequencies. Comparisons of the *cis* and *trans* isomers of [$GeF_4(OPMe_3)_2$] showed that the *cis* isomer was only marginally lower in energy (1.31 kJ mol^{-1}) than the *trans* isomer in the gas phase. Both isomers were present in solution during NMR experiments and these results are consistent with this, however the choice of solvent, experimentally, affects the position of equilibrium and the amount of isomer present. The representations of the HOMO and LUMO for these isomers are shown in Figure 3.16

cis-[$GeF_4(OPMe_3)_2$]

trans-[$GeF_4(OPMe_3)_2$]

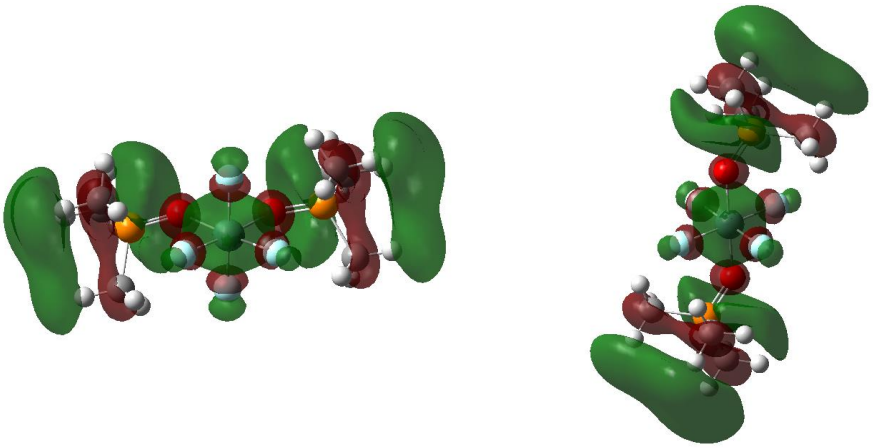

LUMO -0.323 eV

LUMO -0.414 eV

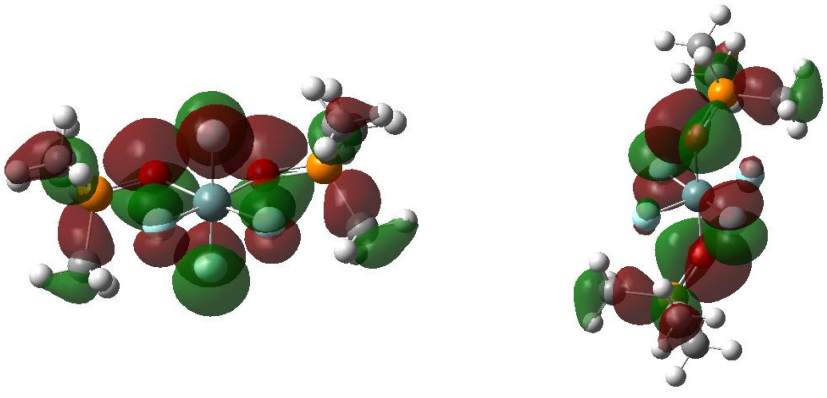

HOMO -7.948 eV

HOMO -7.889 eV

Figure 3.16: Representations of the HOMO and LUMO of *cis*/*trans*-[$GeF_4(OPMe_3)_2$].

The HOMO, HOMO-1 and HOMO-2 for both *cis* and *trans* isomers are combinations of lone pairs based on the fluorine ligands and the oxygens of the $OPMe_3$ ligand. The LUMO and LUMO+2 have Ge-F σ* character with LUMO+1 being entirely based on the $OPMe_3$ ligand.

For the monocationic *mer*/*fac*-$[GeF_3(OPMe_3)_3]^+$ complexes, the geometry of the *mer* isomer was taken from the structure of $[GeF_3(OPPh_3)_3]^+$ with the Ph groups exchanged for Me. For the *fac* isomer the converged structure of *mer*-$[GeF_3(OPMe_3)_3]^+$ was taken as a starting point. The *mer* isomer was more stable than that of the *fac* isomer (by 3.19 kJ mol^{-1}) and this was consistent with the experimental data that showed the *mer*-$[GeF_3(OPMe_3)_3]^+$ isomer was significantly more abundant in solution than *fac*-$[GeF_3(OPMe_3)_3]^+$. The representations of the HOMO and LUMO for these isomers are shown in Figure 3.17

fac-$[GeF_3(OPMe_3)_3]^+$ *mer*-$[GeF_3(OPMe_3)_3]^+$

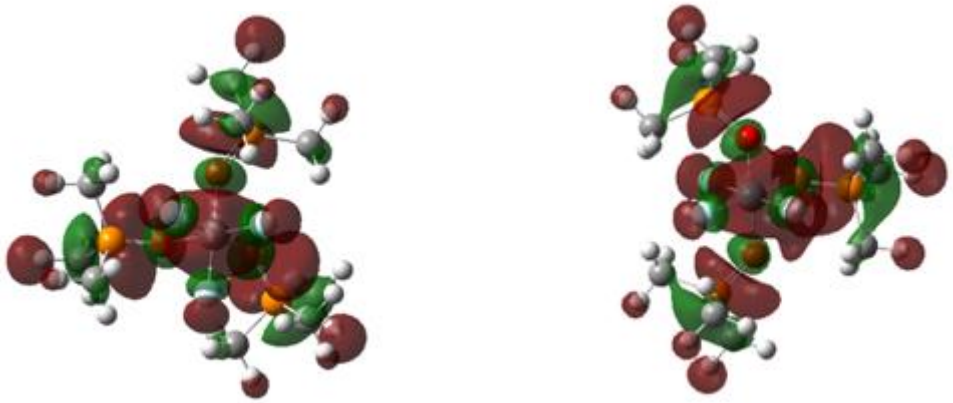

LUMO -0.108 eV LUMO -0.114 eV

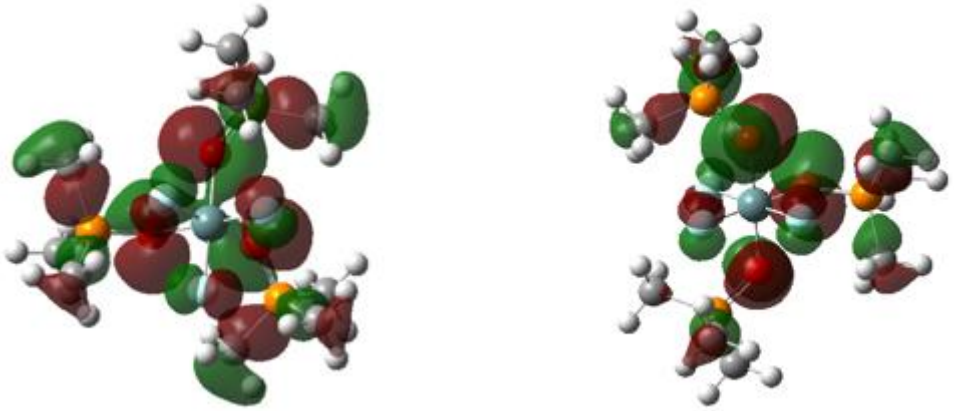

HOMO -0.418 eV HOMO -0.389 eV

Figure 3.17: Representations of the HOMO and LUMO of *fac/mer*-$[GeF_3(OPMe_3)_3]^+$.

The HOMO, HOMO-1, and HOMO-2 of both isomers of $[GeF_3(OPMe_3)_3]^+$ are based on combinations of lone pairs on the F and O atoms. For these complexes the LUMO is mostly Ge-F antibonding and LUMO+1/+2 are mostly ligand based.

The dicationic complexes *trans*/*cis*-$[GeF_2(OPMe_3)_4]^{2+}$ were also modelled, with *trans*-$[SnF_2(OPPh_3)_4]^{2+}$ taken as the starting geometry for the *trans* isomer.[3] For the *cis* isomer the initial geometry was taken from the optimised geometry of *trans*-$[GeF_2(OPMe_3)_4]^{2+}$ and the structure modified to get the *cis*-geometry. For the dications, *cis*/*trans*-$[GeF_2(OPMe_3)_4]^{2+}$ the *cis* isomer is much more stable than the *trans* isomer (18.50 kJ mol^{-1} lower in energy). The representations of the HOMO and LUMO for these isomers are shown in Figure 3.18.

cis-$[GeF_2(OPMe_3)_4]^{2+}$ *trans*-$[GeF_2(OPMe_3)_4]^{2+}$

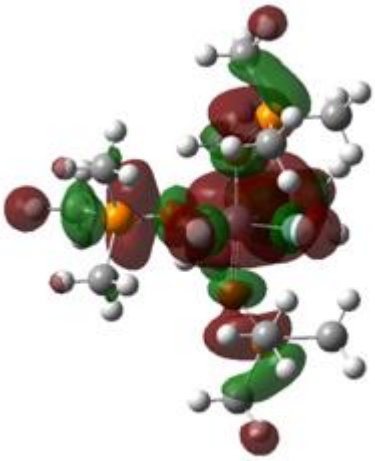

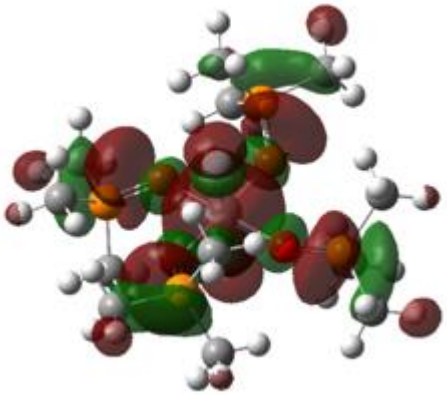

LUMO -0.222 eV LUMO -0.221 eV

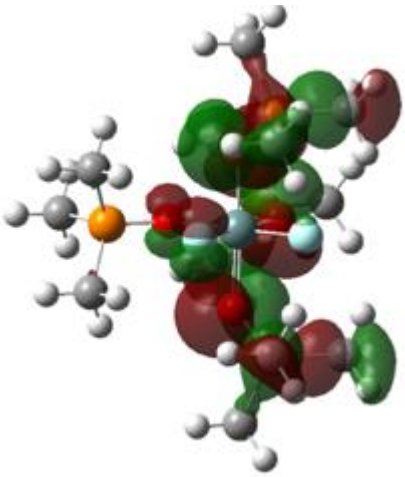

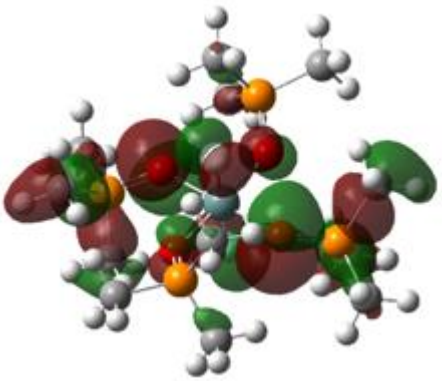

HOMO -0.516 eV HOMO -0.523 eV

Figure 3.18: Representations of the HOMO and LUMO of *cis/trans*-$[GeF_2(OPMe_3)_4]^{2+}$.

For both *cis* and *trans* isomers of $[GeF_2(OPMe_3)_4]^{2+}$ the HOMO and HOMO-1/-2 are based on the lone pairs of the O and F atoms with the LUMO being mostly Ge-F antibonding and LUMO+1/+2 mostly ligand based.

3.3 Conclusions

This Chapter describes the characterisation of the first monocationic complexes of the GeF_3^+ fragment with hard nitrogen and oxygen donor ligands (L = dmso, dmf, pyNO, py, $OPPh_3$, $OPMe_3$). A large amount of spectroscopic data on these complexes have been obtained and been compared directly to the tin analogues described in Chapter 2. Structural data of the novel $[GeF_3(OPPh_3)_3][OTf]$ has also been obtained and compared directly to its neutral counterpart, $[GeF_4(OPPh_3)_2]$.[1] Attempts to prepare dications by the removal a further fluoride were only partially successful for L = $OAsPh_3$. The $[GeF_3(L)_3][OTf]$ are similar to $[SnF_3(L)_3][OTf]$ but appear to be less stable in solution, with the reaction of $[SnF_4(L)_2]$ or $[SnF_3(L)_3][OTf]$ with TMSOTf and more ligand, producing $[SnF_3(L)_3][OTf]$ and $[SnF_2(L)_4][OTf]_2$, but in the germanium systems the removal of a second fluoride did not occur for most of the ligands investigated in this work. However, notably, $[GeF_2(OAsPh_3)_4][OTf]_2$ was clearly identified in a mixture with the monocationic system and is the first reported complex of its kind. This is in contrast with the OPR_3-type ligands that show no sign of being able to form a dicationic complex with the Ge(IV) centre, therefore suggesting that $OAsPh_3$ is a stronger donor ligand towards the Ge(IV) centre. This work is consistent with earlier crystallographic data on early transition metal pnictine oxide complexes that showed that the M-OAs bond length was shorter than that for M-OP and thus signifying a stronger binding mode for $OAsPh_3$ towards hard acceptors.

Information on the bond dissociation energies of Sn-F and Ge-F show that they do not differ significantly (456 *vs* 464 kJ mol^{-1}, respectively), there may be a significant kinetic barrier in the germanium systems.[4]

DFT calculations have provided evidence for trends in stability of the isomers, although it should be noted that the calculations are for gas phase ions, and cation/anion interactions, packing effects in the solids and solvation in solution will significantly affect the relative stabilities.

3.4 Experimental

The germanium(IV) fluoride complexes $[GeF_4(py)_2]$, $[GeF_4(OPPh_3)_2]$, $[GeF_4(OPMe_3)_2]$ and $[GeF_4(OAsPh_3)_2]$ were made by literature methods and had spectroscopic data consistent with that published.[1, 2]

3.4.1 $[GeF_4(dmf)_2]$

$[GeF_4(MeCN)_2]$ (0.500 g, 2.2 mmol) was suspended in excess DMF and left to stir for 2 h at 50 °C, a white precipitate formed. The mixture was filtered, washed in hexane (3 x 2 mL) and the solid dried *in vacuo*. Yield 125 mg, 60%. Required for $C_6H_{14}F_4N_2O_2Ge$ (294.81): C, 24.44; H, 4.79; N, 9.50. Found: C, 24.04; H, 5.39; N, 9.32%. IR (Nujol/cm^{-1}): ν = 1654s (C=O) 642br, 622br (Ge-F). ^{1}H NMR (CD_3NO_2, 250 K): δ ppm = 8.5 (s, $(CH_3)_2NCO$-**H**), 8.16 (s, $(CH_3)_2NCO$-**H**), 8.13 (s, $(CH_3)_2NCO$-**H**), 3.28 (s, *cis* isomer, (C**H**$_3$)$_2$NCOH), 3.25 (s, *trans* isomer, (C**H**$_3$)$_2$NCOH)), 3.12 (s, *cis* isomer, (C**H**$_3$)$_2$NCOH), 3.07 (s, *trans* isomer, (C**H**$_3$)$_2$NCOH)), 2.94 (s, *cis* isomer, (C**H**$_3$)$_2$NCOH), 2.79 (s, *cis* isomer, (C**H**$_3$)$_2$NCOH). ^{19}F{^{1}H} NMR (CD_3NO_2, 250 K): δ ppm = -135.8 (t, $^2J_{FF}$ = 59 Hz), -125.4 (s), -124.9 (t, $^2J_{FF}$ = 59 Hz).

3.4.2 $[GeF_4(dmso)_2]$

GeF_4 was bubbled through a stirred solution of dmso (0.5 mL) in hexane for 2 minutes. The solution was then stirred for 1 h. The solvent was filtered off and the solid dried *in vacuo*. Required for $C_4H_{12}F_4O_2S_2Ge$ (304.88): C, 15.76; H, 3.97. Found: C, 15.91; H, 3.31%. IR (Nujol/cm^{-1}): ν = 632br, 618br, 596br (Ge-F).^{1}H NMR (CD_3NO_2, 250 K): δ ppm = 3.03 (br s, CH_3), 2.91 (s, CH_3). ^{19}F{^{1}H} NMR (CD_3NO_2, 250 K): δ ppm = -129.8 (t, $^2J_{FF}$ = 61 Hz)), -115.4 (s), -115.3 (t, $^2J_{FF}$ = 61 Hz).

3.4.3 $[GeF_4(pyNO)_2]$

$[GeF_4(MeCN)_2]$ (0.264 g, 1.14 mmol) was dissolved in CH_2Cl_2 and pyNO (0.517 g, 2.28 mmol) was added to the solution and left to stir for 2 h, a white precipitate formed. The mixture was filtered, washed in hexane (3 x 2 mL) and the solid dried *in vacuo*. Yield 0.320 g, 41%. Required for $C_{10}H_{10}F_4N_2O_2Ge.2H_2O$ (374.9): C, 32.00; H, 3.76; N, 7.47. Found: C, 31.95;H, 3.31; N, 7.28%. IR (Nujol/cm^{-1}): ν = 675s (Ge-F) ^{1}H NMR (CD_3NO_2, 253 K): δ ppm = 8.7 (m, [2H]), 8.4 (m, [1H]), 8.0 (m, [2H]), 5.44 (residual CH_2Cl_2), 2.46 (H_2O). ^{19}F{^{1}H} NMR (CD_3NO_2, 253 K): δ ppm = -142.76 (br s)

3.4.4 $[GeF_3(dmso)_3][OTf]$

$[GeF_4(dmso)_2]$ (0.705 g, 0.23 mmol) was suspended in CH_2Cl_2 and a solution of TMSOTf (0.514 g, 0.23 mmol) was added. The reaction mixture was allowed to stir for 2 h, a solution of dmso in MeCN was then added (0.23 mmol) and left to stir for 72 h. The solvent was then concentrated *in vacuo* and hexane (5 mL) was added which yielded a white precipitate. Yield 0.082 g, 69%. Required for $C_7H_{18}F_6O_6S_4Ge.3H_2O$ (598.00): C, 14.82; H, 34.27. Found: C, 14.84; H, 3.69%. IR (Nujol/cm^{-1}): ν = 3437br (H_2O), 639s (Ge-F). ^1H NMR (CD_3NO_2, 298 K): δ = 3.06 (s), 2.99 (s), 2.98 (s), 2.51 (s, dmso). $^{19}F\{^1H\}$ NMR (CD_3NO_2, 298 K): δ = -122.2 (s), -121.7 (t, $^2J_{FF}$= 71 Hz), -109.8 (d, $^2J_{FF}$= 71 Hz), -79.8 (s, OTf).

3.4.5 $[GeF_3(dmf)_3][OTf]$

$[GeF_4(dmf)_2]$ (0.170 g, 0.50 mmol) was suspended in CH_2Cl_2 and a solution of TMSOTf (0.128 g, 0.50 mmol) was added. The reaction mixture was allowed to stir for 2 h, a solution of DMF was then added (0.50 mmol) and left to stir for 72 h. The solvent was then concentrated *in vacuo* and hexane (5 mL) was added which yielded a white precipitate. Yield 0.110 g, 38%. IR (Nujol/cm^{-1}): ν = 638 (br Ge-F). ^1H NMR (CD_3NO_2, 298 K): δ = 8.52 (s, $(CH_3)_2NCO$-**H**), 8.22 (s, $(CH_3)_2NCO$-**H**), 8.10 (s, $(CH_3)_2NCO$-**H**), 5.44 (residual CH_2Cl_2), 3.30-3.42 (m, $(CH_3)_2NCOH$)), 3.14-3.24 (m, $(CH_3)_2NCOH$)), 3.02. $^{19}F\{^1H\}$ NMR (CD_3NO_2, 298 K): δ = -134.5 (s), -135.0 (t, $^2J_{FF}$= 64 Hz), -126.1 (d, $^2J_{FF}$= 64 Hz).

3.4.6 $[GeF_3(pyridine)_3][OTf]$

$[GeF_4(pyridine)_2]$ (0.131 g, 0.43 mmol) was suspended in CH_2Cl_2 (10 mL) and a solution of TMSOTf (0.095 g, 0.43 mmol) was added. After stirring for 2 h, pyridine (0.03 g, 0.43 mmol) was added to the solution. The reaction mixture was stirred for 15 h. The solvent was concentrated to ca. 5 mL, *n*-hexane (15 mL) was added and the solid was filtered off and dried *in vacuo*. Yield 0.10 g, 47%. Required for $C_{16}H_{15}F_6N_3O_3SGe.CH_2Cl_2$ (600.92): C, 33.98; H, 2.85; N 6.99. Found C, 33.96; H, 2.87; N, 7.21%. IR (Nujol): $\tilde{\nu}$ = 627 (br), 615 (br) (Ge-F) cm^{-1}. ^1H NMR (400 MHz, CD_2Cl_2, 298 K): δ = 8.93 (m), 8.76 (m), 8.70 (m), 8.20 (m), 7.91 (m), 7.82 (m), 7.73 (m), 7.73 (m). $^{19}F\{^1H\}$ NMR (CD_2Cl_2, 298 K): δ = -79.0 (s, OTf), -122.0 (t, $^2J_{FF}$ = 55 Hz), -124.4 (s, F^-), -137.3 (d, $^2J_{FF}$ = 55 Hz), -149.2 (s) ppm.

3.4.7 $[GeF_3(pyNO)_3][OTf]$

$[GeF_4(pyNO)_2]$ (0.037 g, 0.11 mmol) was suspended in CH_2Cl_2 (10 mL) and a solution of TMSOTf (0.024 g, 0.11 mmol) was added at room temperature. After stirring for 2 h, pyNO (0.095 g, 0.11 mmol) in MeCN (1 mL) was added. The reaction mixture was stirred for 72 h. The resulting white precipitate was filtered off, washed in n-hexane (15 mL) and dried *in vacuo*. Yield 0.54 g, 77%.

Required for $C_{16}H_{15}F_6GeN_3O_6S$ CH_2Cl_2 (648.9): C, 31.46, H 2.64, N 6.48. Found C 31.62, H, 2.94, N, 7.18%. IR (Nujol): $\tilde{\nu}$ = 639 (s), 590 (w) (Ge-F) cm^{-1}. ^1H NMR (400 MHz, CD_3NO_2, 298 K): δ = 8.7 (m, 2H), 8.3 (m, H), 7.9 (m, 2H). $^{19}F\{^1H\}$ NMR (CD_3NO_2, 298 K): δ = –79.6 (s), -129.8 (s), -133.0 (t, $^2J_{FF}$ = 58 Hz), -136.1 (t, $^2J_{FF}$ = 58 Hz), -136.9 (d, $^2J_{FF}$ = 65 Hz), -141.8 (s), -143.0 (t, $^2J_{FF}$ = 65 Hz).

3.4.8 [$GeF_3(OPPh_3)$][OTf]

[$GeF_4(OPPh_3)_2$] (0.144 g, 0.20 mmol) was suspended in CH_2Cl_2 and a solution of TMSOTf (0.046 g, 0.20 mmol) was added, the reaction mixture was allowed to stir for 2 h. To this, $OPPh_3$ (0.056 g, 0.20 mmol) was then added and the solution was stirred for 15 h. The solution was concentrated *in vacuo* and excess hexane was added, the solvent was removed, and the resulting white powder was dried *in vacuo*. Yield 0.150 g, 67%. Required for $C_{55}H_{45}F_6O_6P_3SGe.1.25CH_2Cl_2$ (1219.72): C, 55.39; H, 3.93. Found: C, 55.22; H, 3.98%. IR (Nujol/cm^{-1}): ν = 1116sh, 1049m (P=O), 637sh (Ge-F). ^1H NMR (CD_2Cl_2, 298 K): δ = 7.7-7.3 (m). $^{19}F\{^1H\}$ NMR (CD_2Cl_2, 298 K): δ = -79.0 (s, OTf), -89.0 (d, $^2J_{FF}$ = 76 Hz), -100.4 (t, $^2J_{FF}$ = 76 Hz), -100.9 (s). $^{31}P\{^1H\}$ NMR (CD_2Cl_2, 298 K): δ = 44.1 (s), 43.7 (s), 41.7 (m).

3.4.9 [$GeF_3(OPMe_3)$][OTf]

[$GeF_4(MeCN)_2$] (92 mg, 0.40 mmol) was suspended in CH_2Cl_2 and a solution of TMSOTf (0.089 g, 0.40 mmol) was added, the reaction mixture was allowed to stir for 2 h. To this $OPMe_3$ (110 mg, 1.20 mmol) was then added and the solution was stirred for 15 h, a white solid precipitated out which was separated by filtration, washed in hexane, and dried *in vacuo* Yield 0.160 g, 72%. Required for $C_{10}H_{27}F_6O_6P_3SGe$ (554.92): C, 21.64; H 4.90. Found C, 21.44; H 4.25%. IR (Nujol/cm^{-1}): ν = 1078sh (P=O), 639sh (Ge-F). ^1H NMR (CD_3NO_2, 298 K): δ = 1.90 (d, $^2J_{PH}$ = 14 Hz), 1.83 (d, $^2J_{PH}$ = 14 Hz), 1.82 (d, $^2J_{PH}$ = 14 Hz). $^{19}F\{^1H\}$ NMR (CD_3NO_2, 298 K): δ = -79.8 (s, OTf), -93.0 (s). -95.7 (d, $^2J_{FF}$ = 62), -106.6 (t, $^2J_{FF}$ = 64 Hz). $^{31}P\{^1H\}$ NMR (CD_3NO_2, 298 K): δ = 70.4 (s), 67.4 (m), 66.9 (m).

3.4.10 [$GeF_3(OAsPh_3)$][OTf] and [$GeF_2(OAsPh_3)_4$)][OTf]$_2$

[$GeF_4(MeCN)_2$] (92mg, 0.40 mmol) was suspended in CH_2Cl_2 and a solution of TMSOTf (89 mg, 0.40 mmol) was added, the reaction mixture was allowed to stir for 2 h. To this $OAsPh_3$ (322 mg, 1.20 mmol) was then added and the solution was stirred for 15 h, a white solid precipitated out which was separated by filtration, washed in hexane, and dried *in vacuo.* Yield 0.12 g. IR (Nujol): $\tilde{\nu}$ = 845 (sh) (As = O), 636 (Ge-F) cm^{-1}. ^1H NMR (CD_3NO_2, 298 K): 7.3–7.9 (m). $^{19}F\{^1H\}$ NMR (CD_3NO_2, 298 K): δ = −89.9 (s), −89.5 (t, $^2J_{FF}$ = 66 Hz), −79.9 (s, OTf), −79.3 (d, $^2J_{FF}$ = 67 Hz), −65.1 (s),

−59.1 (s).We were unable to obtain microanalytical data for this complex due to a mixture of species present in the $^{19}F\{^{1}H\}$ NMR spectrum, see Results and Discussion (Section 3.2.2).

3.4.11 [GeF_3(terpy)][OTf]

TMSOTf (0.115 g, 0.52 mmol) was added to a solution of [$GeF_4(MeCN)_2$] (0.119 g, 0.52 mmol) in CH_2Cl_2 (10 mL) at room temperature. After stirring for 2 h, terpyridine (0.120 g, 0.52 mmol) was added to the solution. The reaction mixture was stirred for 15 h. A white solid precipitated and the solid was separated by filtration and washed with hexane (3 x 5 mL) dried *in vacuo*. Yield 0.150 g, 56%. IR (Nujol): $\tilde{\nu}$ = 637 (br), 573 (s) [(Ge-F)] cm^{-1}. ^{1}H NMR (400 MHz, CD_2Cl_2, 298 K): δ = 9.3 (m, [2H]), 8.9 (m, [2H]), 8.8 (m, [2H]), 8.7 (m, [1H]), 8.6 (m, [2H]), 8.2 (m, [2H]). $^{19}F\{^{1}H\}$ NMR (CD_2Cl_2, 298 K): δ = -79.0 (s, OTf), -115.9 (d, $^{2}J_{FF}$ = 68 Hz), -153.0 (t, 68 Hz). Despite attempts on different batches both before and after attempted recrystallisation, satisfactory elemental analyses for this compound could not be obtained, most likely due to the very poor solubility of the complex and co-precipitation of inorganic materials with the complex. However, the spectroscopic data are consistent with that expected for the formulation, *mer*-[GeF_3(terpy)][OTf].

3.5 X-ray crystallographic data

a

Compound	$[GeF_3(OAsPh_3)_3][OTf]$
Space group (no.)	P-1 (2)
a /Å	17.9880(3)
b /Å	18.9588(2)
c /Å	19.7554(3)
α /°	61.380(1)
b /°	70.394(1)
g /°	64.978(1)
U /Å^3	5283.71(15)
Z	4
m(Mo-K_α) /mm^{-1}	3.570
F(000)	2448
Total number reflns	100585
R_{int}	0.040
Unique reflns	21188
No. of params, restraints	1351, 0
R_1, wR_2 [I > 2σ(I)] [b]	0.033, 0.083
R_1, wR_2 (all data)	0.037, 0.094

[a] Common items: T = 293 K; wavelength (Mo-K_α) = 0.71073 Å; θ(max) = 27.5°; [b] $R_1 = \Sigma||Fo|-|Fc||/\Sigma|Fo|$; $wR_2=[\Sigma w(Fo^2-Fc^2)^2/\Sigma wFo^4]^{1/2}$

3.6 References

1. Cheng, F.; Davis, M. F.; Hector, A. L.; Levason, W.; Reid, G.; Webster, M.; Zhang, W., *European Journal of Inorganic Chemistry* **2007,** *2007*, 2488-2495.

2. Cheng, F.; Davis, M. F.; Hector, A. L.; Levason, W.; Reid, G.; Webster, M.; Zhang, W., *European Journal of Inorganic Chemistry* **2007,** *2007*, 4897-4905.

3. King, R. P.; Woodward, M. S.; Grigg, J.; McRobbie, G.; Levason, W.; Reid, G., *Dalton Transactions* **2021,** *50*, 14400-14410.

4. Dean, J. A., L*ange's Handbook Of Chemistry*, Eleventh Edition ed.; McGraw Hill, New York, 1973; Vol. 13, p 12A-12A.

5. Weinert, C. S., *ISRN Spectroscopy* **2012,** *2012*, 718050.

6. Muetterties, E. L., *Journal of the American Chemical Society* **1960,** *82*, 1082-1087.

7. D. Tudela, F. P., Wiley, *Inorganic Syntheses*: 1997; Vol. 31.

8. Kupče, Ē.; Upena, E.; Trušule, M.; Lukevics, E., *Polyhedron* **1989,** *8*, 2641-2644.

9. Ault, B. S., *Journal of the American Chemical Society* **1983,** *105*, 5742-5746.

10. Walther, A. M.; Ault, B. S., *Inorganic Chemistry* **1984,** *23*, 3892-3897.

11. Davis, M.The Synthesis and Characterisation of Complexes of Tin and Germanium Fluorides with Soft Donor Ligands. PhD Thesis, University of Southampton, 2008.

12. Benjamin, S. L.; Levason, W.; Reid, G., *Chemical Society Reviews* **2013,** *42*, 1460-1499.

13. Davis, M. F.; Levason, W.; Reid, G.; Webster, M.; Zhang, W., *Dalton Transactions* **2008**, 533-538.

14. Suter, R.; Swidan, A. a.; Macdonald, C. L. B.; Burford, N., *Chemical Communications* **2018,** *54*, 4140-4143.

15. MacDonald, E.; Doyle, L.; Chitnis, S. S.; Werner-Zwanziger, U.; Burford, N.; Decken, A., *Chemical Communications* **2012,** *48*, 7922-7924.

16. King, R. P.; Levason, W.; Reid, G., *Dalton Transactions* **2021,** *50*, 17751-17765.

17. Woodward, M. S.; King, R. P.; Bannister, R. D.; Grigg, J.; McRobbie, G.; Levason, W.; Reid, G., *Inorganics* **2022,** *10*, 107.

18. Tran, D.; Zavalij, P.; Oliver, S., *Acta Crystallographica, Section E: Structure Reports Online* **2002,** *E58*, m742-m743.

19. Bhalla, R.; Levason, W.; Luthra, S. K.; McRobbie, G.; Monzittu, F. M.; Palmer, J.; Reid, G.; Sanderson, G.; Zhang, W., *Dalton Transactions* **2015,** *44*, 9569-9580.

20. Griffiths, J. E.; Irish, D. E., *Inorganic Chemistry* **1964,** *3*, 1134-1137.

21. Jura, M.; Levason, W.; Petts, E.; Reid, G.; Webster, M.; Zhang, W., *Dalton Transactions* **2010,** *39*, 10264-10271.

22. Levason, W.; Patel, B.; Popham, M. C.; Reid, G.; Webster, M., *Polyhedron* **2001,** *20*, 2711-2720.

23. Benjamin, S. L.; Levason, W.; Pugh, D.; Reid, G.; Zhang, W., *Dalton Transactions* **2012,** *41*, 12548-12557.

4 Synthesis and characterisation of cationic Sn(IV), Ge(IV), and Si(IV) complexes with neutral aza-macrocycles

4.1 Introduction

Following on from the work in Chapters 2 and 3, which aided in the underlying understanding of Sn(IV) and Ge(IV) fluoride chemistries in respect to their reactivity and formation of cationic complexes, this chapter describes further work on these systems using macrocyclic ligands and their assessment as carriers of [^{18}F]fluoride towards PET imaging applications. This chapter therefore discusses the experiments undertaken to explore the synthesis of Sn(IV), Ge(IV) and also Si(IV) cationic complexes with the ligands; terpyridine, RMe_2tacn (R = Me or Bn), Me_4-cyclen and Me_4-cyclam. Due to the strength of the Si-F bond and the difficulty in exploring its coordination chemistry directly, this work has explored the heavier halides, chloride, and iodide, with the aim of forming the fluoride complexes through subsequent halide exchange reactions.[1, 2]

4.1.1 Macrocycles

A more thorough analysis of macrocycles and macrocyclic complexes used in this work is outlined in Section 1.2 to 1.4. Tacn derivatives coordinate *facially* and lock the geometry of an octahedral complex. Previous work in the Southampton group has shown that tacn derivatives do form very stable complexes with Group 13 metal fluorides, such as [GaF_3($BnMe_2$tacn)] and [AlF_3($BnMe_2$tacn)] ($BnMe_2$tacn = 1-benzyl-4,7-dimethyltriazacyclonane) and that these complexes can be successfully ^{18}F-radiofluorinated in aqueous MeCN (the latter can only be formed from halide exchange from the chloride analogue due to the strength of the Al-F bond).[3-5] The chemical structures of Me_3tacn and $BnMe_2$tacn are shown in Figure 4.1.

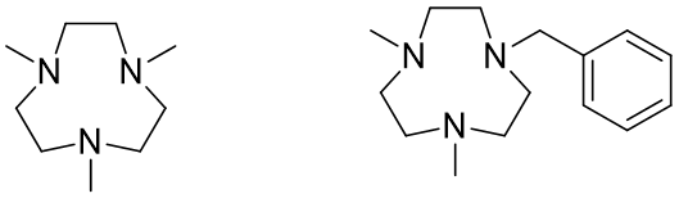

Figure 4.1: Structures of Me_3tacn and $BnMe_2$tacn.

1,4,8,11-Tetraazacyclotetradecane (cyclam, Figure 4.2 when n = 1) derivatives are also known to form highly stable macrocyclic complexes with many metal ions due to their thermodynamic and kinetic stability. Their pendant arm functionalised derivatives are also prevalent in diagnostics, as

targeted radiopharmaceuticals for therapeutic use in nuclear medicine and also as contrast agents in MRI.[6-8] Cyclic complexes have an added benefit over acyclic counterparts due to their ability in being able to adopt a pre-organised conformation, this aids in additional inertness when bound to a metal ion. This is important as the metal macrocyclic complex formed must be able to withstand physiological pH and competition from a range of competitive ions in the body, such as Cl^-, PO_4^{3-}, OAc^-, CO_3^{2-}. In ^{18}F-based PET imaging, the M-F fragment must remain bound to the macrocycle to avoid accumulation and binding to non-target organs.[9]

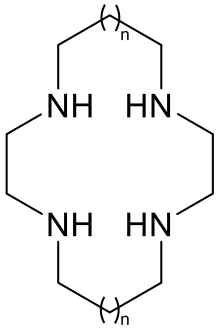

Figure 4.2: Structure of cyclen (n=0) and cyclam (n=1).

It is unlikely that 12-membered ring 1,4,7,10-tetraazacyclododecane (cyclen) derivatives (Figure 4.2, where n=0) will be large enough to encapsulate any of the Group 14 (IV) metal ions, however there is a potential that the 14-membered cyclam may form the encapsulated metal ion species. For example, Delgado and co-workers reported Zn(II) complexes with the cyclen derivative H_2dota and cyclam derivative H_2teta and showed that in the former complex the metal ion adopts a *cis*-distorted octahedral geometry and the macrocycle takes on a *trans*-I folded conformation.[9] However in the latter complex, the macrocycles are not folded and the metal centres are encapsulated by the macrocycle and adopt a *trans*-III configuration (see isomer nomenclature in Figure 4.3). Zn(II) has an ionic radius of 0.74, whereas Sn(IV) has an ionic radius of 0.69.[10]

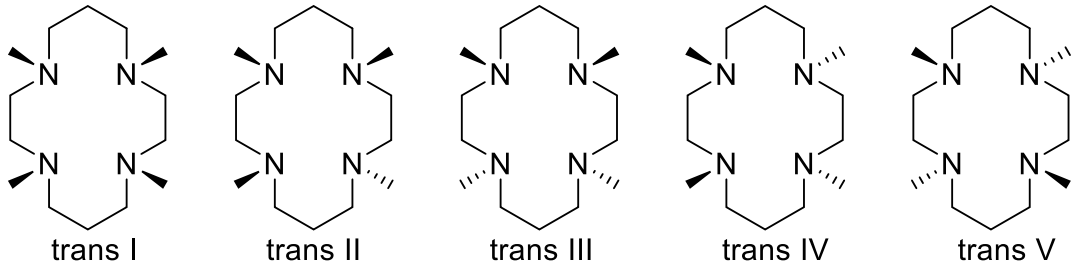

Figure 4.3: Five *trans* isomers of Me_4-cyclam, following Bosnich's nomenclature.[11]

An example of two bifunctional cyclam derivatives are shown in Figure 4.4 and these have been used to complex two different radioactive isotopes of copper, ^{64}Cu and ^{67}Cu, for diagnostic imaging.[12]

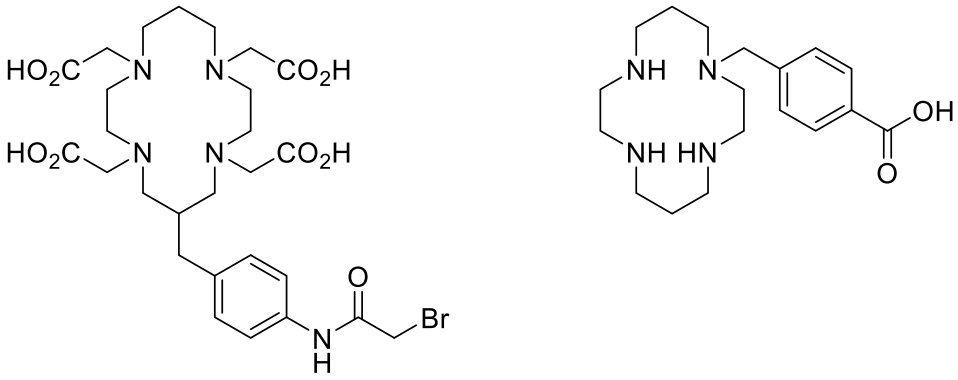

Figure 4.4: Two examples of a cyclam derivatives as bifunctional chelators (BAT and CPTA) used to complex ^{64}Cu and ^{67}Cu to bioconjugates for PET imaging.[12]

A select range of transition metal ions that have been shown to be encapsulated by cyclam derivatives is shown in Table 14.[13]

Table 14: Table of select Group 14 and transition metal ions ionic radii. Data taken from Shannon and co-workers.[10]

Ion	Coordination Number	Radius / Å
Si (IV)	6	0.40
Ge (IV)	6	0.53
Sn (IV)	6	0.69
Ni (II)	6	0.69
Cu (II)	6	0.73
Zn (II)	6	0.74

The tetra-aza macrocycles are neutral, hard donor ligands and provide additional thermodynamic stability and kinetic inertness in their metal complexes over their open chain counterparts, owed to the macrocyclic effect. Only few reports of Group 14 complexes with these types of nitrogen macrocycles exist, with previous work conducted in Southampton on these types of complexes in the +2 and +4 oxidation states, such as $[Ge(Me_4\text{-cyclam})][OTf]_2$ and $[GeF_4(\kappa^2\text{-}Me_4\text{-cyclam})]$.[14-16] The aza-macrocycle of Ge(II) presented an unusual halide-free dicationic complex which was stabilised by the neutral donor ligand, leading to endocyclic coordination to the Ge(II) centre,

whilst the Ge(IV) complex showed the *meso* conformation at the coordinated nitrogens with the two other nitrogens bent away from the metal centre (Figure 4.5).

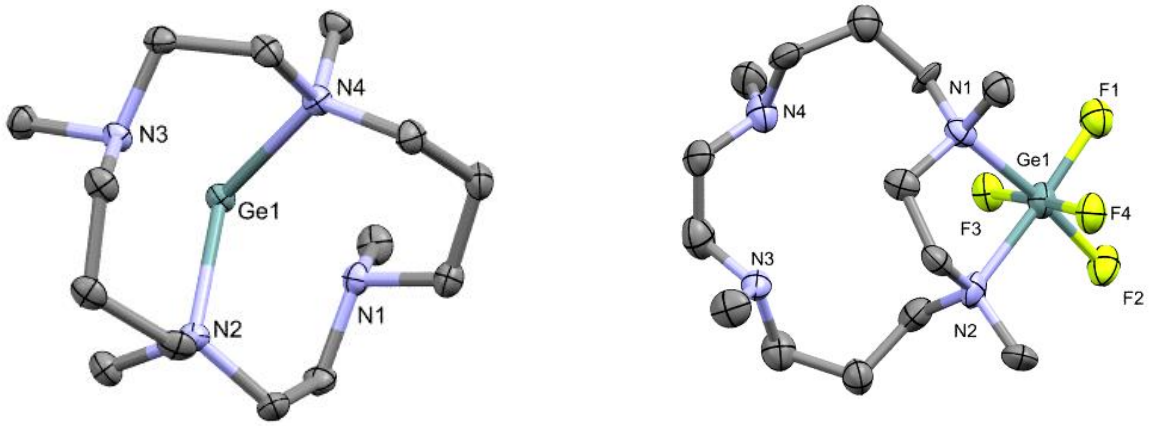

Figure 4.5: Crystal structure of as $[Ge(Me_4\text{-cyclam})]^{2+}$ and $[GeF_4(\kappa^2\text{-}Me_4\text{-cyclam})]$. Redrawn from References.[14, 16]

4.1.2 Sn(IV) and Ge(IV) bromide and chloride containing complexes with nitrogen donor macrocyclic ligands

Willey and co-workers showed the reactions of Me_3tacn with MCl_4 (where M = Sn or Ge) forms ionic complexes containing a MX_3^+ fragment, isolated as *fac*-$[GeCl_3(Me_3tacn)]_2[H_3O][Cl]_3$ and *fac*-$[SnCl_3(Me_3tacn)]_2[SnCl_6]$. MBr_4 reacts with 3,5-trimethyl-1,3,5-triazacyclohexane (Me_3tach) to form a κ^3-coordinated complex as $[GeBr_3(Me_3tach)]_2[MeNH_3]Br_3$.MeCN and $[SnBr_3(Me_3tach)]_2[SnBr_6]$. It can be noted that the germanium complexes contain halide counter anions, whereas for both tin complexes the hexahalostannate dianion, $[SnX_6]^{2-}$, is the counter anion and this was also seen in the reaction of $SnCl_4$ with soft donor ligand $[9]aneS_3$ to form $[SnCl_3([9]aneS_3)]_2[SnCl_6]$.[17] An example of each triaza complex is shown in Figure 4.6.

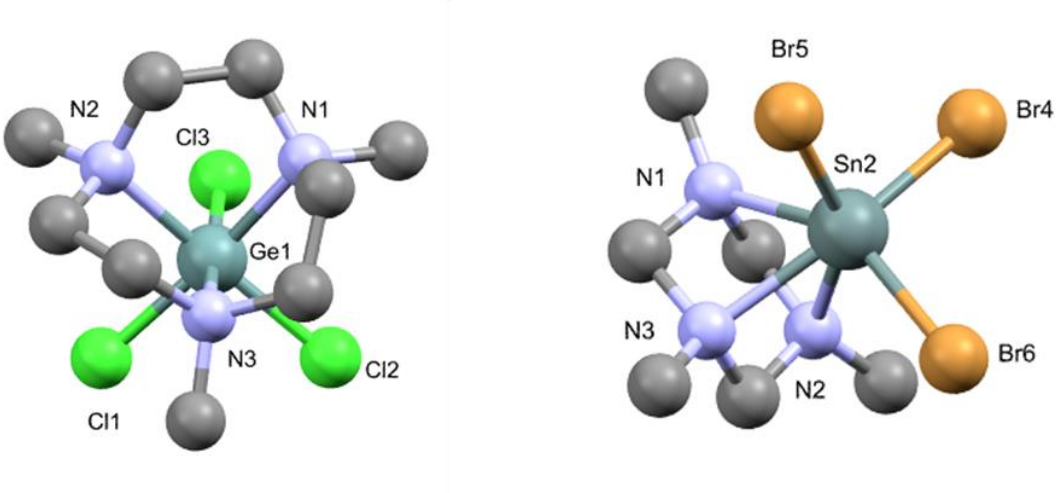

Figure 4.6: Crystal structures of cations $[GeCl_3(Me_3tacn)]^+$ and $[SnBr_3(Me_3tach)]^+$ in the complexes $[GeCl_3(Me_3tacn)][Cl]$ and $[SnBr_3(Me_3tach)]_2[SnBr_6]$, respectively. Redrawn from Reference.[17] No ellipsoid data available.

The MX_3^+ cations are stabilised by κ^3 coordination of the macrocyclic ligand to form stable, octahedral complexes with *facial* geometry. Previously in the Reid Group, the reaction of $[GeF_4(MeCN)_2]$ with Me_3tacn in CH_2Cl_2 produced a colourless solid that was identified as the desired product $[GeF_3(Me_3tacn)]_2[GeF_6]$ by microanalysis, but no solution data were obtained to corroborate its identity due to poor solubility in common NMR solvents. However, crystals isolated from slow evaporation of MeCN have the structure *fac*-$[GeF_3(Me_3tacn)]Cl$ (Figure 4.7), this chloride ion was believed to have arisen from the displaced fluoride ion reacting with the chlorocarbon solvent used in the reaction.

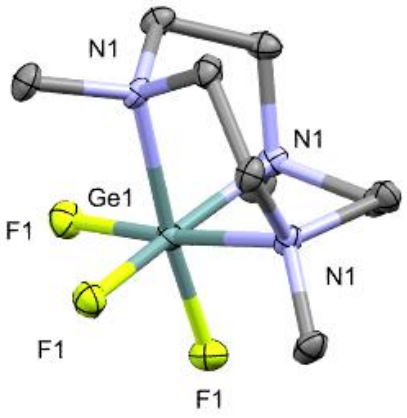

Figure 4.7: Crystal structure the cation in *fac*-$[GeF_3(Me_3tacn)]Cl$. Redrawn from Reference.[14]

There are fewer examples of Sn(IV) complexes with thioether macrocycles, despite extensive research on compounds containing a Sn-S bond in tin chemistry.[18-21] Willey and co-workers demonstrated the synthesis of both cationic $[SnCl_3([9]aneS_3]_2[SnCl_6]$ and neutral κ_2 coordinated

[$SnCl_4$([18]aneS_6)] Sn-S containing macrocyclic complexes.[22] A range of Sn(IV) chloride complexes of the type [R_2SnCl_2(L)], where L is a bipy derivative have been reported, the driving force in this area of research is due to the reported anti-tumour activity of such complexes.[23, 24]

4.1.3 Cationic silicon halide complexes

In the 1960s, the ionic compound [$SiCl_3(PMe_3)_2$][ClO_4] was first reported in the literature and it was shown that it can be synthesised *via* two different pathways. One by reacting $AgClO_4$ with $SiCl_3$ in benzene, with the resultant [$SiCl_3$][ClO_4] being separated from the AgI precipitate and reacted with PMe_3 *via* the addition of two equivalents. The second method reacts two equivalents of PMe_3 with the silicon amine complex, [$SiCl_3(NMe_3)_2$][ClO_4] in MeCN.[25] However, characterisation for this complex was extremely limited, with only partial microanalysis recorded. This was the only known cationic silicon halide complex with a phosphine ligand, up until 2022 when work in the Reid group showed the first examples of cationic silicon iodide phosphine complexes, plus additional characterisation of the $[SiCl_3(PMe_3)_2]^+$ cation.[26]

The reaction of PMe_3 with SiI_4 leads to spontaneous iodide displacement, without the addition of a halide abstractor, and forms the cationic complex [$SiI_3(PMe_3)_2$][I], the crystal structure of which is shown in Figure 4.8, and this contrasts directly with analogous chemistries with the heavier Group 14 element, tin, whereby only the neutral [$SnX_4(PMe_3)_2$] complexes were observed.[27]

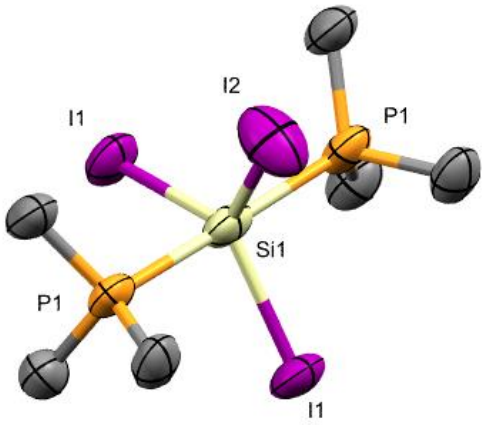

Figure 4.8: Crystal structure of the cationic complex $[SiI_3(PMe_3)_2]^+$. H atoms, I^- counterion and the lattice CH_2Cl_2 molecules are omitted for clarity.[26]

Spontaneous displacement of the lighter halides from the silicon centre was shown not to be possible, this difference in reactivity reflects the weaker Si-I bond and the small size of the silicon centre.[15] It was shown that reactions of SiI_4 with bidentate phosphine ligands, such as

$Et_2P(CH_2)_2PEt_2$ and *o*-$C_6H_4(PMe_2)_2$, only yield the neutral six coordinate complexes of the type $[SiI_4(L\text{-}L)]$, with no evidence of iodide displacement. This difference is likely due to the bidentate phosphines being adequately good donor ligands, but not strong enough to cause "auto-ionisation", even with an excess of ligand.[26]

Following on from these results, the halide abstractor, $Na[BAr^F]$, was used to assess whether a series of lighter cationic silicon halide complexes could be synthesised. The reactions of $[SiX_4(PMe_3)_2]$ with $Na[BAr^F]$ was shown to successfully form the five coordinate species of the type $[SiX_3(PMe_3)_2][BAr^F]$ (where X = Cl or Br). Addition of a second equivalent of $Na[BAr^F]$ did not abstract a second halide. An alternative halide abstractor, TMSOTf, was then utilised to try to form a dicationic complex, however the reactions of $[SiCl_4(PMe_3)_2]$ with one and two equivalents of TMSOTf yield neutral *mono*- and *bis*-triflate containing compounds, $[SiCl_3(PMe_3)_2(OTf)]$ and $[SiCl_2(PMe_3)_2(OTf)_2]$, the crystal structure of the latter is shown in Figure 4.9.[28]

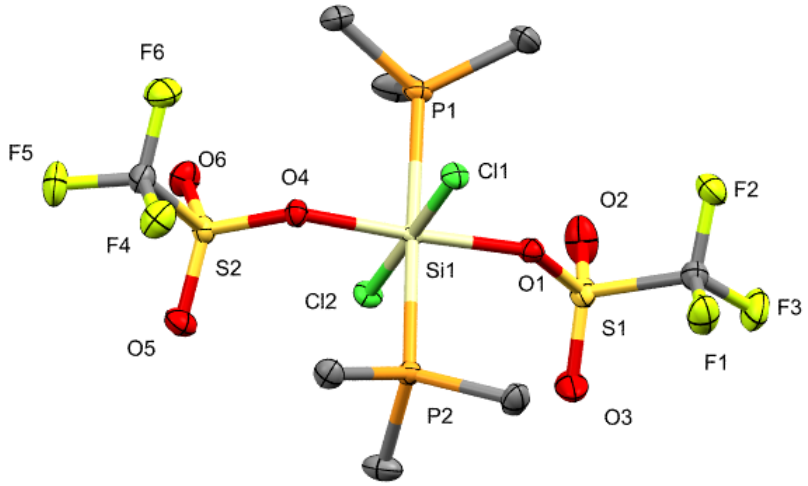

Figure 4.9: The crystal structure of the complex $[SiCl_2(PMe_3)_2(OTf)_2]$.[26]

The crystals of $[SiCl_2(PMe_3)_2(OTf)_2]$ were grown by layering a CH_2Cl_2 solution with *n*-hexane and the structure showed an "all *trans*" complex. This is in direct contrast to the Ge(IV) analogue, $[GeCl_2(PMe_3)_2(OTf)_2]$, where triflates only bind weakly and are mutually *cis*.[29]

There are many examples of silicon(IV) halide complexes with NHC ligands in the literature (however, it is worth noting that there are currently no known neutral silicon(IV) iodide complexes that contain NHCs). For example, the reactions of SiX_4 (where X= Br or I) with 1,2-bis(2,6-diisopropylphenyl)imidazole-2-ylidene) (Dipp) leads to the formation of the cationic complexes $[SiX_3(NHC)][X]$, via the displacement of one halide, the structure of which can be seen in Figure 4.10.[30]

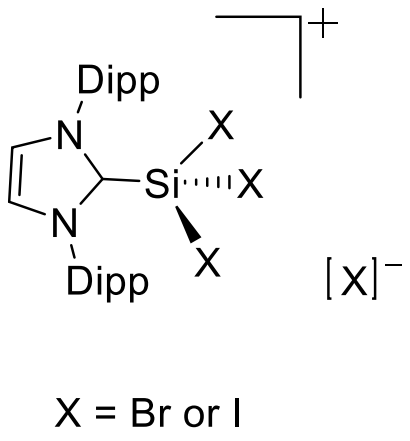

Figure 4.10: Structure of $[SiX_3(NHC)][X]$ where X = Br or I.[30]

4.1.4 Aims

The aim of this Chapter was to develop the chemistry of Group 14 macrocyclic complexes of Sn(IV), Ge(IV) and Si(IV). This work focused on:

i. their ability to form monocationic and dicationic complexes with tridentate and tetradentate aza-macrocyclic ligands;
ii. to assess their suitability as candidates for ^{18}F radiolabelling, through assessment of their synthesis route and stability;
iii. attempt radiofluorination reactions of the complexes deemed suitable.

Complexes have been predominantly characterised by ^{1}H and $^{19}F\{^{1}H\}$ NMR, and IR spectroscopy, microanalysis, and single crystal X-ray analysis.

4.2 Results and discussion

Previous published works have demonstrated that Group 13 metal fluorides are promising in the development of PET radiotracers. In this chapter the coordination chemistry of the Group 14 elements, with neutral N-donor macrocyclic ligands, were explored to assess their feasibility as a platform to PET imaging. Sn(IV) was chosen initially due to the ease in handling and accessibility through the synthon $[SnF_4(MeCN)_2]$ and due to it having several NMR active isotopes and therefore more diagnostic NMR data, with the aim of moving up the Group, with increasing M-F bond strength. The neutral Me_3tacn and $BnMe_2$tacn ligands were synthesised from literature preparations, with the latter ligand being of particular interest with regards to radiolabelling experiments due to the benzyl group, this acts as a chromophore and can be tracked by HPLC during these radiolabelling reactions.[31, 32] The benzyl group can also act as a site for bioconjugation, thus creating biologically active imaging agents.[33, 34] Preliminary work was done using the ligand Me_3tacn, instead of $BnMe_2$tacn, as the Me_3tacn ligand can be synthesised in greater yields and is significantly cheaper to make than that of the benzyl analogue and it is expected to behave in a very similar way.

4.2.1 Synthesis of $[SnF_3(RMe_2tacn)][OTf]$ complexes where R = Me or Bn

The reaction of one molar equivalent of each $[SnF_4(MeCN)_2]$, TMSOTf and RMe_2tacn in MeCN, yields pale yellow solids, which are filtered off and washed in anhydrous hexane to remove unreacted ligand (Scheme 22).

Scheme 22: General synthetic route to $[SnF_3(RMe_2tacn)][OTf]$ where R = Me or Bn.

Anhydrous MeCN was the reaction solvent of choice after seeing unwanted peaks in the ^1H NMR and $^{19}F\{^1H\}$ NMR spectrum when using only CH_2Cl_2, this may be due to the Lewis acid promotion of the metal centre or due to Cl^- in the solvent reacting.

The $^{19}F\{^1H\}$ NMR spectrum of $[SnF_3(Me_3tacn)][OTf]$ (Figure 4.11) clearly shows the formation of a *facially* coordinated Me_3tacn complex, with a singlet at -186.7 ppm and this also has well resolved $^1J_{19F\text{-}119Sn}$ and $^1J_{19F\text{-}117Sn}$ spin couplings. The magnitudes of the coupling constants are consistent

with the expectation based on $\gamma^{119}Sn/\gamma^{117}Sn$ (1.046), where γ is the gyromagnetic ratio for each isotope.[35] This is in clear contrast to the spectrum for the $[SnF_3(dmso)_3][OTf]$ analogue, shown in Chapter 2 (Figure 2.15), which has a mix of both *fac* and *mer* complexes.

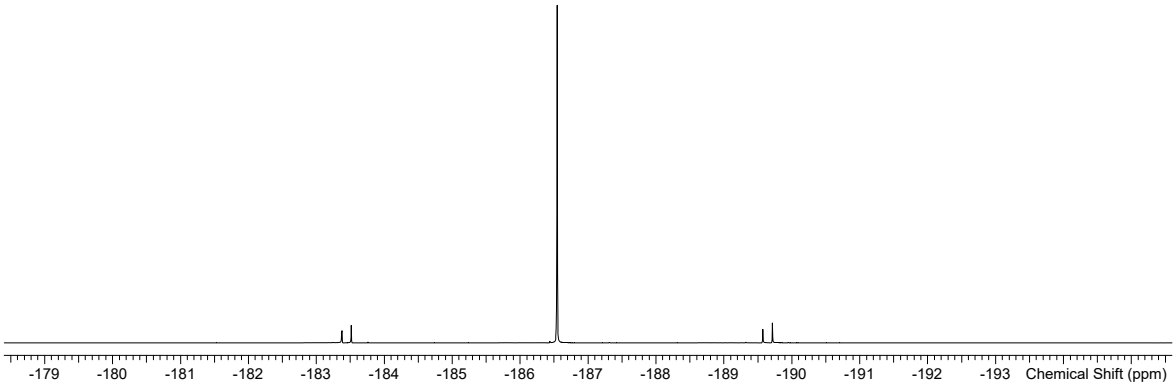

Figure 4.11: $^{19}F\{^1H\}$ NMR spectrum of $[SnF_3(Me_3tacn)][OTf]$ (298 K, CD_3NO_2). Triflate resonance omitted for clarity.

The ^{119}Sn NMR spectrum of $[SnF_3(Me_3tacn)][OTf]$ is shown in Figure 4.12, it proved difficult to get a fully resolved ^{119}Sn NMR spectrum due to the relatively poor complex solubility, and low receptivity of the ^{119}Sn isotope, however it does seem to be in line with the expected 1:3:3:1 quartet and the coupling constant for $^1J_{19F\text{-}119Sn}$ is similar to those obtained from the $^{19}F\{^1H\}$ NMR spectrum.

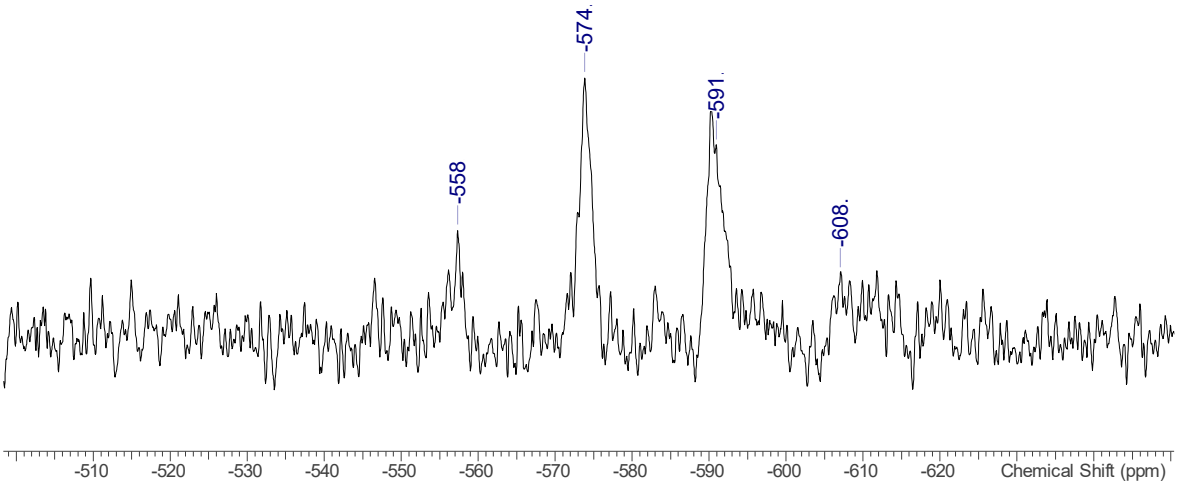

Figure 4.12: $^{119}Sn\{^1H\}$ NMR spectrum $[SnF_3(Me_3tacn)][OTf]$ (298 K, 1:5 CD_3NO_2/CH_3NO_2).

Table 15 outlines key NMR spectroscopic results for $[SnF_3(Me_3tacn)][OTf]$.

Table 15: ^{119}Sn and $^{19}F\{^{1}H\}$ NMR data for $[SnF_3(Me_3tacn)][OTf]$.

Compound	Isomer	δ ^{119}Sn (ppm)	δ $^{19}F\{H\}$ (ppm)	$^{1}J(^{19}F\text{-}^{119}Sn)$ (Hz)
$[SnF_3(Me_3tacn)][OTf]$	*fac*	-582.9 (q)	-186.7 (s)	2388

The infrared spectrum for this complex, recorded using CsI salt plates as a Nujol mull, also indicates the presence of the desired complex, with two IR active bands in the Sn-F region at 579 and 563 cm^{-1} (A_1 and E). Two peaks in this region are expected for an octahedral complex with *facially* coordinated Me_3tacn with C_{3v} symmetry. The ESI^+ mass spectrum gave an *m/z* and isotope pattern consistent with the tin species $[SnF_3(Me_3tacn)]^+$ (*m/z* = 348; 100%), as shown in Figure 4.13.

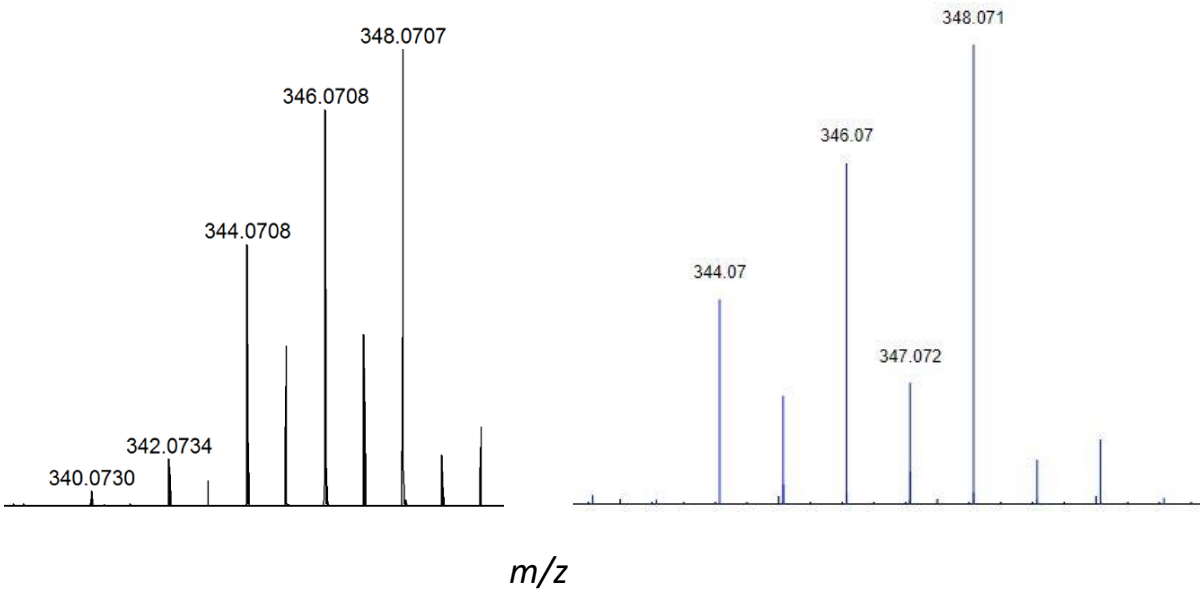

Figure 4.13: LRMS (ESI^+) mass spectrum of $[SnF_3(Me_3tacn)]^+$ in CH_3NO_2 (actual: left) and simulated ESI^+ mass spectrum of $[SnF_3(Me_3tacn)]^+$ (simulated: right).

Colourless crystals suitable for single crystal X-ray crystallography were isolated by slow evaporation from a CH_3NO_2 solution (Figure 4.14). The structure of the cation shows an octahedral Sn(IV) centre with *facial* coordination of the ligand. The cation is *iso*-structural to the neutral Group 13 gallium analogue, $[GaF_3(Me_3tacn)]$.[33]

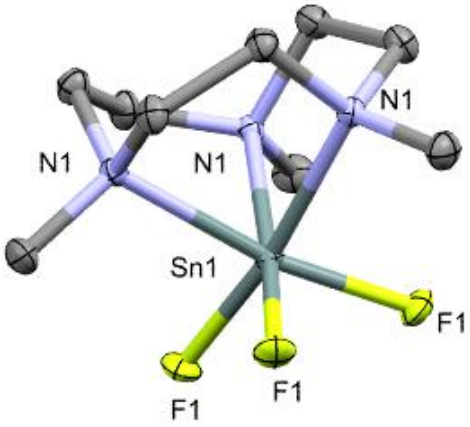

Figure 4.14: Crystal structure of the cation, $[SnF_3(Me_3tacn)]^+$, in the complex $[SnF_3(Me_3tacn)][OTf]$. Hydrogens and OTf^- omitted for clarity. Ellipsoids are drawn at the 50% probability level. The molecule has three-fold symmetry. Selected bond lengths (Å) and angles (°) are: Sn1-F1 = 1.937(2), Sn1-N1 = 2.206(3), N1-Sn1-N1 = 81.21(10), F1-Sn-N1 = 92.46(6), F1-Sn1-N1 = 170.08(9).

When compared to the chloride analogue as reported in the literature, the Sn-N bond is slightly shorter (2.206 *vs* 2.244 Å) and the Sn-F bond is significantly shorter at 1.937 Å versus 2.368 Å for the Sn-Cl.[36] This is expected due to the more electronegative fluorine and higher bond dissociation energies associated with it, and due to the fact F is smaller than Cl.

Attempts were made to find a milder route to the Me_3tacn complex through ligand substitution of a pre-formed *tris* cationic complex, such as $[SnF_3(dmso)_3][OTf]$, whilst the spectroscopic data looked promising, due to the highly coordinating nature of dmso it proved difficult to fully remove all of the residual dmso, as reported with the analogous $[GaF_3(RMe_2tacn)]$ chemistry reported in Chapter 5. This could become a problem at a radiolabelling stage due to only requiring ng concentrations and any impurities at this level can create significant problems and therefore was not further explored using the dmso complex.

4.2.1.1 Stability studies of $[SnF_3(Me_3tacn)][OTf]$ via $^{19}F\{^1H\}$ NMR spectroscopy

$^{19}F\{^1H\}$ NMR stability studies on the 'cold' ^{19}F complex, $[SnF_3(Me_3tacn)][OTf]$, were undertaken on a ~ 20 mg scale to test the behaviour of the complex under a variety of conditions. However, it is worth noting that during a radiolabelling experiment, only very small quantities of complex are used (ng) in combination with $[^{18}F]$fluoride target water, hence the reactivities and stabilities at each scale may differ significantly. The NMR scale experiments were carried out in a 10% $EtOH/D_2O$ solution.

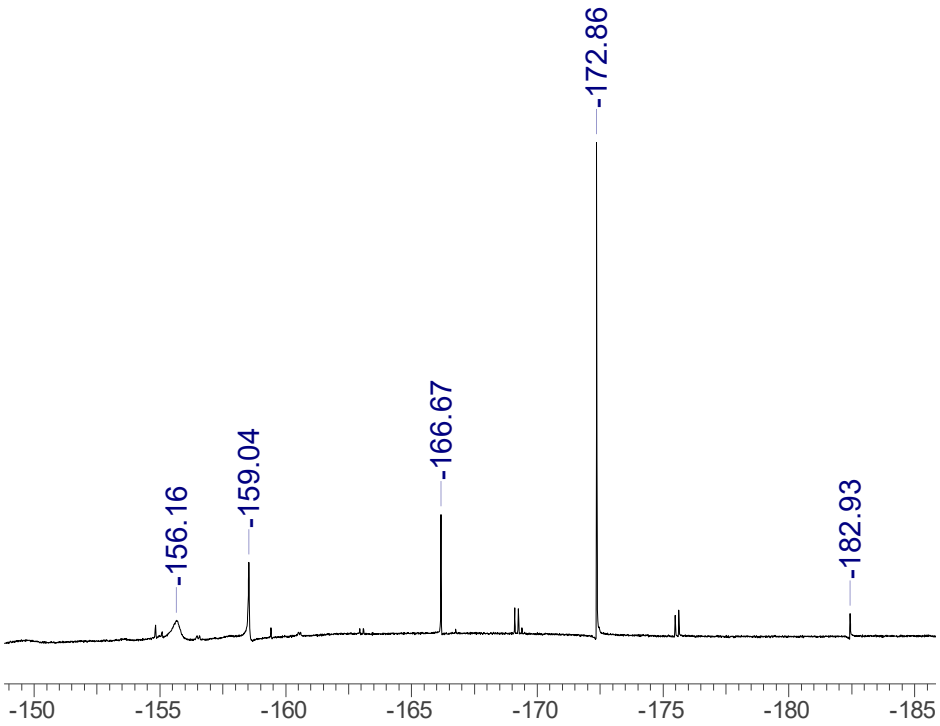

Figure 4.15: $^{19}F\{^{1}H\}$ NMR spectrum of $[SnF_3(Me_3tacn)][OTf]$ (298 K, 10% $EtOH/D_2O$).

Figure 4.15 shows the resonance of $[SnF_3(Me_3tacn)][OTf]$ as a sharp singlet with tin satellites at -172.9 ppm, which is closely matched to the spectrum in Figure 4.11, with the chemical shifts differing slightly due to the different solvent system. There are other minor species present, without Sn satellites, between -156.2 and -183.0 ppm, which are not present in the original spectrum and are likely minor degradation products due to hydrolysis.

Further NMR scale studies were undertaken in competitive media containing a 10 fold excess of each $NaHCO_3$ Na_3PO_4 and NaOAc, and their $^{19}F\{^{1}H\}$ NMR spectra are shown in Figure 4.16.

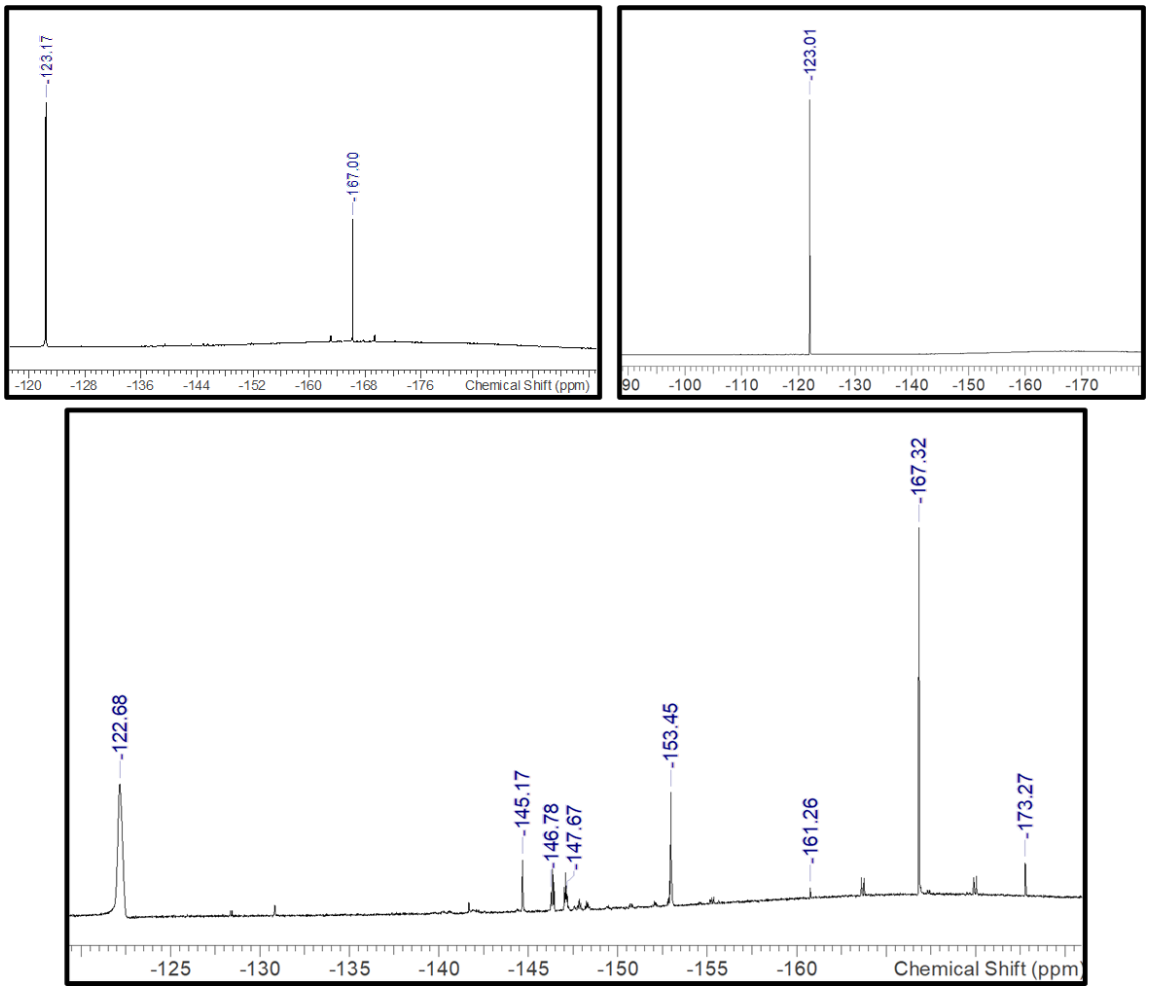

Figure 4.16: Top:$^{19}F\{^{1}H\}$ NMR spectrum of $[SnF_3(Me_3tacn)][OTf]$ in the presence of a 10-fold excess of $NaHCO_3$ (left) and in the presence of a 10-fold excess of Na_3PO_4 (right) Bottom: $^{19}F\{^{1}H\}$ NMR spectrum of $[SnF_3(Me_3tacn)][OTf]$ in the presence of 10-fold excess of NaOAc.

The data shows that the complex is not stable in PO_4^{3-}, leading to immediate and complete degradation to F^- (-123.0 ppm). This instability is likely to be due to a pH effect rather than the presence of the PO_4^{3-} anions, however in Na_2CO_3, whilst a significant amount of F^- was formed, the complex resonance was clearly visible. The presence of a 10-fold excess of NaOAc, NaCl and KF did not affect the NMR spectra significantly, only causing a minor amount of degradation that did not worsen over time.

Further studies were conducted in media that replicate those *in vivo*, the $^{19}F\{^{1}H\}$ NMR spectra of $[SnF_3(Me_3tacn)][OTf]$ in PBS and HSA solutions after four hours are shown in Figure 4.17, with the red bands indicating the presence of tin satellites.

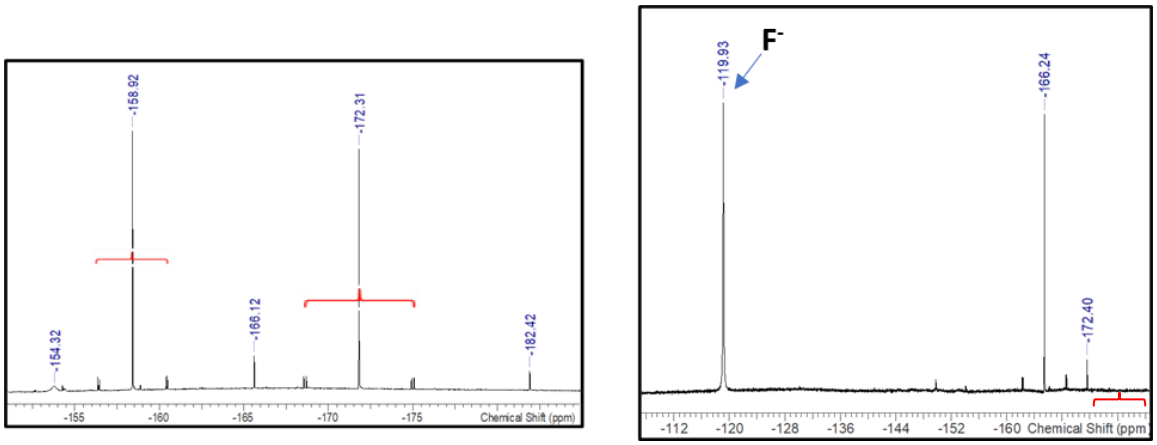

Figure 4.17: $^{19}F\{^{1}H\}$ NMR spectrum of $[SnF_3(Me_3tacn)][OTf]$ in 80% PBS/D_2O solution (left) and in an 80% HSA/D_2O solution (right).

The complex in PBS forms a second tin species directly after addition to the solution, indicated by the second set of tin satellites either side of the peak at -158.9 ppm. However, in HSA, the complexes $^{19}F\{^{1}H\}$ NMR spectrum only showed two resonances, a sharp resonance at -119.9 ppm indicated the presence of F^-, this is indicative of some decomposition, however it did not increase in size over time and the complex peak remained the major compound in solution, demonstrating a reasonable level of stability in this medium.

4.2.2 Synthesis of $[GeF_3(RMe_2tacn)][OTf]$ where R = Me or Bn

Scheme 23: General synthetic route to $[GeF_3(RMe_2tacn)][OTf]$ where R= Me or Bn.

Similar syntheses to the above were conducted using the Ge(IV) analogue, $[GeF_4(MeCN)_2]$, with TMSOTf and RMe_2tacn (R = Me or Bn) in a mixture of MeCN and CH_2Cl_2. The solubility issues and lack of solution data provided from previous work was overcome by the use of the halide abstractor TMSOTf and forming the counterion $[OTf]^-$, instead of $[GeF_6]^{2-}$. This complex was shown to be soluble enough in CD_3NO_2 to acquire good NMR data.[14]

The $^{19}F\{^{1}H\}$ NMR spectrum shows a single resonance for $[GeF_3(Me_3tacn)]^+$ cation at -151.7 ppm and this is consistent with the expected geometry, with the ligand coordinating *facially* to the Ge(IV) centre only (Figure 4.18). The analysis of the data for this germanium complex is aided by the initial synthesis of the tin analogue.

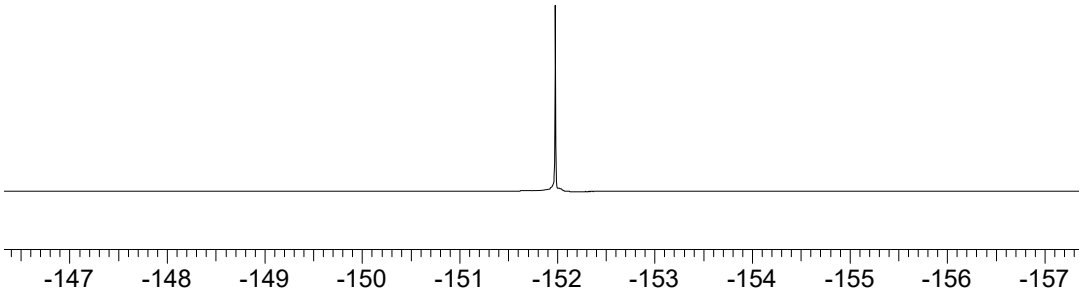

Figure 4.18: $^{19}F\{^{1}H\}$ NMR spectrum of $[GeF_3(Me_3tacn)][OTf]$ (298 K, CD_3NO_2). Triflate region omitted for clarity.

The ESI^+ mass spectrum gave an *m/z* and isotope pattern consistent with the germanium species $[GeF_3(Me_3tacn)]^+$ (*m/z* = 302; 100%), as shown in Figure 4.19.

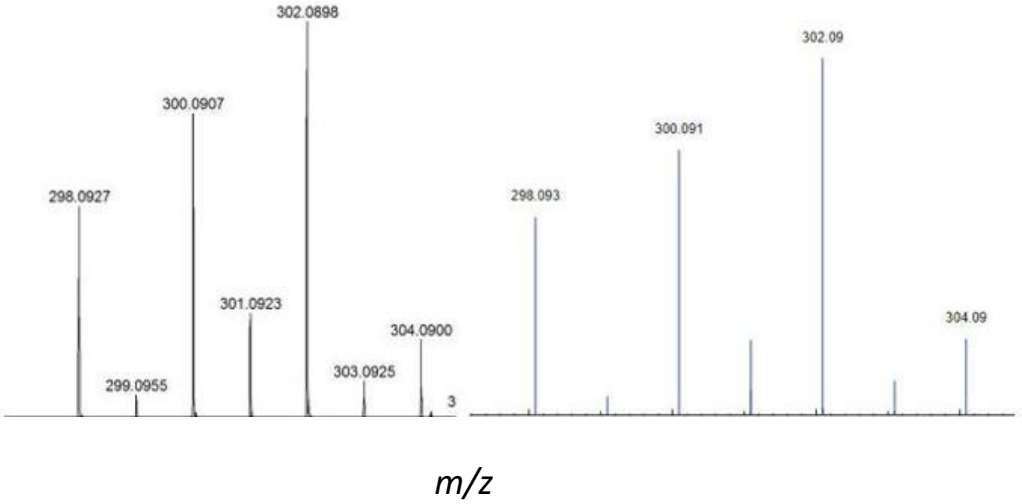

Figure 4.19: LRMS (ESI^+) mass spectrum of $[GeF_3(Me_3tacn)]^+$ in CH_3NO_2 (left) and simulated ESI^+ mass spectrum of $[GeF_3(Me_3tacn)]^+$ (right).

Despite several different attempts, crystals suitable for single crystal X-ray diffraction were not grown, however as described previously, earlier work had shown the structure of $[GeF_3(Me_3tacn)]Cl$ with *facial* geometry.

4.2.2.1 Effect of competitive anions on $[GeF_3(Me_3tacn)][OTf]$ using $^{19}F\{^{1}H\}$ NMR spectroscopy as a probe

The stability of $[GeF_3(Me_3tacn)][OTf]$ was challenged in the presence of chloride and acetate anions, and PBS at pH 7.4. The experiments were carried out in CD_3NO_2 and D_2O for the latter experiment and tracked using $^{19}F\{^{1}H\}$ NMR spectroscopy. The stability of the chelate complex to the competitive anions Cl^- and OAc^-, in a 10-fold excess, which were added as sodium salts, was tested and the $^{19}F\{^{1}H\}$ NMR spectra were unchanged upon addition of the salts, as shown in Figure 4.20 and 4.21.

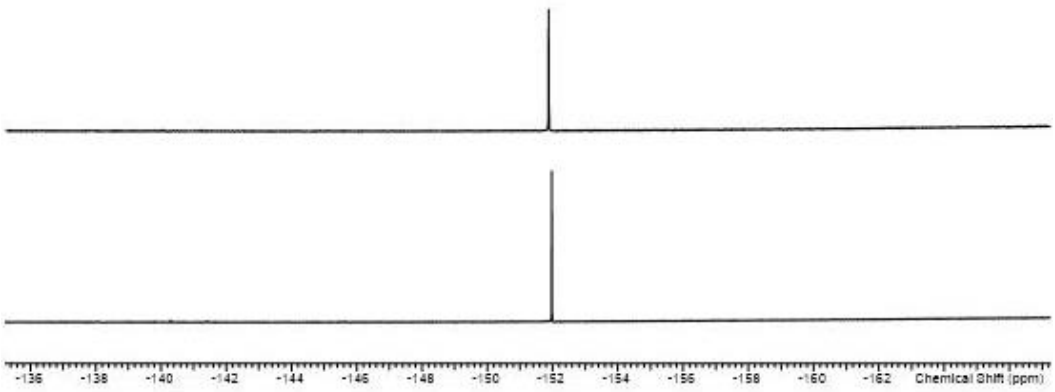

Figure 4.20: $^{19}F\{^{1}H\}$ NMR spectrum of $[GeF_3(Me_3tacn)][OTf]$ in a 10-fold excess of Cl^- ions (CD_3NO_2, 298 K). Top spectrum, t= 0. Bottom spectrum, t = 21 h.

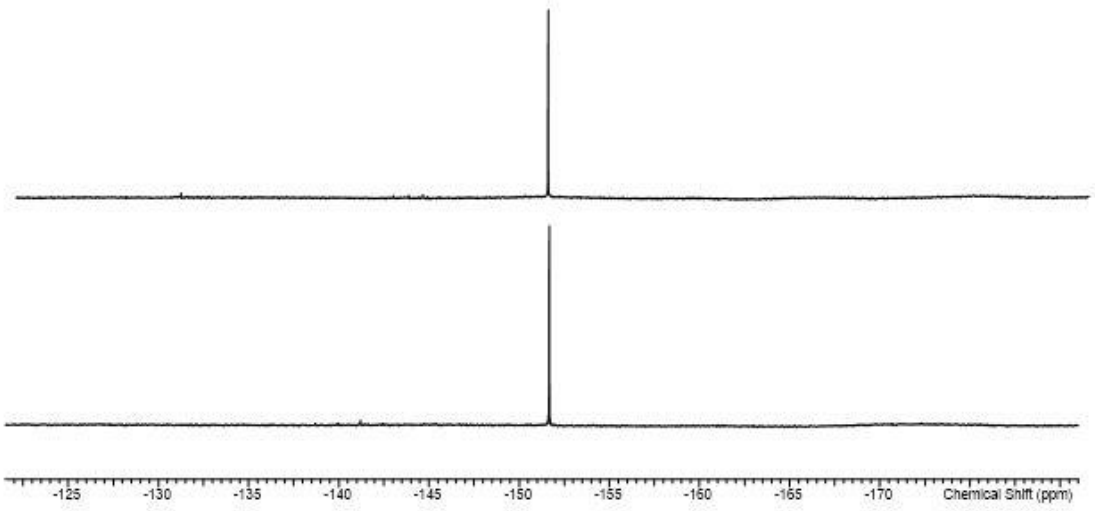

Figure 4.21: $^{19}F\{^{1}H\}$ NMR spectrum of $[GeF_3(Me_3tacn)][OTf]$ in a 10-fold excess of OAc^- anions (CD_3NO_2, 298 K). Top spectrum, t= 0. Bottom spectrum, t = 21 h.

The stability study of the complex in PBS and D_2O showed the appearance of an additional small peaks in the $^{19}F\{^{1}H\}$ NMR spectrum (Figure 4.22), likely attributed to F^- and HF_2^- and organofluorine degradation products, however the chelate complex remained the major product peak after 21 h in solution.

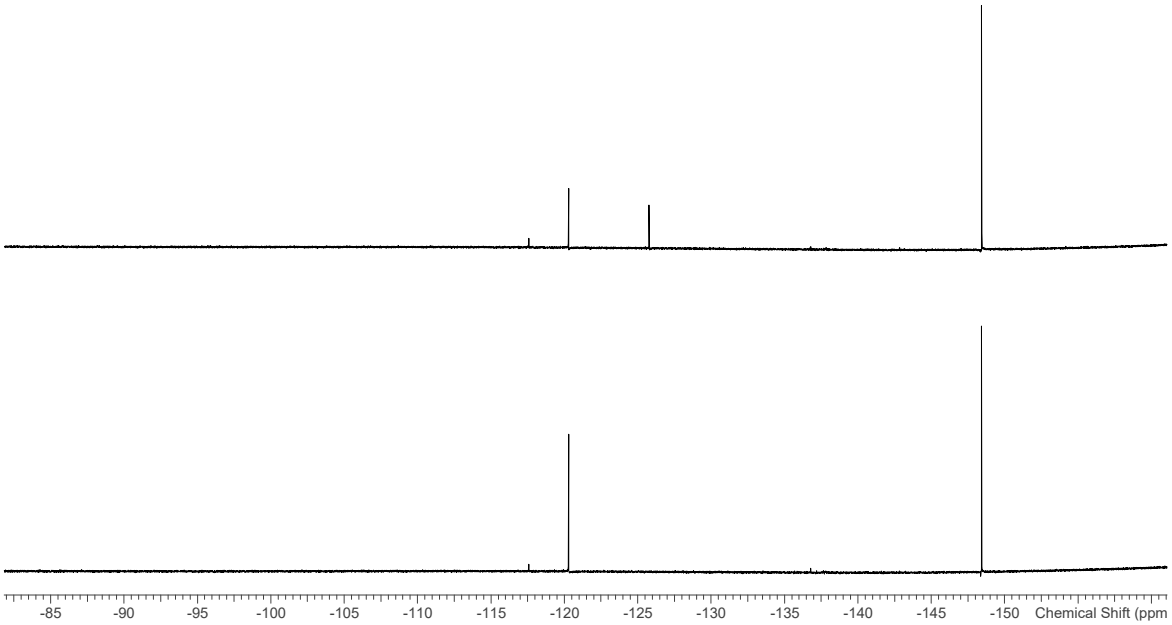

Figure 4.22: $^{19}F\{^{1}H\}$ NMR spectrum of $[GeF_3(Me_3tacn)][OTf]$ in PBS/D_2O mixture. Top spectrum, t= 0. Bottom spectrum, t = 21 h.

4.2.3 Synthesis of $[SiX_3(L)][OTf]$ complexes where L = terpyridine or RMe_2tacn (R = Me or Bn X = F, Cl, or I)

Initially, due its smaller impact on cost and time, terpy was used as the tridentate ligand to explore the synthesis of SiX_3^+ containing complexes. $SiCl_4$ was combined with one molar equivalent of each terpy and TMSOTf in CH_2Cl_2 and stirred at room temperature for 17 h (Scheme 24). An off-white solid of *mer*-$[SiCl_3(terpy)][OTf]$ precipitated out of solution overnight and was filtered, washed in pentane, and produced in good yield (66%).

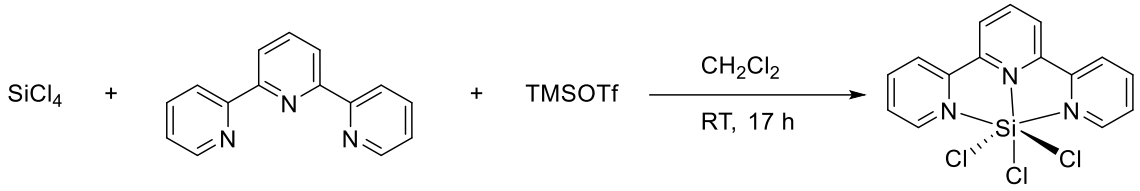

Scheme 24: Schematic for the synthesis of *mer*-$[SiCl_3(terpy)][OTf]$, from $SiCl_4$, terpy and TMSOTf, in CH_2Cl_2.

The complex was analysed by ^{1}H and ^{29}Si NMR spectroscopy, as well as IR spectroscopy, elemental analysis, and X-ray crystallography. The ^{1}H NMR spectrum showed four different environments and the expected shift to a higher frequency upon ligand coordination. The ^{29}Si NMR spectrum (Figure 4.23) was acquired with the help of the relaxation agent tris(2,2,6,6-tetramethyl-3,5-heptanedionato)chromium(III) (TMHD) and the spectrum showed one

resonance at -170.0 ppm, due to the presence of a single silicon environment, this is owed to the locking of the *mer* geometry and symmetry of the complex.

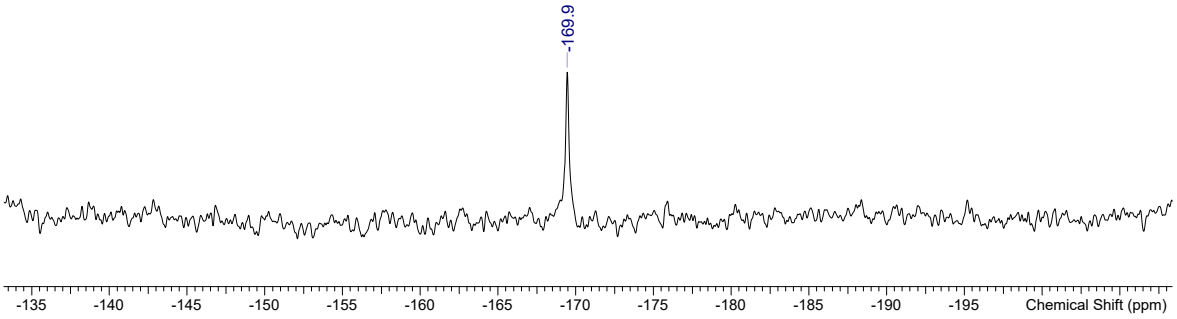

Figure 4.23: ^{29}Si NMR spectrum of $[SiCl_3(terpy)][OTf]$ (d_3-MeCN, 298 K). Range from 0 to –500 ppm was explored; the spectrum was expanded for clarity and only the -170 ppm resonance was observed throughout.

Crystals of $[SiCl_3(terpy)][OTf]$ grown from the slow evaporation of a MeCN solution show the chlorides are coordinated to the metal in a *meridional* configuration, as expected for the structurally rigid ligand. The complex has a distorted octahedral coordination environment around the metal due to terpy locking the geometry (Figure 4.24).

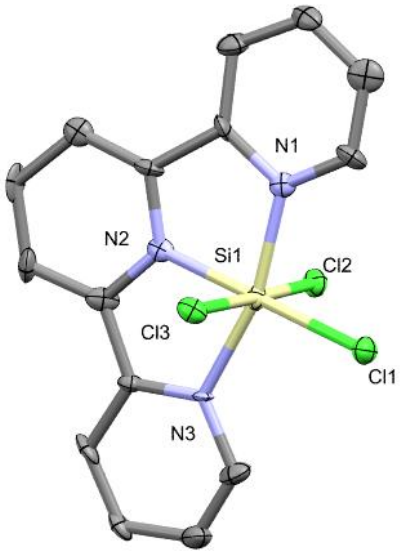

Figure 4.24: Crystal structure of the cation, $[SiCl_3(terpy)]^+$, in the complex $[SiCl_3(terpy)][OTf]$. Ellipsoids shown at 50% probability. H atoms and OTf omitted for clarity.

A number of crystals were isolated and they showed a significant amount of disorder, so a definitive assignment cannot be made by X-ray crystallography alone. However, the cationic

complex structure is not in doubt and has been identified several times, however the bond lengths cannot be compared due to the poor quality data.

An isotopic $^{19}F/Cl$ exchange reaction was undertaken to assess the potential suitability of Si-Cl systems to undergo ^{18}F radiolabelling. To a solution of $[SiCl_3(terpy)][OTf]$.in hexane, 3.5 equivalents of TMAF was added and the reaction mixture was allowed to stir for 1 h. Surprisingly, a blue solid precipitated out of solution, however, on analysis of the $^{19}F\{^1H\}$ NMR spectrum, it showed the expected resonances of a doublet and triplet at -127.4 and -143.6 ppm, respectively. This is the expected number of peaks due to the terpy ligand locking the geometry of the complex meridionally and creating two distinct fluorine environments. An additional smaller singlet resonance was also present in the $^{19}F\{^1H\}$ NMR spectrum at -138.4 ppm, this is likely a small amount of an organofluorine degradation product. Repeats of this reaction to yield a colourless solid with clean elemental analyses was not successful and each time a blue solid was made, despite careful attempts to ensure all starting materials were dry and pure and the solvent used was rigorously anhydrous.

$[SiF_3(Me_3tacn)][SiF_5]$ had been synthesised previously by the Reid Group, by the reaction of SiF_4 gas with the triaza macrocycle, Me_3tacn, in anhydrous CH_2Cl_2 or toluene, as demonstrated in Scheme 25. Crystals of $[SiF_3(Me_3tacn)][Cl]$ were isolated during this work, the chloride anions being attributed to attack on the solvent by the liberated fluoride ion. However, this auto-ionisation was not observed with other tridentate amine ligands, where no other cationic complexes were formed.[37]

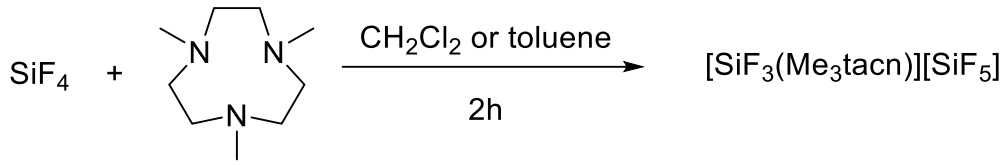

Scheme 25: Schematic to show the synthesis of $[SiF_3(Me_3tacn)][SiF_5]$ developed by Reid and co-workers in 2009.[37]

SiF_4 gas is highly toxic, hard to access, and difficult to control when it comes to the stoichiometries during a reaction. Therefore, an alternative, more controlled and easier to handle route was sought, using the chemistry developed in this thesis. In contrast to SiF_4, $SiCl_4$ and SiI_4 are liquids and significantly easier to handle and control.

One molar equivalent of TMSOTf was added to a solution of $SiCl_4$ in CH_2Cl_2 and stirred for 2 h, followed by the addition of one molar equivalent of Me_3tacn and the reaction mixture was allowed to stir for an additional 14 h. This yielded a colourless solid of $[SiCl_3(Me_3tacn)][OTf]$, which was then dissolved in rigorously anhydrous MeCN and 3.5 molar equivalents of anhydrous

tetramethylammonium fluoride (purified *via* sublimation) was added to the reaction vessel, immediately a colourless solid precipitated out from solution and the reaction was allowed to stir for 1 h (Scheme 26).

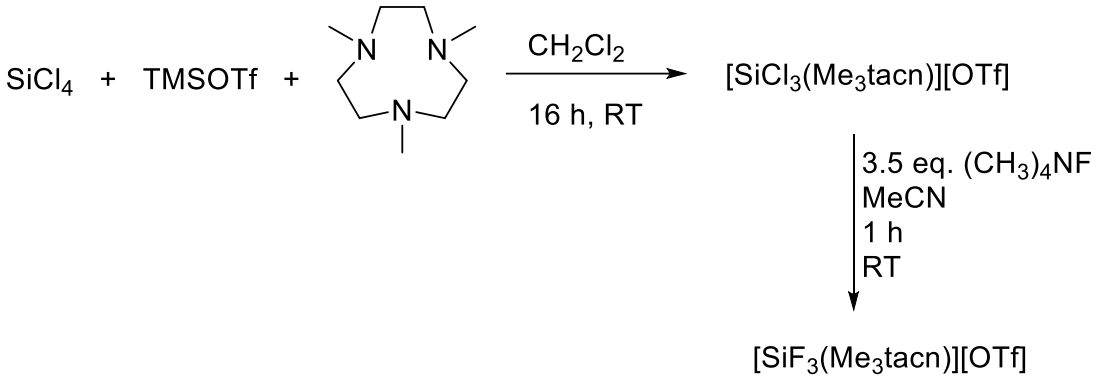

Scheme 26: Schematic to show the newly developed synthetic pathway to $[SiF_3(Me_3tacn)][OTf]$.[15]

The $^{19}F\{^1H\}$ NMR spectrum for this complex can be seen in Figure 4.25, with the triflate anion present at -79 ppm and the cation present at -151.3 ppm, this is close to the reported figure of -148.2 ppm for $[SiF_3(Me_3tacn)][SiF_5]$.[37] It is worth noting that the slight change in chemical shift is likely due to the differing counterion present in each complex.

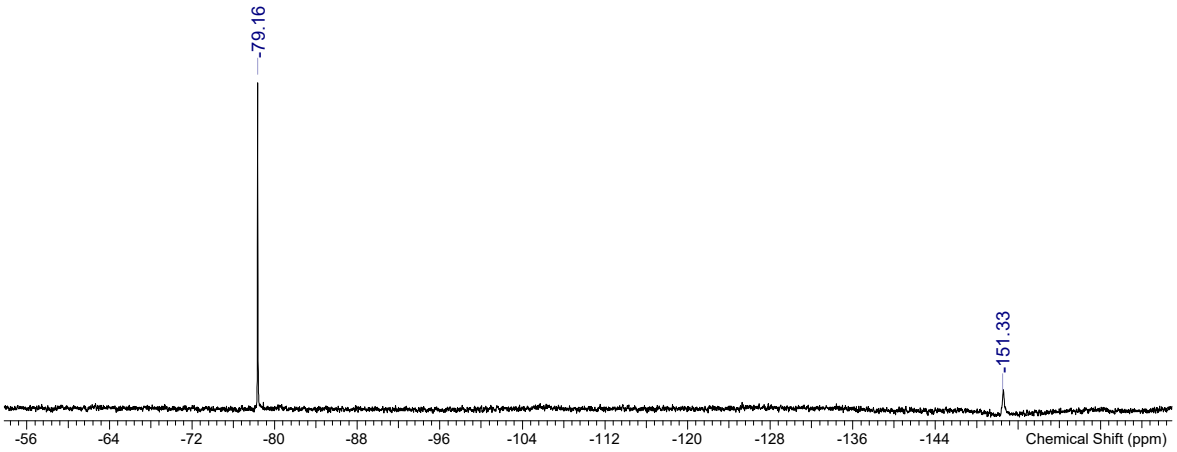

Figure 4.25: $^{19}F\{^1H\}$ NMR spectrum of $[SiF_3(Me_3tacn)][OTf]$ (CD_2Cl_2, 298 K).

The analogous complex containing the $BnMe_2tacn$ ligand was synthesised in the same way through an NMR scale reaction.

A similar reaction was undertaken using SiI_4, $[SiI_3(Me_3tacn)]^+$ was synthesised in the absence of the halide abstractor, TMSOTf, this was done due to the weak Si-I bond likely being broken easily *via* an "auto-ionisation" reaction, with the driving force strongly towards forming a more stable macrocyclic complex with Me_3tacn. It proved to be difficult to isolate due to high sensitivity to air

and moisture, however limited analytical data was acquired. The ^{1}H NMR spectrum in d_3-MeCN showed the presence of two Me_3tacn environments – possibly attributed to the desired complex, which can be distinguished from free ligand due to its downfield shift, and also a small amount of protonated ligand.

Due to its difficulty in handling, an *in situ* NMR-scale reaction was undertaken by adding an excess of $(CH_3)_4NF$ (TMAF) to the reaction mixture to, firstly, understand whether the desired complex had in fact been synthesised successfully and secondly, if the fluoride could be accessed via I/F halide exchange. The latter point would enable us to identify the iodide retrospectively. The $^{19}F\{^{1}H\}$ NMR for this reaction showed a small peak at - 137 ppm, this is significantly more downfield than expected for the $[SiF_3(Me_3tacn)]^+$ cation and is unlikely to be that of the desired complex.

4.2.4 Synthesis of $[MF_2(L)][OTf]_2$ complexes where M = Sn, Ge or Si, and L = Me_4-cyclen or Me_4-cyclam

4.2.4.1 Synthesis of Sn(IV) fluoride complexes with Me_4-cyclen and Me_4-cyclam

Two molar equivalents of TMSOTf were added to a solution of $[SnF_4(MeCN)_2]$ in rigorously anhydrous MeCN and/or CH_2Cl_2, followed by the addition of one molar equivalent of the appropriate tetra-aza macrocycle at room temperature (Figure 4.26), which yielded mildly moisture sensitive yellow-orange solids.

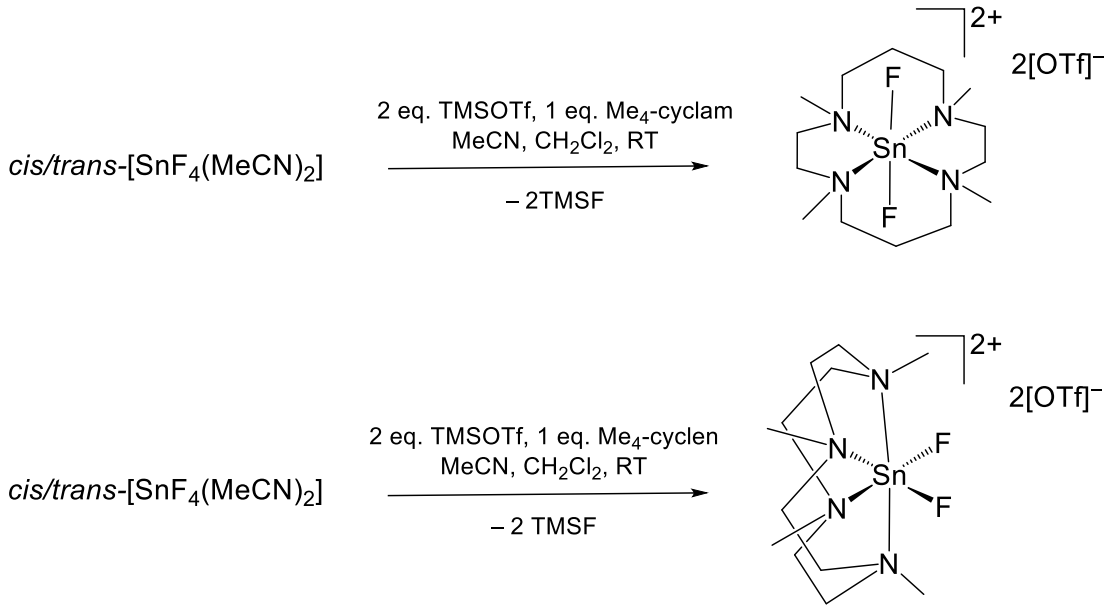

Figure 4.26: Synthesis of the dicationic, *endocyclic* Sn(IV) tetra-aza macrocyclic complexes.

The ^{1}H NMR spectrum of [SnF_2(Me_4-cyclam)][OTf]$_2$ is complex and displays many overlapping broad features from 3.0-4.2 ppm, this is in contrast to free Me_4-cyclam which shows a singlet and two multiplets, corresponding to the methyl and methylene protons, respectively. This is consistent with coordination of the ligand to the metal centre. The CH_2 protons in the backbone of cyclam give a complex second order pattern, which is consistent with proton inequivalency upon coordination to the metal. The ^{1}H NMR spectrum aids in understanding what complex has been synthesised, however it cannot provide much detail on its own due to the presence of a mixture of isomers which is dependent on the rate of interconversion of the isomers in solution.

The ^{19}F{^{1}H} NMR spectrum of [SnF_2(Me_4-cyclam)][OTf]$_2$ (Figure 4.27) reveals the presence of two isomers in solution, with two pairs of doublet resonances present with the $^{1}J_{19F\text{-}119Sn}$ also clearly visible, therefore confirming complexation to the Sn centre. These are mostly likely attributable to two isomers that contain fluorines in different environments. From this data, it is likely that the *trans* I and *trans* II isomers (shown in

Figure 4.3) were present in solution when the NMR was run. It is likely that interconversions between different stereoisomers may occur over time. A singlet at -79.4 ppm is not shown but is present and corresponds to the presence of triflate and this is omitted from view for clarity. The complex was shown to be remarkably stable, a stability study of this complex over 10 days was conducted using ^{19}F{^{1}H} NMR as a probe and it remained stable, with no signs of degradation.

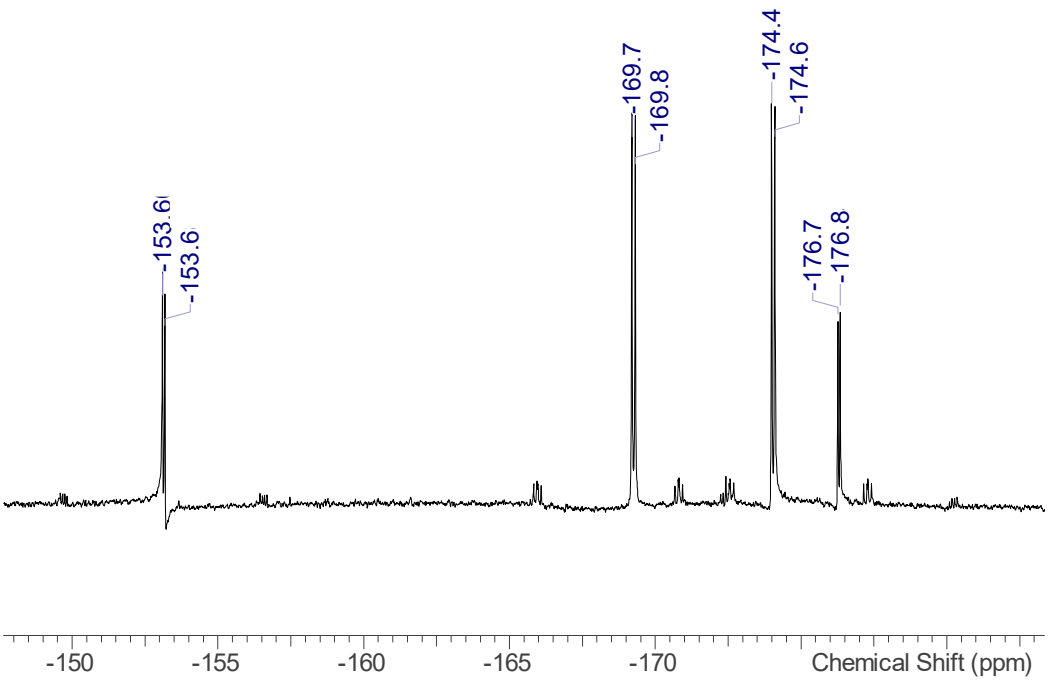

Figure 4.27: $^{19}F\{^{1}H\}$ NMR spectrum $[SnF_2(Me_4\text{-cyclam})][OTf]_2$ (298 K, CD_3NO_2). Triflate region omitted for clarity.

To aid in identifying the complex, electrospray mass spectrometry (ESI) was utilised. The ESI^+ gave an *m/z* and isotope pattern consistent with the tin species $[SnF_2(Me_4\text{-cyclam})]^{2+}$ (*m/z* = 207; 100%), as shown in Figure 4.28.

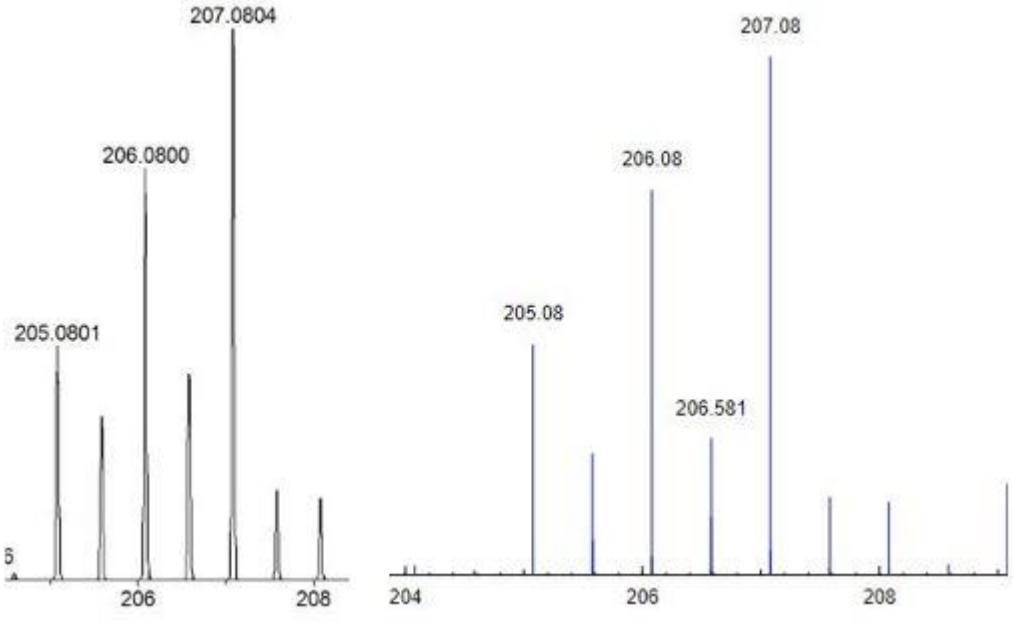

Figure 4.28: ESI^+ mass spectrum and isotope pattern of $[SnF_2(Me_4\text{-cyclam})]^{2+}$ in CH_3NO_2 (left) and predicted spectrum and isotope pattern of $[SnF_2(Me_4\text{-cyclam})]^{2+}$ simulated spectrum (right).

The cavity of the 12-membered macrocycle, Me_4-cyclen, was expected to be too small to encapsulate the metal ion, hence Me_4-cyclen is likely to adopt a folded conformation upon complexation.[9] The corresponding reaction to form the tin fluoride complex, yielded a bright orange solid, which was filtered and washed in hexane. The $^{19}F\{^1H\}$ NMR spectrum contains a large singlet with tin satellites, at -172.4 ppm, this is expected for the *trans*-I configuration due to equivalent fluorides. A small set of unknown doublets at -166.5 and -177.8 ppm were also present, likely attributed to a small amount of degradation (Figure 4.29).

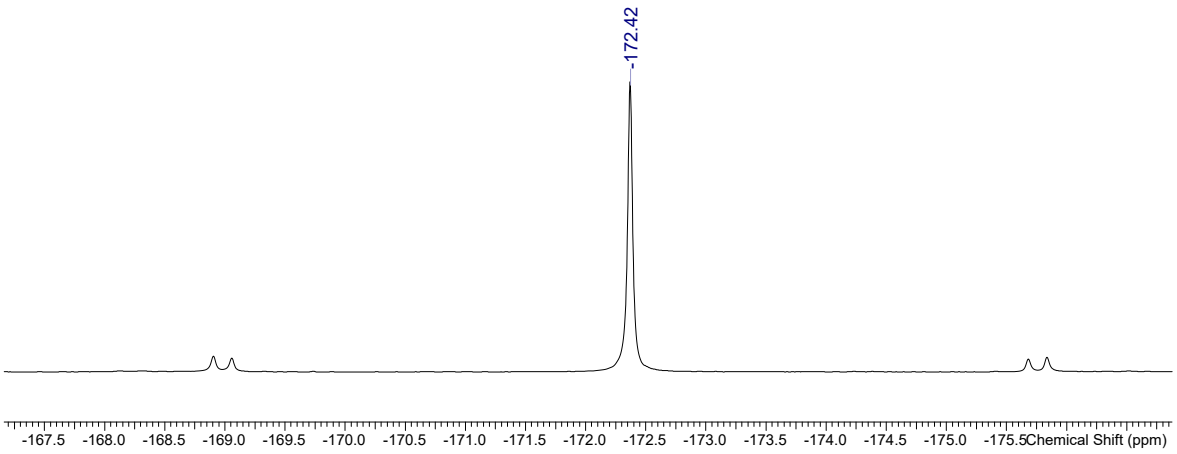

Figure 4.29: $^{19}F\{^1H\}$ NMR spectrum $[SnF_2(Me_4\text{-cyclen})][OTf]_2$ (298 K, CD_3NO_2). Triflate resonance omitted for clarity.

The ESI^+ mass spectrum confirmed the presence of the desired complex in CH_3NO_2, with an *m/z* and isotope pattern consistent with the tin species $[SnF_2(Me_4\text{-cyclen})]^{2+}$ (*m/z* = 207; 100%) (Figure 4.30). Microanalytical measurements of the bulk solid confirmed the expected formulation. Despite several attempts, no crystals suitable for X-ray crystallography were grown for either complex.

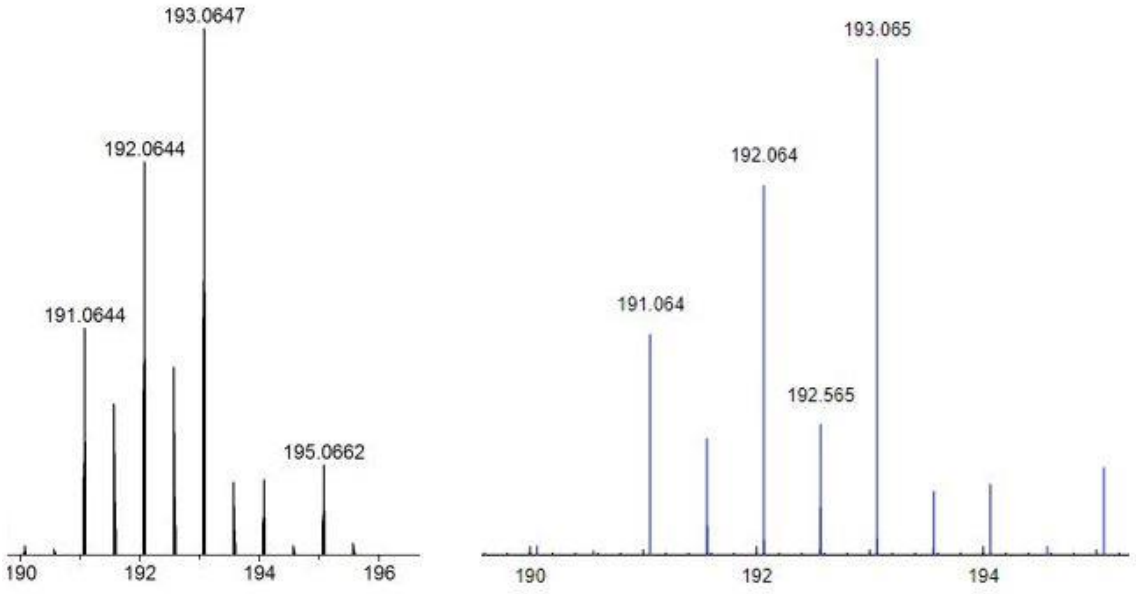

Figure 4.30: ESI$^+$ mass spectrum and isotope pattern of $[SnF_2(Me_4\text{-cyclen})]^{2+}$ in CH_3NO_2 (left) and predicted spectrum and isotope pattern of $[SnF_2(Me_4\text{-cyclen})]^{2+}$ simulated spectrum (right).

4.2.4.2 Synthesis of Ge(IV) fluoride complexes with Me_4-cyclen and Me_4-cyclam

The analogous Ge(IV) reactions were conducted similarly to the Sn(IV) chemistry described above but a longer reaction times were required (72-88 h) for the reactions to go to completion, the complexes were produced in good yield and were yellow-orange solids. The general synthesis pathway to $[GeF_2(Me_4\text{-cyclam})][OTf]_2$ and $[GeF_2(Me_4\text{-cyclen})][OTf]_2$ are shown in Scheme 27.

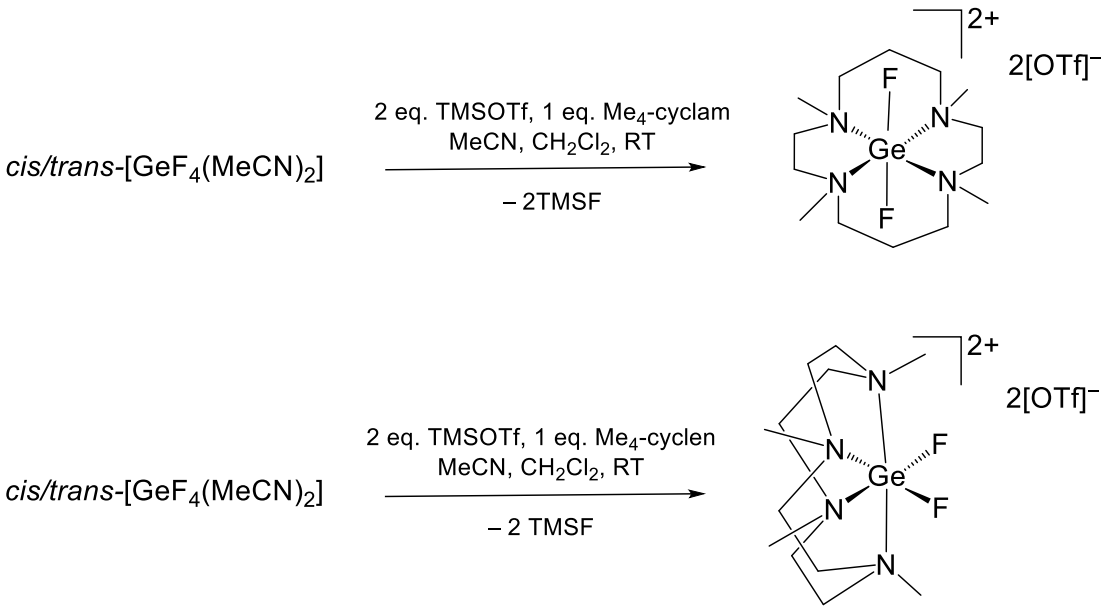

Scheme 27: Synthesis of the dicationic Ge(IV) fluoride tetra-aza macrocyclic complexes $GeF_2(Me_4\text{-cyclam})][OTf]_2$ and $[GeF_2(Me_4\text{-cyclen})][OTf]_2$.

The reaction of $[GeF_4(MeCN)_2]$ with Me_4-cyclam was conducted similarly to the tin complex and was allowed to react for three days. A complex ^1H NMR spectrum was acquired, likely due to the mix of symmetric and asymmetric isomers present in solution. The $^{19}F\{^1H\}$ NMR spectrum contains an additional two singlets in comparison to the spectrum shown for the tin complex above (Figure 4.27), totalling four doublets and two singlets and indicating the presence four (out of a possible five) conformational isomers. These stereoisomers include; the Me groups '*all up*', '*up,up,up,down*', '*up,up,down,down*'—2 variants and '*up,down,up,down*' relative to the GeN_4 plane) of a *trans* octahedral geometry, with slow pyramidal inversion at the nitrogen. Cyclam is a larger, 14-membered ring and this allows germanium to sit within the ring itself (this is in contrast to the smaller, 12-membered Me_4-cyclen).

The coordinated fluorides in the '*all up*' and '*up,up,up,down*' stereoisomers are inequivalent and these account for the four doublets present in the $^{19}F\{^1H\}$ NMR spectrum (Figure 4.31). The two singlets likely account for the other stereoisomers with equivalent coordinated fluorides, however it cannot be ruled out that one of these singlets corresponds to the *cis* isomer.

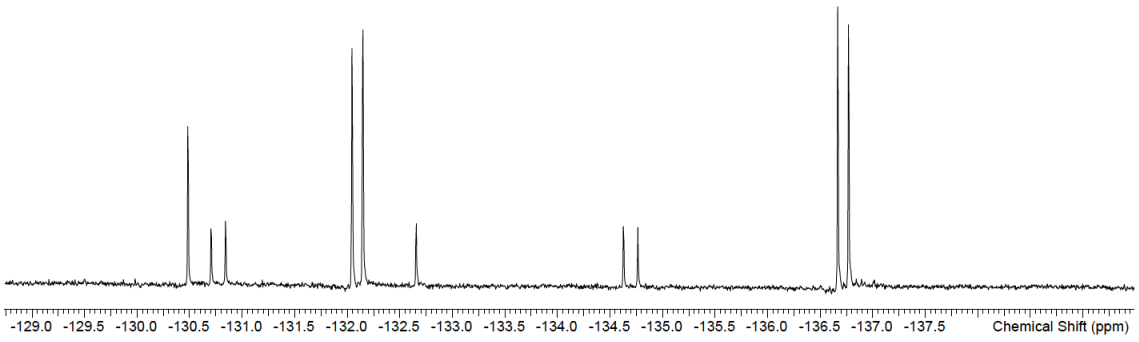

Figure 4.31: $^{19}F\{^1H\}$ NMR spectrum of $[GeF_2(Me_4\text{-cyclam})][OTf]_2$. (298 K, CD_3NO_2). Triflate resonance omitted for clarity.

The Ge(IV) Me_4-cyclen analogue was synthesised over 86 h and resulted in the formation of the desired 6-coordinate complex, $[GeF_2(Me_4\text{-cyclen})][OTf]_2$, as a pale yellow solid in good yield (see Scheme 27). The ^1H NMR spectrum shows an expected pattern of two multiplets between 3.5-4.0 ppm corresponding to the methylene protons within the ring of the macrocycle, and two singlets upfield corresponding to two CH_3 groups each. Germanium has a nuclear spin of 9/2 and a large quadrupolar moment which can lead to line broadening in NMR spectra, the spectrum is shown in Figure 4.32.

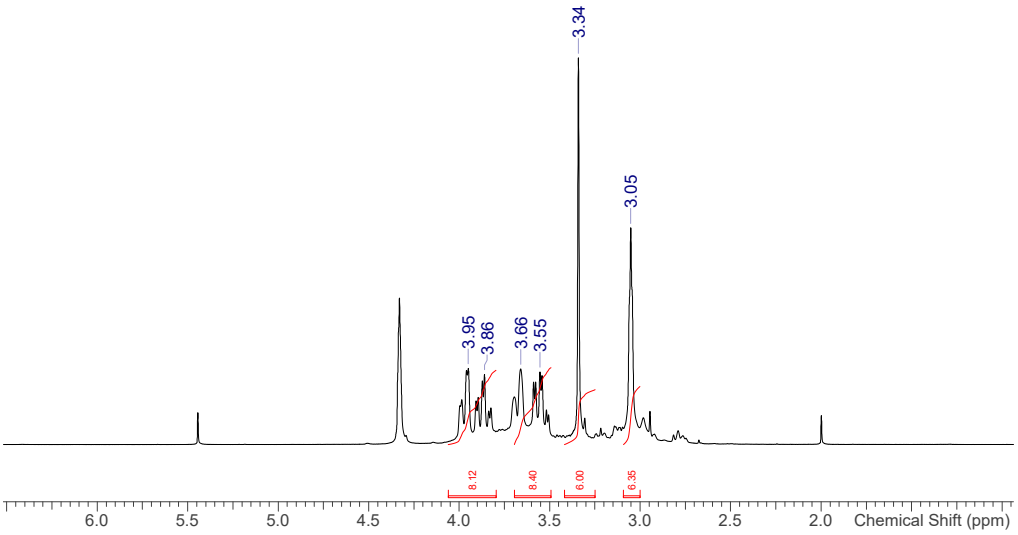

Figure 4.32: ^{1}H NMR spectrum of $[GeF_2(Me_4\text{-cyclen})][OTf]_2$ (298 K, CD_3NO_2)

The second order splitting pattern of the methylene protons in the Me_4-cyclen ring can be seen between 3.55 and 3.95 ppm. In contrast to the complex corresponding $^{19}F\{^{1}H\}$ NMR spectrum of $[GeF_2(Me_4\text{-cyclen})][OTf]_2$ (Figure 4.33), a singlet resonance at -132.3 ppm for the cyclen complex indicates that all the fluorides are equivalent and that the 12-membered ring generated the *cis*-octahedral isomer and this geometry is confirmed *via* the crystal structure shown in Figure 4.35.

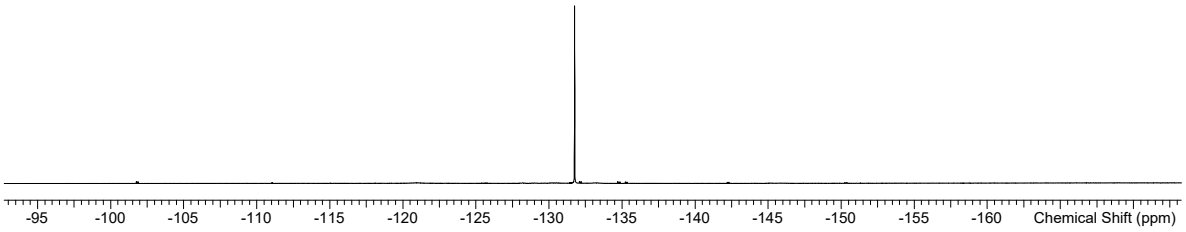

Figure 4.33: $^{19}F\{^{1}H\}$ NMR spectrum of $[GeF_2(Me_4\text{-cyclen})][OTf]_2$ (CD_3NO_2, 298 K). Triflate resonance omitted for clarity.

To aid in unambiguously identifying the complex, positive ion electrospray mass spectrometry was utilised (ESI^+ MS), analysis of the ESI^+ mass spectrum gave an *m/z* and isotope pattern consistent with the species $[GeF_2(Me_4\text{-cyclen})]^{2+}$ (*m/z* = 170.07) (Figure 4.34).

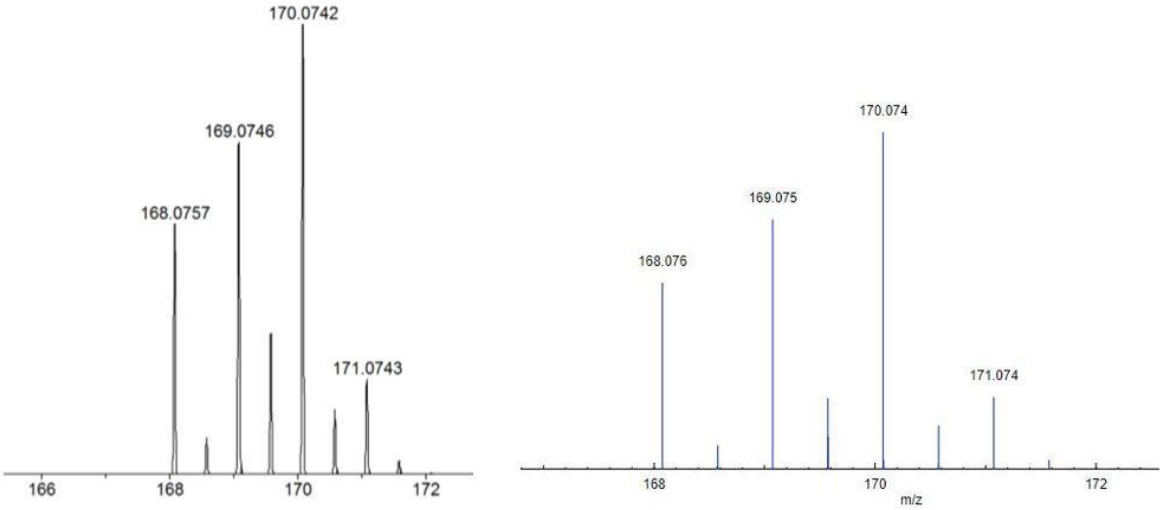

Figure 4.34: ESI$^+$ mass spectrum and isotope pattern of $[GeF_2(Me_4\text{-cyclen})]^{2+}$ in CH_3NO_2 (left) and predicted spectrum and isotope pattern of $[GeF_2(Me_4\text{-cyclen})]^{2+}$ simulated spectrum (right).

An ESI$^-$ mass spectrum was also recorded to confirm the presence of the triflate anion (*m/z* = 148.95; 100%).

X-ray crystallographic analysis of $[GeF_2(Me_4\text{-cyclen})][OTf]_2$, crystals of which were formed *via* slow evaporation of a CH_3NO_2 solution, confirmed that the macrocycle was in a folded conformation (Figure 4.35).

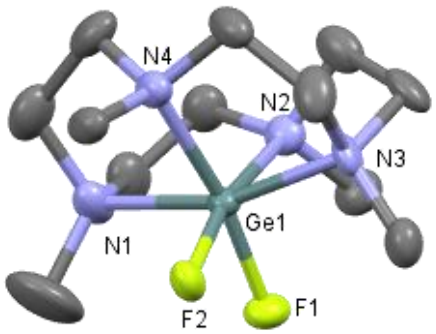

Figure 4.35: The crystal molecular structure of one of the 14 crystallographically independent *cis*-$[GeF_2(Me_4\text{-cyclen})][OTf]_2$ within the unit cell, with the triflates and hydrogens omitted for clarity, (see Experimental for details). Ellipsoids are drawn at the 50% probability level and H-atoms are omitted for clarity. Selected bond lengths (Å) and angles (°): Ge1-F1 = 1.755 (8), Ge1-F2 = 1.792 (8), Ge1-N1 = 2.101 (12), Ge1-N2 = 2.084 (11), Ge1-N3 = 2.035 (11), Ge1-N4 = 2.107 (11), F1-Ge1-F2 = 84.5 (4), N1-Ge1-N4 = 83.8

(5), N2-Ge1-N1 = 84.9 (5), N2-Ge1-N4 = 106.2 (4), N3-Ge1-N1 = 161.7 (5), N3-Ge1-N2 = 84.8 (5), N3-Ge1-N4 = 84.6 (5). The bond distances and angles in the other molecules are broadly similar, but the combination of the unexpectedly large unit cell and the inversion twin preclude detailed comparisons.

Due to the difficulty in solving the $[GeF_2(Me_4\text{-cyclen})][OTf]_2$ crystal structure, Dr Rob Bannister assisted in its refinement. Analysis of the data revealed an inversion twin with a large unit cell in the space group $P2_1$, with the asymmetric unit cell containing 14 cations and 28 anions, and four CH_3NO_2 solvent molecules.

This structure of $[GeF_2(Me_4\text{-cyclen})]^{2+}$ is the first known example of a tetra-aza Ge(IV) dicationic complex. When comparing the difficulties faced when attempting to make analogous dicationic complexes with monodentate ligands, as presented in Chapter 3.2.2, it is clear that there is a significantly greater driving force for the successful synthesis of dications bearing a macrocycle. This is likely due to the thermodynamic and kinetic stability of the macrocyclic complex and the entropic driving force pushing the reaction to completion.

It is worth noting that the analogous tetra-aza reactions were also performed on both Sn(IV) and Ge(IV) systems using the ligands Bn_4-cyclam and Bn_4-cyclen, and whilst the results looked promising and the desired complexes are likely to have formed, the systems proved to be very insoluble in all common NMR solvents and proved too difficult to acquire data for and so were not pursued further.

In contrast to these results, attempts to obtain thioether complexes using the ligands [9]aneS_3, [12]aneS_4 and [14]aneS_4 of Sn(IV) and Ge(IV) fluoride using an analogous approach, proved unsuccessful (Figure 3.15).

4.2.4.3 Attempted synthesis of Si(IV) halide complexes with Me_4-cyclen and Me_4-cyclam

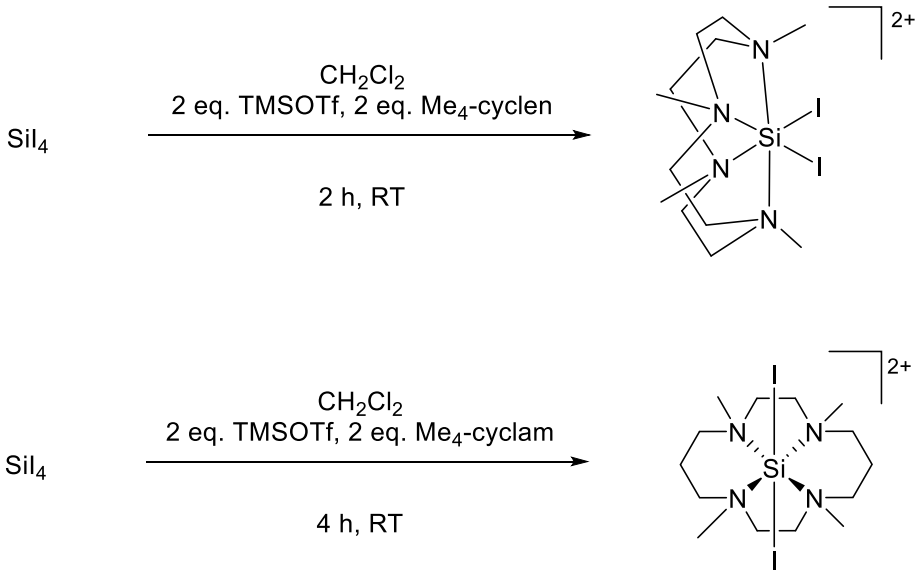

Scheme 28: Synthesis of the Si(IV) tetra-aza macrocyclic complexes and expected structures.

The reaction of SiI_4 with two equivalents of TMSOTf and appropriate ligand produced highly sensitive, yellow solids in good yield and were dried under a flow of nitrogen. Both complexes degraded immediately under a dynamic vacuum and immediately on exposure to air or moisture, this prevented a full and detailed analysis of the complexes, with no crystals suitable for X-ray crystallography due to rapid decomposition. However, the IR spectrum for both complexes showed a medium band at 207 and 210 cm^{-1} for the cyclen and cyclam complex, respectively, likely attributed to the Si-I stretch within the complexes.

The chloride analogues proved even more challenging to isolate, despite many attempts under different conditions, the products from these reactions were viscous and difficult to acquire full detailed analysis.

4.2.5 Attempted radiofluorination reactions

Following on from previous radiolabelling work in the Reid group on the Group 13 system, [GaF_3($BnMe_2$tacn)], and after stability studies on both [MF_3(Me_3tacn)][OTf] (where M = Sn or Ge) showed promising results, work was done at St Thomas' Hospital to establish whether these Group 14 systems could successfully undergo [^{18}F]fluoride radiolabelling reactions or not.

Firstly, [GeF_3($BnMe_2$tacn)][OTf] was chosen as the initial precursor to attempt radiolabelling due to a combination of its properties; Ge-F bond strength, of which is similar to that of Ga-F and its stability in aqueous media over time (as seen in Section 4.2.2.1). However, in practice, no ^{18}F/^{19}F

exchange in the conditions that were explored occurred. The Lewis acidity of Ge(IV) and strong Ge-F bond, coupled with the complex being cationic, likely adding to the strength of the Ge-F bond, may be the reasons for the failure of this reaction.

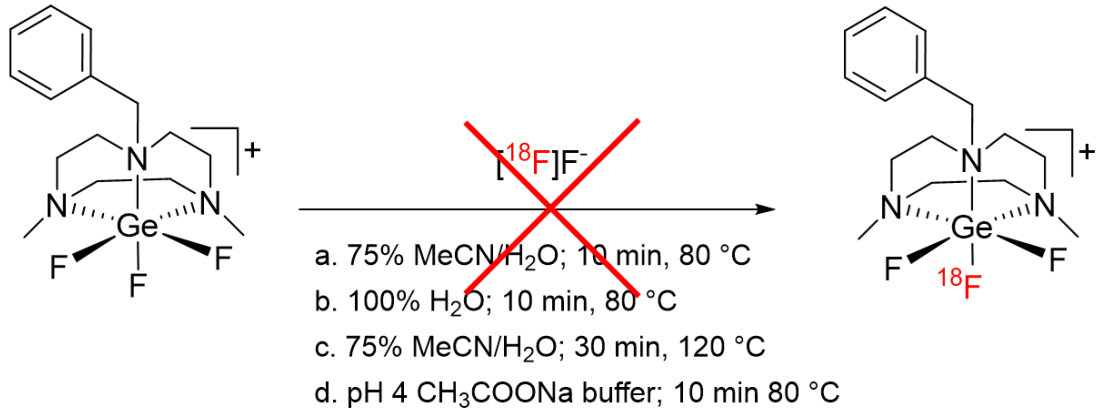

Scheme 29: Attempted $^{18}F/^{19}F$ isotopic exchange reactions on $[GeF_3(BnMe_2tacn)][OTf]$.

The only radioactive species present was unreacted [^{18}F]fluoride. Confirmation that the $^{18}F/^{19}F$ isotopic exchange reaction is not happening but the complex is remaining present and not being broken down is shown by the UV trace, shown in blue in Figure 4.36, showing that the inactive complex $[Ge^{19}F_3(BnMe_2tacn)]^+$ is eluting off the HPLC column intact and present at Rt = 5.74 min.

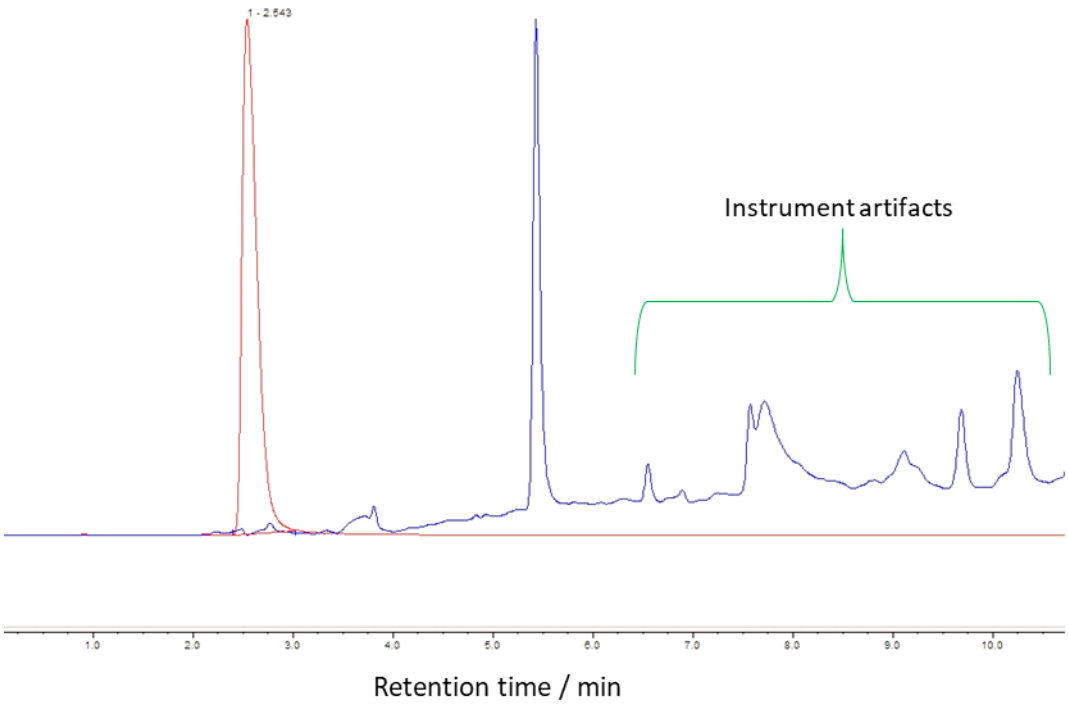

Figure 4.36: Radio-HPLC chromatogram (red) and the corresponding UV tracer (blue) of the crude product from the attempted $^{18}F/^{19}F$ isotopic exchange reaction on $[GeF_3(BnMe_2tacn)][OTf]$ (0.1 m, 0.27 μmol) in 75% MeCN/H_2O. Radio-HPLC chromatogram: Rt = 2.54, 100% ($^{18}F^-$); UV trace: Rt = 5.74 ($[Ge^{19}F_3(BnMe_2tacn)]$)

Two radiofluorination experiments of [SnF_3($BnMe_2$tacn)][OTf] were attempted in 75% MeCN/H_2O, one at 80° C and one at 100 °C for 10 min and both failed to result in the desired radio-product, with signs of degradation of the inactive complex in the UV trace and only [^{18}F]fluoride present in the HPLC radio-trace.

4.3 Conclusions

This work demonstrates a series of Group 14 complexes, in the +4 oxidation state, with neutral aza-macrocyclic co-ligands; Me_3tacn, $BnMe_2$tacn, Me_4-cyclen, and Me_4-cyclam and terpy.

This Chapter reports the first synthesis of a series of Group 14 dicationic complexes with N_4 donor macrocycles, Me_4-cyclam and Me_4-cyclen. This work has proven that a driving force to form a κ_4 macrocyclic complex is present if you actively remove two fluorides using the halide abstractor, TMSOTf. Whilst previously, only κ_2 coordinated complexes had been synthesised, in the absence of a halide abstractor.[14] The kinetic barriers to overcome this is clear, as some of the work on the Ge(IV) tetra-aza systems required over 3 days to go to completion, this is more common in transition metal chemistry where partially filled *d*-orbitals give rise to very substantial kinetic barriers.

Stability studies on [GeF_3(Me_3tacn)][OTf] showed that the chelate complex was stable in a 10 x excess of chloride and acetate anions, and also showed great stability in PBS at pH 7.4. Radiofluorination attempts of [MF_3($BnMe_2$tacn)][OTf] (where M = Sn or Ge) were trialled and no routes to their successful radiolabelling was found to form the desired radio-product.

Considering the PET aspect of this work, the macrocyclic complexes were synthesised and studied to assess their suitability for applications as PET radio-imaging agents, preliminary stability studies were conducted over a variety of physiologically relevant conditions, with both Ge and Sn systems tested under ^{18}F radiolabelling conditions. Whilst the work in this Chapter demonstrated that the Group 14 tetradentate dications were not suitable for ^{18}F radiofluorination, future work on functionalising a ligand with fewer benzyl substituents and more solubilising groups could enable these studies to be undertaken.

As part of the future work, further exploration of halide exchange reactions of Si(IV) chloride and iodide systems to access the fluoride complex and exploit the strong Si-F bond in reference to radio-fluorination and its potential as a PET radiotracer.

4.4 Experimental

4.4.1 [$SnF_3(Me_3tacn)$][OTf]

[$SnF_4(MeCN)_2$] (0.129 g, 0.46 mmol) was dissolved in MeCN (20 mL). To this TMSOTf (0.102 g, 0.46 mmol) was added in MeCN (5 mL). After stirring for 2 h, Me_3tacn (0.080 g, 0.46 mmol) was added and an immediate colour change was observed to cloudy yellow. The suspension was stirred further for 2 h and the yellow precipitate was separated by filtration and dried *in vacuo.* Yield 0.08 g, 39%. IR (Nujol/cm^{-1}): ν = 1261 (CF_3), 1227 (C-CF_3), 1157 (-OSO_2), 563 (s), 518 (s) (Sn-F). ^{1}H NMR (CD_3NO_2, 298 K): δ = 3.5 (s, CH_3, [9H]), 2.3 (s, tacn-CH_2, [12H]). $^{19}F\{^1H\}$ NMR (CD_3NO_2, 298 K): δ =-79.5 (OTf), -187.5 (s, $^1J_{119SnF}$ = 2388 Hz). ^{119}Sn NMR (CH_3NO_2, 253 K): δ =-582.9 (q). LRMS (ESI^+): *m/z* calculated for M^+ = 347.00, found: 348.07. (ESI^-): *m/z* calculated for OTf^- = 149.07, found: 148.95.

4.4.2 [$SnF_3(BnMe_2tacn)$][OTf]

Method as above, using [$SnF_4(MeCN)_2$] (0.078 g, 0.28 mmol), $BnMe_2$tacn (0.070 g, 0.28 mmol) and TMSOTf (0.063 g, 0.28 mmol). ^{1}H NMR (CD_3NO_2, 298 K): δ = 7.41 (m, [5H], ArH), 3.43 (m, [2H], Ar-CH_2), 3.08 (m, [4H], tacn-CH_2), 2.94 (m, [4H], tacn-CH_2), 2.82 (m, tacn-CH_2, [2H]), 2.71 (m, tacn-CH_2, [2H]), 2.61 (s, CH_3, [6H]). $^{19}F\{^1H\}$ NMR (CD_3NO_2, 298 K): δ =-79.4 (OTf), -154.3 (s, $^1J_{119SnF}$ = 1585 Hz), -184.6 (d, $^1J_{119SnF}$ =2441 Hz, $^2J_{FF}$ = 38 Hz), -186.2, (t, $^1J_{119SnF}$ =2466 Hz, $^2J_{FF}$ = 38 Hz). LRMS (ESI^+): *m/z* calculated for M^+ = 424.10, found: 422.11. (ESI^-): *m/z* calculated for OTf^- = 149.07, found: 148.95.

4.4.3 [$SnF_2(Me_4$-cyclen)][OTf]$_2$

[$SnF_4(MeCN)_2$] (0.254 g, 0.92 mmol) was dissolved in CH_2Cl_2 .To this TMSOTf (0.408 g, 1.84 mmol) was added in CH_2Cl_2 (5 mL) to the reaction mixture allowed to stir for 2 h. A solution of Me_4-cyclen (0.210 g, 0.92 mmol) in CH_2Cl_2 was then added and the reaction mixture was left to stir for 86 h. The yellow solid was filtered and washed in hexane (3 x 5 mL) and dried under a flow of nitrogen. Yield 0.45 g, 69%. Required for $C_{16}H_{28}F_8N_4O_6SnS_2.2H_2O$ (743.3): C, 23.38; H, 4.48; N 7.79. Found: C, 23.20; H, 4.79; N, 8.10%. IR (Nujol/cm^{-1}): ν = 574, 518 (Sn-F). ^{1}H NMR (CD_3NO_2, 298 K): δ ppm = 3.8 (m, CH_2, [16H]), 3.2 (s, CH_3, [12H]). $^{19}F\{^1H\}$ NMR (CD_3NO_2, 298 K): δ ppm = -172.4 (s, $^1J_{119SnF}$ = 2610 Hz). LRMS (ESI^+): *m/z* calculated for M^{2+} = 192.54, found: 193.06. (ESI^-): *m/z* calculated for OTf^- = 149.07, found: 148.95

4.4.4 $[SnF_2(Me_4\text{-cyclam})][OTf]_2$

TMSOTf (0.533 g, 2.40 mmol) was added to a solution of $[SnF_4(MeCN)_2]$ (0.332 g, 1.2 mmol) in CH_2Cl_2 and allowed to stir for 2 h. A solution of Me_4-cyclam (308 mg, 1.2 mmol) in CH_2Cl_2 was then added and the reaction mixture was left to stir for 72 h. The orange solid was filtered and washed in hexane (3 x 5 mL) and dried *in vacuo***.** Yield 0.59 g, 69%**.** Required for $C_{16}H_{28}F_8N_4O_6SnS_2.2H_2O$: C, 23.38; H, 4.48; N 7.79. Found: C, 23.20; H, 4.79; N, 8.10%. IR (Nujol/cm^{-1}): ν = 574, 518 (Sn-F). ^1H NMR (CD_3NO_2, 298 K): δ ppm = 3.4-3.9 (br m), 3.6 (s), 3.1-3.2 (overlapping m), 2.8 (overlapping s), 2.7 (s), 2.5 (s), 2.1 (br s), 1.7 (br s). $^{19}F\{^1H\}$ NMR (CD_3NO_2, 298 K): δ ppm =-176.8 (d, $^2J_{FF}$ = 30 Hz), -174.5 (d, $^2J_{FF}$ = 43 Hz), -169.7 (d, $^2J_{FF}$ =43 Hz), -153.6 (d, $^2J_{FF}$ = 30 Hz). LRMS (ESI^+): *m/z* calculated for M^{2+} = 206.57, found: 207.08. (ESI^-): *m/z* calculated for OTf^- = 149.07, found: 148.95.

4.4.5 $[GeF_3(Me_3tacn)][OTf]$

Method 1 $[GeF_4(MeCN)_2]$ (0.302 g, 1.1 mmol) was suspended in a solution of TMSOTf (0.243 g, 1.1 mmol) and $MeCN/CH_2Cl_2$ (10 mL) and allowed to stir at RT for 2 h. Me_3tacn (0.188 g, 0.46 mmol) was then added and immediately a colourless solid precipitated. The suspension was stirred for a further 15 h and the solid was separated *via* filtration and recrystalised from CH_3NO_2/Et_2O, and dried in vacuo. Yield 0.260 g, 79%. Required for $C_{10}H_{21}F_6N_3O_3SGe.H_2O$ (467.99): C, 25.67; H, 4.95; N, 8.98. Found: C, 25.81; H, 4.96; N, 8.79%. $^{19}F\{^1H\}$ NMR (CD_3NO_2, 298 K): δ ppm = -151.7 (s), -78.7 (s, OTf). LRMS (ESI^+): *m/z* calculated for M^+ = 300.92, found: 302.09. (ESI^-): *m/z* calculated for OTf^- = 149.07, found: 148.95.

Method 2 $[GeCl_3(Me_3tacn)][OTf]$ (80 mg, 0.16 mmol) was suspended in CH_2Cl_2 and 3.5 eq. of $[NMe_4]F$ was added. The reaction was allowed to stir for 16 h, the insoluble $[NMe_4]Cl$ was filtered off and hexane (10 mL) was added to the filtrate, which afforded a colourless solid. Yield 0.035 g, 73%. Spectroscopic data as Method 1.

4.4.6 $[GeF_3(BnMe_2tacn)][OTf]$

$[GeF_4(MeCN)_2]$ (0.057 g, 0.25 mmol) was suspended in a solution of TMSOTf (0.055 g, 0.25 mmol) in 1:1 $MeCN/CH_2Cl_2$ (10 mL) and allowed to stir for 2 h. A solution of $BnMe_2$tacn (0.061 g, 0.25 mmol) in CH_2Cl_2 was then added and the reaction mixture was left to stir for 15 h. The resulting off-white precipitate was filtered and washed in hexane (3 x 5 mL) and dried *in vacuo*. Yield 0.075 g, 57%. Required for $C_{16}H_{25}F_6GeN_3O_3S.3CH_2Cl_2$: C, 29.23; H, 4.00; N, 5.38. Found: C, 29.53; H, 4.91; N, 5.81. IR (Nujol/cm^{-1}): ν = 638s (Ge-F). ^1H NMR (CD_3NO_2, 298 K): δ ppm = 7.41 (m, ArH, [5H]), 4.45 (s, Ar-CH_2, [2H]), 3.67 (m, tacn-CH_2, [2H]), 3.45 (m, tacn-CH_2, [4H]), 3.07 (s, CH_3, [6H]), 2.88 (m, tacn-CH_2, [4H]), 2.72 (m, tacn-CH_2, [2H]). $^{19}F\{^1H\}$ NMR (CD_3NO_2, 253 K): δ ppm = -79.53 (s, OTf),

-121.05 (s), -149.87 (d, $^2J_{FF}$ = 48 Hz), -151.64 (t, $^2J_{FF}$ = 48 Hz). LRMS (ESI$^+$): *m/z* calculated for M^+ = 378.21, found: 378.12. (ESI$^-$): *m/z* calculated for OTf^- = 149.07, found: 148.95.

4.4.7 $[GeF_2(Me_4\text{-cyclen})][OTf]_2$

$[GeF_4(MeCN)_2]$ (284 mg, 1.23 mmol) was suspended in a solution of TMSOTf (0.547 g, 2.46 mmol) in CH_2Cl_2 and allowed to stir for 2 h. A solution of Me_4-cyclen (281 mg, 1.23 mmol) in MeCN was then added and the reaction mixture was left to stir for 86 h. The resulting yellow precipitate was filtered and washed in hexane (3 x 5 mL) and dried under a flow of nitrogen. Yield 0.520 g, 63%. Required for $C_{16}H_{28}F_8GeN_4O_6S_2$: C, 26.39; H, 4.43; N, 8.79. Found: C, 25.98; H, 4.65; N, 8.59. IR (Nujol/ cm^{-1}): ν = 639 (m), 574 (m) (Ge-F). ^{1}H NMR (CD_3NO_2, 298 K): δ ppm = 3.82-4.00 (m, CH_2, [8H]), 3.51-3.70 (m, CH_2, [8H]), 3.34 (s, CH_3, [6H]), 3.05 (s, CH_3, [6H]). $^{19}F\{^1H\}$ NMR (CD_3NO_2, 298 K): δ ppm = -79.34 (s, OTf), -132.26 (s). LRMS (ESI$^+$): *m/z* calculated for M^{2+} = 169.51, found: 170.07. (ESI$^-$): *m/z* calculated for OTf^- = 149.07, found: 148.95.

4.4.7.1 X-ray experimental for $[GeF_2(Me_4\text{-cyclen})][OTf]_2$

Analysis of the data for $[GeF_2(Me_4\text{-cyclen})][OTf]_2$ xCH_3NO_2 revealed an inversion twin with a surprisingly large unit cell in space group P 21 , with the asymmetric unit containing 14 cations, 28 anions and four CH_3NO_2 solvent molecules that were resolved, and a further 5.5 CH_3NO_2 solvent molecules per asymmetric unit were accounted for by solvent masking. There appeared to be no plausible higher symmetry space group and no missed symmetry. While the $[GeF_2(Me_4\text{-cyclen})]^{2+}$ cations were generally well-defined, some of the OTf groups showed evidence of some rotational disorder, most of which were modelled satisfactorily. Given the very large cell and the inversion twin, while the identity of the complex and the *cis* octahedral coordination geometry at Ge are not in doubt, detailed comparisons of the geometric parameters are not justified.

4.4.8 $[GeF_2(Me_4\text{-cyclam})][OTf]_2$

$[GeF_4(MeCN)_2]$ (0.321 g, 1.4 mmol) was suspended in a solution of TMSOTf (0.618 g, 2.78 mmol) in CH_2Cl_2 and allowed to stir for 2 h. A solution of Me_4-cyclam (0.357 g, 1.4 mmol) in MeCN was then added and the reaction mixture was left to stir for 72 h. The resulting red-orange precipitate was filtered and washed in hexane (3 x 5 mL) and dried under a flow of nitrogen. Yield 0.42 g, 45%. Required for $C_{18}H_{32}F_8N_4O_6GeS_2$.MeCN: C, 31.86; H, 4.70; N, 9.06. Found: C, 31.09; H, 5.10; N, 9.24%. IR (Nujol/cm^{-1}): ν = 639 (Ge-F). ^{1}H NMR (CD_3NO_2, 298 K): δ ppm = 3.16 (br s, CH_2), 2.70 (s, CH_3). $^{19}F\{^1H\}$ NMR (CD_3NO_2, 298 K): δ ppm = -136.77 (d, $^2J_{FF}$ = 38 Hz), -134.75 (d, $^2J_{FF}$ = 52 Hz), -

132.71 (s), -132.15 (d, $^2J_{FF}$ = 38 Hz), -130.82 (d, $^2J_{FF}$ = 52 Hz), -130.53 (s). LRMS (ESI^+): *m/z* calculated for M^{2+} = 183.54, found: 184.09. (ESI^-): *m/z* calculated for OTf^- = 149.07, found: 148.95

4.4.9 [$SiCl_3$(terpy)][OTf]

$SiCl_4$ (0.175 g, 1.03 mmol) was dissolved in CH_2Cl_2 (5 mL) and terpyridine (0.240 g, 1.03 g) in CH_2Cl_2 (10 mL) was added. TMSOTf (0.229 g, 1.03 mmol) was added to the solution at room temperature. The reaction mixture was stirred for 17 h. An off white solid precipitated and the solid was separated by filtration and washed with pentane (3 x 5 mL) and dried *in vacuo*. Yield 0.350 g, 66%. Required for $SiCl_3C_{15}H_{11}N_3CF_3SO_3.0.25CH_2Cl_2$ (538.0): calcd. C 36.28, H 2.15, N 7.81%. Found C 36.47, H 2.41, N 7.66%. IR (Nujol): $\tilde{\nu}$ = 555 (m), 544 (s) (Si-Cl) cm^{-1}. ^1H NMR (400 MHz, d_3-MeCN, 298 K): δ = 9.9 (m, [2H]), 8.9 (m, [6H]), 8.7 (m, [2H]), 8.3 (m, [2H]). ^{29}Si NMR (d_3-MeCN, 298 K): δ = -169.6 (s)

4.4.10 Attempted synthesis of [SiF_3(terpy)][OTf]

[$SiCl_3$(terpy)][OTf] was dissolved in hexane and 3.5 equivalents of TMAF (0.100 g, 0.063 mmol),was added, a dark blue solid immediately precipitated and the suspension was allowed to stir for 1 h. The precipitate was filtered and washed with hexane (3 x 5 mL) and dried *in vacuo*. IR (Nujol): $\tilde{\nu}$ = 780 (m), 739 (m), 722 (s) (Si-F) cm^{-1}. ^1H NMR (400 MHz, d_3-MeCN, 298 K): δ = 9.13 (m, [2H]), 8.94 (m, [4H]), 8.82 (m, [1H]), 8.67 (m, [2H]), 8.16 (m, [2H]). $^{19}F\{^1H\}$ NMR (d_3-MeCN, 298 K): δ = -127.4 (d, $^2J_{FF}$ = 12 Hz), -143.6 (t, $^2J_{FF}$ = 12 Hz). Repeat microanalyses did not give desired results.

4.5 References

1. Denmark, S. E.; Eklov, B. M., *Chemistry – A European Journal* **2008,** *14*, 234-239.

2. Schirrmacher, R.; Bradtmöller, G.; Schirrmacher, E.; Thews, O.; Tillmanns, J.; Siessmeier, T.; Buchholz, H. G.; Bartenstein, P.; Wängler, B.; Niemeyer, C. M.; Jurkschat, K., *Angewandte Chemie International Edition* **2006,** *45*, 6047-6050.

3. Bhalla, R.; Levason, W.; Luthra, S. K.; McRobbie, G.; Sanderson, G.; Reid, G., *Chemistry – A European Journal* **2015,** *21*, 4688-4694.

4. Bhalla, R.; Darby, C.; Levason, W.; Luthra, S. K.; McRobbie, G.; Reid, G.; Sanderson, G.; Zhang, W., *Chemical Science* **2014,** *5*, 381-391.

5. Monzittu, F. M.; Khan, I.; Levason, W.; Luthra, S. K.; McRobbie, G.; Reid, G., *Angewandte Chemie International Edition* **2018,** *57*, 6658-6661.

6. Silversides, J. D.; Burke, B. P.; Archibald, S. J., *Comptes Rendus Chimie* **2013,** *16*, 524-530.

7. Morphy, J. R.; Parker, D.; Kataky, R.; Eaton, M. A. W.; Millican, A. T.; Alexander, R.; Harrison, A.; Walker, C., *Journal of the Chemical Society, Perkin Transactions 2* **1990**, 573-585.

8. Broan, C. J.; Jankowski, K. J.; Kataky, R.; Parker, D.; Randall, A. M.; Harrison, A., *Journal of the Chemical Society, Chemical Communications* **1990**, 1739-1741.

9. Delgado, R.; Félix, V.; Lima, L. M. P.; Price, D. W., *Dalton Transactions* **2007**, 2734-2745.

10. Shannon, R. D., *Acta Crystallographica Section A* **1976,** *32*, 751-767.

11. Cabbiness, D. K.; Margerum, D. W., *Journal of the American Chemical Society* **1969,** *91*, 6540-6541.

12. Anderson, C. J.; Welch, M. J., *Chemical Reviews* **1999,** *99*, 2219-2234.

13. Liang, X.; Sadler, P. J., *Chemical Society Reviews* **2004,** *33*, 246-266.

14. Cheng, F.; Davis, M. F.; Hector, A. L.; Levason, W.; Reid, G.; Webster, M.; Zhang, W., *European Journal of Inorganic Chemistry* **2007,** *2007*, 4897-4905.

15. Everett, M.; Jolleys, A.; Levason, W.; Light, M. E.; Pugh, D.; Reid, G., *Dalton Transactions* **2015,** *44*, 20898-20905.

16. Cheng, F.; Hector, A. L.; Levason, W.; Reid, G.; Webster, M.; Zhang, W., *Angewandte Chemie International Edition* **2009,** *48*, 5152-5154.

17. R. Willey, G.; J. Woodman, T.; Somasundaram, U.; R. Aris, D.; Errington, W., *Dalton Transactions* **1998**, 2573-2576.

18. Hilbert, J.; Näther, C.; Bensch, W., *Inorganic Chemistry* **2014,** *53*, 5619-5630.

19. Qi, B.; Zhao, X.; Wang, S.; Chen, K.; Wei, Y.; Chen, G.; Gao, Y.; Zhang, D.; Sun, Z.; Li, F., *Journal of Materials Chemistry A* **2018,** *6*, 14359-14366.

20. Robinson, F.; Curran, P. J.; de Groot, C. H.; Hardie, D.; Hector, A. L.; Holloway, K.; Huang, R.; Newbrook, D.; Reid, G., *Materials Advances* **2021,** *2*, 4814-4823.

21. Gurnani, C.; Hawken, S. L.; Hector, A. L.; Huang, R.; Jura, M.; Levason, W.; Perkins, J.; Reid, G.; Stenning, G. B., *Dalton Transactions* **2018,** *47*, 2628-2637.

22. Willey, G. R.; Jarvis, A.; Palin, J.; Errington, W., *Dalton Transactions* **1994**, 255-258.

23. Crowe, A. J., Fricker, S. P., Antitumour activity of tin compounds. In *Metal Compounds in Cancer Therapy.* Ed. Springer Netherlands: Dordrecht, 1994; pp 147-179.

24. Crowe, A. J.; Smith, P. J.; Cardin, C. J.; Parge, H. E.; Smith, F. E., *Cancer Letters* **1984,** *24*, 45-48.

25. Beattie, I. R.; Ozin, G. A., *Journal of the Chemical Society A: Inorganic, Physical, Theoretical* **1969**, 2267-2269.

26. King, R. P.; Dyke, J. M.; Levason, W.; Reid, G., *Inorganic Chemistry* **2022,** *61*, 16905-16913.

27. Levason, W.; Pugh, D.; Reid, G., *Inorganic Chemistry* **2013,** *52*, 5185-5193.

28. King, R. P.Coordination chemistry of group 14 with Pnictine Ligands and the development of precursors for the electrodeposition of antimony chalcogenides. PhD Thesis. University of Southampton, 2022.

29. King, R. P.; Levason, W.; Reid, G., *Dalton Transactions* **2021,** *50*, 17751-17765.

30. Böttcher, T.; Steinhauer, S.; Lewis-Alleyne, L. C.; Neumann, B.; Stammler, H.-G.; Bassil, B. S.; Röschenthaler, G.-V.; Hoge, B., *Chemistry – A European Journal* **2015,** *21*, 893-899.

31. Belousoff, M. J.; Duriska, M. B.; Graham, B.; Batten, S. R.; Moubaraki, B.; Murray, K. S.; Spiccia, L., *Inorganic Chemistry* **2006,** *45*, 3746-3755.

32. Wieghardt, K.; Chaudhuri, P.; Nuber, B.; Weiss, J., *Inorganic Chemistry* **1982,** *21*, 3086-3090.

33. Bhalla, R.; Levason, W.; Luthra, S. K.; McRobbie, G.; Monzittu, F. M.; Palmer, J.; Reid, G.; Sanderson, G.; Zhang, W., *Dalton Transactions* **2015,** *44*, 9569-9580.

34. Levason, W.; Monzittu, F. M.; Reid, G., *Coordination Chemistry Reviews* **2019,** *391*, 90-130.

35. Davis, M.The Synthesis and Characterisation of Complexes of Tin and Germanium Fluorides with Soft Donor Ligands. PhD Thesis, University of Southampton, 2008.

36. Dean, J. A., Eleventh Edition ed.; McGraw Hill, New York, 1973; Vol. 13, p 12A-12A.

37. Cheng, F.; Hector, A. L.; Levason, W.; Reid, G.; Webster, M.; Zhang, W., *Chemical Communications* **2009**, 1334-1336.

5 Exploring new synthetic routes to [$GaF_3(RMe_2tacn)$] and $^{18}F/^{19}F$ isotopic exchange reactions

5.1 Introduction

This Chapter focuses on the experiments undertaken to explore the synthesis and radiolabelling work to form [$Ga^{18}F^{19}F_2(BnMe_2\text{-tacn})$]. [$GaF_3(BnMe_2\text{-tacn})$] can be successfully radiolabelled under fast conditions (10 min), with moderate heating at 80 °C, using [^{18}F]fluoride target water without the need for Lewis acid promotion and produced high RCY's of up to 77% in MeCN.[1, 2]

Previous work by the Reid group on the formation of [$Ga^{18}F^{19}F_2(BnMe_2\text{-tacn})$] from a halide exchange reaction (on [$GaCl_3(BnMe_2\text{-tacn})$]) showed high stability over time, with an RCP greater than 98% after two hours.[2, 3] However, the chemically identical product formed *via* the isotopic exchange reaction from [$Ga^{19}F_3(BnMe_2\text{-tacn})$], whilst a big advantage was that it was able to be labelled at much lower concentrations (<30 nM), it also showed a quicker drop in RCP over time when compared to the complex produced from halide exchange. This was an unexpected result due to the Ga-F bond being significantly more stable than the Ga-Cl bond, with a greater bond dissociation energy and a lower tendency to undergo hydrolysis, which the Ga-Cl bond is highly susceptible to.[4]

The work in this Chapter was undertaken to probe why these systems showed unexpected trends in RCP and to try and discover a new synthetic pathway to [$Ga^{19}F_3(BnMe_2\text{-tacn})$] that does not contain any highly coordinating solvents or competitive anions. A thorough analysis of Group 13 (B, Al, and Ga) coordination complexes with applications with PET imaging is outlined in Chapter 1.[5]

5.1.1 Routes to [$GaF_3(RMe_2tacn)$]

Only in more recent work has the chemistry of Group 13 fluorides with hard nitrogen ligands been explored extensively, this is likely down to the metal fluorides being highly polymerised and having poor solubility and so are unreactive towards neutral ligands. However, development in the Reid Group showed that using the trifluoride trihydrate, $GaF_3.3H_2O$, overcame some of the solubility questions and gave rise to a variety of complexes with nitrogen donor ligands, by employing harsher hydrothermal synthesis techniques (Scheme 30).[6-9]

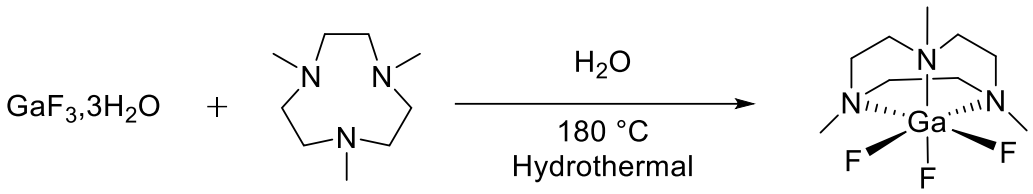

Scheme 30: Synthetic procedure for the formation of [GaF_3(Me_3-tacn)] hydrothermally.[10]

The product was isolated as a pale brown solid, Figure 5.1 shows the $^{19}F\{^1H\}$ NMR spectrum of the solid isolated from this reaction.

The proton NMR spectrum shows clear second-order effects on the tacn-CH_2 protons, due to H-H couplings, as well as a sharp singlet at 2.6 ppm corresponding to the methyl protons on Me_3tacn. Indicating that the ligand is coordinated to the metal centre.[9] Me_3tacn binds *facially* to the metal centre and so the geometry is locked and the methylene protons are in two distinct environments, this is why the second order pattern is seen.

Figure 5.1 shows the $^{19}F\{^1H\}$ NMR spectrum of [GaF_3(Me_3tacn)] produced by hydrothermal synthesis.

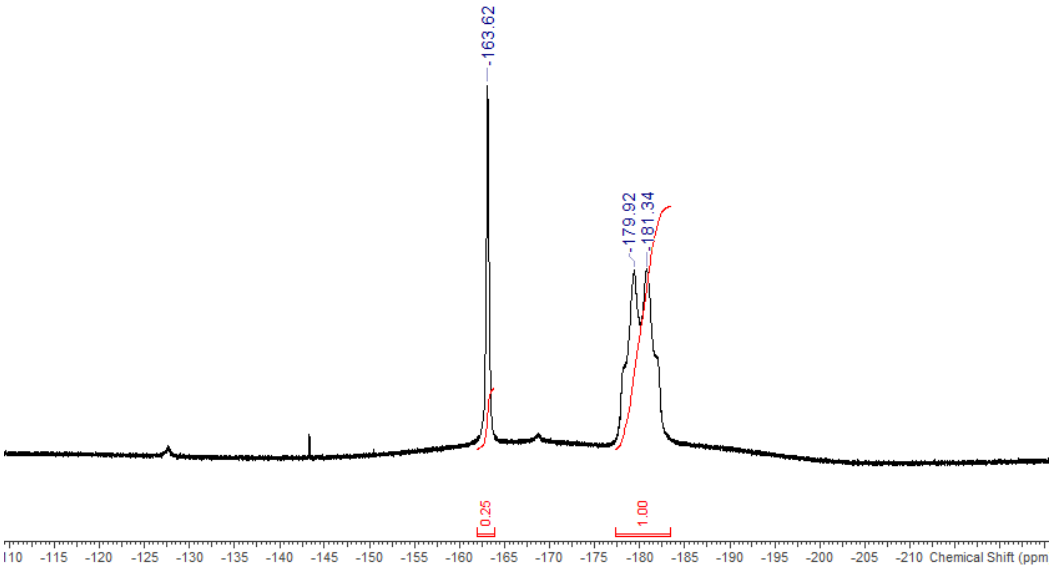

Figure 5.1: $^{19}F\{^1H\}$ NMR spectrum of [GaF_3(Me_3tacn)] produced by hydrothermal synthesis (298 K, d_3-MeCN). Note that the slight rolling baseline is due to the Teflon in the probe.

The collapsed quartet at -181.0 ppm is that of the product.[9] The quartet is present due to the coupling to the two NMR active gallium isotopes and the overlapping of two sets of four-line (1:1:1:1) patterns. An additional substantial unidentifiable peak at -163.62 ppm is present, this is

around the fluorocarbon region and a small peak at -127 ppm is likely to be F^-, a common feature in $^{19}F\{^1H\}$ spectra.

It is also worth noting that analogous chemistries were also undertaken with the other Group 13 elements, as $AlF_3.3H_2O$ and $InF_3.3H_2O$, with successful synthesis of both the Me_3tacn complex counterparts.[6]

The reaction of equimolar amounts of $[GaF_3(OH)_2(dmso)]$ with Me_3tacn was performed at 70 °C and stirred for 2 hours in CH_2Cl_2 (Scheme 31).[9]

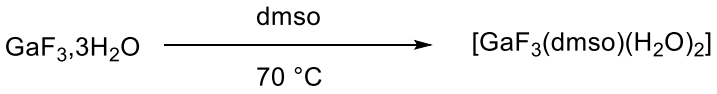

Scheme 31: Synthetic procedure for the formation of $[GaF_3(OH)_2(dmso)]$.

$[GaF_3(Me_3tacn)]$ was obtained as a white solid.[11] The ^{71}Ga NMR spectrum (Figure 5.2) portrayed a broad peak at 47 ppm, most likely the partially collapsed quartet is derived from the three equivalent fluorides in the highly symmetrical complex coupling to the quadrupolar ^{71}Ga centre.

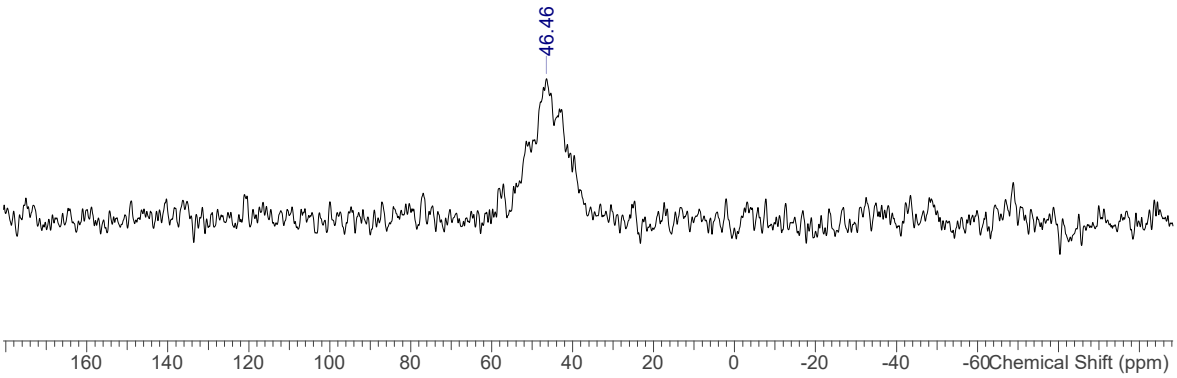

Figure 5.2: ^{71}Ga NMR spectrum of $[GaF_3(Me_3tacn)]$ (D_2O, 298 K).

5.1.2 Aims

The aim of this chapter was to develop a new synthetic protocol to the complex, $[GaF_3(BnMe_2tacn)]$, avoiding the presence of dmso and any other coordinating anions or solvents that may lead to contamination of the final produc. This work focused on:

i. synthesising a precursor to the synthesis of $[GaF_3(BnMe_2tacn)]$ that had no coordinating solvents or anions in its reaction pathway, unlike research demonstrated previously with $[GaF_3(dmso)(H_2O)_2]$;[11]
ii. whether this can be radiolabelled using [^{18}F]fluoride;[2]
iii. to test the hypothesis that the trace dmso retained in the original precursor used to synthesise $[GaF_3(BnMe_2tacn)]$ was the cause of the poor radiochemical stability of $[Ga^{18}F^{19}F_2(BnMe_2tacn)]$ over time, in comparison to the same radio-product formed from the Cl/^{18}F exchange reaction.

5.2 Results and discussion

The desired metal complex, [GaF_3($BnMe_2$-tacn)], was synthesised from [GaF_3(dmso)(H_2O)$_2$], as shown in Scheme 32. Radiolabelling experiments conducted previously suggested that there was some quenching of the reaction due to trace amounts of highly coordinating dmso still present from the precursor[2], so to test if this, synthesis in a dmso and chloride free environment of the [GaF_3($BnMe_2$-tacn)] was undertaken, with the aim of radiolabelling *via* isotopic exchange and testing the radio-products stability over time.

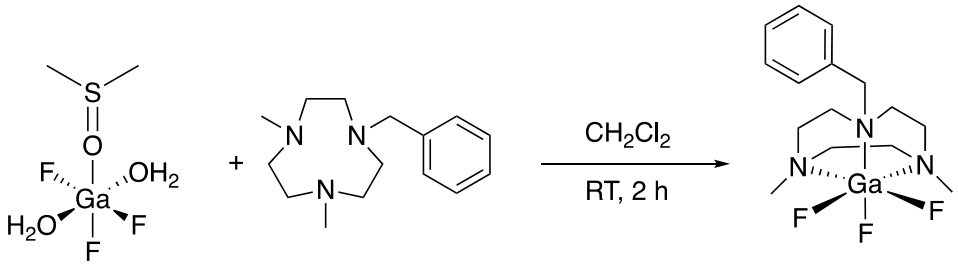

Scheme 32: Synthesis of [GaF_3($BnMe_2$-tacn)] from [GaF_3(dmso)(H_2O)$_2$].[2]

5.2.1 Exploring new synthetic routes to [GaF_3($BnMe_2$-tacn)]

An exploratory set of experiments was undertaken to find a new route to [GaF_3($BnMe_2$tacn)] by exploring which molecular synthon could be used as a precursor, that does not contain any coordinating or competitive solvents or ions; ensuring that any coordinating ligands can be removed fully from the final product. Whilst in previous work it has been demonstrated that metal chloride based chelates can be successfully radiolabelled with [^{18}F]fluoride, MCl_3 based complexes (where M = Al, Ga or In) are moisture sensitive and performing such reactions on a sub-milligram scale can prove to be challenging. It is optimal to find routes to the chelates from an aqueous source of the trivalent metal.

[GaF_3(pyNO)(H_2O)$_2$] was synthesised from literature methods, by reacting the pre-formed complex [GaF_3(dmso)(H_2O)$_2$] with one equivalent of pyNO in MeOH, as shown in Scheme 33, and tested whether it could act as a synthon to the macrocyclic complex [GaF_3(Me_3tacn)].[11] The latter, known complex, was successfully synthesised, and confirmed *via* its spectroscopic signatures. Most importantly, the NMR spectra did not show any traces of residual pyNO in the product.

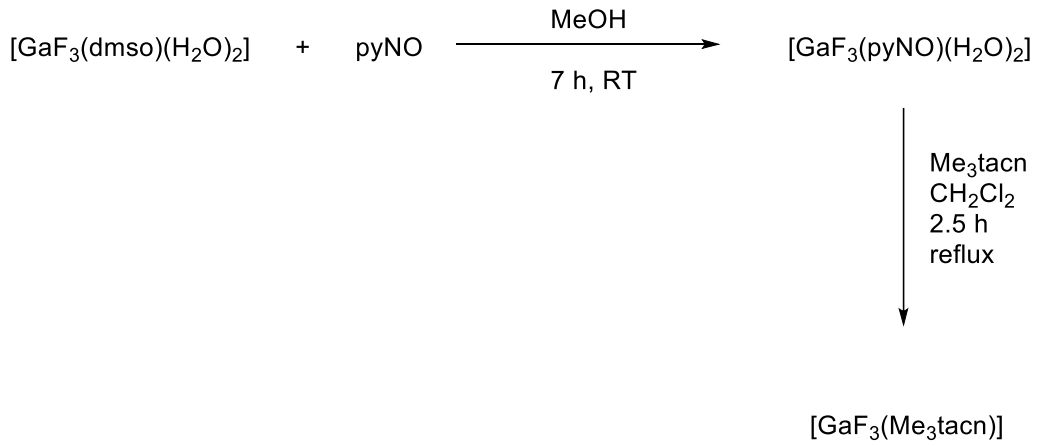

Scheme 33: Schematic for the synthesis of $[GaF_3(pyNO)(H_2O)_2]$ from literature methods, followed by the new synthetic pathway towards $[GaF_3(Me_3\text{-tacn})]$. [11]

An alternative route was then developed to obtain the complex $[GaF_3(pyNO)(H_2O)_2]$ free from dmso (and other competitive solvents or anions) to use as a synthon to the macrocyclic complex, $[GaF_3(BnMe_2\text{-tacn})]$ (Scheme 34). Hydrothermal methods have a number of advantages over traditional solution phase chemistry, it can produce clean and high-yielding complexes and the high pressure system provides a driving force towards complexation, this can also be done free of competing anions and solvents.

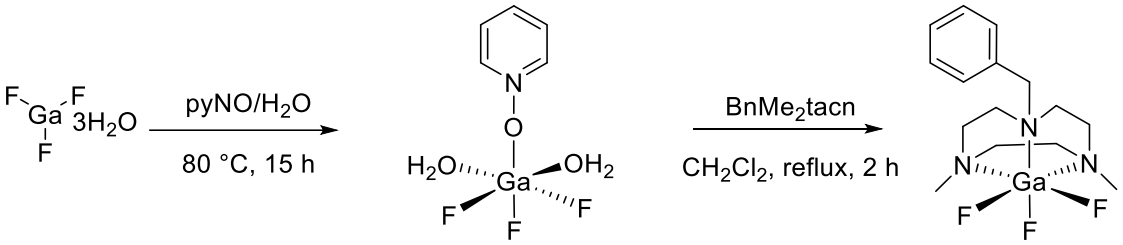

Scheme 34: Schematic for the new hydrothermal synthesis of $[GaF_3(pyNO)(H_2O)_2]$ followed by its reaction with $BnMe_2$tacn to form $[GaF_3(BnMe_2tacn)]$ free of chloride ions and dmso.

The hydrothermal reaction of $GaF_3.3H_2O$ with pyridine N-oxide produced a white solid in high yield and spectroscopic analysis of the bulk solid confirmed the desired product, $[GaF_3(pyNO)(H_2O)_2]$, when comparing to that of the literature. The ^{1}H NMR spectrum of this complex in CD_3OD exhibited three resonances in a 2:1:2 ratio for the pyNO and there is a complete absence of any uncoordinated pyNO in the product (Figure 5.3).

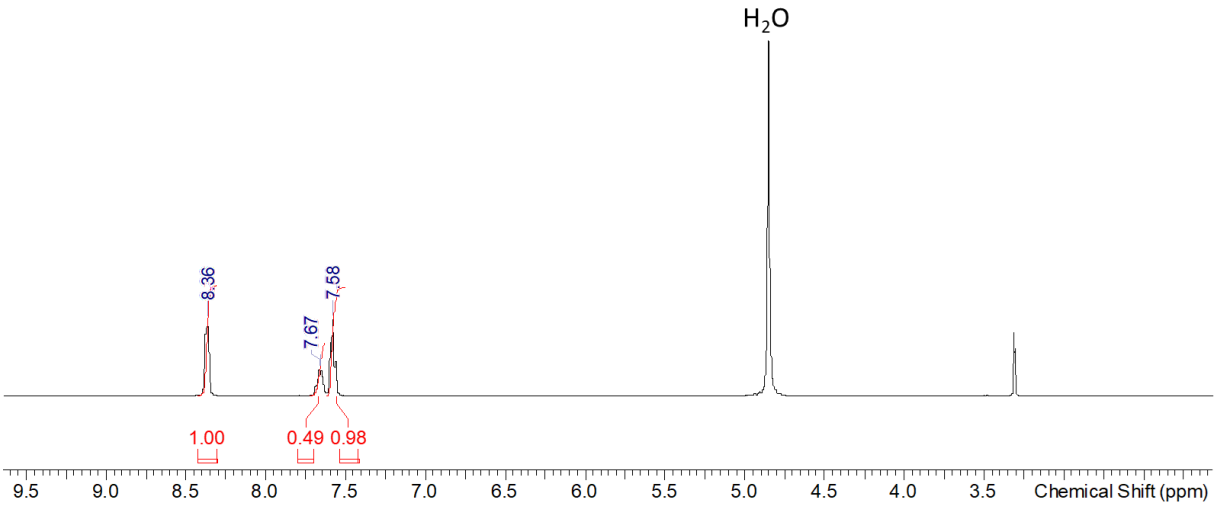

Figure 5.3: ^{1}H NMR spectrum of $[GaF_3(pyNO)(H_2O)_2]$.

A broad resonance at -176.4 ppm in the $^{19}F\{^{1}H\}$ spectrum is present, this broadness shows that the complex is likely exchanging in solution (Figure 5.4). It can be noted that in previous work, it proved difficult for O-donor ligands to fully displace all the water molecules.[1]

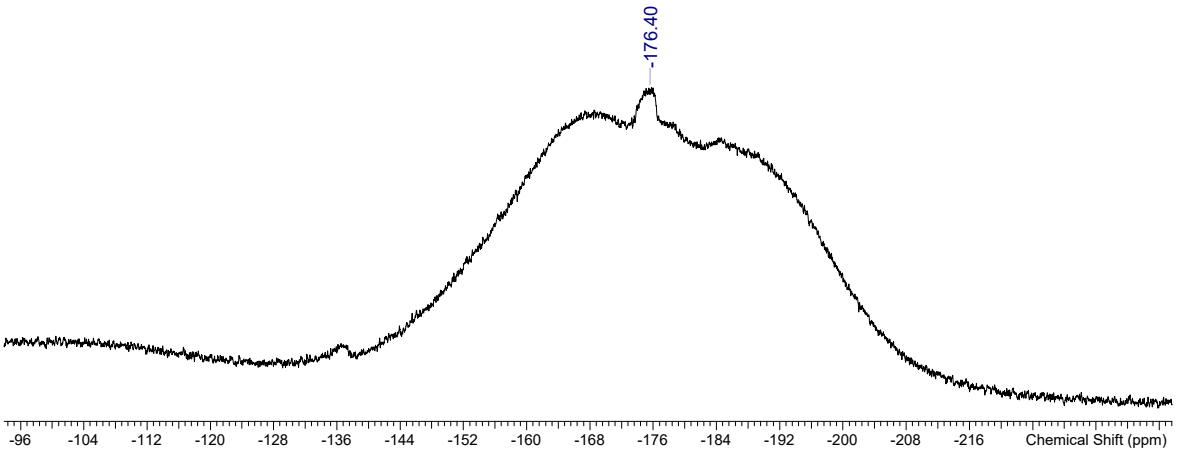

Figure 5.4: $^{19}F\{^{1}H\}$ spectrum of $[GaF_3(pyNO)(H_2O)_2]$ (298 K, CD_3OD). The rolling baseline is due to the Teflon in the probe.

The reaction of $[GaF_3(pyNO)(H_2O)_2]$ with one equivalent of the tridentate $BnMe_2tacn$ in CH_2Cl_2 at reflux produced a pale yellow solid in good yield. The $^{19}F\{^{1}H\}$ spectrum recorded in D_2O gives a collapsed quartet at -172.2 ppm (Figure 5.5), this is consistent with the literature.[11]

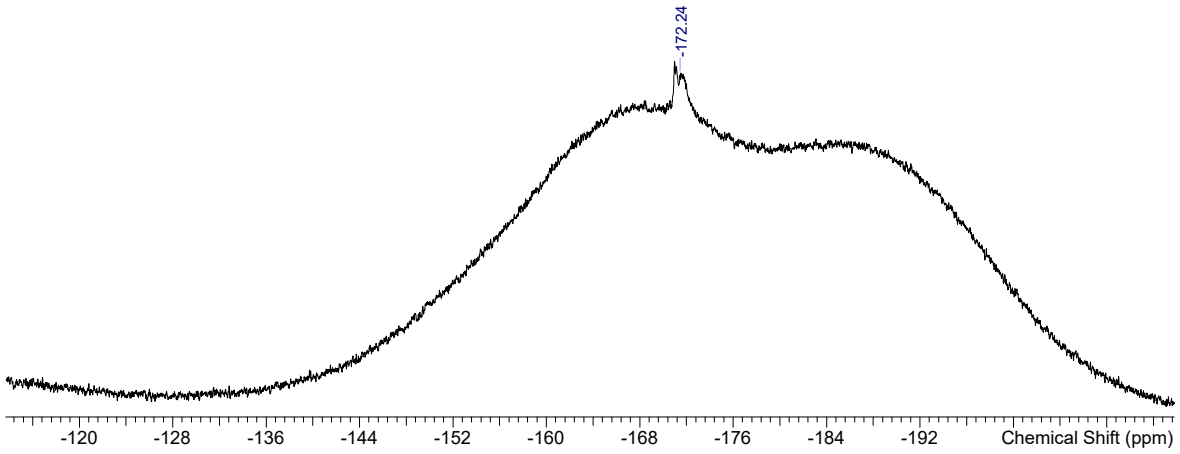

Figure 5.5: $^{19}F\{^{1}H\}$ spectrum of [GaF_3($BnMe_2$tacn)] (298 K, D_2O). The rolling baseline is due to the Teflon in the probe.

Elemental analysis data are consistent with the formation of the desired complex, with one water molecule also present. A common attribute seen in these macrocyclic systems.

However, the direct hydrothermal reaction of $GaF_3.3H_2O$ with $BnMe_2$tacn does not form the desired [GaF_3($BnMe_2$tacn)] complex (unlike with Me_3tacn), and likely causes the ligand to degrade under the high pressure and temperature conditions.

The synthesis of the [GaF_3(Me_3tacn)] complex was also investigated from the precursor $Ga(OTf)_3.3H_2O$, to provide a dmso-free and chloride-free route. Equimolar amounts of $Ga(OTf)_3.3H_2O$ and Me_3tacn were combined in CH_2Cl_2 and allowed to react for 2 h at room temperature.

$$Ga(OTf)_3.H_2O + Me_3tacn \xrightarrow[CH_2Cl_2,\ RT]{2\ h} [Ga(OTf)_3(Me_3tacn)]$$

Scheme 35: Synthesis of [$Ga(OTf)_3$Me3tacn].

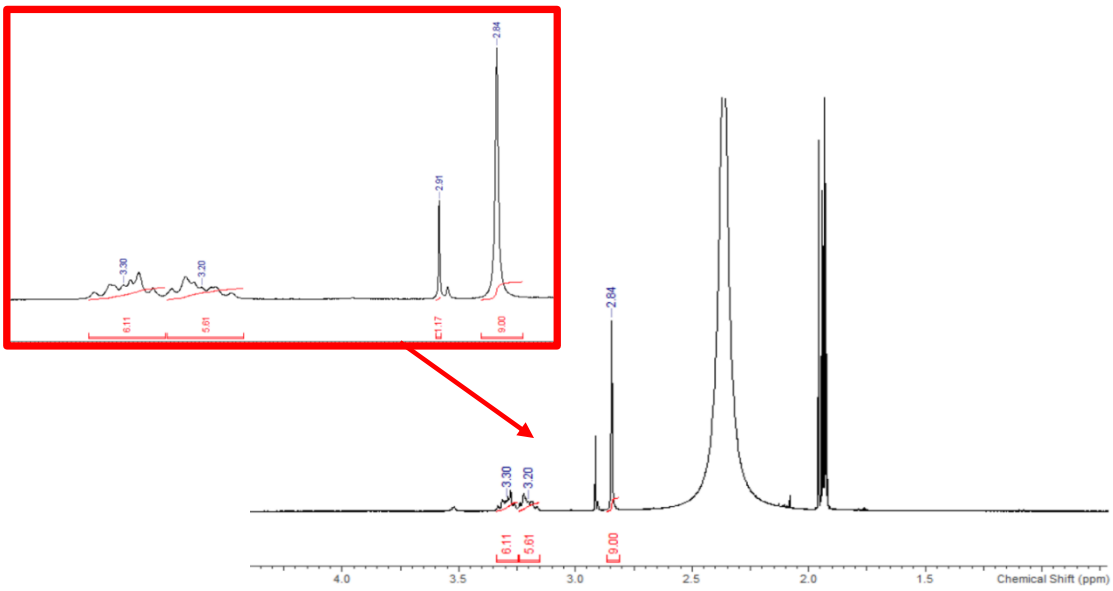

Figure 5.6: ^{1}H NMR spectrum of attempted synthesis of [Ga(OTf)$_3$Me$_3$tacn]. xH_2O (298 K, d_3-MeCN). Region from 2.8-3.5 ppm is expanded in red for clarity.

The proton NMR spectrum of the product obtained from this reaction is shown in Figure 5.6. The spectrum shows two multiplets at 3.3 and 3.2 ppm, these are indicative of second order tacn-CH_2 multiplets associated with tridentate coordination and show a significant downfield shift from free tacn, as well as a sharp singlet at 2.8 ppm owing to the methyl protons on Me_3tacn. The quadrupolar gallium nucleus couples to the methylene protons which causes the broadening and formation of these multiplets. A significant, broad resonance for water was also observed at 2.4 ppm. The *mer* isomer is of a lower symmetry and so has a significant electric field gradient (efg) at the ^{71}Ga nucleus, the fast quadrupolar relaxation is the reason for being unable to observe this complex in the ^{71}Ga spectrum. There are some minor peaks at 2.9 and 2.5 ppm, likely to be impurities, microanalysis failed to show the desired product, indicating that the product is likely to be impure. The ^{19}F{^{1}H} NMR spectrum shows one singlet at -79.3 ppm, this is expected and consistent with there being one triflate environment present (Figure 5.7).

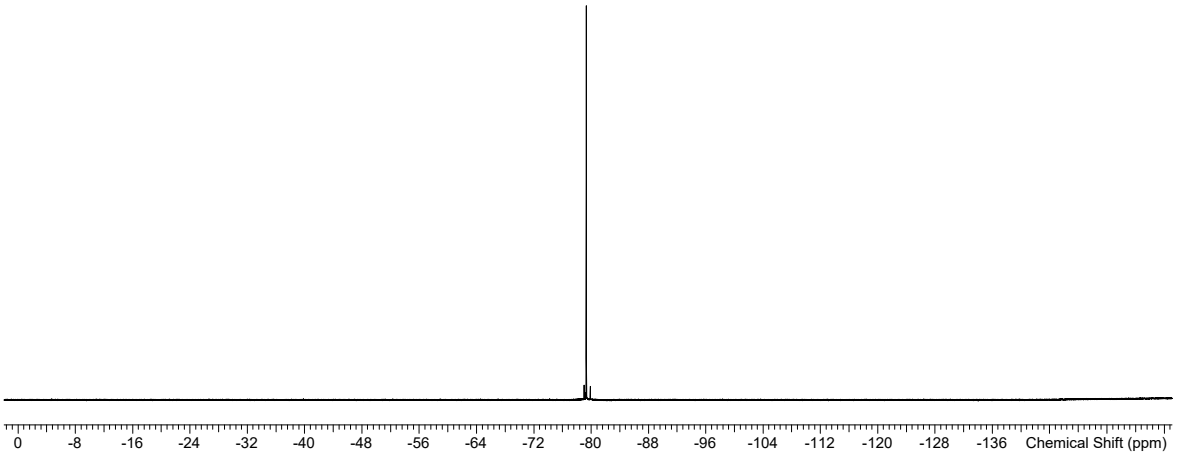

Figure 5.7: $^{19}F\{^{1}H\}$ spectrum of $[Ga(OTf)_3Me_3tacn].xH_2O$ (298 K, d_3-MeCN).

The addition of 3.5 equivalents of TMAF to a solution of $[Ga(OTf)_3Me_3tacn]$ in MeCN, produced an off white solid, analysis of the $^{19}F\{^{1}H\}$ spectrum showed that it contained a large triflate resonance at -79.6 ppm, and a smaller broad resonance at -154.4 ppm, the latter peak being significantly less negative than expected for the desired product, $[GaF_3(Me_3tacn)]$, even when accounting for solvent effects and therefore, is unlikely to be that of $[GaF_3(Me_3tacn)]$.

5.2.2 Radiochemistry

As mentioned in Chapter 1.5, the radiolabelling experiments performed in this work were undertaken at St Thomas' Hospital in London. The complex $[GaF_3(BnMe_2tacn)]$ synthesised from $[GaF_3(dmso)(H_2O)_2]$ was originally made and radiolabelled successfully by a previous Reid group member, Dr Francesco Monzittu, the same radiolabelling experiment was performed to familiarise with the chemistry, equipment, and radiochemistry laboratory and to check that it could be replicated. The desired product of $[Ga^{18}F^{19}F_2(BnMe_2tacn)]$ was successfully synthesised in MeCN, with an RCY of 74% and, of the purified product, an RCP of 95% at t = 0 (analytical radio-HPLC chromatogram and UV-trace shown in Figure 5.9). It was found in this repeat study that using FASTlab™ reaction vessels *versus* Eppendorf vials, the latter of which are often used in radiolabelling reactions, created higher yields of the desired product (an image of a FASTlab reaction vessel can be seen in Figure 5.8). This is thought likely due to enhanced thermal conductivity, as the FASTlab vessels have greater contact with the heat source and it is therefore likely to be at the desired temperature for a longer period of time. This product was purified thorough a HLB SPE protocol.

Figure 5.8: A photo of a reaction vessel used on the GE FASTlab, attached to a cassette

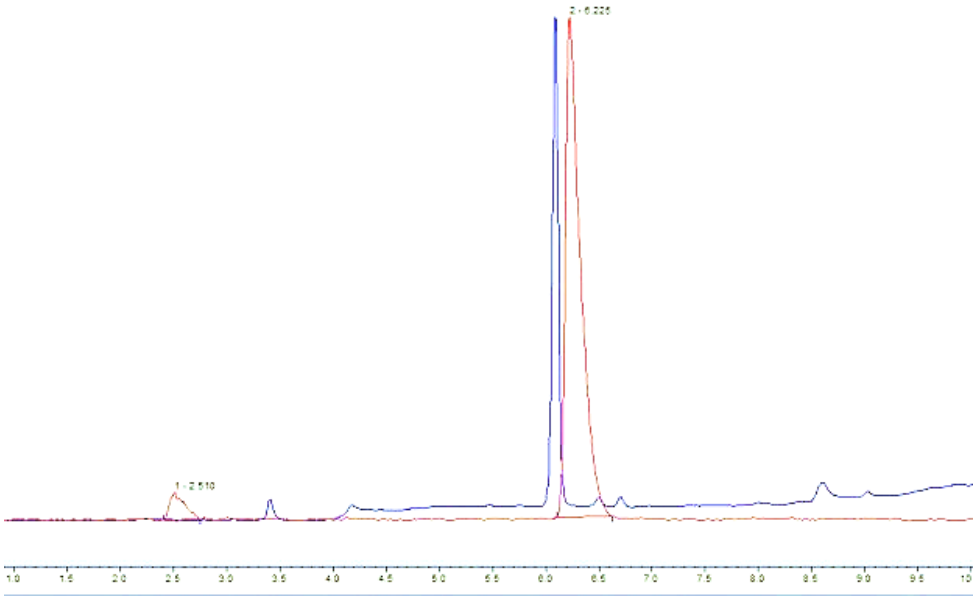

Figure 5.9: Analytical radio-HPLC chromatogram of the SPE purified [$Ga^{18}F^{19}F_2(BnMe_2tacn)$] (1 mg, 2.68 μmol). Peak 1 (red): 2.51 min 5% (^{18}F-) and peak 2 (red): 6.23 min 95% ([$Ga^{18}F^{19}F_2(BnMe_2tacn)$]) at t = 0 min. Synthesis replicated from the work in Reference.[2]

The following reaction (Scheme 36) was then conducted to investigate whether the radiofluorination of the [$GaF_3(BnMe_2tacn)$] complex, synthesised from the pyNO precursor, can yield a higher and more stable RCP overtime than that of the dmso precursor.

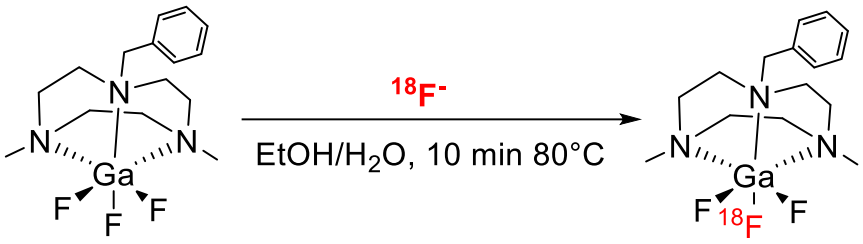

Scheme 36: Radiofluorination method for [GaF_3($BnMe_2$tacn)].

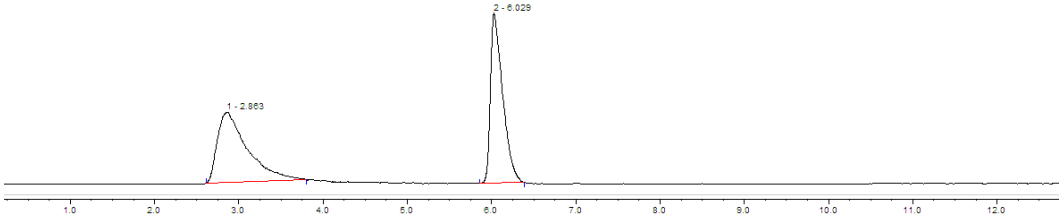

Figure 5.10: Radio-HPLC chromatogram of the crude product from the radiofluorination of [GaF_3($BnMe_2$tacn)] (synthesised from pyNO adduct) (0.1 mg, 268 nmol). Peak 1: Rt = 2.86 min, 51% ($^{18}F^-$). Peak 2: Rt = 6.03, 49% ([$Ga^{18}F^{19}F_2$($BnMe_2$tacn)]).

A simple purification method protocol was established using a hydrophilic-lipophilic balanced (HLB) solid-phase extraction (SPE). The target radio-product was formulated in a mixture of 10% EtOH/H_2O and gave an RCP of approximately 99% at t=0.

Figure 5.11 shows a stacked radio-HPLC plot of [$Ga^{18}F^{19}F_2$($BnMe_2$tacn)] from t = 0 to t = 3 h at 1 h intervals.

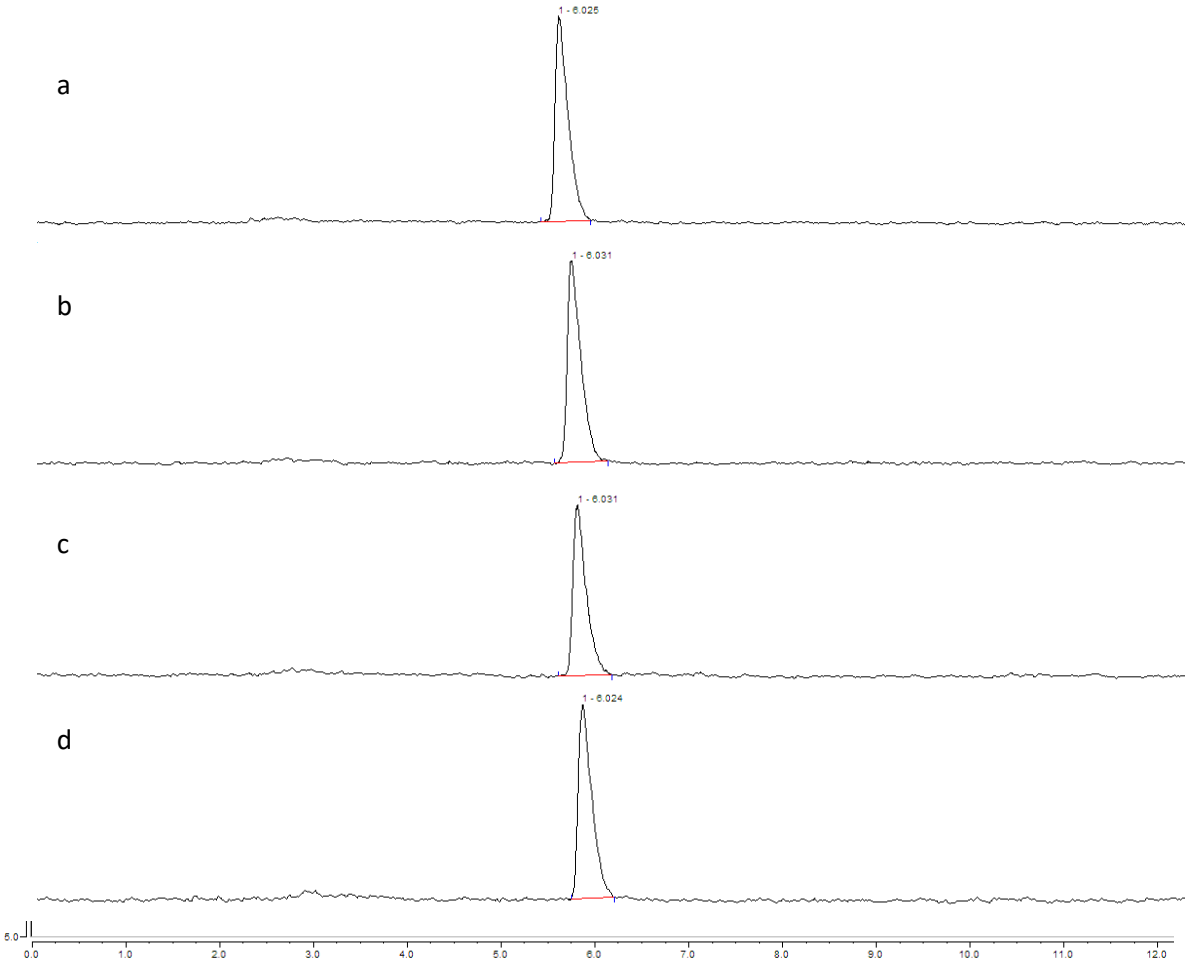

Figure 5.11: Stacked radio-HPLC (red) of the purified product, $[Ga^{18}F^{19}F_2(BnMe_2tacn)]$ (0.1 mg, 268 nmol), produced from the reaction of $[GaF_3(pyNO)(H_2O)_2]$ and $BnMe_2tacn$ and radiolabelled under conditions outlined in 5.4.4, at varying time points: a: t = 0 min., b: t = 1 h., c: t = 2 h, d: t = 3 h.

The radio-HPLC traces above shows the purified product from the radiofluorination reaction on $[GaF_3(BnMe_2tacn)]$, which was produced *via* the $[GaF_3(pyNO)(H_2O)_2]$ route illustrated in Scheme 34. In contrast to the poor RCP over time from the product synthesised using the dmso precursor, this $[Ga^{18}F^{19}F_2(BnMe_2tacn)]$ complex remained completely stable over three hours, with the RCP still at 99% at t = 3 h and with no sign of any other radio-products in the spectrum.

However, subsequent repetitions of this reaction have not had the same outcome, with all of them degrading over time, with the RCP ranging from 77-79% after three hours. Post-purification, the sample was split into two vials, with one being doped with a small amount of dmso (10 μL) and one remaining the same.

5.3 Conclusions

The work in this chapter demonstrates the rationale behind finding a new synthetic route towards [GaF_3($BnMe_2$tacn)]. In this, a new route to the synthesis of [GaF_3(pyNO)(H_2O)$_2$] was developed, free of chloride anions or competing dmso solvent, and it was shown that it can act as a viable synthon towards synthesising the [GaF_3($BnMe_2$tacn)] complex. This provides an easier route into Ga(III) fluoride complexes.

A new route for the synthesis of [GaF_3($BnMe_2$tacn)] was successfully developed after testing several new reaction pathways and radiofluorination was undertaken to assess its stability over time when compared to the same product synthesised from [GaF_3(dmso)(H_2O)$_2$].

Whilst it is clear that the presence of a small amount of dmso does degrade [GaF_3($BnMe_2$tacn)] overtime and that it is likely that in producing this complex from the dmso adduct, it is the highly coordinating solvent that is interfering with the stability of the radio-product over time. This work has not conclusively determined this and further experiments will be needed to confirm. Considering all the experiments performed, the explanation for the RCP is not fully explained, and further experiments using [GaF_3(pyNO)(H_2O)$_2$] as the precursor could be performed; this could include a “one-pot” reaction whereby [GaF_3(pyNO)(H_2O)$_2$], $BnMe_2$tacn and [^{18}F]fluoride are all added to the reaction vessel or[GaF_3($BnMe_2$tacn)] is synthesised from [GaF_3(pyNO)(H_2O)$_2$] on the same day as the subsequent radiofluorination reaction to ensure optimal purity and stability. Ultimately, this complex will be conjugated to a biomolecule, such as PSMA, and further work will need to be undertaken to optimise the reaction conditions for this specific molecule. Work in the Reid group has begun on exploring the bioconjugation side of this work using other sterically bulky tacn ligands with carboxylate and phosphate functional groups.

5.4 Experimental

5.4.1 $[GaF_3(pyNO)(H_2O)_2]$

In a Teflon vessel, $GaF_3.3H_2O$ (0.038 g, 0.21 mmol) was suspended in freshly distilled water (10 mL). A solution of pyNO (0.060 g, 0.63 mmol) in water (5 mL) was added. The reaction vessel was placed in a Parr stainless steel autoclave and heated to 150 °C for 16 h. The mixture was allowed to cool to ambient temperature, causing the precipitation of colourless $[GaF_3(pyNO)(H_2O)_2]$. The product was filtered off and dried *in vacuo.* Yield 0.045 g, 83%. Spectroscopic data match that reported in the literature.[11]

5.4.2 $[GaF_3(RMe_2tacn)]$

Method 1 The compound was prepared as reported in the literature.[11] $[GaF_3(OH_2)_2(dmso)]$ (0.43 g, 0.17 mmol) was suspended in CH_2Cl_2 (4 mL), after two minutes Me_3tacn (0.05 mL, 0.17 mmol) dissolved in 1 mL of CH_2Cl_2 was added, which gave a clear solution. After two hours hexane (10 mL) was added and a white solid precipitated. The solid was filtered and washed in hexane (5 mL), to give a white powder. Yield 0.181 g, 35%. ^{1}H NMR (CD_3CN, 298 K): δ ppm = 2.85 (m, 6H), 2.71 (m, [6H]), 2.64 (s, [9H]). $^{19}F\{^1H\}$ NMR (CD_3CN, 298 K): δ ppm = -181.50 (br). ^{71}Ga (D_2O, 298 K): δ ppm = 46.24 (br)

Method 2 The compound was prepared as reported in the literature.[9] $GaF_3.3H_2O$ (0.050 g, 0.28 mmol) was suspended in freshly distilled water (2 mL). Me_3tacn (0.047 g, 0.28 mmol), was then added and the pale yellow suspension was transferred into a Teflon container and loaded into a stainless steel, high pressure vessel (Parr) and heated to 180 °C for 15 h. The vessel was then allowed to cool. A yellow solution containing brown particulates was formed and filtered off, the resulting filtrate was treated with anhydrous hexane, this yielded a pale brown solid. Spectroscopic data as for Method 1.

Method 3 This method was adapted from the literature.[9] $[GaCl_3(BnMe_2tacn)]$ (0.053 g, 0.125 mmol) was suspended in MeCN (5 mL) and $[NMe_4]F$ (0.034 g, 0.125 mmol) was added. The solution was stirred at room temperature for 1 h. The $[NMe_4]Cl$ formed was filtered off and the filtrate treated with Et_2O, which yielded a white precipitate. Yield 0.030 g, 64%. Spectroscopic data matches literature.[9]

Method 4 from $[GaF_3(pyNO)(H_2O)_2]$

$[GaF_3(pyNO)(H_2O)_2]$ (0.140 g, 0.54 mmol) was suspended in CH_2Cl_2 (10 mL) and $BnMe_2tacn$ (0.134 g, 0.54 mmol) was added, the reaction was allowed to reflux for 2.5 h. The reaction mixture was

allowed to cool to RT and filtered to remove any unreacted starting material. Hexane (40 mL) was added to the solution and the colourless solid formed was filtered and dried *in vacuo* (0.110 g, 56%). Required for $C_{15}H_{25}N_3F_3Ga.H_2O$ (392.12): C, 45.95; H, 6.94; N, 10.72. Found: C, 46.37; H, 6.68; N, 10.61%. Spectroscopic data matches that of the literature.

5.4.3 [Ga(OTf)$_3$Me$_3$tacn]

$Ga(OTf)_3$ (151 mg, 0.29 mmol) was dissolved in CH_2Cl_2 (5 mL) and Me_3tacn (50 mg, 0.29 mmol) was added. The mixture was allowed to stir for 2 h, the white precipitate was filtered and washed in hexane and dried *in vacuo* (54 mg, 64%). ^{1}H NMR (CD_3CN, 298 K): δ ppm = 3.28 (m, [6H]), 3.22 (m, [6H]), 2.84 (s, [9H]). $^{19}F\{^1H\}$ NMR (CD_3CN, 298 K): δ ppm == -78.71 (OTf). IR (Nujol/cm^{-1}): ν = 1260 ($-OSO_2$), 1227 ($C-CF_3$), 1157 ($C-CF_3$), 639 (Ga-O).

5.4.4 ^{18}F/^{19}F isotopic exchange radiolabelling procedure

[GaF_3($BnMe_2$tacn) (0.1 mg, 268 nmol) was dissolved in EtOH (0.75 mL). To this an aqueous solution containing [^{18}F]fluoride in cyclotron target water (0.25 mL) was added and the reaction vessel was heated to 80 °C for 10 mins. The crude reaction mixture was diluted with 10 mL of water and a small sample was removed for analysis by analytical HPLC.

5.4.5 SPE purification protocol

HLB cartridges were conditioned using EtOH (10 mL), followed by H_2O (10 mL).

The diluted reaction mixture was trapped on a pre-conditioned HLB cartridge, washed with water (2 x 10 mL) to remove the unreacted $^{18}F^-$ and eluted with EtOH (1 mL) and 0.9% saline solution (3 mL) into water to result in a formulated product in <10% EtOH. The formulated product was analysed by HPLC at t = 0 and at time intervals up to 180 mins.

5.4.6 Analytical HPLC system

Experiments were analysed using an Agilent 1290 HPLC system with an Agilent 1260 DAD UV detector. Mobile phase A = 10 mM ammonium acetate, B = MeCN. Column : Phenomenex Luna 5 um C18(2) 250 x 4.6 mm. Gradient 0-15 min (10-90% B), 15-20 min (90% B), 20-21 min (90-10% B) and 21-26.5 min (10% B).

5.5 References

1. Monzittu, F.Main group and transiton metal-based chelates for PET applications. PhD Thesis. University of Southampton, Southampton, 2018.

2. Monzittu, F. M.; Khan, I.; Levason, W.; Luthra, S. K.; McRobbie, G.; Reid, G., *Angewandte Chemie International Edition* **2018,** *57*, 6658-6661.

3. Bhalla, R.; Levason, W.; Luthra, S. K.; McRobbie, G.; Sanderson, G.; Reid, G., *Chemistry – A European Journal* **2015,** *21*, 4688-4694.

4. Blower, P. J.; Levason, W.; Luthra, S. K.; McRobbie, G.; Monzittu, F. M.; Mules, T. O.; Reid, G.; Subhan, M. N., *Dalton Transactions* **2019,** *48*, 6767-6776.

5. Bhalla, R.; Levason, W.; Luthra, S. K.; McRobbie, G.; Reid, G.; Sanderson, G.; Zhang, W., *Chemical Communications* **2014,** *50*, 12673-12675.

6. Bhalla, R.; Levason, W.; Luthra, S. K.; McRobbie, G.; Monzittu, F. M.; Palmer, J.; Reid, G.; Sanderson, G.; Zhang, W., *Dalton Transactions* **2015,** *44*, 9569-9580.

7. Benjamin, S. L.; Levason, W.; Reid, G., *Chemical Society Reviews* **2013,** *42*, 1460-1499.

8. Downs, A. J., C*hemistry of aluminium, gallium, indium, and thallium*. Blackie Academic & Professional: London; New York, 1993.

9. Bhalla, R.; Darby, C.; Levason, W.; Luthra, S. K.; McRobbie, G.; Reid, G.; Sanderson, G.; Zhang, W., *Chemical Science* **2014,** *5*, 381-391.

10. Sanderson, G.Coordination complexes of group 13 halides: towards a new class of PET imaging agents. PhD Thesis. University of Southampton, Southampton, 2015.

11. Bhalla, R.; Burt, J.; Hector, A. L.; Levason, W.; Luthra, S. K.; McRobbie, G.; Monzittu, F. M.; Reid, G., *Polyhedron* **2016,** *106*, 65-74.

6 Translation of the radio-fluorination of [$FeF_3(BnMe_2tacn)$] onto the FASTlab™

Translating radiopharmaceuticals from the laboratory into a clinical setting requires automation of the radiochemical synthesis which must produce a consistent drug product for the patient and limit the exposure of radiation to production staff.[1] GE HealthCare's FASTlab is an automated cassette-based synthesis platform and in this work a protocol for radiolabelling the complex, [$FeF_3(BnMe_2tacn)$], with [^{18}F]fluoride has been developed and optimised using this commercially available synthesis platform.

This chapter discusses the experiments that were undertaken to optimise the automation of the synthesis of [$Fe^{18}F^{19}F_2(BnMe_2tacn)$], including the variation of parameters such as eluent composition and precursor concentration, temperature and organic:aqueous solvent ratio.

At 30 GBq scale, a radiostabiliser may be needed to be added to the formulation to maintain a high radiochemical purity over the shelf-life of 8 hours. Therefore, a series of radiostabilisers was tested for their compatibility with the iron(III) complex and to test their ability at limiting radiolysis at high activity.

6.1 Introduction

For the safety and compliance with good manufacturing practices (GMP), automated radiochemistry is crucial for the production of radiopharmaceuticals and is a requirement in a clinical setting. Automation enables reproducible synthesis and protects the operator from radioactivity dose, as the FASTlab is installed inside a lead-lined hot cell.[2] The cassettes used during the synthesis are single-use and can be disposed of after use. An example of a loaded cassette mounted onto the FASTlab platform is shown in Figure 6.1.

Figure 6.1: A cassette mounted on the FASTlab (cassette can be seen inside the red rectangle).

The reproducible production of radiotracers is essential for translation into clinical usage. A number of commercially available synthesis modules are currently used for GMP production in addition to pre-clinical research. This includes the FASTlab™ (GE HealthCare, shown in Figure 6.2), TRACERlab™ FXFN (GE HealthCare), E&Z modules (Eckert & Ziegler), Explora® (Siemens Healthcare), and AllInOne (Trasis).[3] Careful optimisation is required at each stage of the synthesis and automation is required to ensure reproducibility. Automation on these systems is often far from trivial.[4]

Figure 6.2: The GE HealthCare's FASTlab™ used in the Addenbrookes research laboratory.

6.1.1 Iron macrocyclic systems

Iron(III) trifluoride complexes with N-donor ligands that have been reported in the literature include *mer*-$[FeF_3(NH_3)_3]$, *mer*-$[FeF_3(terpy)]$ and *fac*-$[FeF_3(Me_3tacn)]$ (Scheme 37).[5-7]

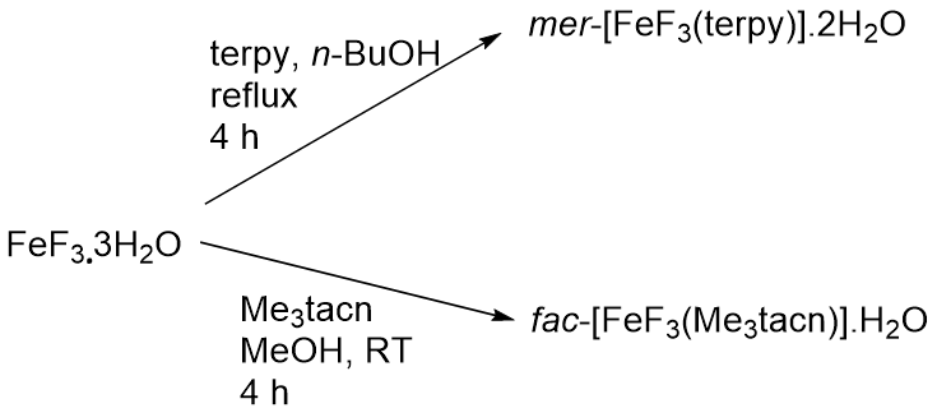

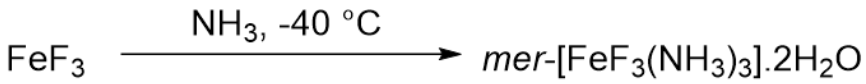

Scheme 37: Schemes for the synthesis of *mer*-$[FeF_3(NH_3)_3]$, *mer*-$[FeF_3(terpy)]$ and *fac*-$[FeF_3(Me_3tacn)]$.[5-7]

$[FeF_3(terpy)]$ and $[FeF_3(RMe_2tacn)]$ (R = Me or Bn) were synthesised in an alcoholic solution over 4 h, with the former at reflux and the latter at room temperature. The IR spectra for *mer*-$[FeF_3(terpy)]$ shows two ν(Fe-F) bands (although three are expected but not resolved) and the *fac*-$[FeF_3(RMe_2tacn)]$ complexes show two ν(Fe-F) bands (as expected). The electronic transitions for the d^5 high spin systems have a d^6A_{1g} ground state and therefore there are very weak spin-forbidden bands in the visible region.[5] Crystals for the complex, *mer*-$[FeF_3(terpy)]$, were grown from a solution in water (Figure 6.3) and the structure shows the *meridional* configuration, as expected with the terpyridine ligand that fixes the geometry and contained three water molecules in the crystal lattice.

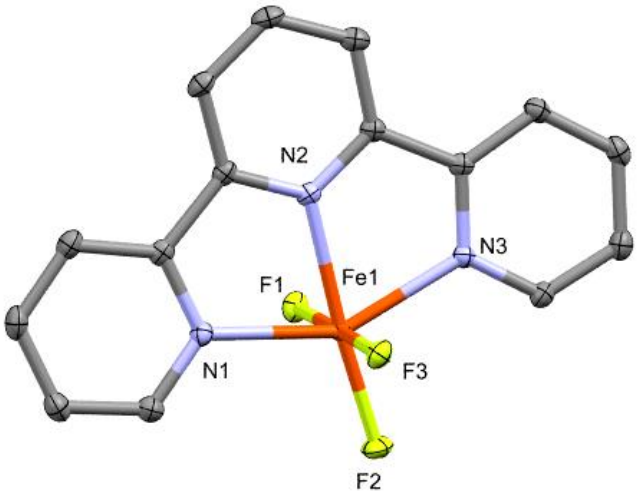

Figure 6.3: Crystal structure of *mer*-[FeF_3(terpy)].3H_2O. Redrawn from Reference.[5]

These previous studies showed that the iron(III) fluoride complexes with tacn-based ligands are worth exploring as a possible platform for PET radiotracer applications, due to their stability, ease of synthesis and solubility in aqueous media. However, it was shown that transition metal terpy complexes of the type [MF_3(terpy)] (M = Cr or Fe) do not have the stability required to be a potential candidate for PET imaging applications. The *fac*-[FeF_3($BnMe_2$tacn)] complex was prepared and crystals suitable for single crystal X-ray analysis were obtained by slow evaporation of a concentrated solution of the complex in water. The crystal structure can be seen in Figure 6.4, the two co-crystallised water molecules in the lattice are not shown.[5]

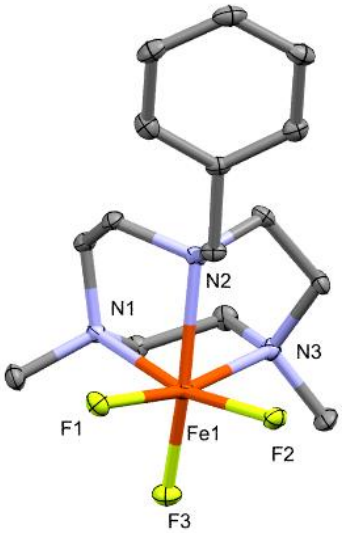

Figure 6.4: Crystal structure of [FeF_3($BnMe_2$tacn)].2H_2O. H atoms and co-crystallised water molecules omitted. Redrawn from Reference.[5]

Fe(III) complexes with cyclam derivatives have also been reported by Wieghardt and co-workers, forming cationic complexes of the type [FeF(L)][PF_6].[8] An example of such a complex with the Me_3cyclam-carboxylate ligand is shown in Figure 6.5.[9-11]

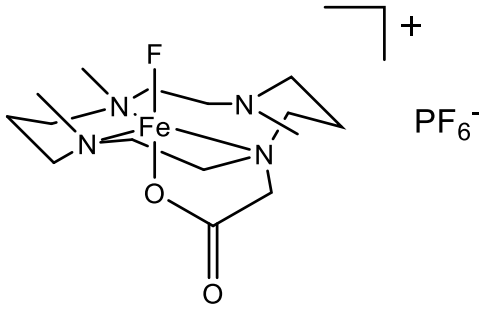

Figure 6.5: Structure of high-spin [FeF(Me_3cyclam-acetate)][PF_6].[10]

This ligand supports an octahedral geometry and occupies four coordination sites on the Fe(III) centre with nitrogen groups and has a carboxylate arm that coordinates to the fifth coordination site, leaving the sixth open to another ligand, in this case, a fluoride.

Iron(III) chloride complexes with nitrogen donor ligands have been more widely researched than those of the fluorides. For example [$FeCl_3$(L)], where L = 2,2',6',2"-terpy, Me_3tacn, tach and $(CN)_3$-tacn and also of the type [$FeCl_3$(L)(OH_2)] where L is a bidentate nitrogen donor such as 2,2'-bipy and 1,10-phen.[12-17]

Morrow and co-workers investigated the properties of two imidazole containing tacn iron(III) systems for paraCSI (paramagnetic chemical shift imaging) and paraCEST (paramagnetic chemical exchange saturation transfer) applications, which could have potential for further studies in magnetic resonance imaging as T_1 relaxation agents and other biomedical applications (an example of which is shown in Figure 6.6).[18]

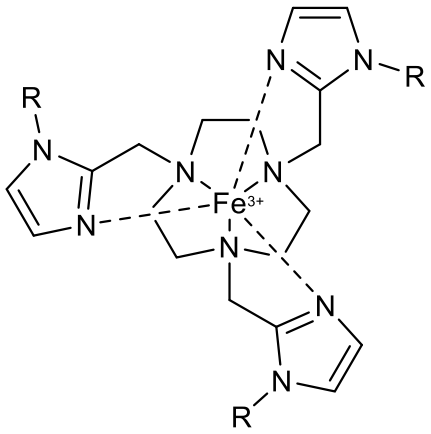

Figure 6.6: Structure of Fe(III) tacn complexes containing N-methyl substituted imidazole pendant arms (R = Me) and unsubstituted imidazole pendant arms (R = H), prepared by Morrow and co-workers with a view towards biomedical applications.[18]

Morrow and co-workers have also reported several macrocyclic ligands for Fe(II) containing cyclen or tacn backbones with pendant arms functionalised with benzimidazole, pyridine or amide donor groups (Figure 6.7), with the aim of finding complexes that could have applications in MRI. Paramagnetic transition metal coordination complexes are a newer class of MRI contrast agent and are of interest due to their effect on ligand proton chemical shifts.[18-23]

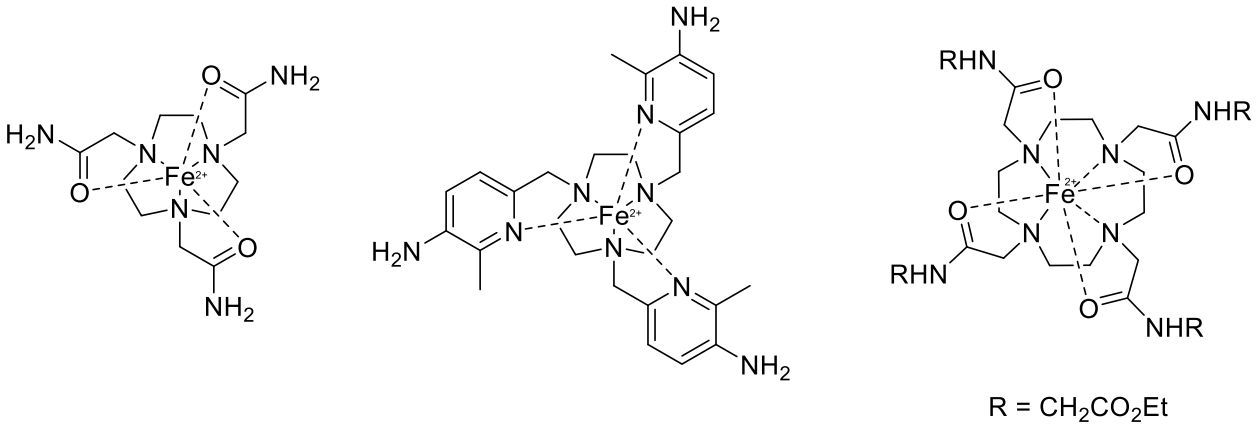

Figure 6.7: A selection of Fe(II) macrocyclic complexes explored as potential MRI contrast agents.[22]

6.1.2 Radiofluorination reactions at low activity

Previous work in the Reid group demonstrated the radiofluorination of [FeF_3($BnMe_2$tacn)] was viable and was conducted through $^{18}F/^{19}F$ isotopic exchange reactions in a 75% MeCN/25% H_2O unbuffered solution.[5]

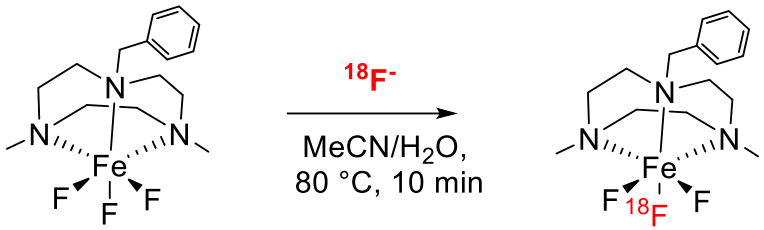

Scheme 38: ^{18}F radiolabelling conditions for isotopic exchange reaction on [Fe$^{19}F_3$(BnMe$_2$tacn)]. Redrawn from Reference.[5]

The water used in these reactions was an aliquot of the cyclotron target water containing [^{18}F]fluoride (between 40-180 MBq) and was used without modification. This reaction produced an RCY of approximately 40% when starting with a precursor mass of 1 mg or 0.1 mg (concentrations of 2360 and 236 nmol, respectively), and unsurprisingly, the RCY was significantly lower when the reaction was performed at room temperature for 10 min (6% when starting with 1 mg of precursor).[24] Radiofluorination was also achieved with a starting precursor mass of 0.01 mg (24 nmol), the RCY was 13% ±5, this is promising work for the development of similar systems.

Table 16: $^{18}F/^{19}F$ isotopic exchange radiolabelling conditions for reactions using the precursor [Fe$^{19}F_3$(BnMe$_2$tacn)]. Table edited from Reference.[5]

Precursor mass / mg	Scale / nmol	T / °C	RCY / %
1	2360	25	6 ±1
1	2360	80	44 ±6
0.1	236	80	40 ±6
0.01	24	80	13 ±5

6.1.3 Radiofluorination reactions at high activity

Practical activity values for ^{18}F-labeled PET imaging probes are at high starting activities (up to 30 GBq).[25] At these levels of radioactivity, radiolysis could be a significant factor that could impact the stability of the desired radio-product. Radiolysis of aqueous solutions forms radicals and reactive species such as ·OH, ·H or H_2O_2. These species could react with the radio-product or chemical impurities and cause its degradation over time.[26-28] There is thorough literature on the use of radiostabilisers to quench radiolysis and preserve high radiochemical purity of the desired product, for example, using gentisic acid (Liu, Edwards and co-workers),[29] sodium ascorbate (Chen and co-workers, and Liu and co-workers),[30-32] methionine (Breeman and co-workers),[33] and ethanol (Chen and co-workers, and Filice and co-workers).[31, 34] Figure 6.8 shows a selection of radiostabilisers used in this field.

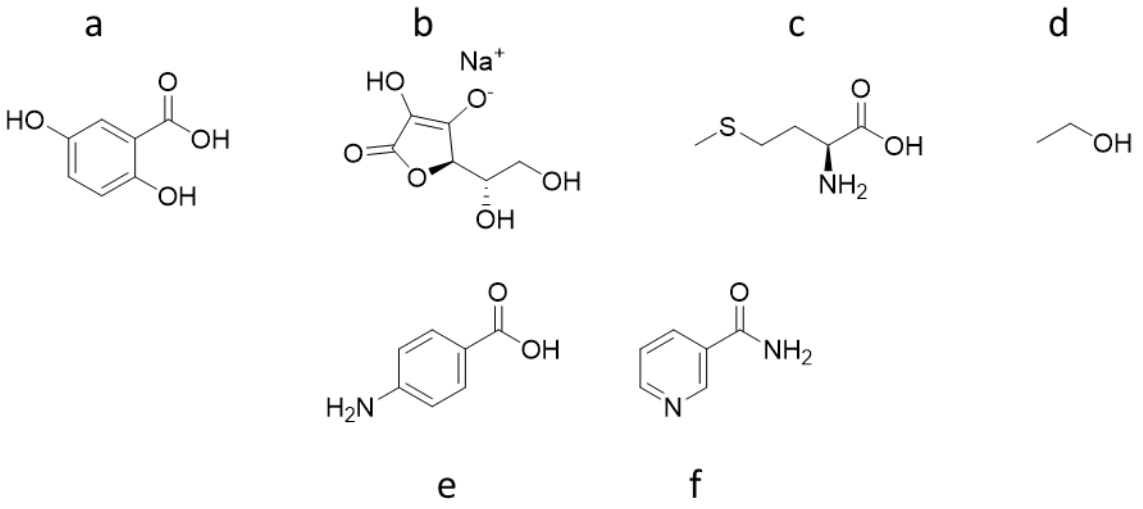

Figure 6.8: Structures of the radiostabilisers gentisic acid **a**, sodium ascorbate **b**, methionine **c**, ethanol **d**, *p*-aminobenzoic acid (*p*ABA) **e**, and nicotinamide **f**, respectively.

A purification method, developed by Engell and co-workers at GE HealthCare, successfully used *p*ABA (**e** in Figure 6.8) as a biocompatible carrier and radioprotectant of the radiotracer [^{18}F]-fluciclatide (Figure 6.9), which is a cyclic tripeptide that is used to selectively image tumour cells and vasculature.[35]

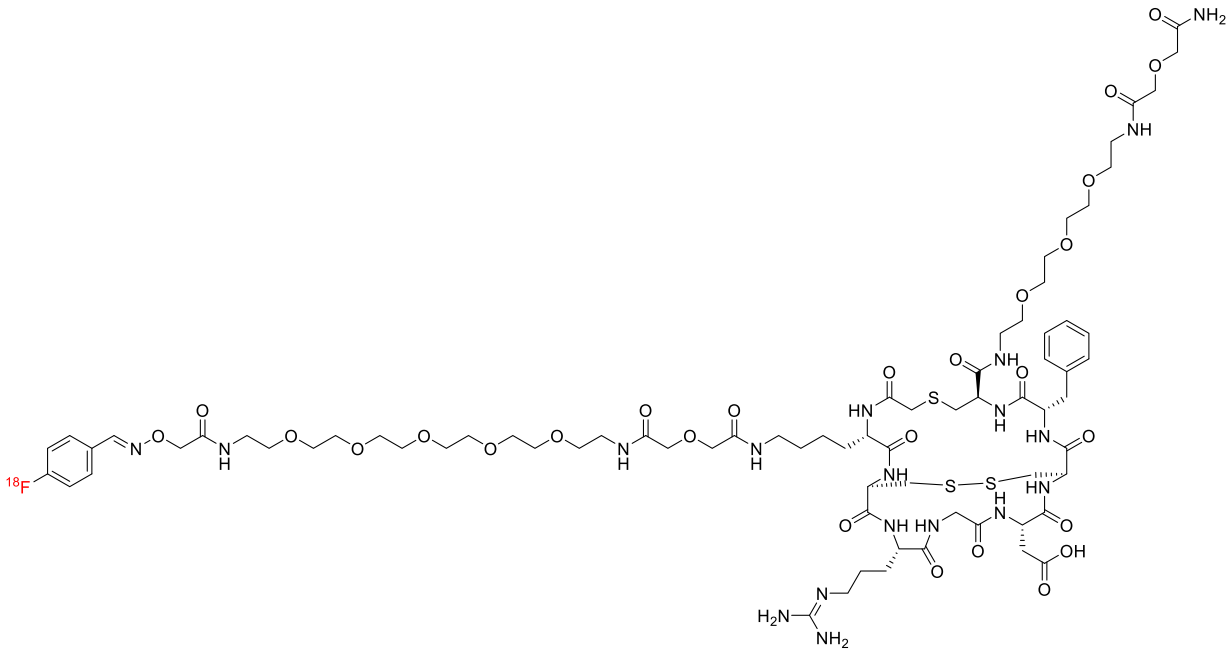

Figure 6.9: The chemical structure of the radiotracer [^{18}F]-fluciclatide.

This radiostabiliser helps to inhibit degradation reactions by trapping highly reactive free-radical species.[36, 37]

Nicotinamide (**f** in Figure 6.8) has been shown to be an effective radiostabiliser and its use has been demonstrated in several patents.[38, 39] For example, it was the preferred stabiliser for a number of radioactive iodine compounds that are used in therapy and diagnostics.[39]

6.1.4 Aims

The aim of this work was to investigate ^{18}F-radiolabelling reactions of [FeF_3($BnMe_2$tacn)] and identify whether this was a promising system for FASTlab automation. This work focussed on:

i. optimisation reactions for the radiofluorination of [FeF_3($BnMe_2$tacn)] using the GE FASTlab synthesis module and assessment of the radiochemical yield and stability of the product over time;
ii. whether this can be scaled to high activity, up to 30 GBq;
iii. the identification of suitable radiostabilisers, if required.

6.2 Results and discussion

The preparation of $[FeF_3(BnMe_2tacn)]$ was undertaken as described in the literature.[5]

6.2.1 Manual experiments

Initially, $[FeF_3(BnMe_2tacn)]$ was radiolabelled manually to establish the yield and purity under these conditions. $[FeF_3(BnMe_2tacn)]$ (0.1 mg, 236 nmol) was dissolved in 750 μL of EtOH and radiofluorinated using $[^{18}F]$fluoride in cyclotron target water (250 μL, 367 MBq) and the reaction was heated to 80 °C for 10 minutes (Scheme 39). The desired radiolabelled product, $[Fe^{18}F^{19}F_2(BnMe_2tacn)]$, was successfully synthesised with a RCY of 72%. The experiments undertaken previously in the Reid group were conducted in MeCN, rather than EtOH, and provided the first example of a transition metal complex where radiofluorination with $[^{18}F]$fluoride was achieved through the formation of an M-^{18}F bond directly.[5] The radio-HPLC and UV chromatogram are shown in Figure 6.10.

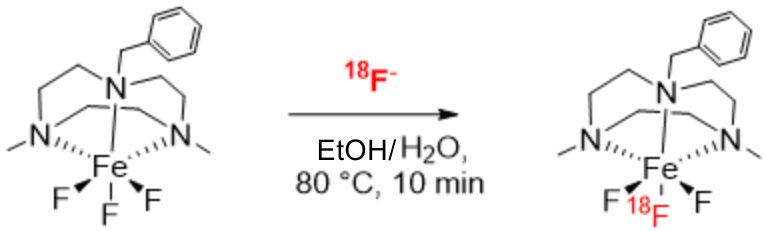

Scheme 39: Schematic to show the synthesis of $[Fe^{18}F^{19}F_2(BnMe_2tacn)]$.

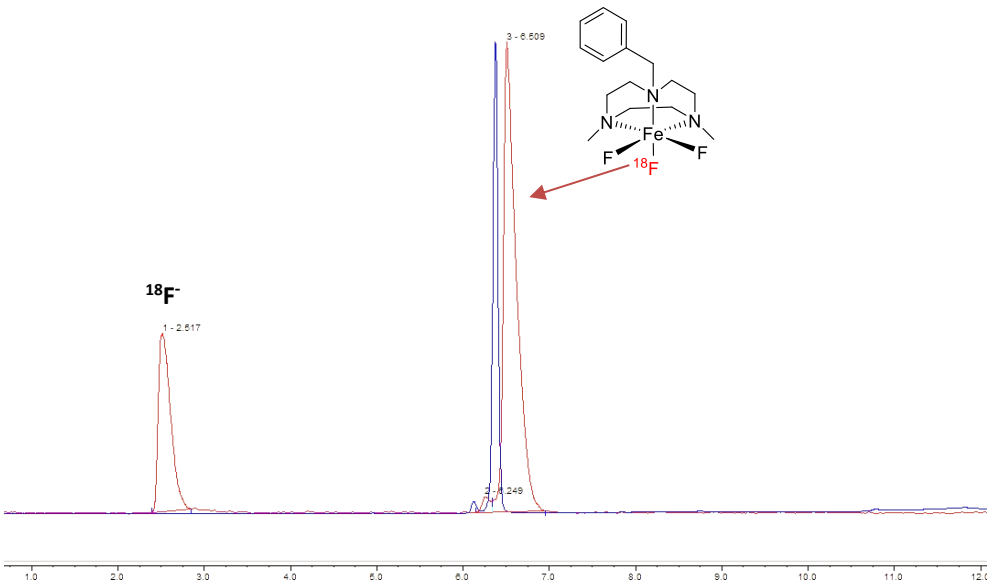

Figure 6.10: Analytical radio-HPLC (red) and UV (blue) chromatogram of the crude product from the reaction of $[FeF_3(BnMe_2tacn)]$ in EtOH with 250 μL of water at 80 °C for 10 min.

The product was purified through a solid phase extraction (SPE) cartridge, which uses a hydrophilic-lipophilic-balanced (HLB) stationary phase to purify the crude reaction mixture. The SPE purification worked well. The RCP of ^{18}F-fluorinated was calculated as 98%, with the RCP remaining constant over at least two hours.

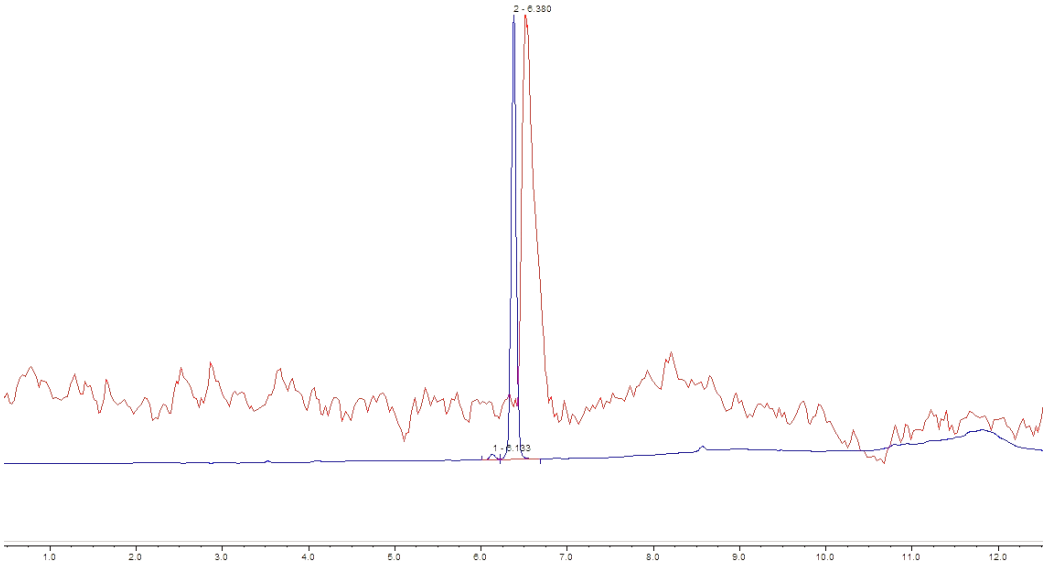

Figure 6.11: Analytical radio-HPLC (red) and UV (blue) chromatogram of the SPE purified [Fe^{18}F^{19}F$_2$(BnMe$_2$tacn)] (red) product after two hours, with an RCP of 98%. The noisy radio-HPLC baseline is due to the low activity (367 MBq) used in this experiment.

6.2.2 FASTlab synthesis

All radiochemistry was performed on the FASTlab using single-use FASTlab cassettes. The protocol sequence was developed on a step-by-step basis, which included vacuum and nitrogen pressure changes and temperature regulation, as well as movement of the syringe. The activity used in these experiments ranged from 100-350 MBq.

Table 17: General FASTlab cassette reagent positions

Cassette Position	**Reagent or hardware**
1	Short tubing to [^{18}F] target water collection vial
2	NaOAc – QMA eluent
3	Syringe 1
4	QMA light SepPak cartridge
5	Short tubing to QMA light SepPak cartridge
6	[^{18}F] inlet
7	Short tubing to left side of reaction vessel
8	Short tubing to middle of reaction vessel
9	N/A
10	Short tubing to crude product
11	Syringe 2
12	Precursor
13	N/A
14	N/A
15	Water bag
16	EtOH – SPE eluent
17	Short tubing to SPE cartridge
18	SPE cartridge
19	N/A
20	N/A
21	N/A
22	N/A
23	Long tubing to external product formulation vial
24	Syringe 3
25	Long tubing to the right side of the reaction vessel

Table 18: Definitions for the ‘Load’, ‘Wash’ and ‘Elute’

FASTlab radiolabelling terminology	Definitions
Load	The solution remaining after the crude product solution was extracted onto the SPE cartridge
Wash	The solution remaining after the product loaded onto the SPE cartridge was washed with water
Elute	The solution remaining after the purified product was eluted from the SPE cartridge with EtOH

An example of the FASTlab cassette layout for the radiosynthesis of [$Fe^{18}F^{19}F_2$($BnMe_2$tacn)] is shown in Figure 6.12.

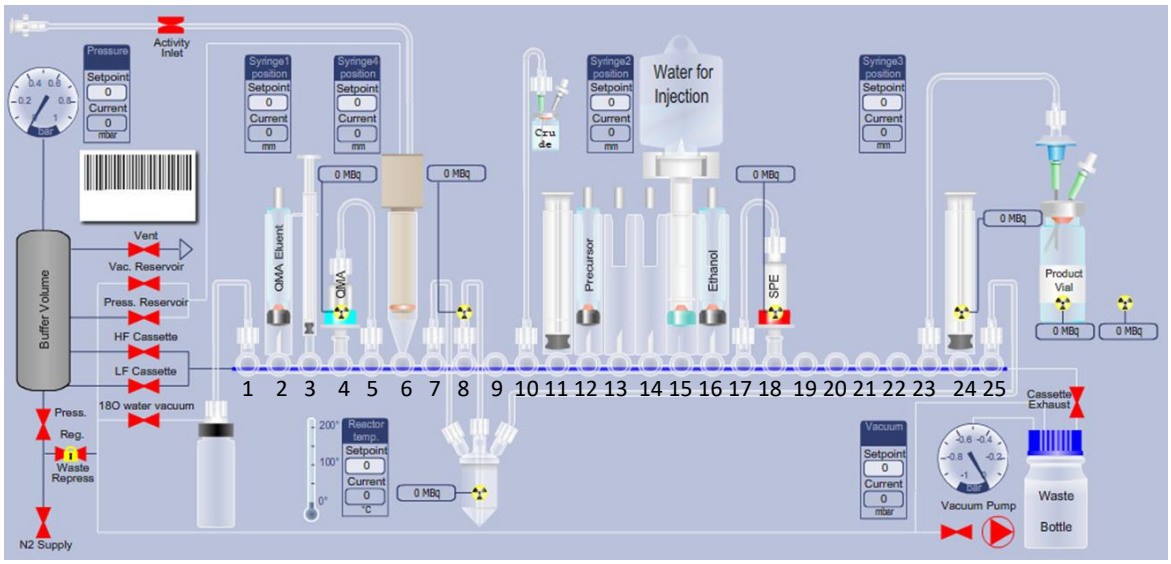

Figure 6.12: FASTlab cassette layout for the radiosynthesis of [$Fe^{18}F^{19}F_2$($BnMe_2$tacn)]. P = position. P1 - tubing to ^{18}F recovery vial; P2 – vial containing NaOAc (QMA eluent); P3 – Syringe 1; P4 – QMA catridge; P5 - tubing to QMA cartridge; P6 - [^{18}F]fluoride inlet resevoir; P7 – tubing to left side of reaction vessel; P8 – tubing to middle of reaction vessel; P9 - N/A; P10 – tubing to crude product; P11 – Syringe 2; P12 – precursor dissolved in EtOH; P13-14 – N/A; P15 – water bag; P16 – EtOH (SPE eluent); P17 – tubing to SPE cartridge; P18 – SPE cartridge; P19-22 – N/A; P23 – tubing to external product formulation vial; P24 – Syringe 3; P25 – tubing to right side of reaction vessel.

Initial optimisation experiments conducted at Addenbrooke's Hospital were performed using a 0.1, 0.6 or 1 mg/mL concentration of [FeF_3($BnMe_2$tacn)] in EtOH/H_2O. [^{18}F]fluoride was trapped onto a QMA cartridge and the ^{18}O water was eluted into a recovery vial for collection; NaOAc eluted (640 μL) the [^{18}F]fluoride through the QMA cartridge into the reaction vessel. During each experiment, the $^{18}F^-$ activity of every solution, vessel and cartridge used was measured using a CRC-25R (Capintec Inc.) to track the radioactivity which can aid in understanding what optimisations need to be undertaken to get the best RCY of the desired radio-product and to calculate the RAC of the reaction. The conditions for these experiments are presented in Table 19.

Table 19: Experimental conditions and small alterations on temperature, organic-to-aqueous solvent content, precursor concentration and time applied to automated protocol for radiofluorination of [$Fe^{18}F^{19}F_2$(BnMe$_2$tacn)] on the FASTlab.

[FeF_3(BnMe$_2$tacn)] Mass / mg	Temperature / °C	EtOH/H_2O ratio	NaOAc eluent conc. / μM	Time / min	Crude RCY* / %
0.1	80	60/40	100	2	0
0.1	120	60/40	100	10	1
1	80	60/40	100	2	0
1	120	60/40	100	10	33
0.6	100	60/40	100	6	35
1	120	75/25	10	10	61

*determined from analytical HPLC chromatograms

Table 19 shows mixed results. It was determined early on that a 100 μM concentration of NaOAc eluent was causing issues, presumably due to the highly concentrated solution preventing the reaction of [^{18}F]fluoride with the iron complex and hindering the radiochemical yield. It is also evident that increasing the temperature and decreasing the concentration of NaOAc to 10 μM significantly improved the RCY. The conditions on the bottom row of Table 19 gave the highest RCY and these conditions were selected for further optimisation of the SPE purification protocol.

A further four experiments were undertaken, with the following remaining constant:

Table 20: Conditions selected for the subsequent optimisation of the [$Fe^{18}F^{19}F_2$(BnMe$_2$tacn)] radiofluorination.

Time / min	10
Temperature / °C	120
NaOAc concentration / μM	10
EtOH/H_2O ratio	75/25

A simple purification protocol was established, and it was found that 19 mL of water was required to effectively trap the radio-product onto the SPE cartridge, diluting the crude product to 10% organic concentration, with lower volume experiments seeing the desired radio-product be

partially present in the Load, this is the remaining solution after extracting the reaction mixture onto the cartridge and the presence of the desired radio-product in the Load indicates that the organic to aqueous ratio needs addressing (see **Error! Reference source not found.** for the definitions of the "Load", "Wash" and "Elute"). SPE cartridges allow for the rapid purification of the crude radio-product. In this method the crude mixture from the reaction vessel was diluted, passed through the SPE cartridge, allowing the unreacted [^{18}F]fluoride to pass through into the waste container, whilst the product was trapped onto the SPE cartridge. Several washes with water ensured the removal of trace [^{18}F]fluoride anions before the purified radio-product was eluted with EtOH (1.5 mL). Thus, [Fe^{18}F^{19}F$_2$(BnMe$_2$tacn)] was successfully purified on the FASTlab, to leave the ^{18}F-bound metal chelate as the main radio-product in the radiotrace (shown in red in Figure 6.13) at Rt = 7.18 min. with an RCP of >99%. The non-decay-corrected yield for this reaction was 45%.

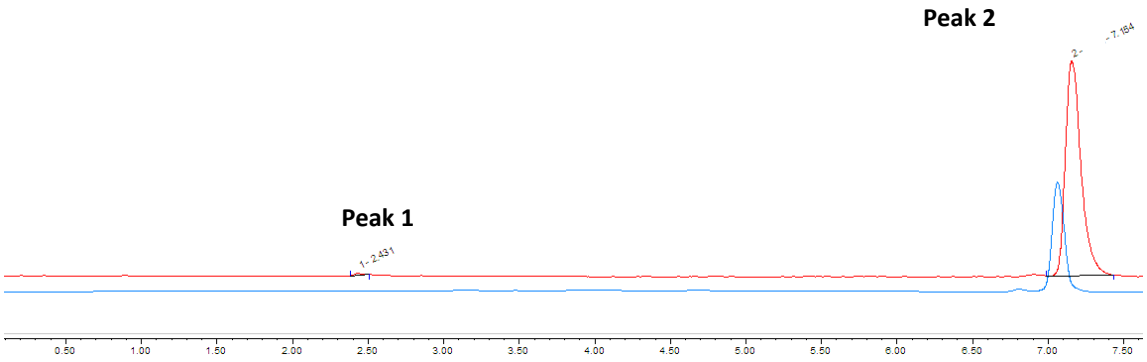

Retention time / min

Figure 6.13: Radio-HPLC (red) and UV chromatogram (blue) of the purified product at t = 0 min. from the low-activity radiofluorination reaction of [FeF$_3$(BnMe$_2$tacn] (1 mg/mL) in 75%/25% EtOH/H$_2$O. Blue trace: Rt = 7.08 ([FeF$_3$(BnMe$_2$tacn)]). Red peak 1: Rt = 2.43 min, <1% (^{18}F$^-$). Red trace, peak 2: Rt = 7.18, >99% ([Fe^{18}F^{19}F$_2$(BnMe$_2$tacn)]).

6.2.3 High activity work

High activity work, up to 30 GBq, was undertaken at the Wolfson Brain Imaging Centre at Addenbrookes Hospital in Cambridge to assess the suitability of the [FeF$_3$(BnMe$_2$tacn)] system to undergo radiolabelling at significantly higher scale than had been attempted previously.

Radiotracers employed in the clinic generally use significantly larger amounts of radioactivity (100-1000 GBq mol^{-1}) than those available in London at St. Thomas' Hospital, where the [^{18}F]F$^-$ produced is used for both the production of [^{18}F]FDG and for research purposes. The radioactivity concentration (RAC) used in these experiments is generally only up to approximately 300 MBq

and this has implications for the molar activity that can be obtained and thus its potential application in a clinical setting.[40] Ideally, for applications in the clinic, a radiotracer should maintain a minimum RCP of 90% over 8 hours.

6.2.3.1 Translation of protocol to high activity

The optimised conditions developed in the low activity work described in Section 6.2.1 were used to test whether the iron(III) complex can undergo similar reactions at high activity. The initial experiment undertaken was performed without any addition of a radiostabiliser, to determine how the complex might be affected by radiolysis; this is the degradation of a product due to radicals produced *via* the interaction of ionising radiation with water. The starting ^{18}F activity for this reaction was 28.2 GBq, with a RAC of 922 MBq/mL at the end of the reaction and a RCY of 42%.

Figure 6.14 presents the radio-HPLC trace, in red, showing the RCP from t = 0 to t = 5 h and the UV trace in blue. The retention time corresponds to that of the reference standard (the precursor).

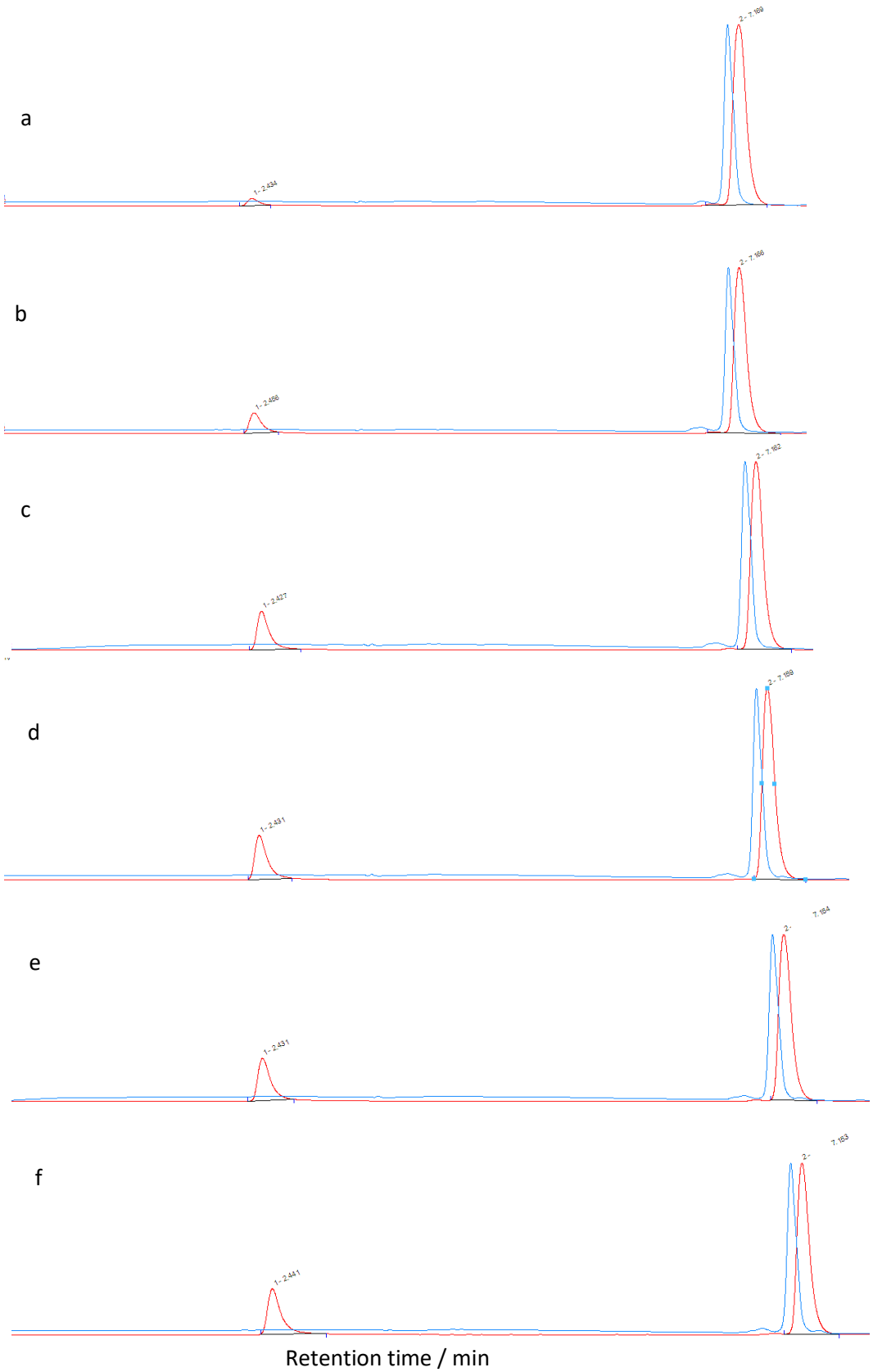

Figure 6.14: Stacked radio-HPLC (red) and corresponding UV chromatogram (blue) of the purified product, [$Fe^{18}F^{19}F_2$($BnMe_2$tacn)], at varying time points: a: t = 0 min., b: t = 1 h., c: t = 2 h, d: t = 3 h, e: t= 4 h, f: t = 5 h.

Table 21: HPLC-chromatogram at time points 0 through to 5 h, corresponding graphs shown in Figure 6.14

HPLC chromatogram	Time / h	RCP / %
a	0	97
b	1	90
c	2	84
d	3	81
e	4	80
f	5	78

The results in Figure 6.14 and Table 21 show that the [$Fe^{18}F^{19}F_2$($BnMe_2$tacn)] complex undergoes degradation over time, with liberation of [^{18}F]fluoride observed over a five hour period, from 3% to 22%.

shows the FASTlab reaction logfile, this is a unique file for this reaction and the FASTlab run and contains data collected at one second intervals throughout the synthesis, with data measured by three different radioactivity detectors, shown in as three different colours (orange, grey and yellow). The blue colour shows the movement of syringe 2 during the synthesis. Data collected also contains values for the programmable process parameters, such as reactor temperature, nitrogen pressure, and syringe position. The x axis is time in seconds and the y axis measures the radioactivity in Bq. These logfiles are useful when doing runs at high radioactivity, as it limits any manual handling that would otherwise be required to track the radioactivity and they provide a diagnostic “fingerprint” that can help establish deficiencies or problems in a synthesis process.[41] The RCY for this reaction was calculated using the data collected in the FASTlab logfile:

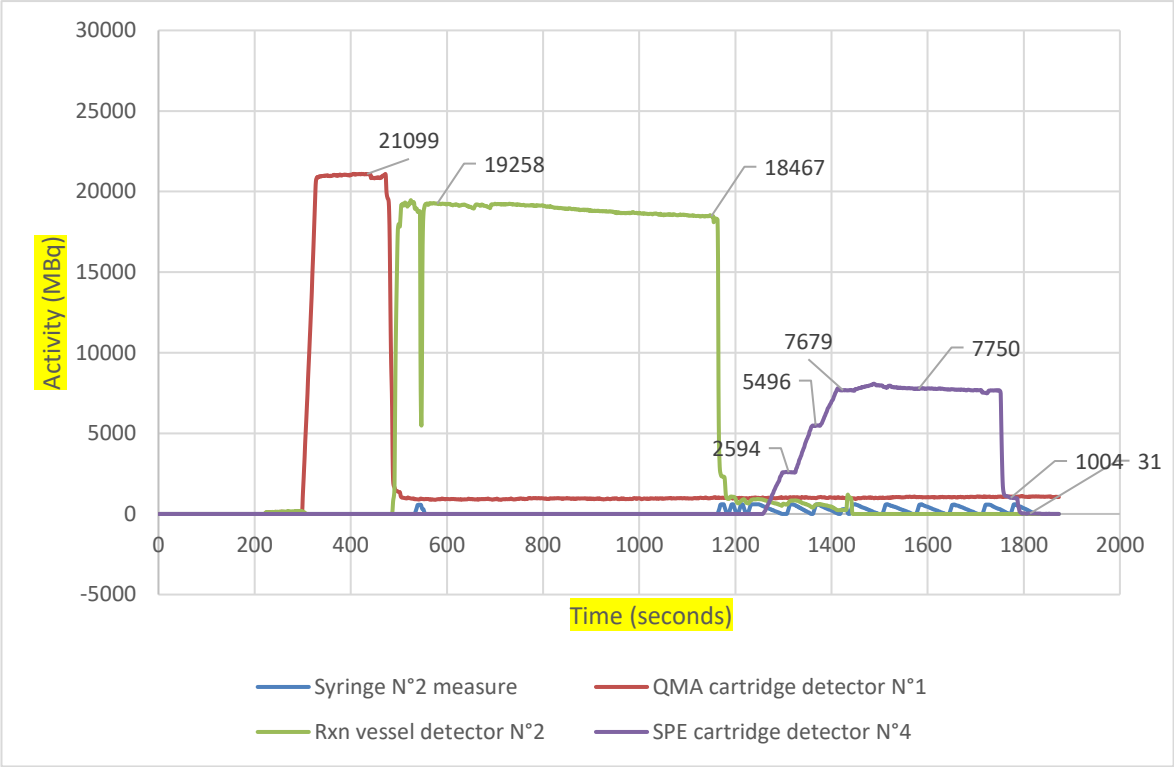

Figure 6.16: FASTlab reaction logfile for the radio-product, [$Fe^{18}F^{19}F_2$($BnMe_2$tacn)], formulated in a 90% H_2O/EtOH solution without the addition of a radiostabiliser.

Peak radioactivity (MBq) of the SPE cartridge containing purified radio-product

$$\frac{7750}{18467} \times 100 = 42\%$$

The radioactivity (MBq) of the reaction vessel at the end of the radiolabelling reaction

Figure 6.15: An equation showing the calculation to determine the RCY for this reaction by dividing the measured radioactivity of the SPE cartridge containing the purified radio-product by the radioactivity of the reaction vessel post-radiolabelling, in MBq.

The crude RCY for this reaction was calculated to be 42%, this is considered a good radiochemical yield. This compares well with the crude RCY data from the low activity experiments described in Section 6.2.2 (which ranged from 0-61%).

Encouraged by these results, a number of radiolabelling experiments were undertaken subsequently with three different potential radiostabilisers to determine whether the lower radiochemical stability observed over time was due to radiolysis and whether this could be improved *via* the addition of the stabiliser.

6.2.3.2 Effect of sodium ascorbate

Radiostabilisers are useful and have been shown to overcome instability of a radioactive product due to radiolysis. Sodium ascorbate is a well-known radiostabiliser and it is non-toxic to humans; it is a mineral salt of vitamin C.[42, 43] For example, it has been shown to be an effective radiostabiliser in the ^{111}In, ^{90}Y and ^{177}Lu radiolabelling of a DOTA conjugate, with applications in diagnostics and therapeutics in endothelial cells of tumour neovasculature.[30, 44] It has also been shown to act as an effective additive to the production of [^{18}F]Fluoropyridine-Candesartan, preventing radiolysis, with the radiochemical purity being >97% after 10 h, this tracer has applications in cardiovascular imaging and AngII type 1 receptors, which are expressed in the kidneys.[45] Sodium ascorbate was chosen as the first potential radiostabiliser to investigate in the high activity radiolabelling of [$FeF_3(BnMe_2tacn)$], since previous work showed that the similar complex, [$GaF_3(BnMe_2tacn)$], was not affected by the addition of sodium ascorbate, albeit in that case the experiment was conducted at low radioactivity.[46]

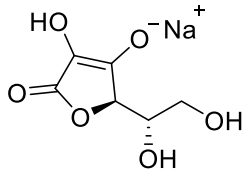

Figure 6.17: Structure of sodium ascorbate.

All conditions remained as described in Table 20, except for the addition of sodium ascorbate to both the solution SPE formulation vial (prior to loading onto the SPE cartridge) and the product formulation vial at a concentration of 50 mg/mL, and with a starting activity of 29.3 GBq.

The RCP at t = 0 was 54%, significantly lower than anticipated (Figure 6.18), and in contrast to the high activity experiment performed without the addition of a further radiostabiliser, where the RCP at t = 0 min was 97% (see chromatogram **a** in Figure 6.14). Furthermore, at t = 15 min in the presence of sodium ascorbate, a dramatic decrease in the RCP of the radio-product was seen, with 99% of the radioactive product now being $^{18}F^-$ (Figure 6.19).

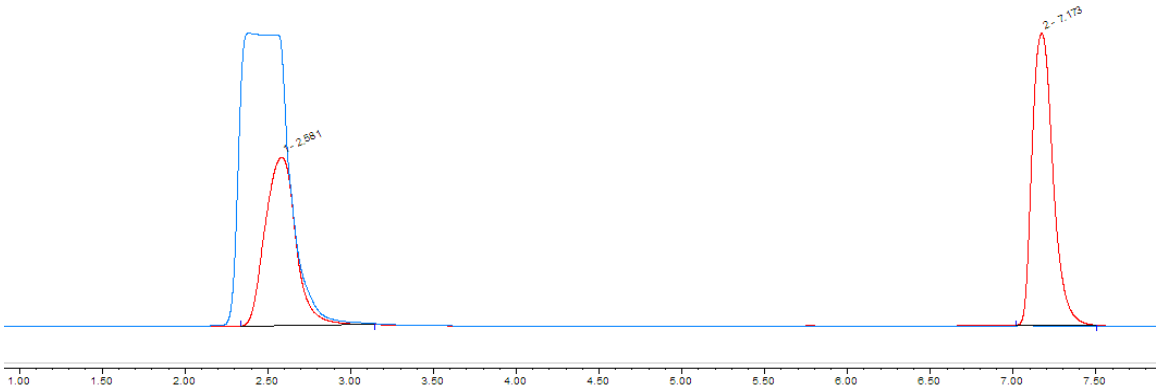

Retention time / min

Figure 6.18: Radio-HPLC (red) and UV chromatogram (blue) of the purified product at t = 0 from the high-activity radiofluorination reaction of $[FeF_3(BnMe_2tacn]$ (1 mg/mL) in the presence of sodium ascorbate (50 mg/mL) in 75%/25% EtOH/H_2O. Blue peak: Rt = 2.49 (sodium ascorbate). Red peak 1: Rt = 2.58 min, 46% ($^{18}F^-$). Red peak 2: Rt = 7.17, 54% ($[Fe^{18}F^{19}F_2(BnMe_2tacn)]$).

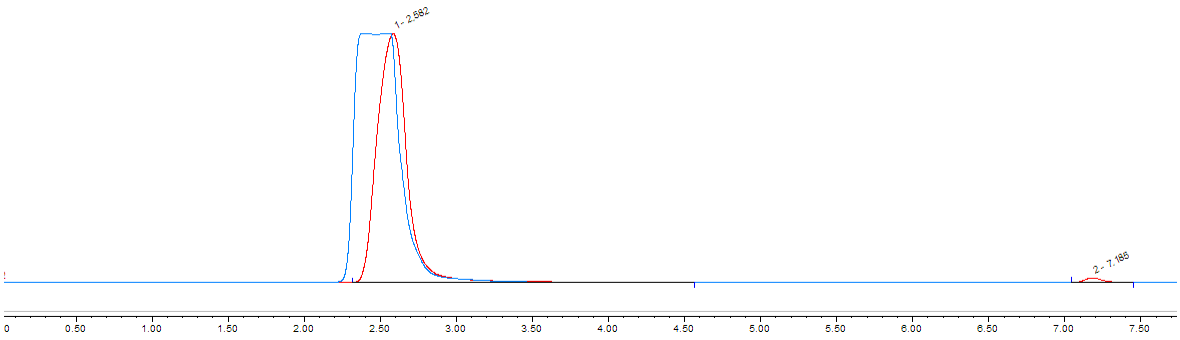

Retention time / min

Figure 6.19: Radio-HPLC (red) and UV chromatogram (blue) of the purified product at t = 15 min from the high-activity radiofluorination reaction of $[FeF_3(BnMe_2tacn]$ (1 mg/mL) in the presence of sodium ascorbate (50 mg/mL) in 75%/25% EtOH/H_2O Blue peak: Rt = 2.49 (sodium ascorbate). Red peak 1: Rt = 2.58 min, 99% ($^{18}F^-$). Red peak 2: Rt = 7.19 min, 1% ($[Fe^{18}F^{19}F_2(BnMe_2tacn)]$).

The UV traces in blue, shown in Figure 6.18 and Figure 6.19, show a major peak at 2.49 min for sodium ascorbate, due to the scale of this peak, the peak associated with the complex cannot be seen as it is concealed in the baseline.

On further research, Fe(III) can be reduced by sodium ascorbate and this is likely to be responsible for the observed behaviour, causing the complete liberation of $^{18}F^-$. This behaviour was not

observed in the Ga(III) complex due to the Ga(III) ion being much less susceptible to reduction compared to Fe(III).[47, 48] However, the FASTlab logfile (Figure 6.20) shows that the radiolabelling reaction proceeded without issue prior to the addition of the radiostabiliser in the formulation vial and produced a similar RCY to that of the reaction without the addition of further radiostabiliser ().

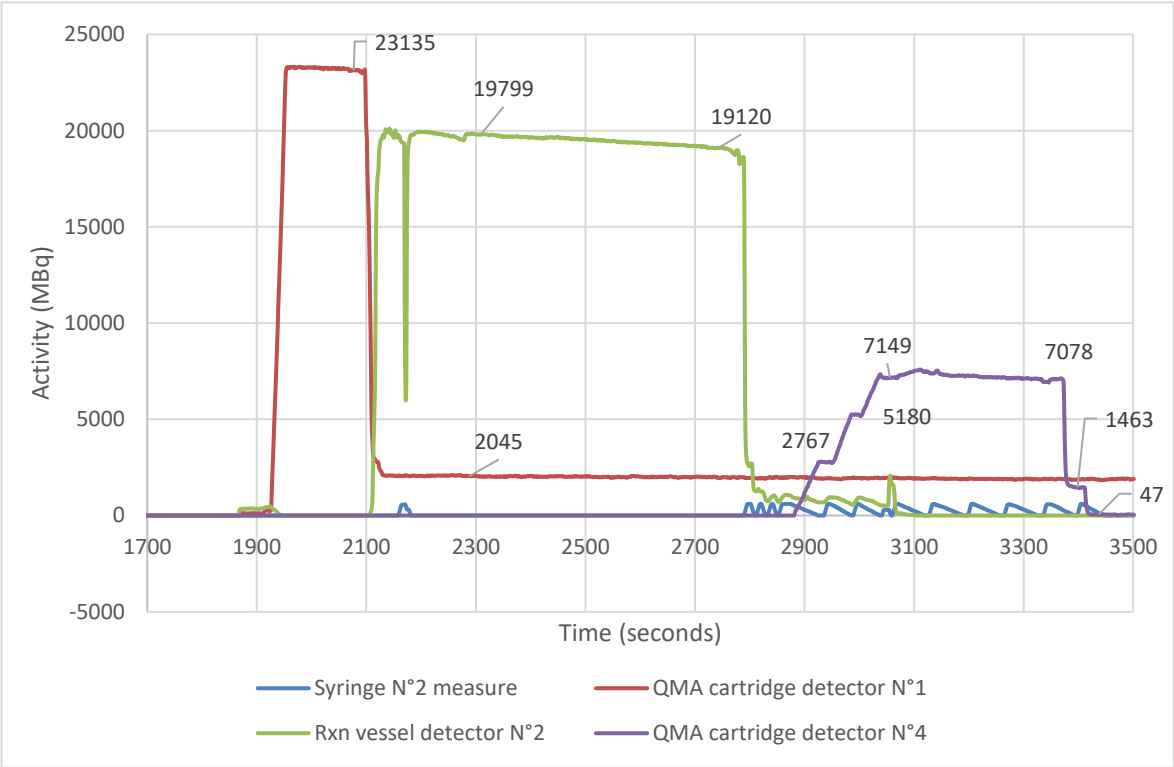

Figure 6.20: FASTlab reaction logfile for the radio-product, $[Fe^{18}F^{19}F_2(BnMe_2tacn)]$, formulated in a 90% H_2O/EtOH with 50 mg/mL sodium ascorbate.

The RCY for this high activity radiofluorination reaction to form $[Fe^{18}F^{19}F_2(BnMe_2tacn)]$ with 50 mg/mL was 38%.

An additional low activity experiment (311 MBq) was subsequently conducted to assess the impact on the RCY of $[FeF_3(BnMe_2tacn)]$ of using a ten-fold lower concentration of sodium ascorbate (5 mg/mL). This experiment showed that the RCP decreased from 90% at t = 0 h to 11% at t = 2 h, and therefore, even at lower radioactive concentration, sodium ascorbate causes the radio-product to degrade. Alternative radiostabilisers that would be less likely to react directly with the Fe(III) complex were therefore sought.

6.2.3.3 Radiostabilising effects of *p*-aminobenzoic acid and nicotinamide

Low-activity experiments were conducted to assess the effects of the radiostabilisers *p*-aminobenzoic acid (pABA, as shown in Figure 6.21) and nicotinamide (Figure 6.24) on the radiochemical stability of [$Fe^{18}F^{19}F_2(BnMe_2tacn)$].[36, 37]

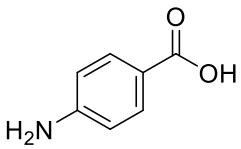

Figure 6.21: The structure of *p*-aminobenzoic acid.

The conditions remained as in Table 20, with the addition of 5 mg/mL of *p*ABA to the product formulation vial only, using a starting activity of 577 MBq.

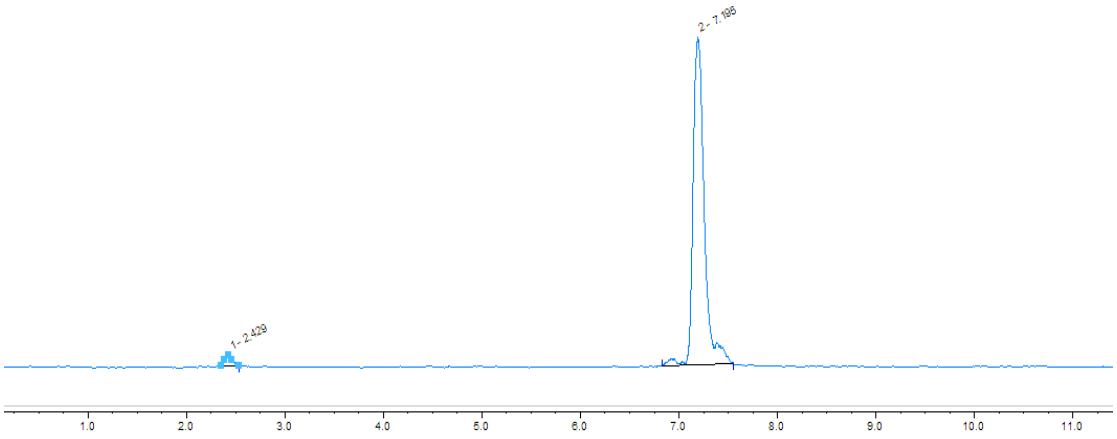

Figure 6.22: Radio-HPLC chromatogram (blue) of the purified product at t = 0 h from the low-activity radiofluorination reaction of [$FeF_3(BnMe_2tacn]$ (1 mg/mL) in the presence of *p*ABA (5 mg/mL) in 75%/25% EtOH/H_2O. Peak 1: Rt = 2.43 min, 2% ($^{18}F^-$). Peak 2: Rt = 7.20, 98% ([$Fe^{18}F^{19}F_2(BnMe_2tacn)$]).

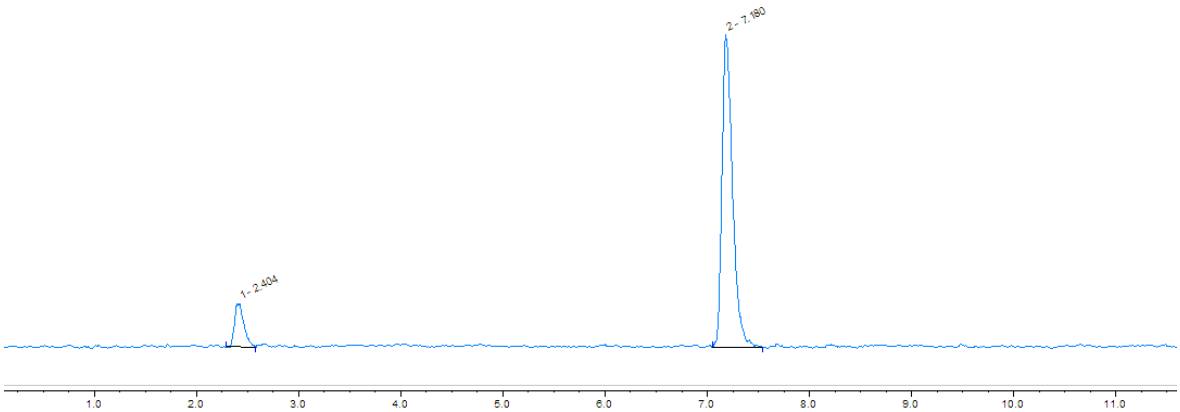

Figure 6.23: Radio-HPLC chromatogram (blue) of the purified product at t = 2 h from the low-activity radiofluorination reaction of [FeF_3($BnMe_2$tacn] (1 mg/mL) in the presence of *p*ABA (5 mg/mL) in 75%/25% EtOH/H_2O. Peak 1: Rt = 2.40 min, 11% ($^{18}F^-$). Peak 2: Rt = 7.18, 89% ([$Fe^{18}F^{19}F_2$($BnMe_2$tacn)]).

The RCP for this reaction decreased from 98% to 89% after two hours.

Nicotinamide is a form of vitamin B_3 and contains a pyridine ring with a primary amide group *meta* to the nitrogen atom in the ring Figure 6.24.

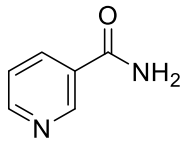

Figure 6.24: The structure of nicotinamide.

A low activity radiofluorination reaction using 5 mg/mL nicotinamide and the RCP decreased from 98% at t = 0 to 91% at t = 2h.

The graph in Figure 6.25 shows that sodium ascorbate is significantly worse than the other two radiostabilisers that were tested, and that *p*ABA and nicotinamide are not significantly different from each other. It was therefore decided to proceed with the high activity experiments using nicotinamide as the radiostabiliser.

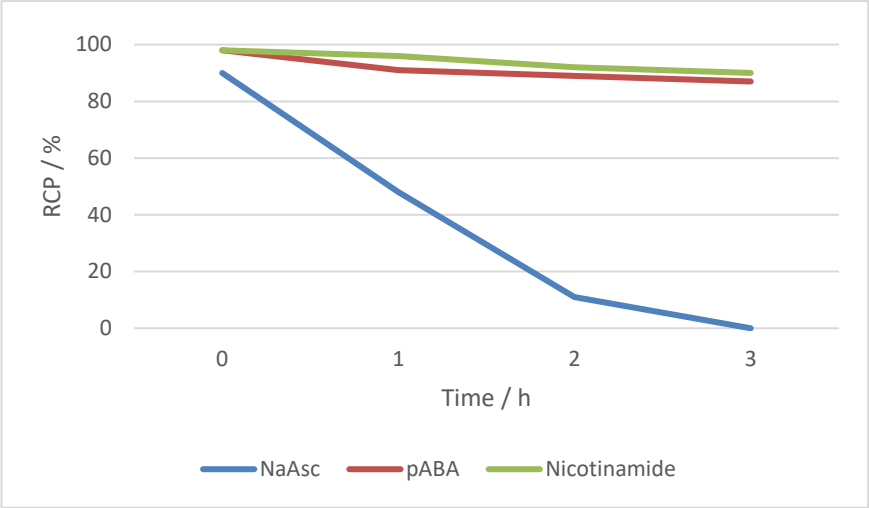

Figure 6.25: Graph showing the trend in radiochemical purity of [$Fe^{18}F^{19}F_2$($BnMe_2$tacn)] over time when radiolabelled in the presence of three different radiostabilisers; sodium ascorbate (NaAsc), *p*-aminobenzoic acid (*p*ABA) and nicotinamide at low-activity.

6.2.3.4 High-activity experiments with nicotinamide

Nicotinamide (5 mg/mL) was added to the product formulation vial, whilst all other conditions remained the same as described in Table 20. The reaction used [^{18}F]fluoride with a starting activity of 26.1 GBq and the RAC was calculated to be 220 MBq/mL with a RCY of 26% once the reaction had completed, the radio-HPLC trace at t = 0 and t = 3 h is shown in Figure 6.26 (the FASTlab logfile can be seen in Figure 6.27).

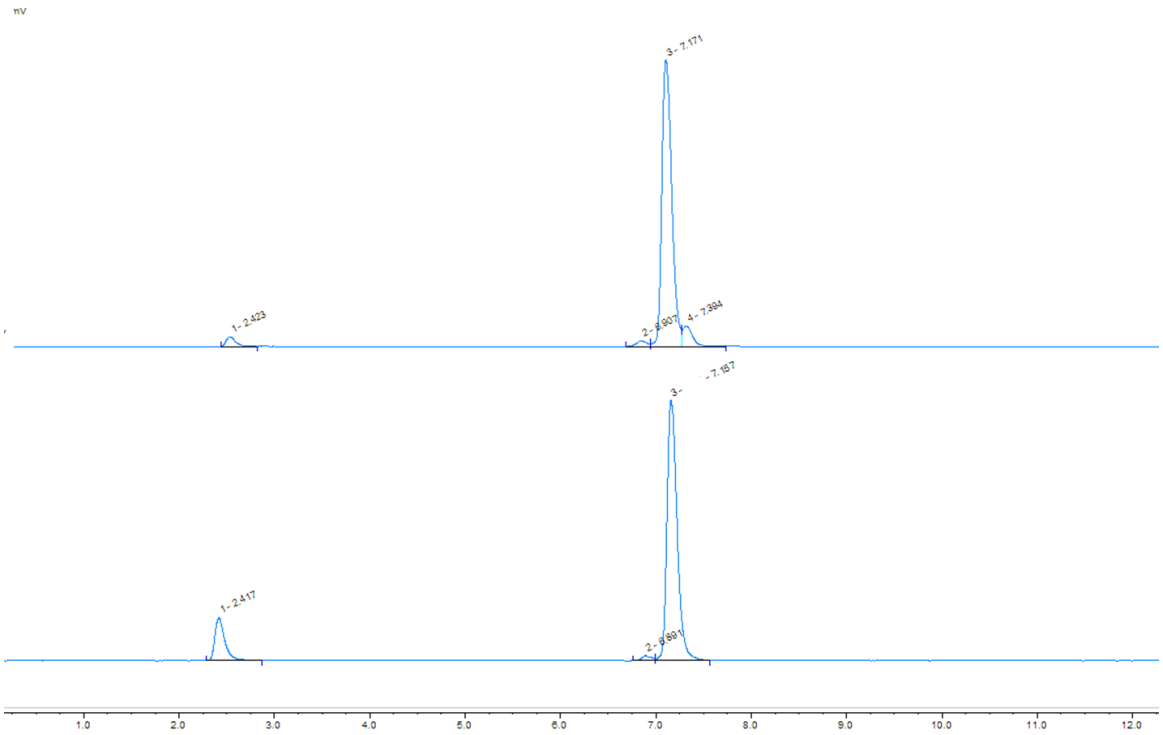

Figure 6.26: Radio-HPLC chromatogram (top spectrum) of the purified product at t = 0 h from the high-activity radiofluorination reaction of [FeF_3($BnMe_2$tacn] (1 mg/mL) in the presence of nicotinamide (5 mg/mL) in 75%/25% EtOH/H_2O. Peak 1: Rt = 2.42 min, 3% ($^{18}F^-$). Peak 2: Rt = 7.17, 97% ([$Fe^{18}F^{19}F_2$($BnMe_2$tacn)]). Radio-HPLC chromatogram (bottom spectrum) of the purified product at t = 3 h from the high-activity radiofluorination reaction of [FeF_3($BnMe_2$tacn] (1 mg/mL) in the presence of nicotinamide (5 mg/mL) in 75%/25% EtOH/H_2O. Peak 1: Rt = 2.42 min, 14% ($^{18}F^-$). Peak 2: Rt = 7.17, 86% ([$Fe^{18}F^{19}F_2$($BnMe_2$tacn)]).

The RCP of [$Fe^{18}F^{19}F_2$($BnMe_2$tacn)] reduced from 97% to 86% after three hours. The FASTlab logfile for this reaction is shown in Figure 6.27 and the crude RCY was calculated to be 26%

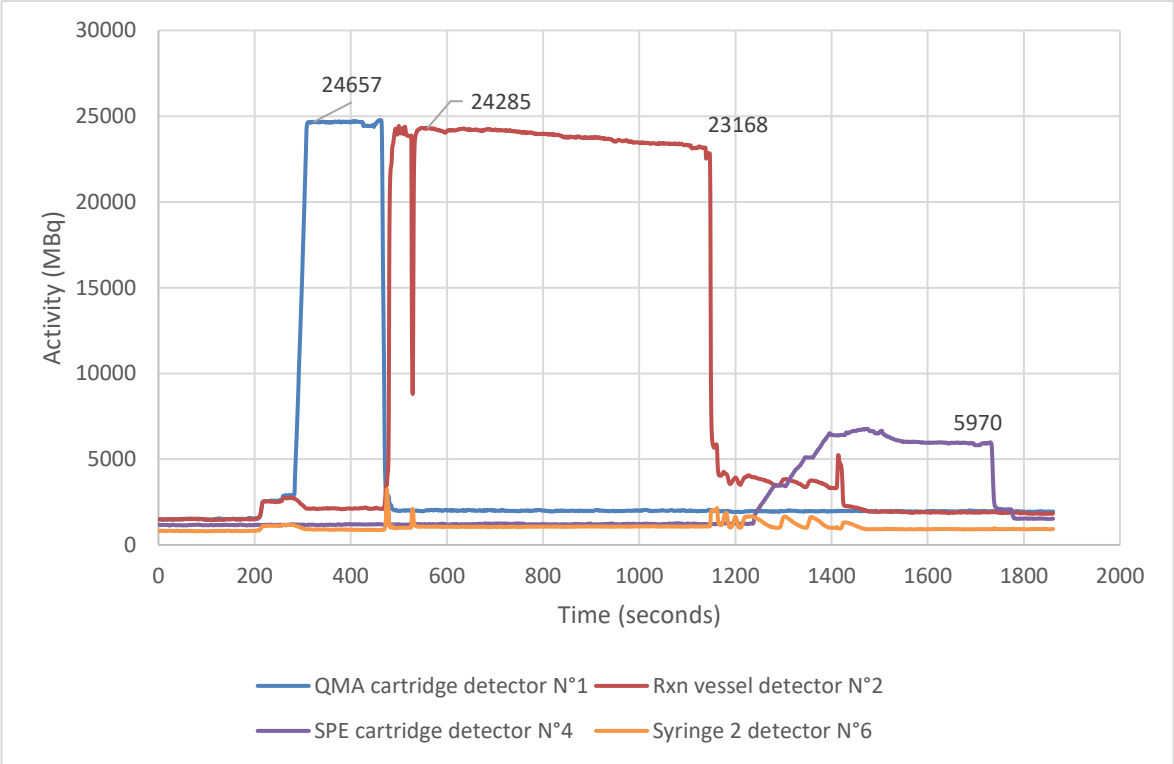

Figure 6.27: FASTlab reaction logfile for the radio-product, $[Fe^{18}F^{19}F_2(BnMe_2tacn)]$, formulated in a 90% H_2O/EtOH with 5 mg/mL nicotinamide.

Figure 6.28 shows that the radio-product degrades rapidly with the addition of sodium ascorbate, but it is more stable with the addition of nicotinamide or *p*ABA compared to the water/EtOH mixture in the absence of additional radiostabiliser.

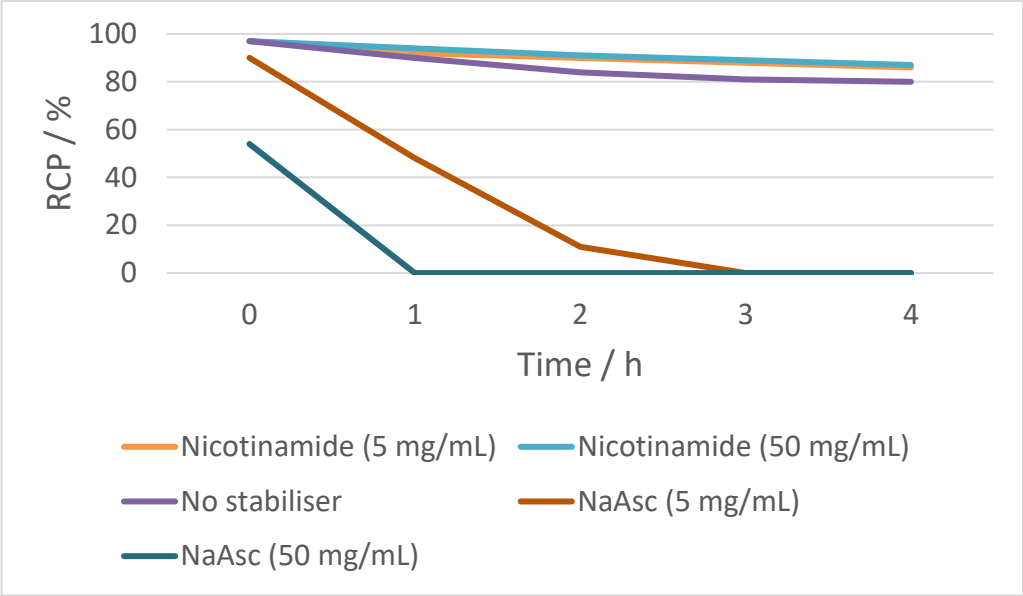

Figure 6.28: Graph representing the RCP (%) of [$Fe^{18}F^{19}F_2$($BnMe_2$tacn)] using different radiostabilisers; nicotinamide (5 mg/mL), nicotinamide (50 mg/mL), sodium ascorbate (5 mg/mL), sodium ascorbate (50 mg/mL) and 10% EtOH in water with no added radiostabiliser.

6.3 Conclusions

[FeF_3($BnMe_2$tacn)] was successfully radiolabelled with [^{18}F]fluoride (from 100 MBq up to 30 GBq), producing [$Fe^{19}F^{18}F_2$($BnMe_2$tacn)]. The $^{18}F/^{19}F$ isotopic exchange reaction at 28.2 GBq, using a GE Healthcare FASTlab platform, in the absence of a radiostabiliser shows degradation from 97% to 78% RCP after 5 hours, suggesting that radiolysis was playing a part in the more rapid degradation of the radio-product compared to the low activity experiments, as might be expected. The addition of nicotinamide as the radiostabiliser improved the radiochemical stability of the radio-product at high activity, with degradation from 97% to 86% after 3 hours. Similar results were found for *p*-aminobenzoic acid, whereas sodium ascorbate caused the complete degradation of the desired radio-product, liberating free $^{18}F^-$.

The successful development of a protocol for the automation of the [^{18}F]fluoride radiolabelling of [FeF_3($BnMe_2$tacn)] has been carried out in this work. This work has shown that it is feasible to automate the synthesis as a "proof of concept" and future work on a similar system containing a bioconjugate can be undertaken using the protocol developed here as a starting point for its optimisation.

Ligands such as NODP, NOTA or NODA, shown in Figure 6.29, conjugated with a biomolecule would bring this system a step closer to a potential PET radiotracer once biological studies on their stability in physiological conditions and *in vitro* and *in vivo* have been performed. The synthesis of some of these ligands and exploration with Fe(III) and other metal ions is currently being undertaken within the Reid Group.

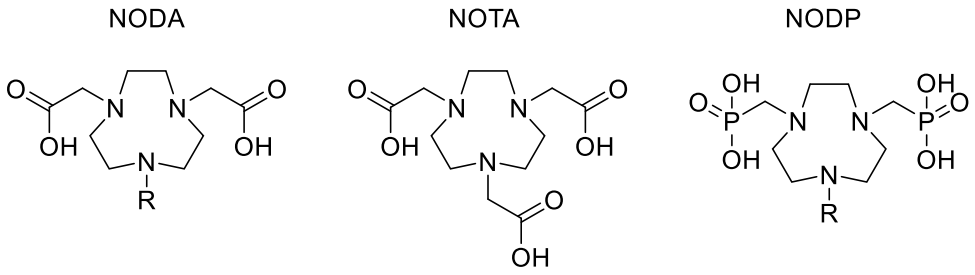

Figure 6.29: Structures of 1,4,7-triazacyclononane-1,4-diacetate (NODA), 1,4,7-triazacyclononane-1,4,7-triacetic acid (NOTA) and 1,4,7-triazacyclononane-1,4-di(methylene phosphonic acid) (NODP).

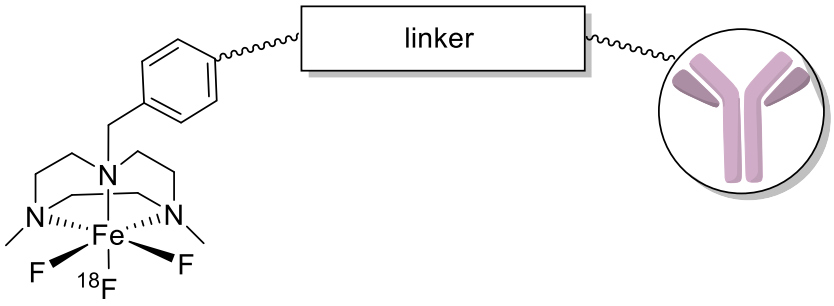

Figure 6.30: The potential future developments of [FeF_3($BnMe_2$tacn)] including a linker to a peptide.

6.4 Experimental

$[FeF_3(BnMe_2tacn)]$ was prepared, purified and characterised as reported in the literature.[5]

6.4.1 Manual radiolabelling procedure: $[Fe^{18}F^{19}F_2(BnMe_2tacn)]$

$[FeF_3(BnMe_2tacn)]$ (0.1 mg, 236 nmol) was dissolved in EtOH (750 μL) and radiofluorinated using $[^{18}F]$fluoride in cyclotron target water (250 μL, 367 MBq) and the reaction mixture was heated to 80 °C for 10 min using the GE FASTlab's reaction vessel heater.

6.4.2 General FASTlab radiolabelling procedure: $[Fe^{18}F^{19}F_2(BnMe_2tacn)]$

$[FeF_3(BnMe_2tacn)]$ (1 mg, 2.68 μM) was dissolved in EtOH (0.75 mL). To this solution, an aqueous solution of $[^{18}F]F^-$ (100 MBq-30 GBq) was eluted from a QMA light SepPak cartridge with NaOAc (640 μL) and added to the reaction vessel and heated to 120 °C for 10 min. The crude reaction mixture was diluted with water (19 mL) so that the SPE formulation vial was <10% EtOH.

6.4.3 SPE purification protocol

The diluted crude reaction mixture was then trapped on a pre-conditioned HLB cartridge, washed with water (2 x 10 mL) to remove unreacted $^{18}F^-$ and then eluted from the HLB cartridge with EtOH (1 mL) into the product formulation vial. The formulated product was analysed by analytical HPLC at t = 0 and various time intervals.

6.4.4 Addition of radiostabilisers

Radiolabelling experiment and SPE purification protocol as above. The product was eluted from the HLB cartridge with 1 mL of EtOH into the product formulation vial containing the radiostabiliser: nicotinamide, sodium ascorbate or *p*-aminobenzoic acid. This gave a final product formulation of either a 5 mg/mL or 50 mg/mL concentration of radiostabiliser.

6.4.5 Analytical HPLC method

Column: Phenomenex Luna 5 μm C18(2) 250 × 4.6 mm. Mobile phase A = water, B = MeCN. Flow rate 1 mL min-1. Gradient 0-15 min (10-90% B), 15-20 min (90% B), 20-21 min (90-10% B), 21-26.5 min (10% B).

6.4.6 Materials and methods

All the experiments were performed within a lead 'castle' made of 50 mm lead bricks. QMA light SepPak cartridge and SPE HLB cartridges were purchased from Waters. QMA light SepPak cartridges were used as received, HLB cartridges were pre-conditioned with EtOH (5 mL), followed by H_2O (5 mL), ensuring the cartridge did not dry out.

Water refers to sterile ultrapure water (18.2 MΩ-cm). Experiments were analysed using an Agilent 1290 HPLC system with an Agilent 1260 DAD UV detector and a Bioscan sodium iodide PMT with rate meter. Dionex Chromeleon 6.8 Chromatography data recording software was used to integrate the peak areas.

The RCY is the amount of activity in the isolated product, expressed as a percentage of the starting activity used in the reaction. The RCP refers to the radioactivity of the desired radio-product, as a percentage or fraction of any other radioactive compounds present, this is measured by a radiodetector that is attached to a HPLC system and can be used to measure stability of the radio-product over time.[24, 49]

6.5 References

1. Allott, L.; Amgheib, A.; Barnes, C.; Braga, M.; Brickute, D.; Wang, N.; Fu, R.; Ghaem-Maghami, S.; Aboagye, E. O., *Reaction chemistry & engineering* **2021,** *6*, 1070-1078.

2. Allott, L.; Aboagye, E. O., *Molecular Pharmaceutics* **2020,** *17*, 2245-2259.

3. Li, S.; Schmitz, A.; Lee, H.; Mach, R. H., *EJNMMI Radiopharmacy and Chemistry* **2016,** *1*, 15.

4. Wickstrøm, T.; Clarke, A.; Gausemel, I.; Horn, E.; Jørgensen, K.; Khan, I.; Mantzilas, D.; Rajanayagam, T.; In 't Veld, D.-J.; Trigg, W., *Journal of Labelled Compounds and Radiopharmaceuticals* **2014,** *57*, 42-48.

5. Blower, P. J.; Levason, W.; Luthra, S. K.; McRobbie, G.; Monzittu, F. M.; Mules, T. O.; Reid, G.; Subhan, M. N., *Dalton Transactions* **2019,** *48*, 6767-6776.

6. Baer, S. A.; Kraus, F., *Zeitschrift für Naturforschung B* **2011,** *66*, 865-867.

7. Pedersen, K. S.; Lorusso, G.; Morales, J. J.; Weyhermüller, T.; Piligkos, S.; Singh, S. K.; Larsen, D.; Schau-Magnussen, M.; Rajaraman, G.; Evangelisti, M.; Bendix, J., *Angewandte Chemie International Edition in English* **2014,** *53*, 2394-7.

8. Berry, J. F.; Bill, E.; Bothe, E.; Neese, F.; Wieghardt, K., *Journal of the American Chemical Society* **2006,** *128*, 13515-13528.

9. Berry, J. F.; Bill, E.; García-Serres, R.; Neese, F.; Weyhermüller, T.; Wieghardt, K., *Inorganic Chemistry* **2006,** *45*, 2027-2037.

10. Berry, J. F.; Bill, E.; Bothe, E.; Weyhermüller, T.; Wieghardt, K., *Journal of the American Chemical Society* **2005,** *127*, 11550-11551.

11. Kent Barefield, E., *Coordination Chemistry Reviews* **2010,** *254*, 1607-1627.

12. Banerjee, A.; Panda, M.; Tolla, A. S.; Li, J.; Brennessel, W. W.; Loloee, R.; Chavez, F. A., *Zeitschrift für anorganische und allgemeine Chemie* **2012,** *638*, 1473-1477.

13. Köhn, R. D.; Kociok-Köhn, G., *Angewandte Chemie International Edition in English* **1994,** *33*, 1877-1878.

14. Eckenhoff, W. T.; Biernesser, A. B.; Pintauer, T., *Inorganica Chimica Acta* **2012,** *382*, 84-95.

15. Zhang, Z.; Geng, Z.-R.; Kan, X.-W.; Zhao, Q.; Li, Y.-Z.; Wang, Z.-L., *Inorganica Chimica Acta* **2010,** *363*, 1805-1812.

16. Cotton, S. A.; Franckevicius, V.; Fawcett, J., *Polyhedron* **2002,** *21*, 2055-2061.

17. Healy, P.; Patrick, J.; Skelton, B.; White, A., *Australian Journal of Chemistry* **1983,** *36*, 2031-2041.

18. Tsitovich, P. B.; Gendron, F.; Nazarenko, A. Y.; Livesay, B. N.; Lopez, A. P.; Shores, M. P.; Autschbach, J.; Morrow, J. R., *Inorganic Chemistry* **2018,** *57*, 8364-8374.

19. Asik, D.; Smolinski, R.; Abozeid, S. M.; Mitchell, T. B.; Turowski, S. G.; Spernyak, J. A.; Morrow, J. R., *Molecules* **2020,** *25*, 2291.

20. Dorazio, S. J.; Tsitovich, P. B.; Gardina, S. A.; Morrow, J. R., *Journal of Inorganic Biochemistry* **2012,** *117*, 212-219.

21. Dorazio, S. J.; Tsitovich, P. B.; Siters, K. E.; Spernyak, J. A.; Morrow, J. R., *Journal of the American Chemical Society* **2011,** *133*, 14154-14156.

22. Tsitovich, P. B.; Morrow, J. R., *Inorganica Chimica Acta* **2012,** *393*, 3-11.

23. McMahon, M. T.; Gilad, A. A.; Bulte, J. W.; Van Zijl, P. C., *Chemical exchange saturation transfer imaging: Advances and applications* **2017**.

24. Coenen, H. H.; Gee, A. D.; Adam, M.; Antoni, G.; Cutler, C. S.; Fujibayashi, Y.; Jeong, J. M.; Mach, R. H.; Mindt, T. L.; Pike, V. W.; Windhorst, A. D., *Nuclear Medicine and Biology* **2017,** *55*, v-xi.

25. Ametamey, S. M.; Honer, M.; Schubiger, P. A., *Chemical Reviews* **2008,** *108*, 1501-1516.

26. Jonah, C. D., *Radiation Research* **1995,** *144*, 141-147.

27. Garrison, W. M., *Chemical Reviews* **1987,** *87*, 381-398.

28. Swiatla-Wojcik, D.; Buxton, G. V., *Radiation Physics and Chemistry* **2005,** *74*, 210-219.

29. Liu, S.; Edwards, D. S., *Bioconjugate Chemistry* **2001,** *12*, 7-34.

30. Liu, S.; Ellars, C. E.; Edwards, D. S., *Bioconjugate Chemistry* **2003,** *14*, 1052-1056.

31. Chen, J.; Linder, K. E.; Cagnolini, A.; Metcalfe, E.; Raju, N.; Tweedle, M. F.; Swenson, R. E., *Applied Radiation and Isotopes* **2008,** *66*, 497-505.

32. Liu, S.; Cheung, E.; Rajopadhye, M.; Williams, N. E.; Overoye, K. L.; Edwards, D. S., *Bioconjugate Chemistry* **2001,** *12*, 84-91.

33. Breeman, W. A. P.; Fröberg, A. C.; de Blois, E.; van Gameren, A.; Melis, M.; de Jong, M.; Maina, T.; Nock, B. A.; Erion, J. L.; Mäcke, H. R.; Krenning, E. P., *Nuclear Medicine and Biology* **2008,** *35*, 839-849.

34. Filice, A.; Fraternali, A.; Frasoldati, A.; Asti, M.; Grassi, E.; Massi, L.; Sollini, M.; Froio, A.; Erba, P. A.; Versari, A., *Journal of Oncology* **2012**.

35. Engell, T.; Mantzilas, D.; Grigg, J. Purification of [18F] - fluciclatide 2013.

36. Engell, T.; Getvoldsen, G. S.; Meijer, A. R.; Khan, I. A.; Nairne, R. J.; Mcrobbie, G. Radiotracer compositions and methods. 2019.

37. Pettitt, R.; Grigg, J.; Engell, T.; Wickmann, C., *Journal of Nuclear Medicine* **2010,** *51*, 530.

38. Solanki, K. K. Stabilization of radiopharmaceutical compositions. 1993.

39. Charleson, F. P. Stabilized radiopharmaceutical compositions 1989.

40. Cleeren, F.; Lecina, J.; Billaud, E. M. F.; Ahamed, M.; Verbruggen, A.; Bormans, G. M., *Bioconjugate Chemistry* **2016,** *27*, 790-798.

41. Torgrim Engell, J. G., Ingvil Gausemel, Knut Dyrstad, Johanthan R. Shales. Method of operating an automated radiopharmaceutical synthesizer 2012.

42. Bhalla, R.; Burt, J.; Hector, A. L.; Levason, W.; Luthra, S. K.; McRobbie, G.; Monzittu, F. M.; Reid, G., *Polyhedron* **2016,** *106*, 65-74.

43. de Blois, E.; Chan, H. S.; de Zanger, R.; Konijnenberg, M.; Breeman, W. A., *Applied Radiation and Isotopes* **2014,** *85*, 28-33.

44. Liu, S.; Edwards, D. S., *Bioconjugate Chemistry* **2001,** *12*, 554-558.

45. Abreu Diaz, A. M.; Drumeva, G. O.; Petrenyov, D. R.; Carrier, J.-F.; DaSilva, J. N., *American Chemical Society Omega* **2020,** *5*, 20353-20362.

46. Monzittu, F.Main group and transiton metal-based chelates for PET applications. PhD Thesis. University of Southampton, Southampton, 2018.

47. Shen, J.; Griffiths, P. T.; Campbell, S. J.; Utinger, B.; Kalberer, M.; Paulson, S. E., *Scientific Reports* **2021,** *11*, 7417.

48. Hynes, M. J.; Kelly, D. F., *Journal of the Chemical Society, Chemical Communications* **1988**, 849-850.

49. Edwards, R.; Greenwood, H. E.; McRobbie, G.; Khan, I.; Witney, T. H., *Molecular Imaging in Biology* **2021,** *23*, 854-864.

7 Summary and Outlook

The work in this thesis has demonstrated a considerable advancement in the chemistry of Group 14 fluoride complexes. A range of distorted octahedral Sn(IV) and Ge(IV) complexes with hard N- and O- donor ligands, of the type $[MF_4(L)_2]$, $[MF_3(L)_3][OTf]$ and even rarer, dicationic $[MF_2(L)_4][OTf]_2$ have been successfully synthesised (M = Sn or Ge). The products have been analysed by infrared spectroscopy, ^1H, $^{19}F\{^1H\}$ and $^{31}P\{^1H\}$ and ^{119}Sn NMR spectroscopy (where applicable) and elemental analysis was obtained when possible. It has been demonstrated that the use of TMSOTf in the presence of additional ligand can reliably remove one fluoride ligand from neutral *cis*/*trans*-$[MF_4(L)_2]$ complexes to form novel monocations as their OTf^- salts, *fac*/*mer*-$[MF_3(L)_3][OTf]$. This is in direct contrast to similar Sn(IV) and Ge(IV) fluoride complexes with soft phosphine donor ligands, that give rise to neutral complexes with coordinated triflate ligand(s). In the case of $[SnF_2(OPPh_3)_4][OTf]_2$, it was shown to be possible to isolate a pure sample of the dication, the first of its kind and this was confirmed as the *trans* isomer in the solid state by single crystal X-ray analysis. $[GeF_2(OAsPh_3)_4][OTf]_2$ was clearly identified in a mixture of products when trying to abstract two fluorides from $[GeF_4(OAsPh_3)_2]$ with the addition of two equivalents of $OAsPh_3$, another very rare example of a Group 14 dicationic complex in the +4 oxidation state. Information on the bond dissociation energies of Sn-F and Ge-F showed that they do not differ significantly (456 *vs* 464 kJ mol^{-1}, respectively), there may be a significant kinetic barrier in the germanium systems.[1]

Work on Group 14 systems was further developed to include macrocyclic ligands, with the aim of assessing these as candidates for radiofluorination and PET imaging. A series of Sn(IV) and Ge(IV) complexes were successfully synthesised with terpy, tacn, cyclen and cyclam ligand derivatives, expanding these systems to Si(IV) proved more challenging and only $[SiCl_3(terpy)][OTf]$ was conclusively made. Si(IV) macrocyclic complexes are worth further exploration and study due to the inherent stability of the Si-F bond that is so important in ^{18}F radiotracers.

$[FeF_3(BnMe_2tacn)]$ had been successfully synthesised and radiolabelled previously, however a greater radiochemical yield during manual experiments was achieved in this work by altering the solvent of choice to EtOH and the reaction vessel used.[2] The synthesis of $[Fe^{18}F^{19}F_2(BnMe_2tacn)]$ was automated and optimised on the GE HealthCare FASTlab module, providing a "proof of concept" and that it is feasible to translate these systems over to automation, this will be the starting block for further work on automation of these systems and to increase the potential for these systems to become translated over into the clinic. The next step for this work would be to conjugate a biomolecule to the system, such as PSMA, through functionalisation of the benzyl

group, this is due to being able to selectively target a specific area in the body to improve the diagnostic capability of certain diseases (for example over expressed cells in prostate cancer, in PSMA's case).

The complex $[GaF_3(BnMe_2tacn)].xH_2O$ was prepared *via* a new synthetic route; *via* developing a dmso and chloride free synthetic pathway to $[GaF_3(pyNO)(H_2O)_2]$ and doing subsequent ligand exchange reactions with the macrocycle $BnMe_2tacn$. Whilst it is clear that the presence of a small amount of dmso does degrade $[GaF_3(BnMe_2tacn)]$ overtime and that it is likely that in producing this complex from the dmso adduct, it is the highly coordinating solvent that is interfering with the stability of the radio-product over time. This work has not conclusively determined this and further experiments will be needed to confirm this.[3]

7.1 References

1. Dean, J. A., *Lange's Handbook Of Chemistry*. Eleventh Edition ed.; McGraw Hill, New York, 1973; Vol. 13, p 12A-12A.

2. Blower, P. J.; Levason, W.; Luthra, S. K.; McRobbie, G.; Monzittu, F. M.; Mules, T. O.; Reid, G.; Subhan, M. N., *Dalton Transactions* **2019,** *48*, 6767-6776.

3. Monzittu, F. M.; Khan, I.; Levason, W.; Luthra, S. K.; McRobbie, G.; Reid, G., *Angewandte Chemie International Edition* **2018,** *57*, 6658-6661.

Appendix A General experimental details

Complex synthesis was carried out by using standard Schlenk line and glovebox techniques, under a dry N_2 atmosphere, unless otherwise stated. Solvents were dried by distillation from CaH_2 (CH_2Cl_2, MeCN, DMSO, DMF, CH_3NO_2), over sodium (pyridine) or Na/benzophenone ketyl (*n*-hexane). All solvents were subsequently stored over 4Å molecular sieves. Aqueous reactions were performed using freshly distilled H_2O.

Ligands $OPPh_3$, $OPMe_3$, pyNO, were obtained from Sigma Aldrich and sublimed before use, cyclam and cyclen were obtained from Chematech and functionalised using literature preparations. TMSOTf was distilled prior to use. GeF_4 was obtained from Fluorochem. Tin (II) fluoride was obtained from Alpha Aesar.

Infrared spectra were recorded over a range of 200-4000 cm^{-1} using a Perkin Elmer Spectrum 100 spectrometer and samples were prepared as Nujol mulls between CsI plates.

NMR spectra were recorded using a Bruker AV400 or DPX400, with ^{1}H and $^{13}C\{^{1}H\}$ being referenced to the solvent resonance. $^{19}F\{^{1}H\}$ spectra were referenced to $CFCl_3$, $^{31}P\{^{1}H\}$ to 85% H_3PO_4, ^{119}Sn to $SnMe_4$ (with $[Cr(acac)_3]$ used as a relaxation agent), ^{29}Si to TMS (with tris(2,2,6,6-tetramethyl-3,5-heptanedionato)chromium(III) as a relaxation agent and ^{71}Ga to $[Ga(H_2O)_6]^{3+}$ at pH 1. Spectra were recorded at 298 K unless otherwise stated.

Mass spectra were obtained using a Waters mass spectrometer, which was equipped with a single quadrupole analyser, ESI MSwas performed in CH_3NO_2 or MeCN. Microanalyses were performed by Medac Ltd or London Metropolitan University.

Single crystal X-ray diffraction data was collected using a Rigaku AFC12 goniometer equipped with an enhanced (HG) Saturn724+ detector mounted at the window of an FR-E+ SuperBright molybdenum (λ = 0.71073 Å) rotating anode generator with VHF or HF Varimax optics (70 or 100 µm), with the crystal held at 100 K. Structure solution and refinement were performed using SHELX(T)-2018/2 and SHELZ-2018/3 through Olex2.[1, 2] H atoms bonded to C were placed in calculated positions using the default C–H distance and refined using a riding model.

The electronic structures of the series $[GeF_4(OPMe_3)_2]$, $[GeF_3(OPMe_3)_3]^+$ and $[GeF_2(OPMe_3)_4]^{2+}$ were investigated by density functional theory (DFT) calculations using the Gaussian 16W program and visualised using GaussView 5.0.[3] The density functional chosen was B3LYP-D3 with

the basis set as 6-311G(d).).[4, 5] Energy minima were confirmed by the absence of imaginary frequencies.

Radiofluorination experiments were performed using $[^{18}F]F^-$ which was obtained via the irradiation of $[^{18}O]H_2O$ target water (97 atom %, Rotem Industries Ltd., Israel) with a CTI RDS 112 cyclotron (11 MeV, 30 μA beam current) used at St. Thomas' Hospital and a GE PETtrace 800 cyclotron (16 MeV, 60 μA beam current) used at Addenbrookes Hospital.

A.1.1 References

1. Sheldrick, G., *Acta Crystallographica Section C* **2015,** *71*, 3-8.

2. Sheldrick, G., *Acta Crystallographica Section A* **2008,** *64*, 112-122.

3. Frisch, M. J.; Trucks, G. W.; Schlegel, H. B.; Scuseria, G. E.; Robb, M. A.; Cheeseman, J. R.; Scalmani, G.; Barone, V.; Petersson, G. A.; Nakatsuji, H.; Li, X.; Caricato, M.; Marenich, A. V.; Bloino, J.; Janesko, B. G.; Gomperts, R.; Mennucci, B.; Hratchian, H. P.; Ortiz, J. V.; Izmaylov, A. F.; Sonnenberg, J. L.; Williams; Ding, F.; Lipparini, F.; Egidi, F.; Goings, J.; Peng, B.; Petrone, A.; Henderson, T.; Ranasinghe, D.; Zakrzewski, V. G.; Gao, J.; Rega, N.; Zheng, G.; Liang, W.; Hada, M.; Ehara, M.; Toyota, K.; Fukuda, R.; Hasegawa, J.; Ishida, M.; Nakajima, T.; Honda, Y.; Kitao, O.; Nakai, H.; Vreven, T.; Throssell, K.; Montgomery Jr., J. A.; Peralta, J. E.; Ogliaro, F.; Bearpark, M. J.; Heyd, J. J.; Brothers, E. N.; Kudin, K. N.; Staroverov, V. N.; Keith, T. A.; Kobayashi, R.; Normand, J.; Raghavachari, K.; Rendell, A. P.; Burant, J. C.; Iyengar, S. S.; Tomasi, J.; Cossi, M.; Millam, J. M.; Klene, M.; Adamo, C.; Cammi, R.; Ochterski, J. W.; Martin, R. L.; Morokuma, K.; Farkas, O.; Foresman, J. B.; Fox, D. J. *Gaussian 16 Rev. C.01*, Wallingford, CT, 2016.

4. Krishnan, R.; Binkley, J. S.; Seeger, R.; Pople, J. A., *Journal of Chemical Physics* **1980,** *72*, 650-654.

5. Lee, C.; Yang, W.; Parr, R. G., *Physical Review B* **1988,** *37*, 785-789.

Appendix B Crystallographic information files

Cif files are located in the supplementary information.

The filenames (CCDC number, when published) correspond to the complexes as follows:

$[SnF_4(py)_2]$ .....2021dept_gr_mw90_auto (2106812)

$[SnF_4(pyNO)_2]$ .....mw121120twins_twin1_hklf4 (2104984)

$[SnF_2(OPPh_3)_4][OTf]_2$.....2021dept_gr_mw98_1 (2104976)

$[GeF_3(OPPh_3)_3][OTf]$ msw107-reprocessed1 (2174295)

$[GeF_2(Me_4\text{-cyclen})][OTf]_2$ .....msw81_2 (2177877)

$[SiCl_3(terpy)][OTf]$.....2022grmwsicl3terpyotf2